# Experimental and mathematical analysis of the central carbon metabolism in cancer and stem cells

Dissertation
zur Erlangung des akademischen Grades

DOCTOR RERUM NATURALIUM
(Dr. rer. nat.)

im Fach Biophysik
eingereicht an der

Lebenswissenschaftlichen Fakultät
der Humboldt-Universität zu Berlin
von

Dipl.-Ing. Christin Zasada, geb. Hess

Präsidentin der Humboldt-Universität zu Berlin
Prof. Dr.-Ing. Dr. Sabine Kunst

Dekan der Lebenswissenschaftlichen Fakultät
Prof. Dr. Bernhard Grimm

---

Gutachter/innen:

1. Prof. Herman-Georg Holzhütter

2. Prof. Edda Klipp

3. Dr. Markus Landthaler

Tag der mündlichen Prüfung: 22. Februar 2017

"Everything should be made as simple as possible, but not one bit simpler."

---

Albert Einstein

# Summary

Metabolic reprogramming of the central carbon metabolism (CCM) is highly debated during the last decade. It describes the rearrangement of nutrient consumption for providing energy and building blocks for cellular proliferation and maintenance. So far, only sparse data are available for an in-depth analysis of metabolic reprogramming events. The herein summarised projects address metabolic programming from different perspectives and show the implementation of cell culture experiments, cutting-edge high-throughput technologies, bioinformatics, and computational modelling into one workflow providing the determination of metabolic flux maps of mammalian cells. The combination of GC-MS and LC-MS-based methodologies enable the quantitative analysis of proteins and metabolites of the CCM. Pulsed stable isotope-resolved metabolomics (pSIRM) experiments allow monitoring the fate of nutrients within the network of the CCM. The time-dependent and position-specific incorporation of carbon-13 leads to an indirect measurement of the metabolic flux, the only one functional readout of a cell.

High-throughput technologieses were applied in four projects to gain insights in metabolic reprogramming in cancer cell lines, human embryonic stem cells (hESCs), induced pluripotent stem (iPS) cells and their derived fibroblasts. A global principal component analysis demonstrated the discrimination of phenotypes by different classes of quantitative data. The comparison of metabolic and protein profiles confirms the presence of the Warburg effect in both cell types. Though, the executing enzymes vary regarding their isoenzyme identity and expression levels.

Methodological improvements provided the implementation of GC-MS derived data for INST-MFA. The mapping of GC-MS derived fragments to the molecule structure enables

an extension of the CCM network. Robustness of the input data has been improved by the development of a R-scripting based quality control tool (MTXQC).

# Zusammenfassung

Die Entstehung von Tumoren und damit einhergehenden Veränderungen wurden insbesondere im letzten Jahrzehnt kontrovers diskutiert. Bisher standen nur wenige Datensätze mit ausreichender Datendichte zur Verfügung um eine umfassende Untersuchung der Regulation des Stoffwechsels durchzuführen. Die in dieser Arbeit zusammengefassten Projekte adressieren verschiedene Aspekte der Stoffwechselregulation und beschreiben die Verknüpfung von Zellkulturexperimenten mit innovativen Hochdurchsatz-Technologien, komplexer Datenanalyse und Computer-basierter Modellierung zur Bestimmung der Stoffwechselflüsse in eukaryotischen Zellen.

Die Kombination von GC-MS und LC-MS basierten Technologien ermöglicht die quantitative Analyse des zentralen Kohlenstoffwechsels. Markierungsexperimente mit stabilen Isotopen (pSIRM) erlauben die dynamische Analyse der Stoffwechselaktivität. In vier Projekten wurden das Proteom und Metabolom von Krebszellen, humanen Stammzellen (hESCs), induzierten pluripotenten Stammzellen (iPS) und deren dazugehörigen differenzierten Vorläufer- oder Nachfolgerzellen bestimmt.

Die multivariate, statistische Analyse der Daten ermöglichte die Differenzierung verschiedener Zelltypen basierend auf der Kombination aller quantitativen Daten. Die Anwendung stabiler Isotope die Detektion der Substrat-spezifischen Verwendung von Nährstoffen im zentralen Kohlenstoffwechsel. Quantitative Bestimmungen der Poolgrössen, Isotopeninkorporationen, sowie der extrazellulären Raten in neuronalen, pluripotenten Vorläuferzellen (Luhmes d0) und Neuronen (Luhmes d6) ermöglichte die Bestimmung der Stoffwechselflusskarte beider Zelltypen unter Verwendung der instationären metabolischenen Flussanalyse (INST-MFA).

Die Etablierung einer Qualitätskontrolle für GC-MS basierte Daten (MTXQC), sowie die Zuordnung der GC-MS Fragmente zur Molekülstruktur, ermöglichten den Ausbau des Netzwerkes des zentralen Kohlenstoffwechsels und die Implementierung der Daten für die metabolische Flussanalyse.

# Acknowledgement

At the end it is hard for me to tell if it is more diligent to summarise an almost six years lasting scientific travel into one PhD thesis, or to thank all the people that have accompanied me in this journey. These years of my PhD were an intensive, exhaustive, inspiring, challenging and overwhelming time and all of you contributed in a very specific manner to the final product you're holding in your hands, therefore just right at the beginning a simple, but pure "Thank you!".

Despite everything I have to start: Dear lab mates, no matter if present or former, I would like to thank you all for your support during the last years. It has been a pleasure to work in a team that shares the joy, frustration and curiosity about science in a way that we are doing. I saw the lab growing from a little team of five persons into a colorful lab of professions, projects and humours. Many of my ideas have been rised with a cup of Italian espresso, cooking zoodles in the kitchen, during shared long nights in the office, or a good drink. Vicariously thank you — Guido, Nadine, Alina, Henning, Fardad, Chris, Jenny, Ela, Birte, Julia, Tobias, Olya and Matthias. I would like to send special acknowledgements to Stefan Kempa — for the guidance and to give me the opportunity to follow my scientific curiosity, to perform "just another little experiment" and to present my work at so many conferences as I did.

Furthermore, I would like to thank my cooperation partners not backing off from the proportions of my experimental plans, supporting the numerous adaptions of protocols and their fruitful comments and discussion. Thank you — Alessandro Prigione and Raul Buckowicki for collecting cells for more than one year across Berlin; to Katharina Nöh, Sebastian Niedenführ and Martin Cerff providing me access to the computational world

of metabolix flux analysis and to Marcel Leist, Simon Gutbier and Johann Delp for your support.
I would also like to thank the scientific commission for supporting the last steps of the PhD — Professor Herman-Georg Holzhütter, Professor Edda Klipp, Dr. Markus Landthaler, Professor Ana Pombo and Professor Thomas Sommer.

Zu guter Letzt möchte ich meiner Familie danken, die mir versucht haben nur jede mögliche Tür zu öffnen, mit Rat, Tat und gutem Rotwein zur Seite stehen und mich in jeder Situation unterstützen — vielen Dank liebe Eltern, Bruderherz und an alle hier ungenannt gebliebenen Familienmitglieder. Insbesondere die letzten Jahre haben mir gezeigt, wie sehr ich auf meine Freunde bauen kann. Die Liste der Personen, denen ich besonders danken möchte, erscheint gerade endlos. Aus diesem Grunde unsortiert und ohne Präferenz — Susi, Oliwia, Doro, Anna & Thomas, Lena, Phuong, Kelly, Magda, Steffi, Heike, Jörg, Barbara, Jordi, Andreas, Heike und Sören.

## Erklärung über die selbstständige Abfassung meiner Dissertation

Hiermit erkläre ich, Christin Zasada, dass die vorliegende Dissertation selbstständig und ohne Benutzung anderer als der angegebenen Hilfsmittel angefertigt wurde. Die aus fremden Quellen — direkt oder indirekt — übernommenen Gedanken wurden als solche gekennzeichnet.
Die Dissertation wurde bisher in dieser oder leicht abgewandelter Form keiner anderen Prüfungsbehörde vorgelegt oder veröffentlicht.

Berlin, den .....

Unterschrift: .....

# Contents

# List of Figures

# List of Tables

# Abbreviations

## General abbreviations

| | |
|---|---|
| ADR | Adriamycin |
| AMP | Adenosine monophosphate |
| ATP | Adenosine triphosphate |
| bFGF | Basic fibroblastic growth factor |
| c | Cytosolic |
| CA | Cinnamic acid |
| CCM | Central carbon metabolism |
| DDA | Data-dependent analysis |
| DM | Differentiation medium |
| DMEM | Dulbeccos modified eagle medium |
| DNA | Deoxyribonucleic acid |
| EI | Electron impact |
| ER | Estrogen receptor |
| er | Endoplasmic reticulum |
| F | Fibroblast |
| FA | Fatty acid |
| FBA | Flux balance analysis |
| FBS | Fetal bovine serum |
| FC | Fold change |
| GC-MS | Gas chromatography - mass spectrometry |
| GO | Gene ontology |
| GOBP | Gene ontology biological process |
| hESC | Human embryonic stem cell |
| hESC-DF | hESC-derived fibroblast |
| HIF1 | Hypoxia-inducible factor 1 |
| IDMS | Isotope dilution mass spectrometry |
| INST-MFA | In-stationary metabolic flux analysis |
| iPS cell | Induced pluripotent stem cell |
| iPS-DF | iPS-derived fibroblast |
| LC-MS | Liquid chromatography - mass spectrometry |
| LFQ | Label-free quantification |
| LI | Label incorporation |
| Luhmes | Lund human mesencephalic cell lines |
| m | Mitochondrial |

| | |
|---|---|
| MCT | Monocarboxylate transporter |
| MEF | Mouse embryonic fibroblasts |
| MeOH | Methanol |
| MeOx | Methoxamine |
| MFA | Metabolic flux analysis |
| MS | Mass spectrometry |
| MSTFA | N-Methyl-N-(trimethylsilyl) trifluoroacetamide |
| mTOR | mammalian Target of rapamycin |
| NAD | Nicotinamide adenine dinucleotide |
| NEAA | Non-essential amino acids |
| NMR | Nuclear magnetic resonance |
| PC | Principal component |
| PCA | Principal component analysis |
| PI3K | Phosphoinositide-3-kinase |
| PLO | Poly-L-ornithine |
| PM | Proliferation medium |
| PPP | Pentose phosphate pathway |
| PR | Progesterone receptor |
| pSIRM | pulsed Stable isotope resolved metabolomics |
| RNA | Ribonucleic acid |
| ROS | Reactive oxygen species |
| TCA-cycle | Tricarboxylic acid cycle |
| Tet | Tetracycline |
| ToF | Time-of-flight |

## Metabolites of CCM

| | |
|---|---|
| 3PGA | 3-Phosphoglyceric acid |
| 6PGA | 6-Phosphogluconic acid |
| aCoA | acetyl-CoA |
| $\alpha$KG | $\alpha$ketoglutaric acid |
| Ala | Alanine |
| Cit | Citric acid |
| DHAP | Dihydroxyacetone phosphate |
| F26P | Fructose-2,6-bisphosphate |
| FBP, F16P | Fructose-1,6-bisphosphate |
| Frc | Fructose |
| Frc1P, F1P | Fructose-1-phosphate |
| Frc6P, F6P | Frutose-6-phosphate |
| Fum | Fumaric acid |
| GA3P | Glyceraldehyde-3-phosphate |
| Glc | Glucose |
| Glc6P | Glucose-6-phosphate |
| Gln | Glutamine |
| Glu | Glutamic acid |
| Gly | Glycine |
| Glyc | Glycerol |

| | |
|---|---|
| Glyc3P | Glycerol-3-phosphate |
| Lac | Lactic acid |
| Leu | Leucine |
| Mal | Malic acid |
| OAA | Oxaloacetic acid |
| PEP | Phosphoenolpyruvic acid |
| Pro | Proline |
| Pyr | Pyruvic acid |
| Ser | Serine |
| Suc | Succinic acid |
| Thr | Threonine |

## Enzymes of the CCM

| | |
|---|---|
| ACLY | ATP-citrate synthase |
| ALDO | Aldolase |
| ASL | Argininsuccinate lyase |
| ASS1 | Argininosuccinate synthase |
| BCAT | Branched-chain-amino-acid aminotransferase |
| CCBL2 | Cysteine-S-conjugate $\beta$-lyase |
| ENO | Enolase |
| FASN | Fatty acid synthase |
| FH | Fumarate hydratase |
| GLS | Glutaminase |
| GOT | Aspartate aminotransferase |
| GS | Glutamine synthetase |
| HK | Hexokinase |
| IDH | Isocitrate dehydrogenase |
| LDH | Lactate dehydrogenase |
| MDH | Malate dehydrogenase |
| ME | Malic enzyme |
| MTHFDL1 | C-1-Tetrahydrofolate synthase |
| OGDH | 2-oxoglutarate dehydrogenase, mitochondrial |
| PC | Pyruvate carboxylase |
| PDHc | Pyruvate dehydrogenase complex |
| PFKP | Phosphofructokinase |
| PGK1 | Phosphoglycerate kinase |
| PHGDH | D-3-phosphoglycerate dehydrogenase |
| PKM | Pyruvate kinase isoenzyme M |
| PSAT | Phosphoserine aminotransferase |
| TALDO | Transaldolase |
| TKT | Transketolase |
| TPI | Triosephosphate isomerase |

# 1 Introduction

## 1.1. Metabolic reprogramming in cancer and stem cells

Metabolic reprogramming describes the rearrangement of nutrient consumption for providing energy and building blocks for cellular proliferation and maintenance occurring during tumorigenesis and cell differentiation (Ito and Suda, 2014b). The oncogenic transformation of a cell results not only in a switch of isoenzyme expression and cell growth, but also in the adjustment of metabolic pathway activities to meet the modified metabolic demands. Metabolic reprogramming occurs also during differentiation of stem and pluripotent cells. The loss of pluripotency results in an increased energy production by oxidative phosphorylation in the mitochondria.

The metabolism is a highly coordinated network and maintains four major goals: (i) the generation of chemical energy by degradation of energy-rich molecules, (ii) the conversion of nutrients into their basic molecules, (iii) the synthesis of macromolecules (proteins, nucleic acid, polysaccharides) and (iv) the generation and breakdown of biomolecules for cellular functions, e.g., membrane lipids or intracellular messengers (Nelson et al., 2009). The arrangement of these reactions in metabolic pathways — in series of enzyme-catalysed reactions — provides the controlled uptake, conversion and production of required nutrients, precursors and macromolecules. Each step within a pathway results in specific, but small chemical modifications of a molecule, e.g., the removal, transfer or addition of a functional group or even a single atom (Nelson et al., 2009).

The core of the central carbon metabolism (CCM) is highly conserved among organism and consists of the pathways: Glycolysis, Tricarboxylic acid cycle (TCA-cycle), the

pentose phosphate pathway (PPP), and the synthesis and degradation of amino and fatty acids. These pathways maintain the uptake of nutrients in form of sugars, amino acids and lipids and their breakdown into smaller compounds (catabolism). The converging catabolic reactions provide the synthesis of precursors in form of two or three-carbon molecules that are used to generate macromolecules (anabolism) for the biosynthesis.
The compartmentation in eukaryotic cell provides a separation of biosynthetic and degradative pathways and their independent regulation, e.g., the degradation of fatty acids solely occurs in mitochondria, whereas the synthesis is taking place in the cytosol.
The interdependent nature of metabolic pathways provides the fine-tuning of the central carbon metabolism. The accumulation of metabolites modifies upstream pathway activities to control their own synthesis rate, e.g., citric acid regulates the rate-limiting glycolytic enzyme phosphofructokinase-1 (PFK-1, cytosolic).

### 1.1.1. Metabolic pathways — a short introduction

**Glycolysis** Glucose accounts for more than 50% of the daily uptake of nutrients. It is the major contributor to biosynthetic reactions and the generation of adenosine triphosphate (ATP). Glycolysis, a series of ten reactions, processes the highest flux of carbons in the cell. One molecule of glucose is converted into two molecules of pyruvic acid (Pyr) and results in the concomitant generation of two molecules of ATP and $NADH/H^+$ (Figure 1.1). The pathway contains of two phases, five reactions each: (i) the preparatory phase, followed by a (ii) pay-off phase. The first phase contains the lysis of glucose — the separation of the six-carbon glucose into two three-carbons molecules glyceraldehyde-3-phosphate (GA3P). Two molecules of ATP are paid for the phosphorylation of glucose-6-phosphate (G6P) and fructose-1,6-bisphosphate (F16P2) in advance of the production of the energy in the second phase. In the pay-off phase the conversion of GA3P into Pyr yields in the synthesis of four molecules of ATP and two molecules of NADH. In the presence of oxygen glycolysis is only the first part of glucose degradation. The subsequent processing of carbons within the mitochondria provides the synthesis of ATP.

The anaerobic breakdown of pyruvic acid into lactic acid, mostly occurring in skele-

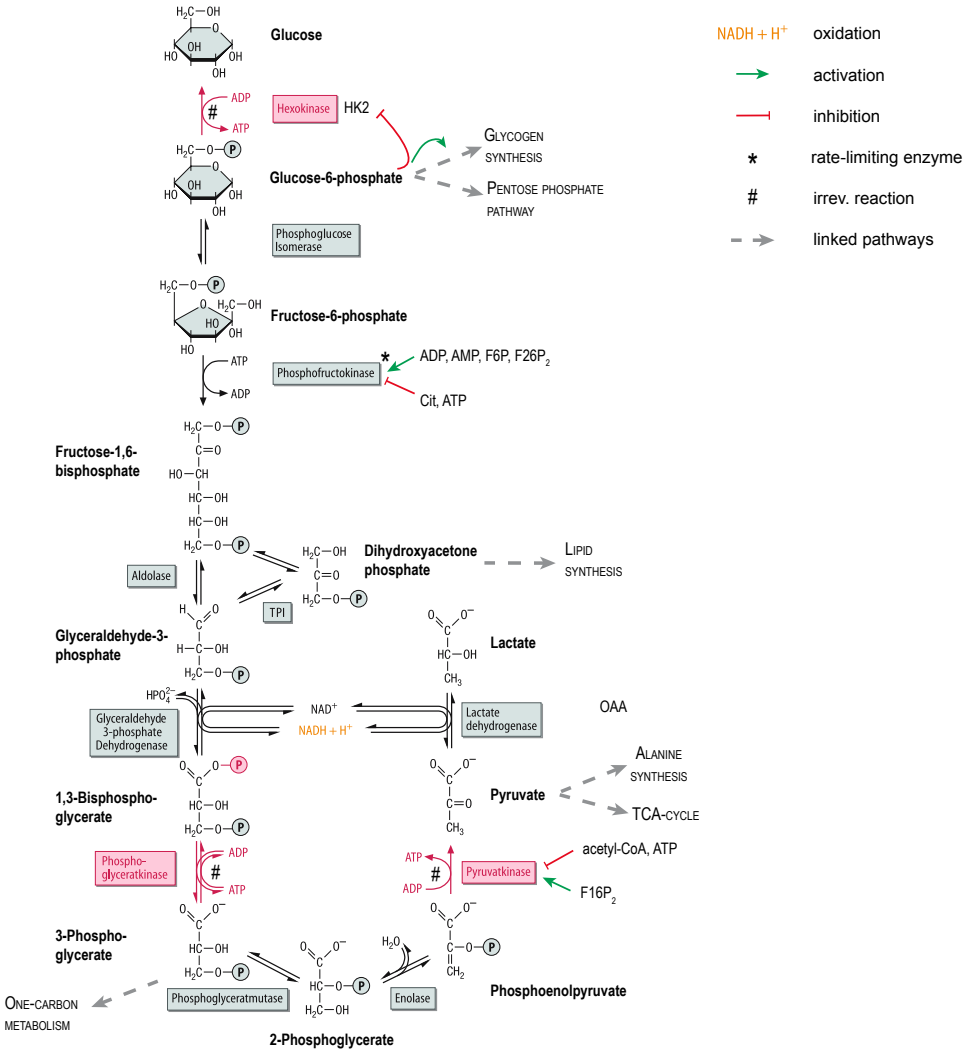


Figure 1.1.: Reaction scheme of glycolysis including regulating intermediates. The breakdown of one molecule glucose into two molecules of glyceraldehyde-3-phosphate (GA3P) requires the investment of two molecules of ATP. In the pay-off phase four molecules of ATP are generated by the synthesis of pyruvic acid (Pyr). The graphic has been taken and modified from Löffler and Schölmerich (2008).

tal muscle, is probably the most conserved reaction of glycolysis. In ancient times living organisms had to cope with an oxygen-depleted environment and were in need of an anaerobic pathway for energy synthesis. The synthesis of Lac replenishes the pool of nicotinamide adenine dinucleotide ($NAD^+$) that is required for the conversion of glyceraldehyde-3-phosphate (GA3P) into 1,3-bisphosphoglycerate (13BPG) the $5^{th}$ reaction of the glycoly-

sis. Erythrocytes, renal medulla, the brain and sperm cells completely rely on this pathway because its their only source of energy.
Interestingly, the amino acid sequence and the structure of glycolytic enzymes are closely related to vertebrates, spinach and yeast. Only the regulation and the subsequent direction of pyruvic acid occurs in a organism-specific manner (Nelson et al., 2009).

The enzyme phosphofructokinase-1 (PFK-1, c) catalyses the committed step of glycolysis and represents at the same time the most regulated point of the pathway. It adds the second phospho-group to fructose-6-phosphate (Frc6P) generating fructose-1,6-bisphosphate (F16P). The activity of the rate-limiting enzyme is allosterically inhibited by increasing product levels of ATP and citric acid (Cit) resulting in a deceleration of the glycolysis. The other way around — the accumulation of AMP activates the enzyme, sensing the demand for ATP synthesis. Fructose-2,6-bisphosphate (F26P2) is the most important regulator of PFK-1 activity. Elevated levels of F26P2 results in an increased affinity of PFK-1 for fructose-6-phosphate (F6P) promoting glycolysis.

Glycolytic intermediates link the central carbon metabolism with adjacent pathways. Glucose-6-phosphate (G6P) fuels the pentose phosphate pathway providing precursors for nucleotide synthesis and the the generation of NADPH.
Dihydroxyacetone phosphate (DHAP) is further metabolised into glycerol-3-phosphate (Glyc3P), an intermediate of lipid synthesis. The *de novo* synthesis of the amino acid serine is formed by the conversion of the glycolytic intermediate 3-phosphoglycerate (3PGA). Serine is an important precursor of the one-carbon metabolism, that has been shown to maintain the methylation status of DNA and histones (Locasale, 2013).

**TCA-cycle** The citric acid or TCA-cycle is one of the few amphibolic pathways combining catabolic and anabolic reactions. Carbohydrates, fatty acids and proteins enter the TCA-cycle in the form of three to five-carbon molecules; the majority as Pyr derived from the glycolysis. The pyruvate dehydrogenase complex (PDHc) facilitates the conversion of mitochondrial imported Pyr into acetyl coenzyme A (acetyl-CoA) that subsequently enters the TCA-cycle (Figure 1.2).

The first enzyme of the cycle — citrate synthase (CS, mitochondrial) — catalyses the

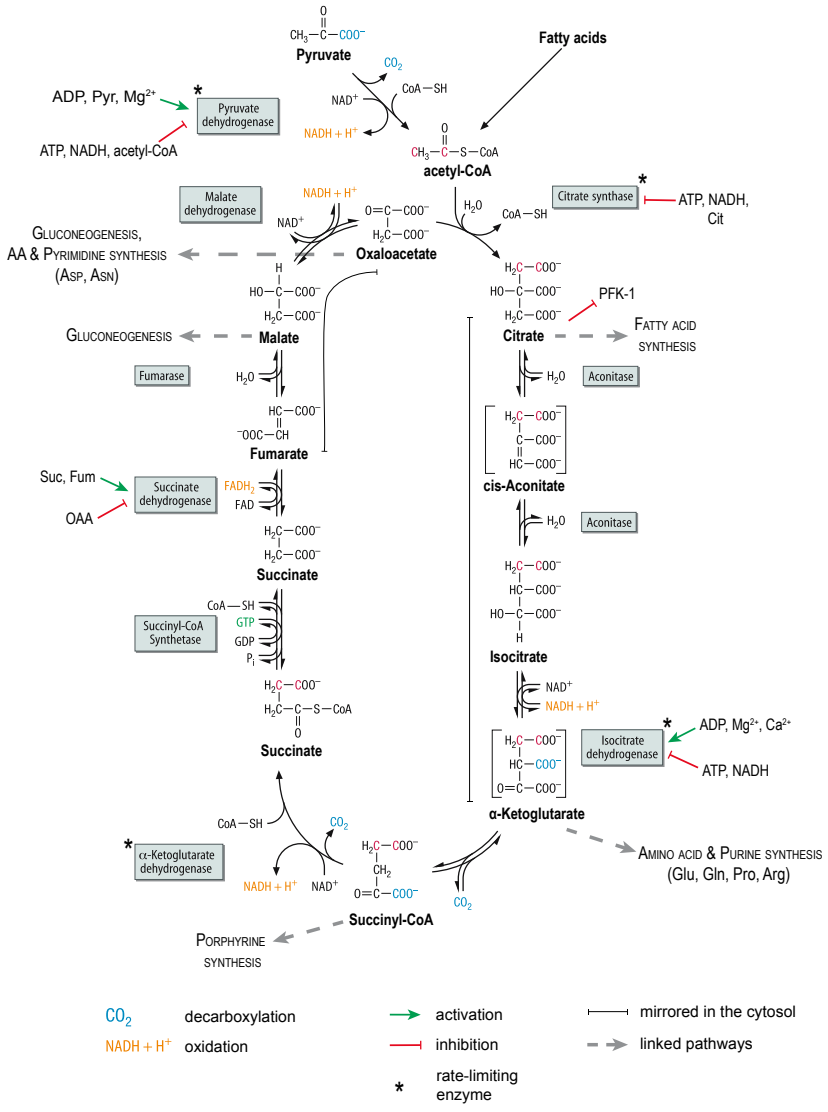


Figure 1.2.: The reactions of the TCA-cycle including linked pathways, activating and inhibiting intermediates. The carbon backbone of the acetyl-group is oxidised into $CO_2$ and oxaloacetate (OAA) converted into succinic acid in the first phase. Subsequently the consumed OAA is reproduced by the conversion of succinate (Suc), a sequence of three reactions similar to the oxidation of fatty acids. The graphic has been taken and modified from Löffler and Schölmerich (2008).

oxidation of oxaloacetic acid (OAA) and acetyl-CoA into citric acid (Cit). Within seven reactions, including two decarboxylation steps, the acetyl-group of Cit is completely oxidised into $CO_2$; the OAA-derived carbon backbone is converted into succinic acid (Suc). The second phase covers the reproduction of the consumed molecule of OAA, closing the TCA-cycle. Interestingly the last phase shares similarities with the $\beta$-oxidation of fatty acids.

One turn of the TCA-cycle produces almost 15× of free energy ($\Delta G^{\circ} = -2881\ kJ/mol$) as much as glycolysis. The conversion of one molecule of acetyl-CoA yields in the generation of three molecules of $NADH/H^+$ and one molecule of $FADH_2$ and GTP. Nine molecules of ATP are produced by one turn of the TCA-cycle in close interaction with respiratory chain.

Though the pool sizes of TCA-cycle intermediates are low abundant, a few metabolites are important precursors for the synthesis of: (i) glucose (oxaloacetic acid, malic acid), (ii) amino acids (oxaloacetic acid, $\alpha$ketoglutaric acid), (iii) fatty acids and sterols (Cit) or (iv) porphyrins (succinyl-CoA).
An extensive usage of these metabolites would impair the TCA-cycle and the ATP synthesis. Therefore anaplerotic reactions prevent the depletion of the cycle. Most important reactions are the direct conversion of Pyr into OAA by the pyruvate carboxylase (PC, m) and the entry of glutamine in form of $\alpha$ketoglutaric acid ($\alpha$KG) facilitated by glutaminolysis.
In addition, a complex system of shuttles connects cytosolic and mitochondrial metabolism to ensure the functioning of the TCA-cycle. In particular the export of citric acid and its conversion into its precursors is important to provide cytosolic acetyl-CoA for the synthesis of fatty acids.
Partially the reactions of the TCA-cycle are mirrored in the cytosol. The sequences (i) from Cit to $\alpha$KG and (ii) from fumaric acid (Fum) to OAA provide the availability of intermediates in case of a decreased export of these intermediates.

The activity of the TCA-cycle is regulated by the demand of cellular energy and the availability of acetyl-CoA provided by the decarboxylation of Pyr or the degradation of fatty acids. Enzymes of the TCA-cycle are activated and inhibited by their products to sensor the conversion of carbons in the TCA-cycle, e.g., an increase of NADH signals that the rate of the respiratory chain, defined by the availability of ATP, is not sufficient to consume the produced reducing equivalent.
Therefore accumulating NADH slows down the TCA-cycle activity. In the same way raised levels of ATP result in a deceleration of the cycle, whereas an increasing pool of ADP

activates the enzymes isocitrate dehydrogenase (IDH) and PDHc. In general accumulating products of a reaction inhibit their own synthesis by feedback regulation, respectively substrates activate their conversion as shown in Figure 1.2. The regulation occurs even beyond the borders of the pathway, e.g., increasing levels of cytosolic Cit inhibits the rate-limiting enzyme PFK-1 and thus the synthesis of pyruvic acid.

### 1.1.2. Key players of the CCM

The metabolic pathways are interconnected by a few important intermediates. Their abundance and the availability of reducing electrons regulates and defines the fate of the intermediates. The following paragraph summarises the fates of glucose-6-phosphate (Glc6P), pyruvic acid (Pyr) and acetyl-CoA, the main key players of the CCM. Because of their essential roles these intermediates are often targeted by metabolic reprogramming.

**Glucose-6-phosphate** The first product of glycolysis is a key player of the central carbon metabolism. Although the majority of the intermediates is metabolised into Pyr, G6P is also a substrate of the pentose phosphate pathway (PPP) and used for glycogen synthe-

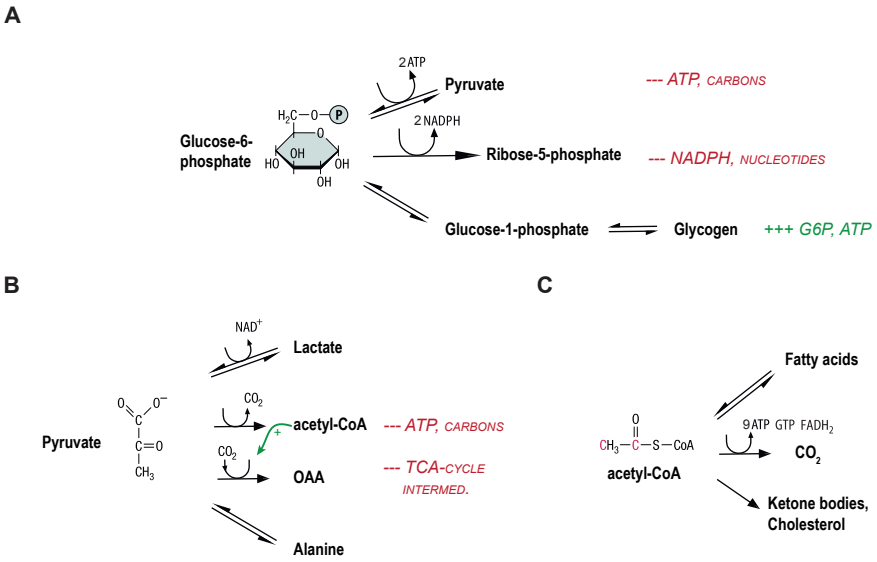


Figure 1.3.: Key players of the CCM, their fate and their regulators: (A) Glucose-6-phosphate (Glc6P), (B) Pyruvic acid (Pyr) and (C) acetyl-coenzyme A (acetyl-CoA).

sis (Figure 1.3-A).

The production of pyruvic acid is coupled to the requirement of ATP and carbons. The pentose phosphate pathway provides the generation of NADPH, required for reductive biosynthesis, and ribose-5-phosphate for the synthesis of nucleotides. Up-regulated enzymes levels of TKT1 and TALDO, rate-limiting enzymes of the PPP, have been detected in cancer cells (Wang et al., 2011a; Xu et al., 2009). Only at high intracellular levels of ATP glucose is stored into glycogen.

G6P is synthesised from its product pyruvic acid by the reversed pathway of glycolysis — the gluconeogenesis. Pyruvic acid enters mitochondria and is converted into OAA and subsequently into Mal. The exported Mal enters glycolysis in form of phosphoenol pyruvate (PEP) and is further processed into Glc6P bypasses the irreversible reaction reactions of the glycolysis.

**Pyruvic acid** Pyruvic acid links cytosolic and mitochondrial metabolism (Figure 1.3-B). Primarily produced from glucose Pyr is either (i) converted into lactic acid, (ii) transaminated into alanine or (iii) enters the mitochondrial metabolism via pyruvate dehydrogenase complex (PDHc) or pyruvate carboxylase (PC). The conversion into Lac restores NADH that is required for the phosphorylation of GA3P.

The decarboxylation by the PDHc complex catalyses the irreversible synthesis of acetyl-CoA in the mitochondria. Multiple allosteric interactions regulate the activity of the complex and fine-tune the usage of mitochondrial imported pyruvic acid. The enzyme PC requires an obligatory activator — acetyl-CoA, another key player of the CCM. Only in the presence of acetyl-CoA the carboxylation of pyruvate is allowed and replenishes the TCA-cycle in form of OAA. This reaction is also part of the gluconeogenesis providing the synthesis of glucose via the conversion of OAA into malic acid (Mal).

**Acetyl-CoA** The two-carbon unit is the major fuel of the citric acid cycle (Figure 1.3-C). It's condensation with oxalic acid (OAA) into citric acid is the first reaction of the TCA-cycle.

Main source of acetyl-CoA is the import of glycolysis-derived pyruvic acid and the $\beta$-

oxidation of fatty acids. The synthesis from Pyr by the PDH complex is a rate-limiting step allosterically regulated. The interplay of pyruvate complex kinases and phosphatases regulates the activity of the PDHc to adjust the import of Pyr into the mitochondria. Besides the complete oxidation of acetyl-CoA into $CO_2$, the intermediate is used for the synthesis of ketone bodies and cholesterol. The export of Cit derived from acetyl-CoA provides carbons for fuelling fatty acid synthesis as described before.

### 1.1.3. Regulatory events in metabolic reprogramming

**Metabolic reprogramming during tumorigenesis** The reprogramming of the metabolism in cancer cells gained increased attention during the last decade. Already in the early 1930s Otto Warburg focused on the biochemical analysis how glycolysis and respiration contributes to the "unstructured cell growth" (Warburg et al., 1924). Those days Otto Warburg postulated that the increased and oxygen-independent conversion of glucose into lactic acid occurs due to impaired mitochondria (Warburg et al., 1927).
Although the Warburg effect is not caused by dysfunctional mitochondria as described by Warburg, but rather an effect of the optimisation of nutrient consumption, still the term is associated with cancer metabolism and describes the elevated synthesis of lactic acid even in the presence of oxygen (Vander Heiden, 2011).
In 2011 Hanahan and Weinberg included the readjustment of energy metabolism occurring during tumorigenesis to their famous hallmarks of cancer (Hanahan and Weinberg, 2011).

Pavlova and colleagues defined six categories of metabolic reprogramming during the development of cancer: (i) the deregulated uptake of main carbon-sources, (ii) the activation of alternative ways to maintain nutrient supply, (iii) the usage of CCM intermediates for NADPH synthesis, (iv) the elevated demand of nitrogen for biosynthesis, (v) the metabolite-driven gene regulation and (vi) metabolic interaction with the tumor environment (Pavlova and Thompson, 2016).

Tumorigenesis results in the modulation of intra- and extracellular metabolite levels, affects the tumor-microenvironment and induces alterations in gene expression levels. The constitutive activation of the nutrient uptake at a maximum rate maintains the limitless

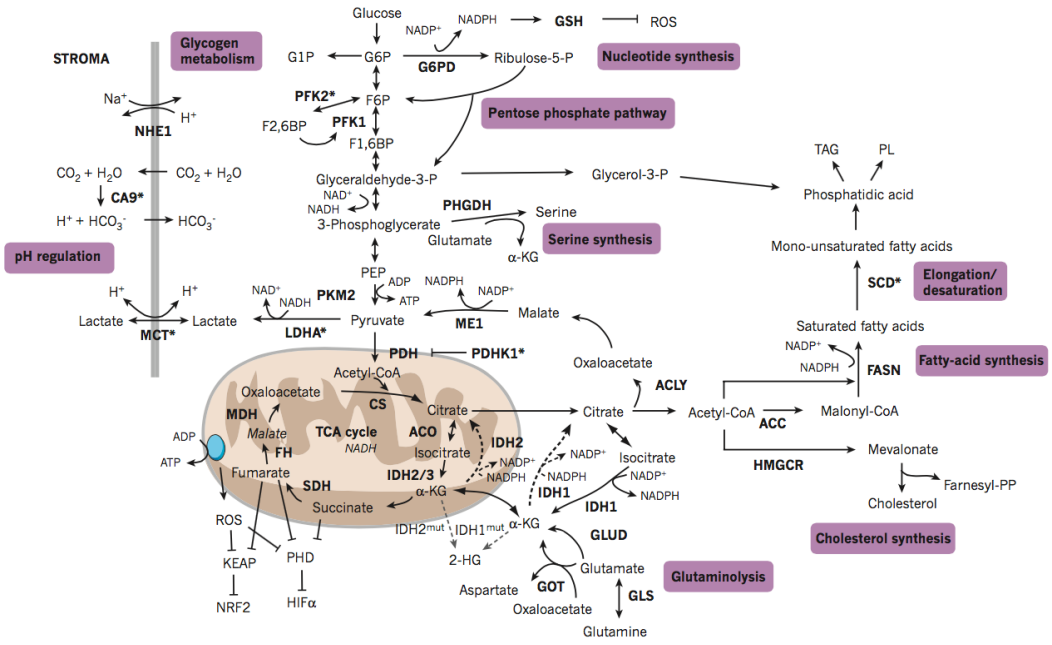


Figure 1.4.: Central carbon metabolism contributing to the macromolecule synthesis and energetic homeostasis. Enzymes are shown in bold. Targets of HIF-1 are marked with an asterisk. Figure has been adapted from Schulze and Harris (2012b).

supply of precursors for tumor cell growth independently from the extracellular environment. The alteration of growth-factor regulated pathway of phosphoinositide 3-kinase (PI3K)/Akt (protein kinase B) and the mammalian target of rapamycin (mTOR) are mostly induced by oncogenic mutations in cancer cells. It has been shown that in cancer cells the PI3-K/AKT pathway leads to an up-regulation of hexokinase 2 (HK2). Increased activity of HK2 traps glucose in form of Glc6P and prevents the efflux of carbons. Subsequently, Glc6P that is not directed towards the synthesis of Pyr and mitochondrial oxidation, is used to generate reducing equivalents (NADPH) and building blocks, e.g., nucleotides and lipids (Deprez et al., 1997; Gottlob et al., 2001).

Central metabolic pathways, their cofactors and known regulators are summarised in Figure 1.4, adapted from Schulze and Harris (2012a). Almost every single enzyme of the central carbon metabolism is a known target of an oncogene, transcription factor or tumor-suppressor. Most prominent regulators of the central carbon metabolism are the oncogene c-myc, the transcription factor HIF-1 or the tumor-suppressor p53.

The oncogene c-myc is a known regulator of a multitude of cellular processes in addition to the regulation of glycolysis and glutaminolysis. Modulated gene expression of glutaminase (GLS-1), the CAD protein and increased levels of the glutamine transporter ASCT2 and SN2 have been detected in broad range of c-myc affected tumor cells (Wang et al., 2011b; Wise et al., 2008). The up-regulated uptake of glutamine, its conversion into glutamic acid replenishes the pools of the TCA-cycle intermediates and contributes to anaplerotic reactions.

Tumor growth results in the temporary deprivation of major nutrients, especially $O_2$, due to insufficient vascularisation of the tumor (Vaupel et al., 1989). A hypoxic environment leads to the stabilisation of the transcription factor hypoxia-inducible factor (HIF1) by dimerisation of the $O_2$-sensitive subunit HIF1-$\alpha$ and constitutively expressed subunit HIF1-$\beta$. In the presence of $O_2$ HIF1-$\alpha$ is directed by prolyl hydroxylation for proteasomal degradation and prevents the activation of glycolysis promoting HIF1. The abundance of the glycolytic enzymes, e.g., PFK2, LDHA, and monocarboxylate transport proteins (MCT) are up-regulated by HIF1 activity and provide a sufficient generation of ATP (Schulze and Harris, 2012a).

Cancer cells prevent a lack of carbons or nitrogen by the development of alternative ways of nutrient acquisition (Schulze and Harris, 2012a). Macropinocytosis, entosis or phagocytosis provide the access to normally unaccessible nutrient sources, e.g., extracellular proteins (Kerr and Teasdale, 2009; Krajcovic et al., 2013). Though nutrient and growth-factor deprived cells do not proliferate, they survive in cell culture for weeks as shown by Lum and colleagues (Lum et al., 2005).

**Metabolic reprogramming during differentiation** A unique feature of pluripotent cells is their dual ability of self-renewal and differentiation into any tissue of the three germ layers. Also induced pluripotent stem (iPS) cells are in the focus of different fields of sciences since the introduction of the stemness cocktail by Takahashi in 2006 (Takahashi and Yamanaka, 2006). The application of Sox2, Oct4, Nanog and Kfl4 transforms somatic cells into pluripotent cells. Originally, Kfl4 replaced the transcription factor and oncogene c-Myc. Due to its increased tumorigenic potential it has been replaced to increase the

applicability of iPS cells in medical therapy.

In their natural environment of the stem cell niche human embryonic stem cells (hESCs) remain in a quiescent state under hypoxic conditions and solely rely on anaerobic glycolysis to produce energy. Reducing equivalents and ATP are solely produced by the conversion of glucose into pyruvic acid and subsequently into lactic acid.

The activation of HIF1, induced by the stabilisation of HIF1-$\alpha$ in the $O_2$-deprived environment, leads to the up-regulation of glycolytic enzymes, e.g., HK2, PFK1 and LDHA (Folmes et al., 2011; Panopoulos and Izpisua Belmonte, 2011; Varum et al., 2011). At the same time HIF1 prevents the entry of glucose-derived pyruvic acid into the mitochondria by the induction of pyruvate dehydrogenase kinase (PDK) inactivating PDHc (Ito and Suda, 2014a). The increased glycolytic activity provides the routing of carbons into the pentose phosphate pathway producing NADPH and thus preventing oxidative stress by an increased production of reactive oxygen species (ROS). The up-regulated activity of the PPP contributes to the synthesis of nucleotides and supports biosynthesis in proliferating stem cells.

Differentiation of stem cells induces a tremendous reprogramming of the CCM. It adjusts the mitochondrial dynamics to meet the elevated demand of energy to sustain the specialised functions of differentiated cells. At the same time the cell proliferation decelerates and minimises anabolic requirements (Folmes et al., 2012). The loss of pluripotency is accompanied by a complex remodelling of mitochondria. Whereas in stem cells mitochondria are functional immature, poorly crystallised and globularly shaped, differentiated cells increase their number of mitochondria with well-developed cristae, dense matrix and branched morphology (Folmes et al., 2012; Varum et al., 2011; Prigione et al., 2010; Suhr et al., 2010). Thus, mitochondrial mass in relation to total cell mass shows equal ratios in pluripotent and differentiated cells. Despite the morphological differences, stem cell mitochondria are functional organelles and able to possess a similar mitochondrial capacity (Birket et al., 2011; Zhang et al., 2011).

The differentiation of hESC and iPS cells results in an increased production of ATP by the electron transport chain, elevated levels of ROS and reduced expression of gly-

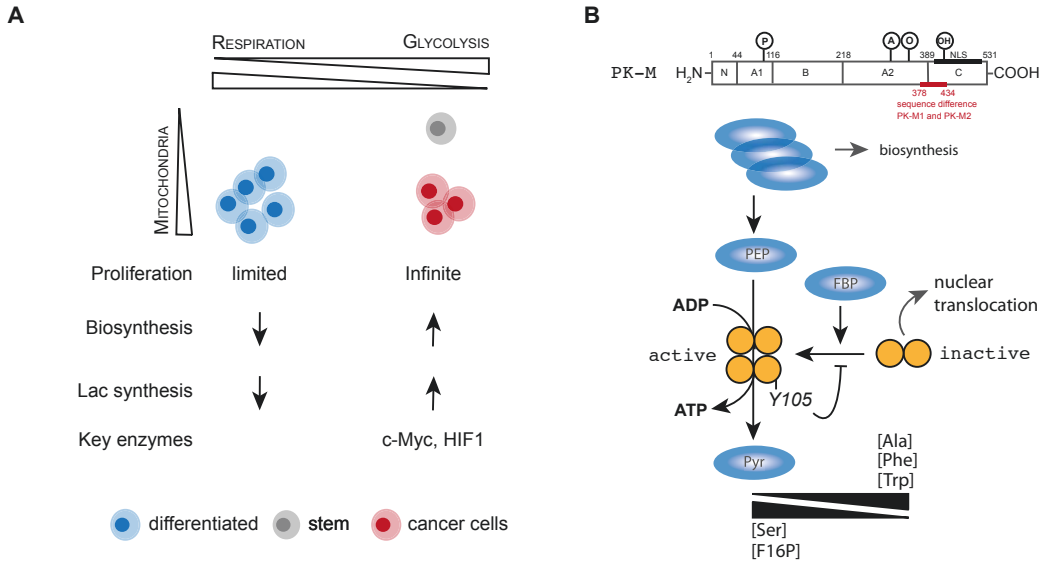


Figure 1.5.: Metabolic modes of different cell phenotypes. (A) Comparison of the metabolic mode of differentiated, stem and cancer cells. (B) Structure and regulation of the pyruvate kinase M (PKM), key regulatory enzyme of glycolysis.

colytic enzymes (Armstrong et al., 2010; Prigione et al., 2010). It has been shown that the stimulation of glycolysis or the inhibition of mitochondrial respiration promotes reprogramming efficiency (Ezashi et al., 2005; Varum et al., 2009), and the other way around — inhibition of glycolysis and induction of respiration impairs the reprogramming of pluripotency (Kondoh et al., 2007). Interestingly, the inhibition of acetyl-carboxylase 1 (ACACA, ACC1) and fatty acid synthase (FASN), enzymes of the fatty acid synthesis results in the repression of pluripotency induction. High levels of both enzymes have been detected in iPS cells.

**The metabolic mode of proliferative cells** At the first glance stem and cancer cells are opposite cell models. Cell proliferation is tightly regulated in stem cells and is in marked contrast to the highly proliferative phenotype of cancer cells.

Thus the metabolic modes of both phenotypes have many characteristics in common as summarised in Figure 1.5-A. Cancer and pluripotent cells require the sufficient generation of energy and building blocks in form of ATP, lipids, fatty acids and other reducing equivalents. At the same time both cell types have to prevent induced oxidative stress damage.

The increased routing of glucose-derived carbons into lactic acid has been detected in both cell types. The enzyme pyruvate kinase (PK) drives the final reaction and actual energy producing step of the glycolysis. Cancer cells preferentially express the isoenzyme PKM2. The distinct regulation of the enzyme provides to adjust the directing of nutrients towards biosynthesis processes or the generation of energy in form of ATP (Figure 1.5-B).
The inactive dimeric form of PKM2 blocks the synthesis of Pyr and concomitant generation of ATP. Although at the first glance counterintuitive, the inactive state of PKM2 provides precursors for cell proliferation. The accumulating glycolytic intermediates are directed into adjacent pathways connected to the synthesis of precursors, e.g., glycerol-3-phosphate synthesis.
The elevated levels of F16P2 induce the tetramerisation and activation of PKM2. The generated Pyr is subsequently directed into the previously described pathways to maintain cellular redox homeostasis and energy synthesis. Also the pool sizes of amino acids (Ser, Ala, Thr and Pro) affect the catalytic state of PKM2. The common roles of the oncogene c-Myc and the transcription factor HIF1 have been described previously. Both key-players elevate the activity of the glycolysis by increasing the transcription of glycolytic isoenzymes, e.g., HK2, PFK-1 or LDHA. Furthermore it has been shown that the regulation of the epigenetic state is highly connected with the metabolic mode of cells (Ryall et al., 2015). Acetyl-CoA and the amino acids serine and glycine are important precursors for histone and DNA acetylation, respectively methylation. Pluripotency is associated with specific histone marks, e.g., histone 3 lysine 27 trimethylation (H3K27me3), and also in cancer cells an distinct regulation of epigenetic modifications has been published (Carey et al., 2014; Jones and Baylin, 2002). Despite all the recent insight, it still remains unclear, how the described similarities in gene regulation and protein expression result in two distinct modes of cell proliferation. The comprehensive analysis of the metabolism in a dynamic and quantitative manner may contribute to the identification of distinct characteristics of both cell types.

## 1.2. High-throughput mass-spectrometry approaches for the quantification of CCM intermediates

The following part of the introduction is partially modified from a recent publication of the thesis author herself and her supervisor Dr. Stefan Kempa (Zasada and Kempa, 2016).

### 1.2.1. Quantification of enzyme expression levels

In 1940s Beadle and Tatum postulated the "one gene, one polypeptide" hypothesis (Beadle and Tatum, 1941). Since then the view on the proteome changed tremendously. Alternative splicing and post-translational modifications (PTMs) provide a complex regulation of isoenzyme expression and enzyme activity in a cell.

The development of liquid chromatography coupled with mass spectrometry (LC-MS) approaches enables the comprehensive high-throughput analysis of the cellular proteome. Three different approaches have been established to aim the quantification of high and medium abundant proteins in a cell: direct, targeted and shotgun proteomics (Domon and Aebersold, 2010). Shotgun-proteomics, also called discovery proteomics, has been widely applied in large-scale studies to create protein inventories (Beausoleil et al., 2006; de Godoy et al., 2008). It is an data-dependent analysis (DDA) methodology and provides the measurement of expressed proteins only. The presence of a protein in a sample is defined by the cellular state, tissue type and organism.

Shotgun-proteomics aims to detect a maximum number of peptides per sample. Tryptic and *in silico* derived peptides are compared for the identification of the proteins. The exclusion of high abundant peptides from fragmentation for a defined time window during the measurement increases the detection of lower abundant ones.

Still low abundant proteins, e.g., transcription factors, are rarely detectable by this approach. A targeted analysis of complex samples complements the proteome determined by shotgun proteomics. Targeted LC-MS based studies require the definition of the amino sequence of proteins and peptides of interest. The selective detection and fragmentation is most frequently operated on LC-MS coupled triple quadrupole instruments. Targeted

LC-MS setups enable the measurement of low abundant proteins with high selectivity and reproducibility in complex cell extracts.

Different strategies have been developed for the quantitative analysis of the proteome during the last decade. Stable isotope labelling of amino acids in cell culture (SILAC) and isotope-coded affinity tag (ICAT) are most commonly applied for LC-MS based proteome quantification.

SILAC and ICAT are designated as metabolic labelling approaches and provide the relative quantification of proteins (Ong et al., 2002; Gygi et al., 1999). Cells utilise the supplemented isotopes in form of modified amino acids in the cell culture media (e.g., Lys-8 instead of Lys-6) and incorporate these into proteins actively synthesised by the cell. The comparison of the coeluting light and heavy peptides at the MS/MS levels provides the relative quantification of isoenzymes.

The absolute quantification of proteins involve the application of isobaric tags for relative and absolute quantification (iTRAQ) or internal isotopic-labeled standards (Wiese et al., 2007; Ross, 2004). The absolute quantification provides the machine-independent and lab-wide comparability of proteome analysis.

Though internal standards are the gold standard regarding accuracy, the application is limited to a defined number of peptides. Standards have to be synthesised and "spiked in" the sample prior the measurement. Label-free quantification approaches, e.g., "spectral counting" and "XICs" are less accurate, but worth to try due to their reduced experimental time and costs (Ono et al., 2006; Old et al., 2005; Ishihama et al., 2005).

### 1.2.2. Quantification of intra- and extracellular metabolite levels

The determination of the complete metabolome of a cell is challenging due to the huge variety of molecules, e.g., such as hexoses, phosphates, amino acids, and lipids. Different molecular sizes, chemical properties and abundance of intermediates require the application of different methodologies.

Mass spectrometry (MS) and nuclear magnetic resonance (NMR) spectroscopy are most commonly applied in the field. Both approaches own complimentary experimental advan-

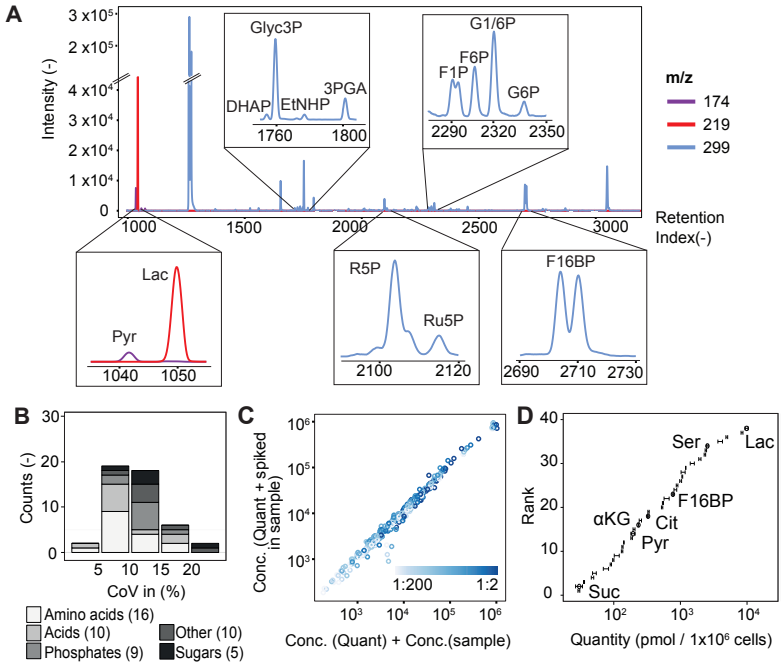


Figure 1.6.: Gas-chromatography coupled mass spectrometry provides the quantification of CCM intermediates. (A) A representative GC-MS selected ion chromatogram obtained from a cell culture sample using temperature-controlled and split injection. Due to the method, the peaks of pyruvate and lactate are baseline separated, detected, and quantified. The majority of phosphates are distinguishable by their retention behaviour. (B) Distribution of the coefficient of variation (CoV) of the measured metabolite quantities derived from five biological replicates. (C) Comparison of single samples and spike-in experiment in order to test recovery of metabolites. (D) Absolute quantities in T98G cells ranked by their concentrations. The graphic has been published in Pietzke et al. (2014).

tages and disadvantages. High sensitivity, broad detection spectra of compounds and the availability of well curated data bases for compound identification are the main benefits of MS-based methodologies (Pietzke and Kempa, 2014).

Though GC-MS based approaches demand the chemical modification of the sample prior the analysis. The process of derivatisation increases the volatility of the compounds and provide the detectability of a broad range of CCM intermediates (Figure 1.6-A). The advantages of NMR analysis are the high precision of metabolite quantification and the analysis of liquid, or even intact, samples, but at the cost of lower sensitivity (Pan and Raftery, 2007).

In general metabolomics studies are based on the relative analysis of peak areas or

intensity levels in the chromatography comparing biological conditions. These studies gain reliable results in the evaluation of clearly impaired metabolic pathways, e.g., inactivation of a specific enzyme, but lack the analysis of minor quantifiable changes of the metabolism (Zasada and Kempa, 2016). Thus, only absolute quantities provide machine- and lab-independent studies.

Absolute quantification of metabolites has been carried out by the application of isotope dilution mass spectrometry (IDMS), introduced by Heumann (1992). Known amounts of isotope compounds are spiked-in the sample. The simultaneously detection allows the absolute quantification, but is limited to a number of available compounds. Furthermore this approach suffers from technical deprivation and matrix effects (Fassett and Paul, 1989).

The determination of external calibration curves overcome these limitations. The measurement of a quantification standard composed of 60 intermediates is measured in eight dilutions prior or subsequent of a batch of samples. The comparison of five biological replicates of a cell extract showed a high reproducibility for the major metabolite classes (Figure 1.6-B). Individual calibration curves for each metabolite and detectable derivate are constituted and provide an estimate of absolute quantities (Figure 1.6-C). An exemplary quantitative profile of T98G cells shows the distribution of metabolic intermediates covering, e.g., glycolytic intermediates, amino acids and phosphate (Figure 1.6-D).

### 1.2.3. Tracing the dynamics of the central carbon metabolism

Glycolysis, TCA cycle, and pentose phosphate pathway link the uptake of nutrients with neighbouring parts of metabolism, resulting in facilitation of lipid, amino acid, and nucleotide synthesis. In the late 1960s, the first studies were carried out with radioactive isotopes to track the routing within the CCM (Wenzel et al., 1966). Nowadays, application of stable isotope-labeled substrates provides a more robust monitoring of nutrient utilisation. Stable isotopes substrates are applied as tracers, either supplemented in cell culture media or directly injected into tissues (Fan et al., 2009).

Depending on the substrate (e.g., glucose, glutamine and essential amino acids) and the kind of isotopic label (e.g., carbon-13, nitrogen-15), the turnover changes the atomic com-

position of intermediates and allows to trace the routing of single atoms along the pathway within the CCM (Pietzke and Kempa, 2014).

Intermediates located closer to the source show higher isotope incorporation than distant ones. GC-MS measurements provide the simultaneous analysis of isotopic incorporation and metabolite abundance in the same measurement (Kempa et al., 2009). The modification of nutrient supplementation or mechanical stress interrupts the metabolic equilibrium of a cell. Within few seconds the central carbon metabolism reacts and readjust the nutrient uptake and utilisation to any kind of perturbation. The developed workflow of pulsed stable isotope resolved metabolomics (pSIRM) studies has been optimised to minimise external stress factors and to shorten the sampling time in cell culture experiments (Pietzke et al., 2014).

Subsequently of the isotopic labelling cells are washed for just a few seconds with a washing buffer containing salts to maintain osmolality and the main nutrients, but lack amino acids and other supplements. These steps provide the continuous fuelling of the main pathways and reduce the carryover of extracellular metabolites in the measurement.

Directly after discarding the washing buffer cells are quenched with ice-cold, 50% methanol, disrupting all cellular processes and initiates the extraction process. The procedure allows a fast handling during the cell harvest and the determination of isotopic incorporation after short incubation times (Pietzke et al., 2014). Only in that way distinct dynamics of isotope incorporation are assignable in the network of the CCM. The evaluation of isotope incorporation in specific branching points of the CCM highlights differences in pathway activities and reveals distinct modes how carbons are incorporated in glycolytic and TCA cycle intermediates.

## 1.3. Computational modelling approaches

The nature of the CCM does not allow a determination of metabolic fluxes without the application of computational tools. Cyclic pathway structures, e.g., the TCA-cycle, and the reversibility of reactions do not provide a correct estimate of absolute fluxes based only on the incorporation of stable isotopes in metabolites.

During the last decade a number of approaches, including and excluding the application of stable isotopes, have been developed to overcome this limitation. The required input of information depends on the method of choice and varies regarding extend and complexity. Flux balance analysis (FBA) and $^{13}C$-metabolic flux analysis (MFA) are the most commonly applied approaches. Genome-scale kinetic models of the CCM are rarely used due its high complexity and to the lack of knowledge about isoform resolved enzyme kinetics. Therefore kinetic models often cover only a smaller subnetwork of the CCM (Niedenführ et al., 2015).

The development of FBA and $^{13}C$-MFA approaches were mainly driven by the optimisation of prokaryotic-based product synthesis in the field of white biotechnology (Varma and Palsson, 1994; Wiechert, 2001). The adaption of existing models to account for the compartment-separated nature of the CCM in eukaryotic cells represents the main challenge across science disciplines (Buescher et al., 2015).

### 1.3.1. Flux balance analysis (FBA)

FBA is a constraint-based approach that provides the determination of steady-state metabolic fluxes in genome-scale models. Constraints are cellular limitations, e.g., physicochemical properties (Raman and Chandra, 2009). FBA allows to predict growth rates or the production of a specific metabolite considering pre-defined constraints (Orth et al., 2010).

The first step of FBA, and common ground for all approaches, is the translation of the biochemical network into a stoichiometric matrix N ($m$ $x$ $v$). Reactants (m, rows) are assigned as biochemically specified to their molar ratios for each reaction (v, columns). The stoichiometric matrix N describes the topology of the network and is independent from time, enzyme kinetics and metabolite concentrations (Niedenführ et al., 2015).

Metabolic fluxes are determined based on the stoichiometric matrix and a biological relevant objective function by linear optimisation, e.g., the maximisation of growth, biomass or ATP-production, the most common objective functions (Raman and Chandra, 2009). According to the applied constraints, a stationary metabolic flux distribution is determined based on the topology of the network (Joyce and Palsson, 2006).

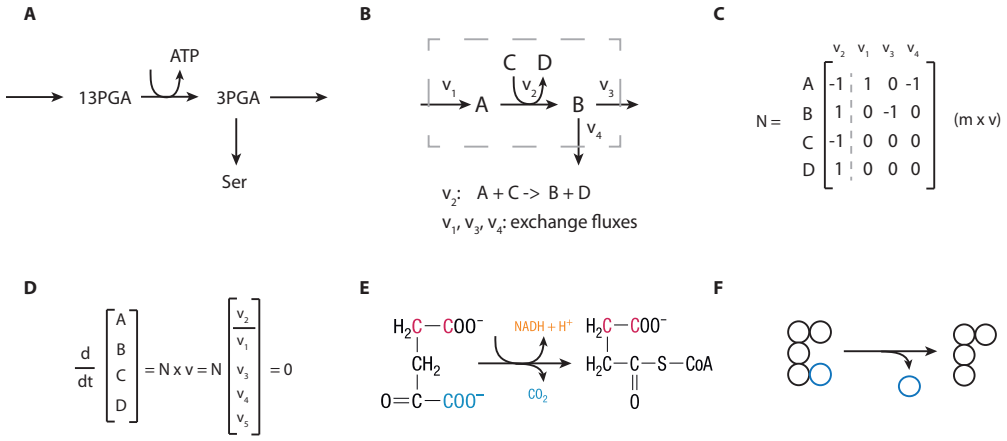


Figure 1.7.: Network construction and mathematical transformations for MFA. (A) Single reaction of the glycolysis showing the dephosphorylation of 1,3-bisphosphoglycerate (13PGA) into 3-phosphoglycerate (3PGA). (B) Conversion of the previous reaction into a scheme of metabolic fluxes. (C) The topology of the simple network in form of the stoichiometric matrix summarising the molarities of substrates and products of each flux. (D) Differential equation for the introduced reaction transforms into a linear equation system at steady-state conditions. (E) $^{13}$C-MFA analysis requires the tracking of carbon introduction and loss within the defined network, here shown for the decarboxylation of succinyl-CoA into succinate (Suc) in the TCA-cycle. (F) Carbon transitions have to be defined for each reaction in the network prior the MFA analysis based on stable isotope incorporation.

Further constraints, e.g., balancing input and output fluxes and the definition of exchange rates, have to be defined prior the determination of metabolic fluxes and reduce the number of feasible flux solutions. Dependent on the optimisation functions FBA empowers to analyse the capabilities and limitations of a network.

The reconstruction of the metabolic network and the selection of bounding criteria are essential steps in the FBA analysis. FBA provides only useful metabolic flux distributions in the case of a well fitting optimisation function. Metabolic gaps in the annotation of proteins reduce the feasibility of FBA. The most commonly applied optimisation function of maximum cell growth is only applicable in few cell systems, e.g., bacterial cells or to an limited extend to cancer cells.

### 1.3.2. Metabolic flux analysis (MFA)

**Stationary metabolic flux analysis** Classical $^{13}$C-MFA is the most frequently applied method in fluxomics targeting stationary metabolic fluxes. MFA approaches use the topology defined in a stoichiometric matrix, similar to FBA. The incorporation of stable isotopes, e.g., $^{13}C$-glucose, is a time-dependent process and provides an indirect measurement of the metabolic fluxes.

The application of isotopic tracers for more than several hours allows the determination of steady state metabolic fluxes by the measurement of macromolecular compounds, such as DNA, RNA, and proteins (Wiechert et al., 2001; Szyperski, 1995). The assumption of constant metabolite pool sizes and steady-state of metabolic fluxes simplifies the mathematical problem into a system of linear equations.

The implementation of carbon transitions for each reaction, describing the transport of carbons through the network, a defined carbon balance and extracellular rates provide the determination of metabolic fluxes. The iterative fitting of experimental-derived and simulation-derived isotopomer distributions for each metabolite results ideally in one, in reality in a number of feasible flux maps for a single network of biochemical reactions.

In 2007, Henry and colleagues introduced thermodynamics- based metabolic flux analysis (TMFA). The feasibility of metabolic fluxes is determined based on the concentration levels of metabolites and the change of free Gibbs energy $\Delta G^{\circ}$. The reversibility of reactions becomes restricted with regard to their likeliness and reduces the number of possible flux maps (Henry et al., 2007).

However, the duration of labelling experiments and the accompanied high experimental cost are two major disadvantages of the classical, stationary $^{13}$C-MFA approach. Recent developments providing the absolute quantification of intracellular metabolites and the improvement of computation power pave the way for non-stationary MFA approaches (INST-MFA) (Nöh and Wiechert, 2011; Young et al., 2007).

**Non-stationary metabolic flux analysis (INST-MFA)** Similar to the stationary approach the experimental system has to fulfil the metabolic steady-state assumption. Intracellular

pool sizes and metabolic fluxes remain constant during the entire experiment. The only time-variant component is the stable isotope incorporation that has to be monitored by extensive sampling in time series experiments (Nöh et al., 2007).
The implementation of absolutely quantified pool sizes complements the information of isotope incorporation and exchange rates. The determination of backward and forward fluxes and an estimate of non-measurable pool sizes of intermediates are the reward of the increased mathematical complexity of INST-MFA (Wahl et al., 2008).
Still, a few challenges remain, e.g., the implementation of sub-cellular compartments, the complex formula of the media, and slow labelling dynamics in the INST-MFA framework (Zamboni, 2011).

Driven by the improvements of bioanalytical techniques and computational methods to analyse the dynamics of metabolism, detailed analyses of cellular metabolism became possible. Todays challenge is to develop tools that enable affordable, simple, rapid, but also detailed analyses of the metabolism to broaden our understanding at a mechanistic level (Zasada and Kempa, 2016).
For example, the combination of pulsed stable isotope resolved metabolomics and mathematical approaches, as non-stationary metabolic flux analysis may be a possible way to streamline dynamic and quantitative metabolomics analyses of cancer, both *in vitro* and *in vivo*. The combination of these approaches may provide the identification of key regulatory steps in cancer or stem cell metabolism and allow to interfere with the metabolic reprogramming (Zasada and Kempa, 2016).

# 2 Materials and Methods

## 2.1. Cell cultivation

All chemicals used for the cultivation of cells are listed in Suppl.A.
Cells were cultivated in Dulbeccos modified Eagle Medium (DMEM / Invitrogen) supplemented with 2.5 g/L glucose and 2 mM glutamine at 21% $O_2$ and 5% $CO_2$ for routine cell cultivation. Stable cell lines has been passaged in appropriate split every 2-3 days using Tryp L/E for cell detachment. Viability was checked by Trypan blue staining on a regular basis.

**Cell number quantification** Calcein-AM staining, labeling live cells, was performed with 1 uM Calcein-AM / 1 ug/mL H-33342 for 30 min at 37 °C. Images were collected in two different fluorescent channels using an automated microscope (Array-Scan VTI HCS Reader (Thermo Fisher, PA). The imaging software (vHCS SCAN, Thermo Fisher, PA) identified nuclei in channel 1 ($36550/46115nm$) as objects according to their size, area, shape, and intensity.
Chanel 2 detected the calcein signal ($47540/52515nm$). An algorithm quantified all calcein positive cells as viable and only H-33342 positive nuclei as not viable cells. Viable cells per well were calculated from area covered by pictures in relation to well area.

## 2.2. Proteomics

### 2.2.1. Sample preparation

Cells were directly harvested from the plate by adding 8 M Urea buffer (Suppl. Table A.2) in appropriate volumes - Nalgene 6-well plate: 250 uL; Nalgene 10 cm dish: 1-2 mL. Protein content were determined by BCA protocol in 96 well-plate format and plate reader. 100–200 ug of protein sample were digested following standard protocol using Trypsin (1:80 w/w, 4 hrs, $30°C$) and Lys-C (1:40 w/w, over night. $30°C$) . Denaturation and alkylation of the proteins were sustained by adding Ditiothreitol (DTT, 11 mM) and Iodacetamine (IAA, 200 mM). Samples were diluted with ammonium bicarbonate between Lys-C and tryptic digestion. After the incubation digestion was stopped through acidification by addition trifluoracetic acid (TFA, 5-10 uL). Samples were desalted and purified by stage tipping for LC-MS analysis. Therefore Empore disc C18 (3M) were mounted three times in a common 200 uL pipette tip. Membranes were activated with 50 uL pure methanol, washed with 50 uL of buffer B (see TABLE) and equilibrated by adding 50 uL of buffer A. Each step was performed on a vacuum system. Per stage tip 18 ug of sample were loaded and desalted by adding buffer A. Stage tips were stored at $4°C$ until proceeding for LC-MS measurement. Peptides were eluted with 50 uL of buffer B. Eluates were dried for 20 min under vacuum and samples resolved in 20 uL of buffer A.

### 2.2.2. LC-MS analysis

Peptides eluted from StageTips were separated by reverse-phase chromatography on a in-house made 25 cm columns C18-Reprosil-Saphir (Dr. Maisch, inner diameter: 75 um, particle diameter: 1.8 um) using nanoflow high-performance liquid chromatography (HPLC) system (Agilent 1200). This system was coupled directly via nano-electrospray ion source (Proxeon) to LTQ Orbitrap Velos (Thermo Fisher Scientific). Peptides were loaded on the column with a flow rate 200 nL/min. Elution was performed with 220 min gradient of buffer B (2 - 50%) at a flow rate of 250 nl/min. Column was washed with 90% buffer B for 10 min and re-equilibrated with buffer A between the runs. Mass spectra were acquired

in a positive mode applying a data-dependent analysis (DDA) switch between survey MS scan (m/z 300-1700m, resolution R=60'000) and MS/MS spectra acquisition. The 20 most intense ions (Top20) of each survey MS scan were selected for fragmentation and MS/MS spectra acquisition. Fragmentation was induced by collision-induced dissociation (CID) with a target value of 3000 ions. Lock mass calibration at m/z+445.12 enabled the improvement of precursor ion accuracy. Mono-charged ions, "potential" contaminants, were excluded fro MS analysis. Fragmented ions were banned for further re-measurement for 30 seconds improving detection of middle-abundant ions. Samples were measured in two technical and at least two biological replicates.

### 2.2.3. Data analysis

Raw files were analysed using MaxQuant (1.4.1.2) - software tool for proteomic analysis developed in the lab of Matthias Mann (Cox and Mann, 2008). MaxQuant provides the identification and label-free quantification of proteins, applying a decoy-International Protein Index (IPI)-human database. Following parameter were set: Proteases - Trypsin (cleavage behind lysine (K) and arginine (R) with restriction after proline (P). Ion masses were searched with a maximum of mass deviation of 7ppm. Variable modifications of methionine oxidation and N-terminal acetylation as well as fixed modification of cysteine carbamidomethylation were set for protein identification. Peptides with at least six amino acids and a maximum of two missed cleavages were selected for analysis. The false discovery rate was fixed for 1%.

## 2.3. pSIRM Methods

### 2.3.1. Cell culture and pSIRM harvest

The number of cells for plating was determined to avoid contact inhibitory effects during the experiment for each cell line and nutrient condition separately. After seeding, the cells were cultured for 2 or 3 days. During that time, cell culture media was replaced 24 and 4 hrs prior to harvest. The adherent growth behavior of the used cell lines allowed the labeling with $^{13}$C-substrates directly on the cell culture dish. Therefore, the cell culture medium was replaced with pre-warmed full label medium containing all carbon sources and supplements like standard cell culture for a defined time range. One carbon source was substituted with its carbon-13 variant according to the setup of the experiment. Hereafter, the cells were quickly flushed with label buffer (140 mM NaCl, 5 mM HEPES (Roth, Karlsruhe, Germany) with pH 7.4, major carbon sources according full label media) to remove extracellular metabolites. Immediately, the cells were quenched with 5 mL 20$°C$ cold 50% methanol (containing cinnamic acid (2 ug/mL)). The cells were scratched from the culture dish in the solvent, transferred into a 15 mL falcon, and stored on ice or at 25$°C$ until proceeding with metabolite extraction. In the pSIRM experiments with an application of $^{13}$C-substrates for less than 5 min, the cells were incubated in label buffer directly.

### 2.3.2. Intracellular metabolite extraction

Methanol-chloroform-water extraction provides an effective extraction and subsequent separation of lipid and polar intermediates. One milliliter chloroform was added to 5 mL of methanol cell extracts, shaken for 30 min at 4$°C$, and centrifuged at maximum speed for 15 min for phase separation. Both phases were collected separately and dried under vacuum. The extracts were stored at 25$°C$.

### 2.3.3. Extracellular metabolite extraction

Fifty microliters per each media sample were extracted in 1 mL of methanol-chlorofom-water (5:2:1 v/v/v, cinnamic acid standard 2 ug/mL) for 30 min overhead shaking at $4°C$. Phase separation was done by adding 0.5 mL of $H_2O$ and centrifugation. A volume of 750 ul per polar phase were dried for GC-MS analysis. Samples were stored at -25$°C$ until preparation for GC-MS measurement.

### 2.3.4. GC-MS analysis

Derivatization was carried out as described with modifications in Kempa et al. (2007). The dried cell extracts were dissolved in 20 uL of methoxyamine hydrochloride solution (Sigma, 40 mg/mL in pyridine (Roth)) and incubated for 90 min at $30°C$ with constant shaking followed by the addition of 80 uL of N-methyl-N-[trimethylsilyl]trifluoroacetamide (MSTFA; Machery-Nagel, Dueren, Germany) and incubation at $37°C$ for 45 min. The extracts were centrifuged for 10 min at 10,000 ×g, and aliquots of 30 uL were transferred into glass vials (Th. Geyer, Berlin, Germany) for gas chromatography-mass spectrometry (GC-MS) measurement.

Retention index standard: Nine alkanes (n-decane, n-dodecane, n-pentadecane, n-octadecane, n-nonadecane, n-docosane, n-octacosane, n-dotriacontane, and n-hexatriacontane) were dissolved in hexane, combined at a final concentration of 2 mg/mL and stored at $4°C$. Retention index standard was added to the solvent (MSTFA) at a final concentration of 2% (v/v) during derivatization.

### 2.3.5. Quantification standard

The quantification mixture was composed of 63 compounds (stock concentration 1 mg/mL, 20% MeOH). A dilution series from 1:1, 1:2, 1:5, 1:10, 1:20, 1:50, 1:100, and 1:200 was prepared, portioned, dried under vacuum, and stored at $20°C$. One set of quantification standard was treated in parallel with cell extracts during derivatization and measured in technical replicates within an experiment.

### 2.3.6. GC-MS measurement

Metabolite analysis was performed on a gas chromatography coupled to time of flight mass spectrometer (Pegasus III- TOF-MS-System, LECO Corp., St. Joseph,MI, USA), complemented with an auto-sampler (MultiPurpose Sampler 2 XL, Gerstel, Mülheim an der Ruhr, Germany). The samples and quantification standards were injected in split mode (split 1:5, injection volume 1 uL) in a temperature-controlled injector (CAS4, Gerstel) with a baffled glass liner (Gerstel). The following temperature program was applied during sample injection: initial temperature of $80°C$ for 30 s followed by a ramp with $12°C$/min to $120°C$ and a second ramp with $7°C$/min to $300°C$ and final hold for 2 min. Gas chromatographic separation was performed on an Agilent 6890 N (Agilent, Santa Clara, CA, USA), equipped with a VF-5 ms column of 30 m length, 250 um inner diameter, and 0.25-um film thickness (Varian, Palo Alto, CA, USA). Helium was used as carrier gas with a flow rate of 1.2 ml/min. Gas chromatography was performed with the following temperature gradient: 2 min heating at $67.5°C$, first temperature gradient with $5°C$/min up to $120°C$; subsequently, a second temperature increase of $7°C$/min up to $200°C$, $12°C$/min up to $320°C$ and a hold of 6 min. The spectra were recorded in a mass range of 60 to 600 mass units with 10 spectra/s at a detector voltage of 1650 V.

### 2.3.7. Data analysis

The vendor software ChromaTOF (Leco) was used for pre-processing of GC-MS derived files: (1) resampling and (2) export of the mass spectra and peak list files. Metabolite identification and quantification are performed with in-house developed software MAUI-SILVIA. Details of algorithms and computational framework are described in Kuich et al. (2014).

Absolute quantities are determined based on external calibration by the measurement of the previously described quantification standards. Known concentrations are correlated with the peak area of top 5 abundant ions m/z of the individual metabolite mass spectra. Fragment masses dependent on the isotope carbon composition and affected by the incorporation of stable isotopes are complemented with corresponding masses (pTop5).

Table 2.1.: GC-MS fragments for determination of stable isotope incorporation.

| Metabolite | Mass fragment m/z Derivate | Abbr. | Carbon-12 | complete labeled | $^{13}$C-Glucose | $^{13}$C-Gln |
|---|---|---|---|---|---|---|
| 3-Phoshphoglyceric acid | 4TMS | 3PGA | 357 | 359 | 359 | / |
| Alanine | 3TMS | Ala | 188 | 190 | 190 | / |
| Aspartic acid | 3TMS | Asp | 232 | 235 | 235 (a) | / |
| Citric acid | 4TMS | Cit | 273 | 278 | 275-277 | 277-278 |
| Citric acid | 4TMS | Cit | 375 | 381 | 375-380 | 380-381 |
| Dihydroxyacetonephosphate | 1MeOX 3TMS | DHAP | 400 | 403 | 403 | / |
| Fructose | 1MeOX 5TMS | Fru | 217 | 220 | 220 | / |
| Fructose-1,6-bisphosphate | 1MeOX 7TMS | F1,6-BP | 217 | 220 | 220 | / |
| Fructose-6-phosphate | 1MeOX 6TMS | F6P | 217 | 220 | 220 | / |
| Fumaric acid | 2TMS | Fum | 245 | 249 | 247 | 249 |
| Glucose | 1MeCX 5TMS | Glc | 319 | 323 | 323 | / |
| Glucose-6-phosphate | 1MeOX 6TMS | G6P | 217 | 220 | 220 | / |
| Gluconic acid-6-phosphate | 7TMS | PG6 | 217 | 220 | 220 | / |
| Glutamic acid | 3TMS | Glt | 246 | 250 | / | 250 |
| Glutamine | 3TMS | Gln | 156 | 160 | / | 160 |
| Glutaric acid | 2TMS | Glut | 261 | 266 | / | 266 |
| Glutaric acid, 2-hydroxy | 3TMS | Glut-OH | 247 | 251 | / | 251 |
| Glutaric acid, 2-oxo | 1MeOX 2TMS | aKG | 198 | 203 | 200 | 203 |
| Glycerol | 3TMS | Glyc | 218 | 221 | 221 | / |
| Glycerol-3-phosphate | 4TMS | Glyc3P | 357 | 359 | 359 | / |
| Glycine | 3TMS | Gly | 276 | 277 | 277 | / |
| Lactic acid | 2TMS | Lac | 117 | 119 | 119 | / |
| Malic acid | 3TMS | Mal | 233 | 236 | 235 | 236 |
| Phosphoenolpyruvic acid | 3TMS | PEP | 369 | 372 | 372 | / |
| Pyruvic acid | 1MeOX 1TMS | Pyr | 174 | 177 | 177 | / |
| Ribose-5-P | 1MeOX 5TMS | R5P | 217 | 220 | 220 | / |
| Serine | 3TMS | Ser | 204 | 206 | 206 | / |
| Succinic acid | 2TMS | Succ | 247 | 251 | 249 | 251 |

An integrated module enabled the targeted evaluation of stable isotope incorporation in GC-MS derived data. Mathematical background is described in detail in Pietzke et al. (2014). Metabolite-specifc mass fragments used for the calculation of isotope incorporation is listed in the Table 2.1. Mass isotopomer distributions of unlabeled metabolites were used for the correction of natural isotope abundance and were automatically selected from measurements of quantification standards or manually defined.

MTXQC, a R-script based tool developed in the frame of this PhD thesis, enabled the assessment of GC-MS derived data quality. Section 3.3.3.2 summarises a detailed description of MTXQC for pSIRM time course experiments, an exemplary output file including the R code is shown in Suppl. Material E.

## 2.4. Experimental setups

### 2.4.1. Fibroblasts, cancer cells, hESCs, iPS cells and their differentiated derivates

Cancer cell lines MDA-MB231, MMCF-7, HT-29, RKO, and SW480 were obtained from ATCC, hESC H1 and H9 from WiCell. Somatic cell lines HFF1, NFH2, and BJ1 and the generation of iPS and iPS-DF cells were kindly provided or generated by Alessandro Prigione, formerly at MPI Berlin and currently at the MDC-Berlin, Germany.
Cancer cells and fibroblasts were cultivated in DMEM media supplemented with 10% fetal bovine serum, non-essential amino acids (NEAA), L-glutamine, Penicillin/Streptomycin, and sodium-pyruvate. Experiments were performed with cell culture passages 2–6.
Human embryonic and iPS cells were cultivated in ko-DMEM media supplemented with 20% ko-serum replacement, NEAA, L-glutamine, Penicillin/Streptomycin, Sodium-Pyruvate, $\beta$-Mercaptoethanol and 8 ng/mL bFGF. Cells were maintained on MEFs and splitted using the cut and paste technique. For experiments cell cultures were transfered to feeder-free conditions on matrigel-coated plates. Experiments were performed between passages 14 and 28. All cell cultures were cultivated at 5% $CO_2$ and ambient oxygen level. Two days prior the experiment cells were seeded for pSIRM labeling experiment in DMEM media supplemented with 2.5 g/L glucose, 0.365 g/L glutamine, and 0.055 g/L pyruvic acid (Table 2.2). Seeding densities were adjusted to maintain maximum of 80% confluency in a petri dish (diameter 10 cm). A media change has been performed four hours prior the labeling to adjust cell culture and nutrient conditions.
Stable isotope labeling and cell harvest were performed as described in the pSIRM methods. $^{13}C$-Glc and $^{13}C$-Pyr were applied for 7 min, $^{13}C$-Gln for 15 min each. For each substrate three ($^{13}C$-Glc), respectively two ($^{13}C$-Gln, -Pyr) biological replicates were harvested and processed for GC-MS measurement as described. A single petri dish has been harvested and prepared for shotgun proteomics analysis as described before.

### 2.4.2. Early differentiation in hESCs H1

Human embryonic stem cells H1 were cultivated in serum-free culture to maintain pluripotency. For detailed information of media composition see Supplement Table B.10. Replacement of the media lacking bFGF and chiemera induced the spontaneous cell differentiation. The parallel replacement of glucose and glutamine by their stable isotopic counterparts provided to monitor the fate of the main carbon-sources within the CCM. $^{13}C$-substrates were applied prior and at 24 hrs and 48 hrs of differentiation. Considering the nutrient turnover cells were labeled with $^{13}C$-Glc for 15 min, $^{13}C$-glutamine has been applied for 60 min.

Cell extracts of two 6-wells were pooled per biological replicate and condition according to the pSIRM protocol. Three biological replicates were prepared for each time point and $^{13}C$-substrate. Quantities of metabolites ($pmol/1 \times 10^6$ cells) were calculated based on protein content determined of the interphase and related to a protein content of 900 $ug/1 \times 10^6$ cells.

Proteome samples were prepared in two biological replicates according to the proteomics protocol. All experimental parameters are summarised in Table 2.3.

### 2.4.3. Neuronal differentiation of Luhmes cells

Experiments were performed in collaboration with Simon Gutbier and Johannes Delp, PhD students of the Leist-Lab. Luhmes d0 and d6 cells were cultivated and differentiated according to the standard protocol in the Leist lab at the University of Konstanz. Briefly, conditionally-immortalized cells (Luhmes d0, tet-off system v-myc transgene) were culti-

Table 2.2.: Human ESCs, iPS cells and their derivates — experimental parameter.

| | **hESC and derivates** |
|---|---|
| Cell lines | 2x breast cancer cell lines<br>3x colon cancer cell lines<br>2x hESC cell lines<br>3x fibroblast cell lines |
| $^{13}C$-Substr. | Glc / Gln / Pyr |
| Labelling Time (min) | 7 / 15 / 7 |
| Nb. of biological replicates | 3 / 2 / 2 |

Table 2.3.: Early differentiation — experimental parameter.

| | **Early differentiation** |
|---|---|
| Cell lines | hESC H1 |
| Time points (hrs of differentiation) | 0, 24, 48 |
| $^{13}$C-Substr. | Glc / Gln |
| Labelling Time (min) | 15 / 60 |
| Nb. of pooled 6-wells | 2 |

vated in proliferation media (PM). 8 $\times 10^6$ Luhmes d0 cells were seeded in a Nunclon T175 tissue flask for differentiation in PM. After 24 h, medium was replaced with differentiation medium (DM).

Pre-differentiated cells were trypsinised after 48 hrs, and seeded in a density of 1.5 $\times$ $10^5$ cells/cm$^2$ in precoated 6-well plates with 50 ug/ml poly-L-ornithine (PLO) and 1 ug/ml bronectin in DM. Differentiated cell culture was maintained in DM for additional four days. Isotopic labeled media ($^{13}C$-Glucose and -Glutamine) were prepared as described before. Initially two experiments were performed to analyse the general nutrient consumption of Luhmes d0 and d6 cells (Exp 1). Therefore Luhmes cells were incubated for 30 min with labelling media and harvested according to the pSIRM protocol for adherent cells in 6-well plates. Every biological replicate consists of two pooled wells of independent differentiations. Cell extracts were stored in 50%-Methanol and shipped on dry-ice for further sample processing at the MDC Berlin-Buch.

50 ul of media sample were collected for each harvested well according to the pSIRM prococol - plain media, prior labelling, and after $^{13}C$-substrate incubation.

In addition time course experiments were conducted for each $^{13}C$-substrate for MFA. Time points, experimental conditions, and additional parameters are listed for each experiment in Table 2.4. Cell counts for each experiment and cell line have been determined by nuclei

Table 2.4.: Neuronal differentiation of Luhmes cells: Experimental conditions and parameter. * Time course experiments have been performed for up to 24 hrs.

| | **Exp 1** | **Exp 2** | **Exp MPP$^+$** | **Exp 2 add-on** |
|---|---|---|---|---|
| Cell lines | d0, d6 | d6 | d6 | d0 |
| $^{13}$C-Substr. | Glc, Gln | Glc, Gln | Glc, Gln | Glc, Gln |
| Treatment | no | no | 5 uM MPP$^+$ | no |
| Labelling Time | 30 min | time course* | time course* | time course* |

Table 2.5.: Applied isotopes for the identification of GC-MS derived fragments

| **Substrate** | **Applied Isotopes** |
|---|---|
| Glucose | u-$^{12}C$,u-$^{13}C$, $^{13}C_1$, $^{13}C_{1,2}$, $^{13}C_{1,2,3}$, $^{13}C_{4,5}$,$^{13}C_{4,5,6}$, $^{13}C_6$ |
| Glutamine | u-$^{12}C$, u-$^{13}C$ |
| other | u-$^{13}C$-Pyr, u-$^{13}C$-$\alpha$KG |

staining in the Leist-Lab as described in Material & Methods 2.1

Multiple wells of each cell line were harvested for shotgun proteome analysis. 8 M Urea buffer has been added directly into the well. Plates have been sealed, stored at -80°C and shipped on dry-ice for further sample preparation at the MDC Berlin-Buch.

### 2.4.4. Mapping of GC-MS fragments

HEK293 and HCT116 cells were labeled with various substrates for the mapping of GC-MS derived fragments to the molecule structure (Table 2.5). Cells were cultivated under standard conditions as described before and labeled for 6 hours with isotopes of glucose and pyruvic acid or over night in the case of the application of glutamine and $\alpha$ketoglutaric acid isotopes. Experiments were performed with DMEM media supplemented with 2.5 g/L glucose and 2 mM glutamine. Cell harvest and metabolite extraction was performed as described in detail in Section 2.3.

## 2.5. Computational methods for omics data analysis

**Volcano plot** Volcano plots are used for the comparison of two proteoms at the same time. Fold changes are calculated related to the primary state; iPS to fibroblast; derived fibroblast to iPS. T-test statistics ($\alpha = 0.05$, two-sided) calculates the significance of the difference of mean values for each protein.

Filled dots (red, blue) represent significant differentially expressed CCM-proteins. Proteins with an absolute $log2FC > 2$ are shown with gene name tag only. Individual clones derived from the same progenitor are summarised as biological replicates for the determination of fold change and t-test.

**Hierachical clustering** Data processing was done with the MaxQuant-related software Perseus 1.4.0.20[1]. LFQ intensities from the MaxQuant output file proteinGroups.txt has been imported into Perseus. Contaminants and reverse proteins were removed prior the analysis.

LFQ intensities were log2-transformed. File annotation has been done in Perseus, thereby samples were grouped regarding experimental setup, cellular status (pluripotent, differentiated) and technical replicate. Data matrix has been filtered for at least three valid values per experimental setup and two technical replicates.

Averaged values of log2 LFQ intensities were transformed into row-wise z-scores. Annotation of GOBP slim and KEGG names were added prior the hierarchical cluster analysis (euclidean distance, average, 300 cluster). Enzymes associated with the central carbon metabolism are mentioned regarding to their expression next to their cluster. Enrichment of GOBP and KEGG pathways are done by Perseus internal algorithms.

**Principal component analysis** Principal component analysis has been carried out complete data matrices without imputation of values. Quantitative data, either metabolite quantities, stable isotope incorporation or protein expression has been log2-transformed prior the analysis. Rank-dependent PCA has been applied in the frame of the combined

[1] http://coxdocs.org/doku.php?id=perseus:start

analysis of all three mentioned kind of data.

**Metabolic profiles** Metabolic profiles were determined based on the absolute quantification of all identified metabolites in a cell line. Only data points fullfiling the quality requirements (described in 3.3.3.2) are taken into account for the calculation of the metabolic profile. Multiple derivates of a metabolite are averaged to a single quantity per metabolite ($pmol/10^6$ cells).

The metabolite abundance is calculated (i) within all quantified metabolites of the corresponding pathway class (x-axis) and (ii) to the total metabolite content (y-axis).

The log2-transformation of the x-axis improves visibility of the metabolite distribution within the pathway. The absolute quantity is reflected in the area of the circle for each metabolite. Metabolites with a fraction less than 1 % within a pathway are excluded from the visualisation. Metabolic profile quantities are shown in the supplement for each cell line. Metabolite-pathway associations are listed in Table 2.6.

## 2.6. Tools and software used for data analysis

- ChromaToF v.4.42 and v.5.2 (Leco); GC-MS derived data processing and annotation
- Illustrator 5.6 (Adobe); data visualisation and general graphical illustration
- MAUI-SILVIA; In-house developed software for GC-MS data annotation and processing. Basic framework is described in Kuich et al. (2014)
- MaxQuant v.1.4.1.2; Protein LFQ quantification of LC-MS derived data (Cox and Mann, 2008)
- MTXQC v.1.6; In-house developed tool for determination of data quality of GC-MS datasets

Table 2.6.: Metabolite-pathway association for the determination of metabolic profiles

| **Pathway** | **Metabolite** |
|---|---|
| Amino acids | Ala, Asp, Gly, Iso, Leu, Lys, Met, Phe, Pro, Ser, Thr, Val |
| Glutaminolysis | 2HG, Glu, Glut |
| Glycolysis | 3PGA, DHAP, FBP, Frc1P, Frc6P, Glc6P, Lac, PEP, Pyr |
| Other | Adenosine, Creatinine, Cytosine, Ery, Frc, Glyc3P, myo-Ino, PanA, Putr, Uracil |
| PPP | 6PGA |
| TCA-cycle | aKG, Cit, Fum, Mal, Suc |

- Perseus; MaxQuant associated tool for LC-MS data analysis and visualisation (Tyanova et al., 2016)
- PTXQC; In-house developed tool for the determination of data quality of LC-MS dataset (Bielow et al., 2016)
- RStudio Desktop; a R for statistics computing working environment, www.rstudio.com
- R packages: dplyr, ggplot2, gplots, plyr, RColorBrewer, reshape2, scales. Please refer for reference to R-project.org
- webgestalt.org (Netherlands); web tool for translating gene lists into biological insights
- bioinformatics.psb.ugent.be (IB, Belgium); generation of venn diagramm

## 2.7. Instationary metabolic flux analysis

A biochemical reaction network of central carbon metabolism for mammalian cell lines has been constructed based on Amaral et al. as well as from the KEGG database (http://www.genome.jp/kegg) (Amaral et al., 2011). The construction of our model was guided by (1) representing biosynthesis and degradation pathways by effluxes from the system and excluding low-abundance biomass components; (2) pooling metabolites due to limited measurement information, e.g., 2-phosphoglycerate and 3-phosphoglycerate, which are represented by one lumped pool 3PGA while preserving the carbon atom transitions; and (3) aggregating parallel fluxes, such as isoenzymes.

The model central carbon metabolism consists of glycolysis, pentose phosphate pathway, TCA-cycle and amino acid synthesis and degradation. Glutaminolysis and de novo synthesis of serine, glycine and alanine were incorporated because time-resolved measurements were available for these pathways. The isotope incorporation information of $^{13}C$-glucose and $^{13}C$-glutamine have been integrated in one network.

The biomass composition for mammalian cells was adopted from Sheikh et al. (2008) and integrated as a set of constraints for the fluxes into building block synthesis. In total, the model contains 67 metabolites and 97 reactions, each supplemented with carbon atom transitions (D.1). We implemented around 1002, respectively 734 isotope patterns derived from the measurement of isotope incorporation at 11 time points (Table 2.7).

The generation of isotopomer balances, the simulation of measurements, the flux estimation, and the statistical assessment of resulting flux confidence intervals were performed using the software tool 13CFLUX2 with an non-stationary extension for simulation of transient labeling distributions (Weitzel et al., 2013).

Fluxes were calculated based on the minimisation of a weighted least squares objective with randomly sampled starting values combined with a globalized optimisation strategy to detect multiple equally good but essentially different flux solutions. Finally, the resulting flux estimations are represented in the context of the metabolic network model by manual illustration in Illustrator. Thickness (pt) of fluxes had been related to the highest

Table 2.7.: Model parameter for INST-MFA in Luhmes d0 and d6 cells.

| **Parameter** | **Luhmes d0** | **Luhmes d6** |
|---|---|---|
| Measured intracell. pools | 15 | 16 |
| Extracellular rates (total) | 23 | 23 |
| Isotope pattern | 1002 | 734 |
| Time points | 11 | 11 |
| Metabolite pools (total / free) | 67 / 33 | 67 / 33 |
| luxes (total / free) | 97 / 36 | 97 / 35 |

(3 pt) metabolic flux in the network for each flux map.

GC-MS derived data have been evaluated by the in-house developed quality control tool MTXQC for time series experiments. The tool evaluates the GC-MS performance, absolute quantification and MID quality using the output from MAUI-SILVA. Absolute pool sizes were taken from the metabolic profile of the cells, considering all requirements regarding absolute quantification as described before.

The following procedure had been applied to achieve an acceptable fit: (1) each mass isotopomer measurement sums up to one and so we used a minimum absolute standard deviation of 0.01 to account for the noise of measurements close to the detection limit of MS instruments, (2) we obtained the best fit by minimising the difference between simulated and measured data, and (3) we excluded those measurements with low abundance that have extraordinary large discrepancies.

# 3 Results

All herein described projects aimed to get insights how metabolic reprogramming affects the central carbon metabolism (CCM) during the induction of pluripotency or tumorigenesis. Quantitative high-throughput mass spectrometry approaches had been applied to a panel of cancer, pluripotent and differentiated cell lines for a comprehensive analysis of the CCM. The application of stable isotopic labeled substrates e.g., $^{13}C$-glucose, provided the time-dependent and carbon-resolved tracing of nutrients within the metabolism and gave an indirect measure of the metabolic flux. Metabolic fluxes are the total outcome of the interaction of all regulatory layers of a cell and therefore the only one functional read-out of a cell.

Four projects have been carried out to address metabolic reprogramming in the context of cell differentiation, induction of pluripotency and tumorigenesis. The methodology has been applied to human embryonic stem cells (hESCs), derived fibroblasts (hESC-DFs) and cancer cell lines; two breast and three colon cancer cell lines. The comparison of proteome and metabolome revealed common and distinct features of the aerobic glycolytic phenotype of potent cells.

A second experiment addressed the reversibility of metabolic reprogramming. Three fibroblasts cell lines, their derived induced pluripotent (iPS) cells and their re-differentiated fibroblasts (iPS-DFs) have been analysed in the same manner as the previous project. Both experiments together allowed to examine similarities and differences of native (hESCs) and reprogrammed (iPS) pluripotency.

In addition events occurring during the early steps of differentiation have been analysed in a third experiments in hESCs H1 cells. At last the analysis of terminal neuronal differ-

entiation of a pluripotent precursor cell lines complements the list of experimental setups.

At first an introduction of each project and an overview of the protein expression, the metabolic profile and the incorporation of main nutrients are given for each project in Section 3.1. The following Section 3.2 summarises the integration of all experimental setups data to identify phenotype specific features of the CCM. Ultimately, the developed workflow from cell culture experiments up to the determination of metabolic fluxes in mammalian cells, including methodological developments, are summarised in Section 3.3.

## 3.1. Quantitative and dynamic analysis of CCM proteome and metabolome during differentiation and reprogramming pluripotency

### 3.1.1. Cancer, stem cells and stem cell derived fibroblasts: common and distinct characteristics of proteome and metabolome

The Warburg effect is known as the main common metabolic characteristic of cancer and stem cells. The shift from mitochondrial respiration towards aerobic glycolysis is a key event occurring during tumorigenesis. The contrary switch is induced in hESCs during differentiation. The metabolism switches from aerobic glycolysis towards an increased activity of oxidative phosphorylation.

Shotgun proteomics and pSIRM experiments have been performed for a quantitative comparison of the CCM in five cancer cell lines (colon cancer: HT-29, RKO, SW480; breast cancer: MCF7, MDA-MB231), two hESC cell lines (H1, H9) and their differentiated counterparts (H1-DF, H9-DF) (Figure 3.1). Every cell line has been incubated with the following stable isotopes for the dynamic analysis of nutrient utilisation: $^{13}C$-glucose (Cambridge isotopes, 7 min), $^{13}C$-glutamine (Cambridge isotopes, 15 min), and $^{13}C$-pyruvic acid (Cambridge isotopes, 7 min). The experiments have been carried out under identical conditions and supply of nutrients.

#### 3.1.1.1. Expression of CCM enzymes and their isoforms

The application of shotgun LC-MS proteomics approach and MaxQuant label-free quantification provided the quantification of 5400 proteins. Duplicated cell lines (H9 and MDA-MB231) are derived from an independent experiment and are included for data validation. Enzymes and their isoforms are highlighted in the green box regarding their position in the cluster, if detected (Figure 3.2). The blue box summarises the enrichment analysis of GO "biological process" (GOBP) of each cluster. The number of proteins located within the cluster are shown in brackets in comparison to the overall number of quantified proteins. The hierarchical cluster analysis of the global proteome revealed similarities between proteome profiles of cancer, stem and differentiated cells. The proteome of the colon cancer cell line HT-29 grouped together with early and late stage breast cancer cell lines MCF7 and MDA-MB231. SW480 colon cancer cells shared a similar proteome profile with hESC derived fibroblasts H1-DF and H9-DF, whereas the proteome of RKO cells showed a closer relation to the proteome of hESCs H1 and H9.

**Differentiation-induced changes of protein expression** The differentiation of hESCs is accompanied by a rearrangement of cell morphology and metabolism, e.g., the maturation of mitochondria, the power plant of a cell running the production of ATP. Despite, a number of TCA-cylce related enzymes showed up-regulated protein levels in pluripotent

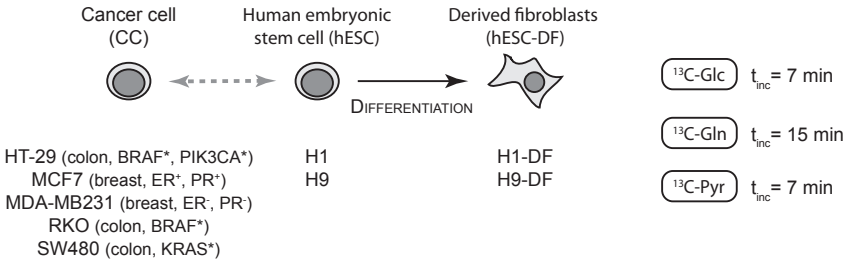


Figure 3.1.: Experimental setup for analysing the proteome and metabolome profile of cancer, stem cells and derived fibroblasts. Isotope labeled substrates ($^{13}C$-glucose, $^{13}C$-glutamine, $^{13}C$-pyruvic acid) are applied to monitor the carbon routing within the CCM in all cell types.

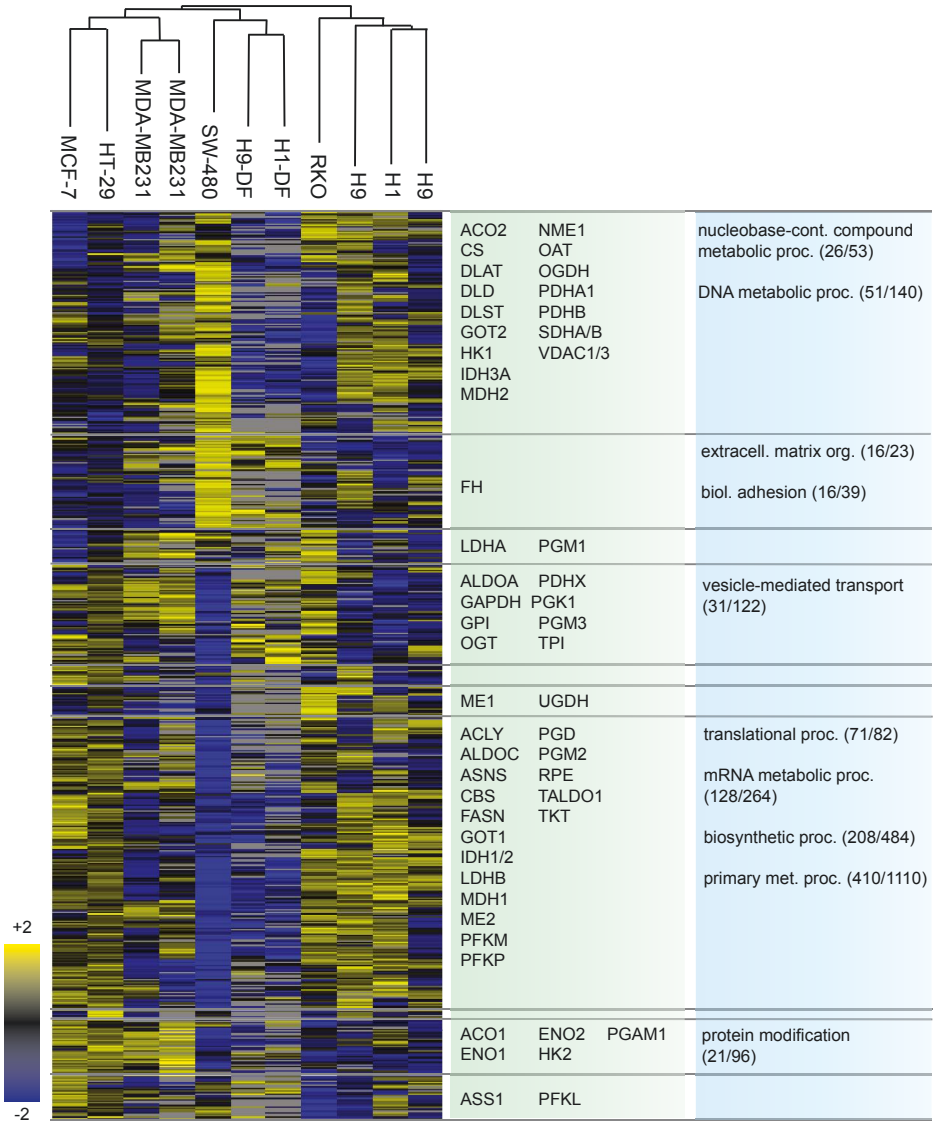


Figure 3.2.: Hierarchical cluster analysis comparing LFQ protein expression of hESCs, derived fibroblasts and cancer cell lines. CCM-associated proteins are shown regarding to their position in the clustering in the green box. Blue box contains the enrichment analysis of GOBP classes including number of proteins within the cluster and number of proteins per GOBP class in total.

hESCs: isocitrate dehydrogenase 1 (IDH1,c), succinate dehydrogenase A (SHDA, m), and both isoenzymes of malate dehydrogenase 1/2 (MDH1 (c)/ MDH2 (m)) (Figure 3.3-A). The pyruvate dehydrogenase complex (PDHc, m) consists of multiple copies of the subunits PDHA, PDHB and DLAT. This complex catalyses the conversion of cytosolic imported

pyruvate into acetyl-CoA, that enters the TCA-cycle. Elevated protein levels have been detected for all subunits in hESCs. Equally, the protein expression of the subunits of the structural related 2-oxoglutarate dehydrogenase complex OGDHc, OGDH and DLST, were increased in the pluripotent cells and decreased with differentiation. The reduced expression of citrate synthase (CS, m), first enzyme of the TCA-cycle and solely expressed in the mitochondria, in hESC-DFs is accompanied by decreased levels of fatty acid synthase (FASN, c).

Differentiation induced a switch in isoenzyme expression of lactate dehydrogenase (LDH, c) and malic enzyme (ME) in hESCs. The levels of LDHB and the NAD-dependent isoenzyme ME2 (m) were increased in hESCs; whereas LDHA and NADP-dependent isoform ME1 (c) were raised in hESC-DFs.

Protein levels of pyruvate kinase M2 (c), one of the rate limiting enzyme of glycolysis, increased with differentiation of hESCs. The complementary isoform PKM1 has not been detected in hESCs, but in hESC-DF cells. Differentiation of hESCs were accompanied by the reduced expression of aspartate aminotransferases (GOT1 (c) / GOT2 (m)). Proteins related to the one-carbon metabolism were highly abundant in hESCs, e.g., 3-phosphoglycerate dehydrogenase (PHGDH, c), cystathionine $\beta$-synthase (CBS, c), and serine hydroxymethyltransferase (SHMT2, c). PHGDH is the first of three enzymes catalysing the *de novo* synthesis of serine (Ser), a major substrate of the one-carbon metabolism. A detailed analysis of the one-carbon metabolism has been summarised in Section 3.2.4.1.

**Proteome similarities between hESC and cancer cell lines** Proteins of the CCM are highly conserved and exist in multiple isoforms. Transcription factors, e.g., c-myc, the hypoxia-inducible factor 1 (HIF-1) and p53 regulate the expression of isoenzymes in the CCM. The proteome profiles of cancer cell lines showed a huge variance of protein expression in general, and especially of proteins related to glycolysis and TCA-cycle, reflecting the complex enzyme expression pattern of those key players in different type of cancer cells.

A comprehensive analysis of CCM protein expression dependent on the cellular status is summarised in Section 3.2. At this point the analysis focusses on the comparison of the

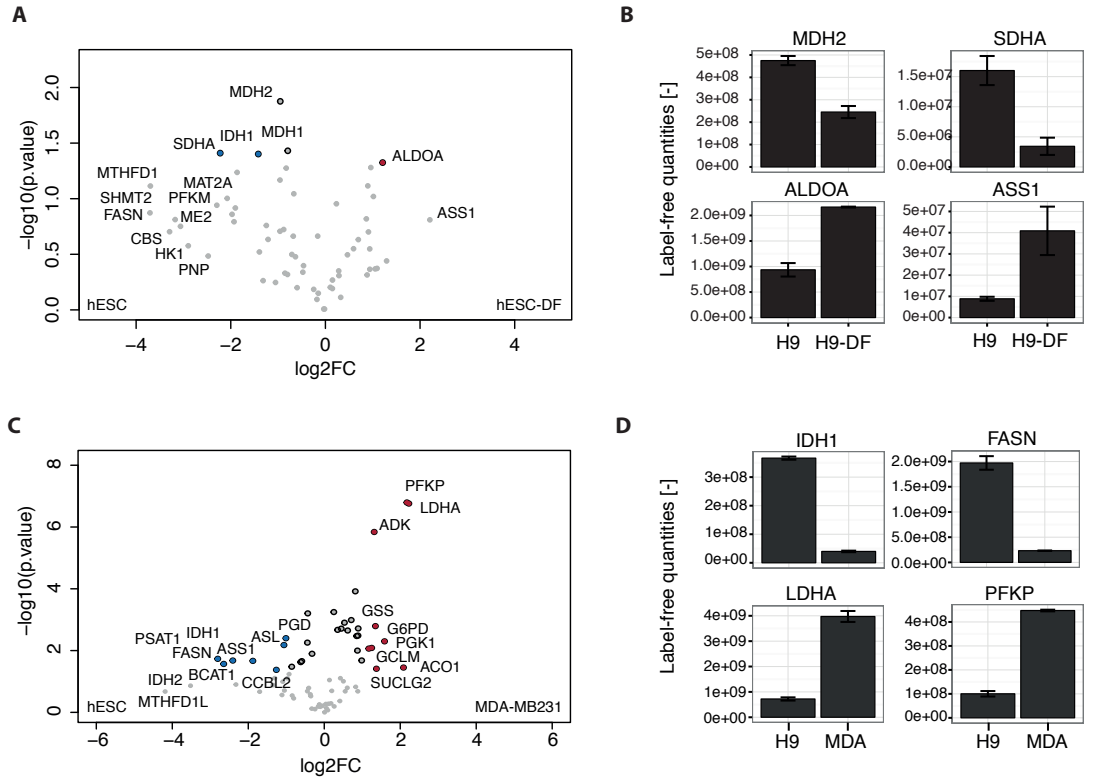


Figure 3.3.: Isoenzyme expression of CCM proteins in hESCs, hESC-DFs and MDA-MB231 cells. (A) Volcano plot comparing CCM related protein expression in hESC and hESC-DF. (B) LFQ-quantities of selected isoenzymes are shown for hESC H9 and H9-DF cells. (C) Volcano plot shows the comparison of expression levels of CCM-enzymes in hESCs and MDA-MB231 cells. (D) LFQ-quantities of selected enzymes of the volcano plot are shown comparing hESCs and MDA-MB231 cells. Coloured circles in the volcano plots show proteins with a $FC > 1$ and $p-value < 0.05$; proteins with $p-value > 0.05$ are shown with name tags only.

proteome of hESCs and breast cancer cells MDA-MB231.

The isoenzymes of LDH were cell-type specifically expressed. MDA-MB231 cells showed high levels of LDHA (Figure 3.3-B). LDHB, second isoform of the enzyme, was more abundant in hESCs. High levels of PKM2, 6-phosphofructokinase (PFKP,c) and phosphoglycerate kinase 1 (PGK1, c) were determined in MDA-MB231 cells.

High abundant proteins in hESCs were mostly related to the one carbon metabolism (MTHFD1L, PSAT1, CCBL2, all cytosolic), fatty acid synthesis (FASN, c) and aspartate metabolism (ASL (c), ASS1 (c,m)). TCA-cycle protein IDH1 (c) showed increased protein levels in hESCs in comparison to MDA-MB231 cells.

A distinct expression of isoenzymes comparing hESCs and MDA-MB231 cells had been detected for the protein branched-chain-amino-acid aminotransferase (BCAT). Pluripotent cells solely expressed the isoenzyme BCAT1 (c), cancer cell lines BCAT2. The cellular localisation of BCAT2 is dependent on the expressed isoform. The mitochondrial isoform BCAT2B lacks the amino acids 9–100 of the cytosolic isoform BCAT2A. The performed MaxQuant analysis did not distinguish between both isoforms based on the detected peptides in that experiment.

#### 3.1.1.2. Metabolic profile of cancer cells, hESCs and hESC-DFs

GC-MS based metabolomics analysis gave the resources for the identification of around 120 compounds of divergent biochemical classes, e.g., amino acids, hexoses and their phosphates. The measurement of a known standard mixture in eight dilutions in sequence with cell extracts provided the estimate of absolute quantities of these compounds. The mixture is composed of 60 metabolites of the pathways: glycolysis, TCA-cycle, pentose phosphate pathway, amino acid metabolism and glutaminolysis. The composition of the standard mixture for absolute quantification and applied quantities are summarised in Supp. Section A.5.

The quantities are visualised in a plot called "metabolic profile" for each cell line. The plot relates the quantities of every intermediate to their proportion within their pathway (x-axis) and to the overall metabolic content (y-axis). The area of the circle of each metabolite corresponds to its absolute pool size. The metabolic profiles of hESCs H9, their derived fibroblasts H9-DF, and MDA-MB231 cells are shown in Figure 3.4.

In general, the comparison of differentiated and potent cells revealed overall lower pool sizes in hESCs and cancer cells, independently from the pathway. Lactic and pyruvic acid belonged to the most abundant intermediates in all cell lines, whereas in relation the pool of Lac exceeded the Pyr pool in hESCs and MDA-MB231 cells. This ratio changed with the differentiation of hESCs into hESC-DF cells.

Amino acids constituted the main class in all three cell types. Threonine, an essential amino acid, is the most abundant amino acid in hESCs and their differentiated counter-

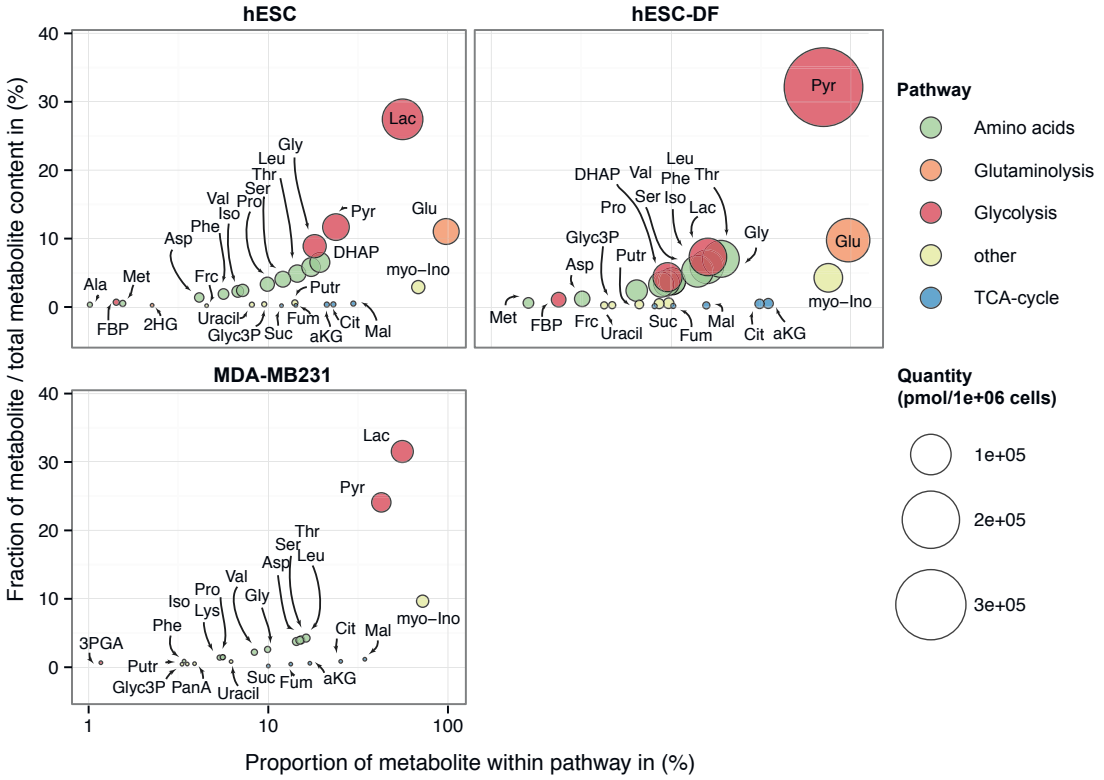


Figure 3.4.: Metabolic profile of hESCs, hESC-DFs, and MDA-MB231 cells. Metabolite quantities are shown regarding their fraction within the pathway of the CCM (x-axis) and to the total metabolic content (y-axis). The circle area correlates to the absolute pool size of the metabolite in $pmol/10^6$ cells.

parts. TCA-cycle intermediates accounted to the low abundant metabolites independently from the cell type. The differentiation of hESCs induced a switch in TCA-cycle quantities. The ratio of malic acid and citric acid, as well as fumaric and $\alpha$-ketoglutaric acid ($\alpha$KG) reversed in hESC-DFs, pointing towards a change of metabolic demands of precursors for biosynthesis processes. Citric, malic and $\alpha$-ketoglutaric acid are important precursors for adjacent pathways and are transported via a number of shuttles across the mitochondrial membrane. Low levels of citric acid may occur due to the increased demand of the metabolite for the production of acetyl-CoA in the cytosol, a precursor for the synthesis of fatty acids.

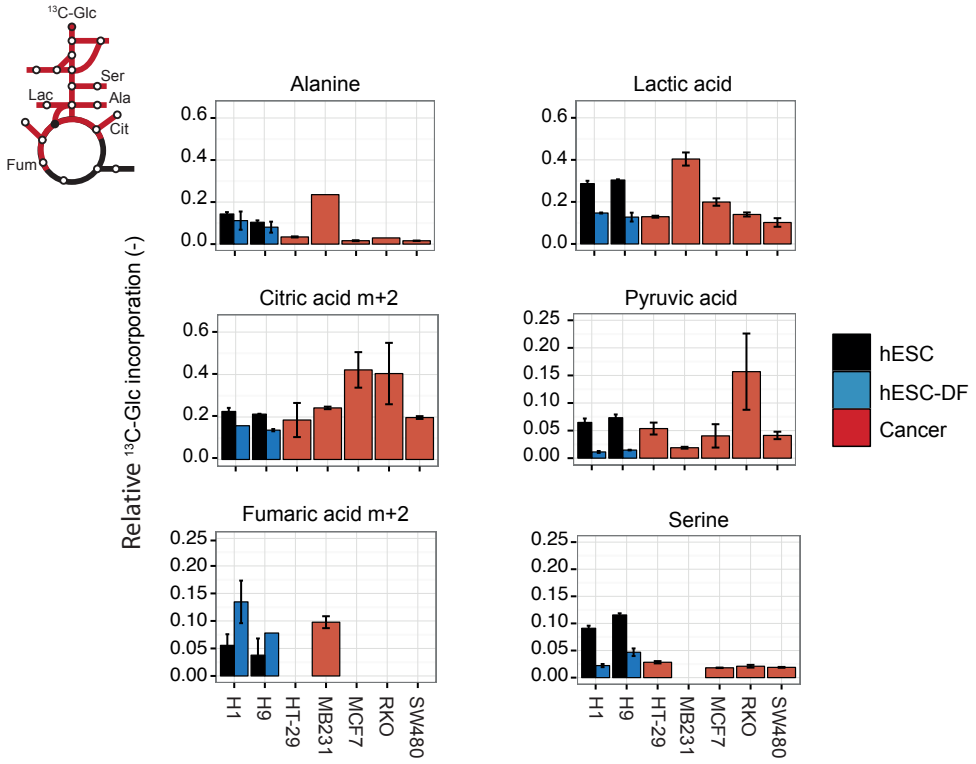


Figure 3.5.: $^{13}C$-Glucose incorporation in human embryonic cells (hESCs), their derivates (hESC-DFs), and cancer cells. Plots show relative average values of three biological replicates. A value of 1 represents 100% carbon-13 incorporation.

#### 3.1.1.3. The routing of nutrient-derived carbons in cancer cells, hESCs and hESC-DFs

**$^{13}$C-Glucose incorporation** GC-MS measurements provides the quantitative determination of stable isotope incorporation in every compound. The incorporation of stable isotopes, e.g., carbon-13, results in shift of intensities within the compounds mass spectra, that is composed of all detected fragments of the metabolite. The shift correlates with the number of incorporated isotopes. For each metabolite and derivate specific fragments were selected for the quantitative analysis of isotope incorporation. A comparison of stable isotope incorporation between different cell lines or cellular states gain insights about similarities and differences in the dynamics of nutrient uptake and utilisation.

The mathematical background and a list of metabolite specific fragments are introduced in Section 2.3. The major claim of the Warburg effect is an increased shuttling of glucose-

derived carbons into the synthesis of Lac. This effect occurs in stem and cancer cells even in the presence of oxygen and therefore bypassing the more efficient synthesis of ATP via mitochondrial respiration.

The levels of carbon-13 incorporation in Lac were similar in hESCs and the breast cancer cells MDA-MB231 and MCF7 (Figure 3.5). The differentiation of hESCs H1 and H9 cells resulted in a drop of incorporation in Lac that is similar to the incorporation rate in colon cancer cell lines RKO, HT-29 and SW480. The same drop of isotope incorporation occurred in Pyr with the differentiation of hESCs into fibroblasts. RKO colon cancer cells showed the highest incorporation rate of $^{13}C$-Glc in Pyr.

The incorporation of two carbon-13 into citric acid (Cit) is an measurement of the entry of glucose-derived carbons via acetyl-CoA into the TCA-cycle. MCF7 and RKO cells showed two times the incorporation rate of $^{13}C$-Glc in comparison to stem cells, HT-29, MDA-MB231 and SW480 cancer cells. The incorporation of $^{13}C$-Glc into Cit decreased with differentiation of hESCs.

The elevated incorporation of $^{13}C$-Glc in Cit observed in hESCs was not further processed into subsequent TCA-cycle intermediates, e.g., fumaric acid (Fum). The data showed a higher incorporation of carbon-13 into Fum in hESC-DF cells, despite their lower levels in Cit, pointed towards an increased turnover of carbons through the TCA-cycle in hESC-DFs in comparison to their pluripotent precursors.

This isotope labelling pattern showed a link of glucose-dependent citric acid production linked to fatty acid synthesis via export of citric acid into the cytosol. In contrast MDA-MB231 and hESC-DF cells cycled glucose-derived carbons through the TCA-cycle for ATP-production.

Further, the differentiation of hESCs has been accompanied by a reduction of glucose-derived carbon routing into serine synthesis. The amino acid represents the link between central carbon and one-carbon metabolism. An increased one-carbon pathway activity meets the raised demand of precursors for DNA and histone methylation, a prerequisite for the maintenance of a pluripotent state. Cancer cell lines incorporated less glucose-derived carbon routing into serine synthesis in comparison to hESCs.

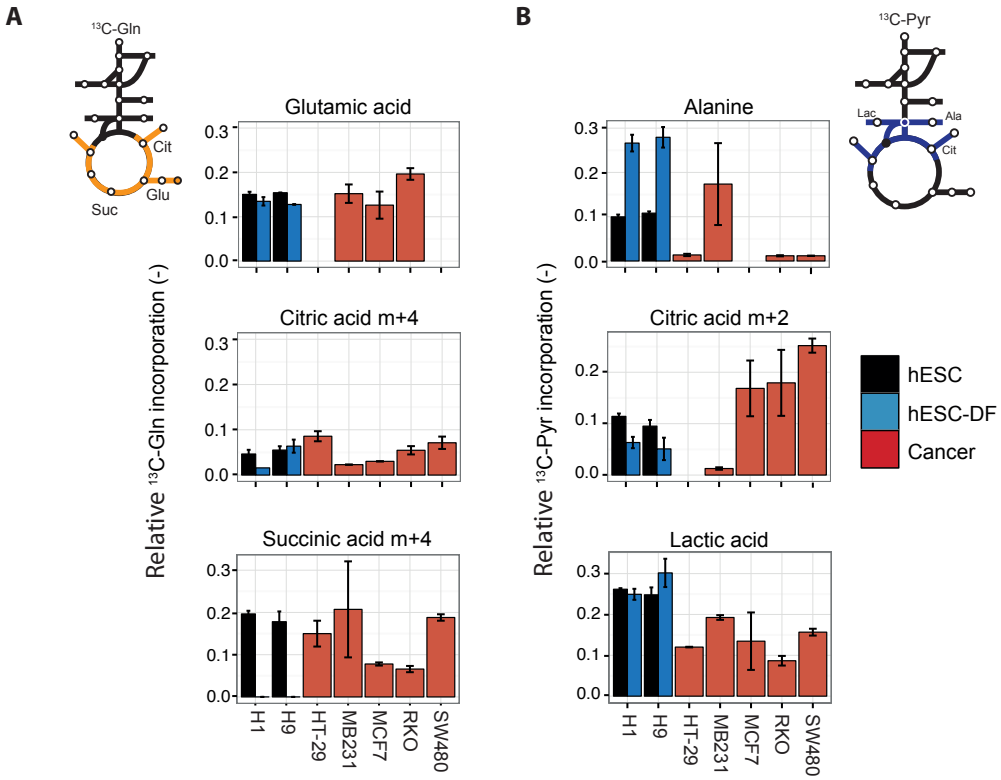


Figure 3.6.: (A) $^{13}C$-glutamine and (B) $^{13}C$-pyruvic acid incorporation in human embryonic cells (hESCs), their derivates (hESC-DFs), and cancer cells. Plots show average values of three (Gln), respectively two (Pyr) biological replicates. Cell lines were incubated for 15 min (Gln), respectively 7 min (Pyr) with each substrate. A value of 1 represents 100% carbon-13 incorporation.

**$^{13}$C-Glutamine** The amino acid glutamine (Gln) replenishes the TCA cycle as a second provider of carbons apart from glucose. Glutamine enters the TCA-cycle in form of $\alpha$-ketoglutaric acid (aKG) after its conversion into glutamic acid (Glu) by the enzyme glutaminase (GLS). The synthesis of glutaminase occurs in both compartments depending on the expression of the isoenzyme GLS.

After 15 minutes of incubation the Glu pool has been replaced up to 20% by carbon-13 in cancer cell lines (Figure 3.6-A). The incorporation rate in hESCs has been slightly lower and decreased further with differentiation into hESC-DFs.

Proceeding clockwise the TCA-cycle the carbon-13 incorporation into succinic acid (Suc) reached similar levels in hESCs and MDA-MB231, SW480, and HT-29. The incorporation of $^{13}C$-glutamine in MCF7 and RKO cancer cells dropped to 10% and has been even not

detectable in hESC-DF cells due to their low pool of succinic acid.
The incorporation of four carbon-13 into citric acid has been below 10% in all cell lines. A comprehensive, phenotype-specific analysis of the incorporation of nutrients into Cit is outlined in Section 3.2.

**$^{13}$C-Pyruvic acid** Pyruvic acid (Pyr) is one of the most interesting metabolites due to its central position linking cytosolic and mitochondrial metabolism. Pyr is converted either into Lac by LDH, simultaneously providing reducing equivalents (NADH), or into the amino acid alanine by alanine aminotransferase GPT1 (c) / GPT2 (m). The enzymes pyruvate carboxylase (PC) and the PDH complex (PDHc) provide the entry of pyruvate-derived carbons into the TCA-cycle either in form of oxaloacetic acid (OAA) or acetyl-CoA.
The analysis of $^{13}C$-Pyr incorporation allows to monitor the activity of these different pathways. A status dependent analysis summarising all projects derived data is shown in Section 3.2.
The differentiation of hESCs resulted in an increased routing of $^{13C}C$-Pyr into alanine synthesis, accompanied by a decreased incorporation via acetyl-CoA into Cit (Figure 3.6-B). The rate of incorporation into Lac did not alter between hESCs and hESC-DFs, opposing the distinct routing of glucose-derived carbons into Lac.
MDA-MB231 cells cancer cell lines shuttled only a minor fraction of $^{13}C$-Pyr into alanine. MCF7, RKO and SW480 cells incorporated up to 25% into Cit and between 10% and 20% into Lac.

### 3.1.2. Rearrangements of proteome and metabolome during reprogramming pluripotency and redifferentiation of somatic cells

A cocktail of four factors (Oct4, Sox2, Kfl4, and Myc) induces pluripotency in differentiated cell. In particular c-myc, a intensively studied oncogene, is known to modify metabolic enzyme expression and their activation, e.g., of the central glycolytic enzymes hexokinase (HK) and pyruvate kinase (PK). The potential of myc is clearly connected with oncogenic transformation and recently labs work on the replacement of c-Myc for the generation of iPS cells to improve their clinical applicability. The ability to define the fate of a iPS cells during differentiation e.g., opens the door towards patient-specific treatments. Until today the literature contains little information about the similarity of the metabolome and proteome of the differentiated precursor and re-differentiated cell after the induction of pluripotency. Only little is known about the comparability of native and reprogrammed pluripotent cells.

Prigione and colleagues showed the modulation of mitochondrial morphology, ATP production, and secretion of lactic acid during the induction of pluripotency (Prigione et al., 2010, 2011). In co-work with Alessandro Prigione we conducted a comprehensive study to investigate the metabolic reprogramming of the CCM combining proteomics and metabolomics

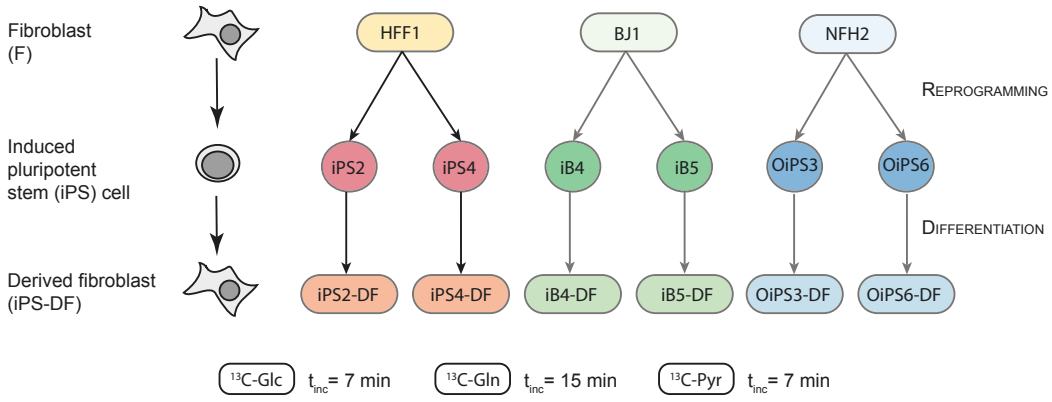


Figure 3.7.: Experimental setup for monitoring metabolic rearrangements during reprogramming pluripotency and redifferentiation of fibroblasts (HFF1, NFH2, BJ1). Application of stable labeled isotopes enable to track the fate of nutrients within the CCM.

approaches. Therefore we reprogrammed three fibroblast cell lines — HFF1, BJ1, and NFH2 — into iPS cells and re-differentiated these iPS cells into somatic cells (Figure 3.7). HFF1 and BJ1 cell lines are derived from the foreskin of male newborns. NFH2 is a dermal fibroblast cell lines, derived from a 84years old female. The comparison of nutrient utilisation in these three stages gained insights about the activity and reversibility of reprogrammed metabolic pathways. We applied stable isotopes, u-$^{13}C$-glucose, u-$^{13}C$-glutamine and u-$^{13}C$-pyruvic acid, to track the fate of carbons in the CCM, and collected samples for proteome and transcriptome analysis.

#### 3.1.2.1. Proteome analysis of fibroblasts, iPS, and iPS-DF cells

LFQ quantities of around 4500 proteins were determined by shotgun proteomics analysis. The different cell lines clustered regarding their cellular status, whereas iPS-DFs proteome profiles were closer related to the iPS cell derived profiles (Figure 3.8). The protein expression of all three native fibroblast cell lines grouped together in a third cluster. Enzymes of the CCM are shown regarding their occurrence in the row clustering in the green box (GOBP enrichment analysis of GOBP class in the blue box).

Induction of pluripotency in fibroblasts reduced the protein expression in a number of glycolytic enzymes (LDHA, GAPDH, ALDOA, and PKM2) and proteins related to GOBP classes cytoskeleton organisation, cell activation, carbohydrate metabolic processes and cell communication. A specific regulation of isoenzyme expression has been shown for the proteins LDHB and IDH. The expression of LDHA and IDH1 increased with induction of pluripotency, whereas LDHB and IDH2/3 were predominantly expressed in native and derived fibroblasts. The expressions levels of proteins related to one-carbon metabolism, subunits of the mitochondrial PDH complex, and TCA-cycle enzymes raised in iPS cells, e.g., CS, PDHB, or SHMT2 (Figure 3.9-A).

The up-regulated protein expression of ACLY and FASN, pointed towards the elevated demand of citric acid for biosynthesis of cholesterol and fatty acids.

The protein carbonic anhydrase (CA2) was the only CCM enzyme significantly up-regulated in iPS-DF cells in comparison to iPS cells (Figure 3.9-B). The protein drives the reversible

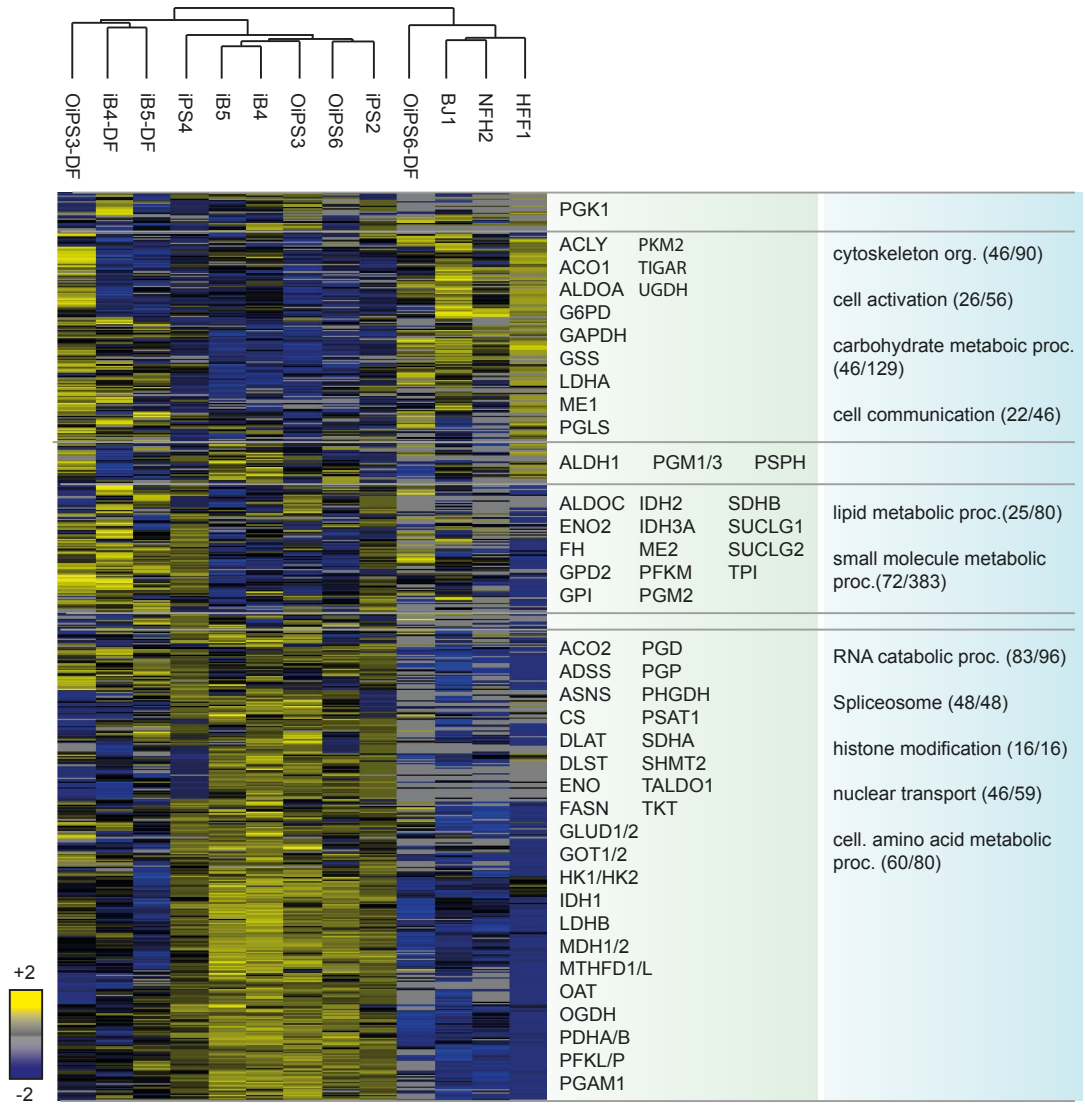


Figure 3.8.: Hierarchical clustering analysis of shotgun-proteomics of native (F) and derived fibroblasts (iPS-DFs) and iPS cells. Enzymes of the CCM are shown in the green box regarding their position in the clustering. The blue box summarises the enrichment analysis of GOBP classes of the cluster.

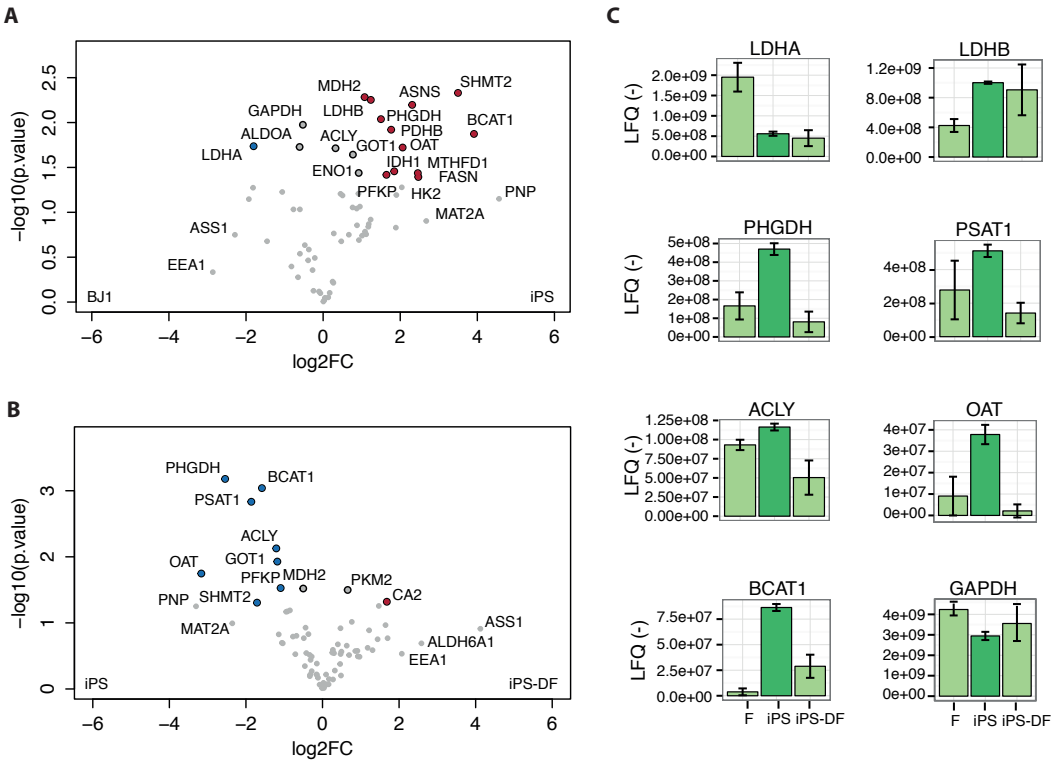


Figure 3.9.: Proteome analysis of the BJ1 derived iPS and iPS-DF cells. (A) Volcano plot comparing BJ1 and derived iPSCs protein expression. Expression levels of enzymes related to one-carbon metabolism and glycolytic enzymes increase with induction of pluripotency. (B) Volcano plot comparing protein expression in iPS and iPS-DF cells. (C) LFQ quantities of selected enzymes comparing native fibroblasts, iPS cells and re-differentiated fibroblasts (iPS-DF) derived from BJ1 cell line.

hydration of carbon dioxide, and stimulates the chloride-bicarbonate exchange.

The expression of PKM2 increased in iPS-DF cells, but the data did not show a significant up-regulated abundance in iPS-DF cells.

The comparison of enzyme levels between all three states indeed revealed a reversible protein expression. Enzymes of the one-carbon metabolism or amino acid synthesis returned to their native level in iPS-DF cells, e.g., PHGDH and BCAT1 (Figure 3.9-C). Both enzyme levels increased in iPS cells and retained in iPS-DFs. Levels of GAPDH altered in a reverse manner and decreased in pluripotent cells.

Figure 3.10.: Metabolic profile of HFF1 fibroblasts, iPS and iPS-DF cells. HFF1 fibroblast are reprogrammed into induced pluripotent stem (iPS2 / iPS4) cells and re-differentiated (iPS2-dDF / iPS4-DF). The area of the bubble represents the absolute metabolite quantity.

#### 3.1.2.2. Metabolic profile of fibroblasts, iPS, and iPS-DF cells

Quantities of CCM-intermediates have been determined by GC-MS analysis as described before. Pool sizes are plotted regarding their abundance within the metabolic pathway and the complete metabolic content for each cell line. A representative metabolic profile is shown for the cell line HFF1, including iPS cells and derived fibroblasts (Figure 3.10). In general the metabolic content decreased with reprogramming pluripotency and have been restored after re-differentiation in iPS-DF cells. Amino acids constituted the major metabolic content in all cell types. Threonine, glycine and serine were the main abundant amino acids, independent from fibroblast origin and phenotype. Pyruvic and lactic acid were highly abundant in pluripotent and differentiated cells. The ratio of both intermediates switched with induction of pluripotency; the pool of Lac exceeded Pyr in iPS cells. Along with differentiation the ratio reversed again in iPS-DF cells. Quantities of the TCA-cylce intermediates were low abundant in all cell lines.

#### 3.1.2.3. Carbon-routing in fibroblasts, iPS and iPS-DF cells

**$^{13}$C-Glucose** The analysis of $^{13}C$-glucose incorporation revealed a reversible reprogramming of glucose routing in all three setups (Figure 3.11). Carbon-13 incorporation in iPS-DF cells retained to the level in the fibroblasts (F) after the alteration of glucose incorporation in iPS cells.

Pluripotency increased the routing of $^{13}C$-Glc through glycolysis towards lactic acid and amino acid synthesis. The low incorporation rate in pyruvic acid pointed towards the presence of a huge non-labeled pyruvic acid pool, e.g., caused by an extensive import of extracellular pyruvic acid. The level of carbon-13 in lactic acid underlined the 'aerobic glycolytic' phenotype of iPS cells and is similar to hESCs.

Pluripotent cells shuttled glucose-derived carbons into the synthesis of the amino acids alanine and serine, in agreement with $^{13}C$-Glc routing in hESCs. The incorporation of glucose-derived carbon into TCA-cycle intermediates has been similar between the three cell types as shown for fumaric acid.

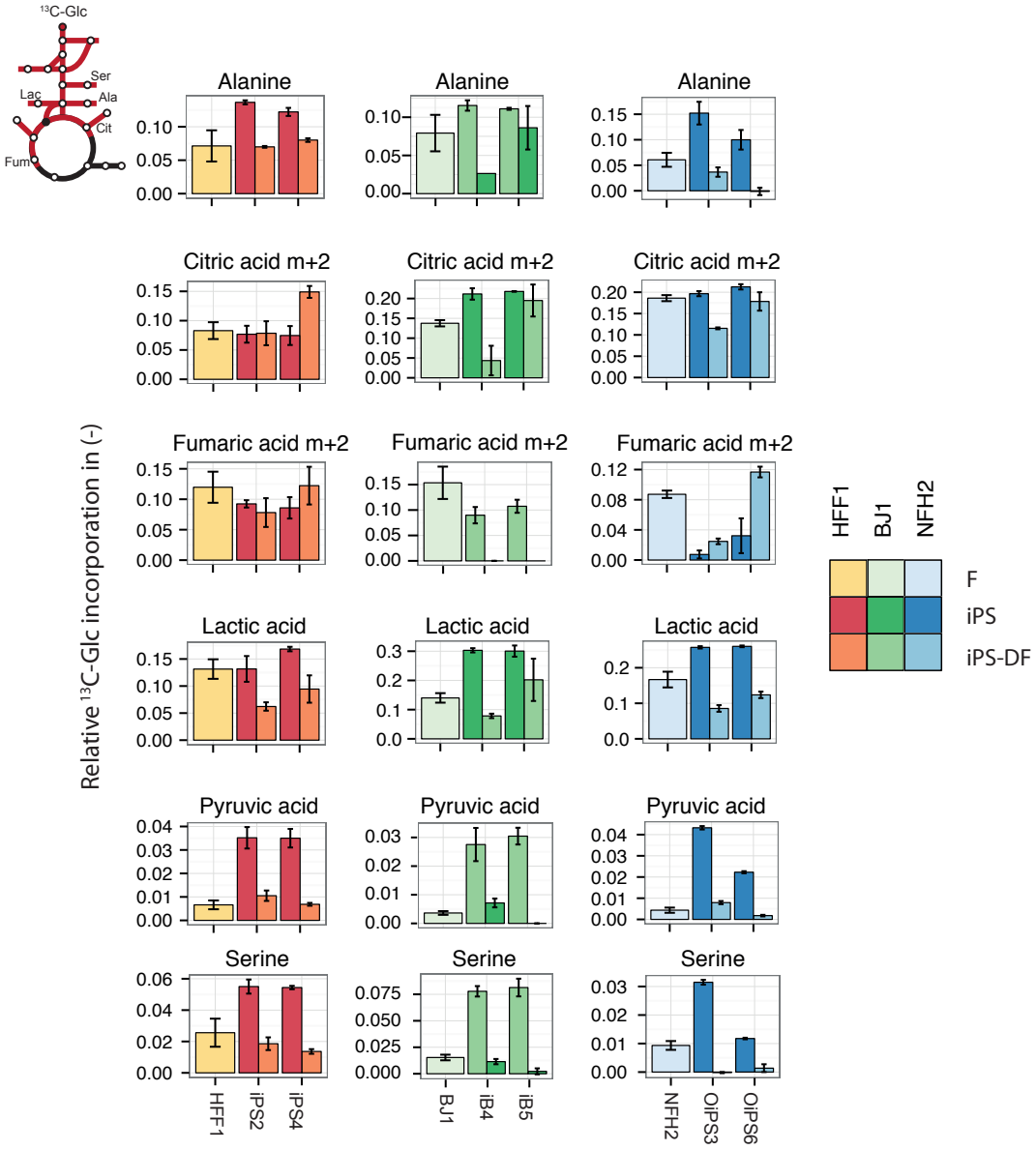


Figure 3.11.: Comparison of $^{13}C$-glucose incorporation of selected metabolites in all three setups HFF1, BJ1 and NFH2. The incorporation in a metabolite is summarised per originating fibroblast line, comparing fibroblast (F), induced pluripotent cells (iPS) and their derived fibroblast (iPS-DF). Data are shown for three biological replicates after 7 min of u-$^{13}C$-Glc incubation. Value of 1 represents 100% carbon-13 incorporation. Data are shown in groups of each native fibroblast cell lines comparing the isotope incorporation of fibroblasts and two iPS-clones and their derived iPS-DF cells. Sample groups: HFF1 (iPS2, iPS4), BJ1 (iB4, iB5), NFH2 (OiPS3, OiPS6).

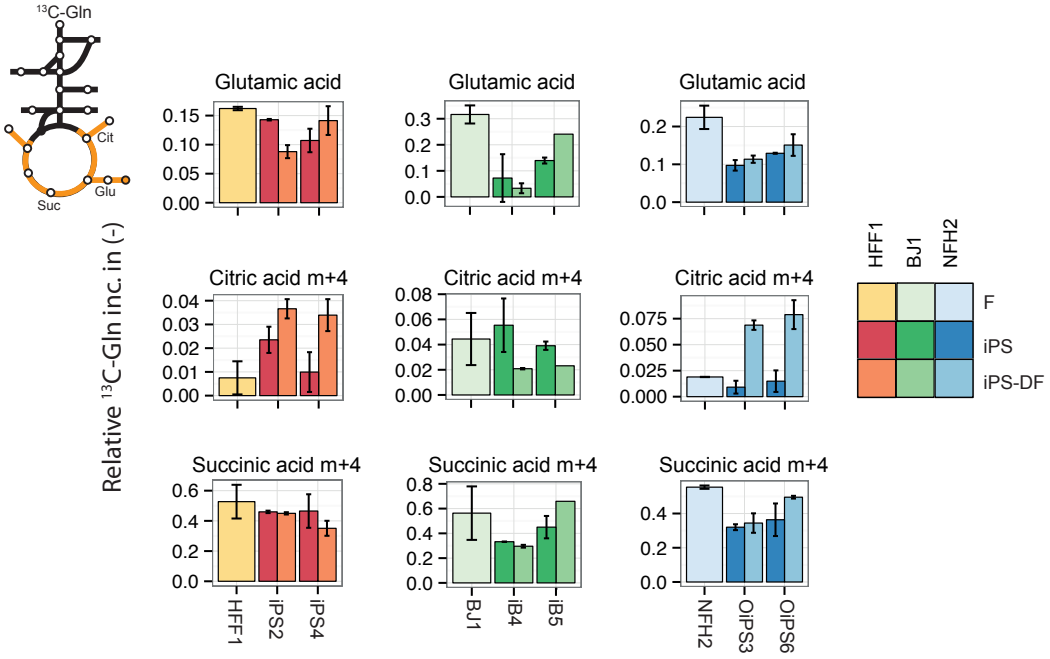


Figure 3.12.: Incorporation of $^{13}C$-glutamine in fibroblasts, iPS, and iPS-DF cells. The carbon-13 incorporation is summarised per native fibroblast line, comparing fibroblast (F), induced pluripotent cells (iPS) and their derived fibroblasts (iPS-DF). Cells were incubated with u-$^{13}C$-Gln for 15 min. Data are shown for two biological replicates and a value of 1 represents 100% carbon-13 incorporation. Data are shown in groups of each native fibroblast cell lines comparing the isotope incorporation of fibroblasts and two iPS-clones and their derived iPS-DF cells. Sample groups: HFF1 (iPS2, iPS4), BJ1 (iB4, iB5), NFH2 (OiPS3, OiPS6).

**$^{13}$C-Glutamine** The conversion of $^{13}C$-glutamine into glutamic acid did not extent 30% after 15 min of substrate incubation in all cell lines, pointing towards additional pathways contributing to the synthesis of glutamic acid (Figure 3.12). The comparison of all three setups did not show a cell status dependent pattern of glutamine uptake. The highest turnover of glutamine into glutamic acid has been observed in native fibroblasts HFF1, NFH2 and BJ1.

The low incorporation rate of $^{13}C$-Gln did not provide an explicit analysis of the oxidative and reductive mode of glutamine usage. The canonical incorporation of $^{13}C$-Gln in Cit increased with re-differentiation of HFF1 and NFH2 derived iPS cells and exceeded the carbon-13 level in the native precursors. BJ1 derived iPS and iPS-DF cells utilised glu-

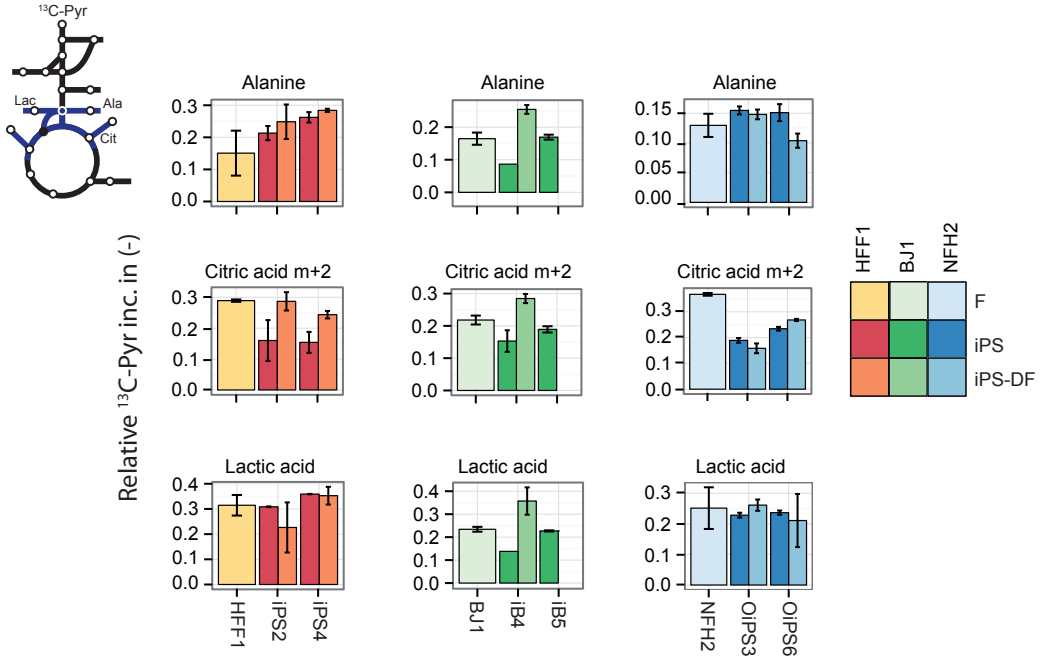


Figure 3.13.: Incorporation of $^{13}C$-pyruvic acid routing during reprogramming and re-differentiation. The isotope incorporation in a metabolite is summarised per originating fibroblast line, comparing fibroblast (F), induced pluripotent cells (iPS) and their derived fibroblasts (iPS-DF). Data is shown for two biological replicates and a value of 1 represents 100% carbon-13 incorporation. Cells were incubated with $^{13}C$-Pyr for 7 min. Data are shown in groups of each native fibroblast cell lines comparing the isotope incorporation of fibroblasts and two iPS-clones and their derived iPS-DF cells. Sample groups: HFF1 (iPS2, iPS4), BJ1 (iB4, iB5), NFH2 (OiPS3, OiPS6).

tamine in a different manner. BJ1 derived iPS cells showed the highest rate of carbon-13 incorporation in comparison to their differentiated precursors or progenitors.

**$^{13}$C-Pyruvate** Tracing the fate of pyruvic acid gains insights about carbon routing at a central point of the CCM. Pyruvate connects mitochondrial and cytosolic metabolism; it fuels the TCA-cycle, as well as Lac and Ala synthesis. The pool of Pyr has been almost completely replaced with its carbon-13 counterpart after 7 min of substrate incubation in all cell types (Supp. Table B.9). The high import rate of extracellular pyruvic acid explains the high level of intracellular $^{13}C$-Pyr and the low $^{13}C$-Glc incorporation in Pyr at the same time.

The incorporation rate of $^{13}C$-Pyr into Lac has been similar in all cell types, a difference to the cell status specific routing of $^{13}C$-Glc into Lac as shown before (Figure 3.13).
HFF1, BJ1, and NFH2 and their corresponding derived fibroblasts showed an increased transport of Pyr-derived carbons via acetyl-CoA into Cit up to 30%. Associated iPS cells incorporated less $^{13}C$-Pyr into the TCA-cycle via PDH complex, with exception of NFH2-derived iPS cells.
The conversion of Pyr into Ala has been individual in all setups. Only in BJ1-derived cells we observed an reduction of $^{13}C$-Pyr in iPS cells in comparison to the somatic cells, as shown during differentiation of hESCs.

### 3.1.3. Early differentiation in human embryonic stem cells H1

Each cell is primed to run a distinct metabolic program to meet its special demand regarding cellular maintenance, proliferation and energetic homeostasis. The herein described project addresses the question which events of metabolic reprogramming occur during early stem cell differentiation.

The hESC cell line H1 has been analysed at 0, 24, and 48 hours after the onset of spontaneous differentiation, induced by an exchange of cell culture media lacking the growth factor bFGF. Human ESCs were labeled with u-$^{13}C$-Glc (15 min) and u-$^{13}C$-Gln (60 min) to monitor changes of nutrient consumption during early differentiation, complementing the quantitative analysis of protein expression and metabolite pool sizes (Figure 3.14).

#### 3.1.3.1. Early events of proteome rearrangement during differentiation of hESCs H1

Global protein abundance has been determined by shotgun, label-free quantification proteomics approach. In total 3300 proteins were quantified, isoenzymes are distinguished based on unique peptides using MaxQuant software v 4.2.14.

Proteins, only identified in each sample, have been taken into account for the hierarchical cluster analysis, shown in (Figure 3.15. CCM-related proteins are highlighted according to their appearance in the cluster analysis. Enrichment analysis of GOBP and KEGG pathway are shown in the blue box. The hierarchical cluster analysis did not reveal an enriched expression of CCM enzymes in any of the identified cluster.

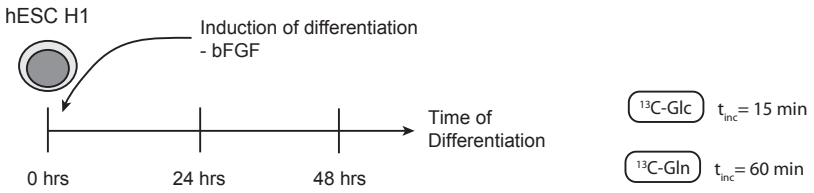


Figure 3.14.: Experimental setup for the analysis of early events in metabolic reprogramming during differentiation of hESC H1 cells. Spontaneous induction of differentiation has been induced by the replacement of cell culture media lacking bFGF. H1 cells were labeled after 0, 24, and 48 hrs with stable isotope substrates: u-$^{13}C$-Glc (15 min) and u-$^{13}C$-Gln (60 min).

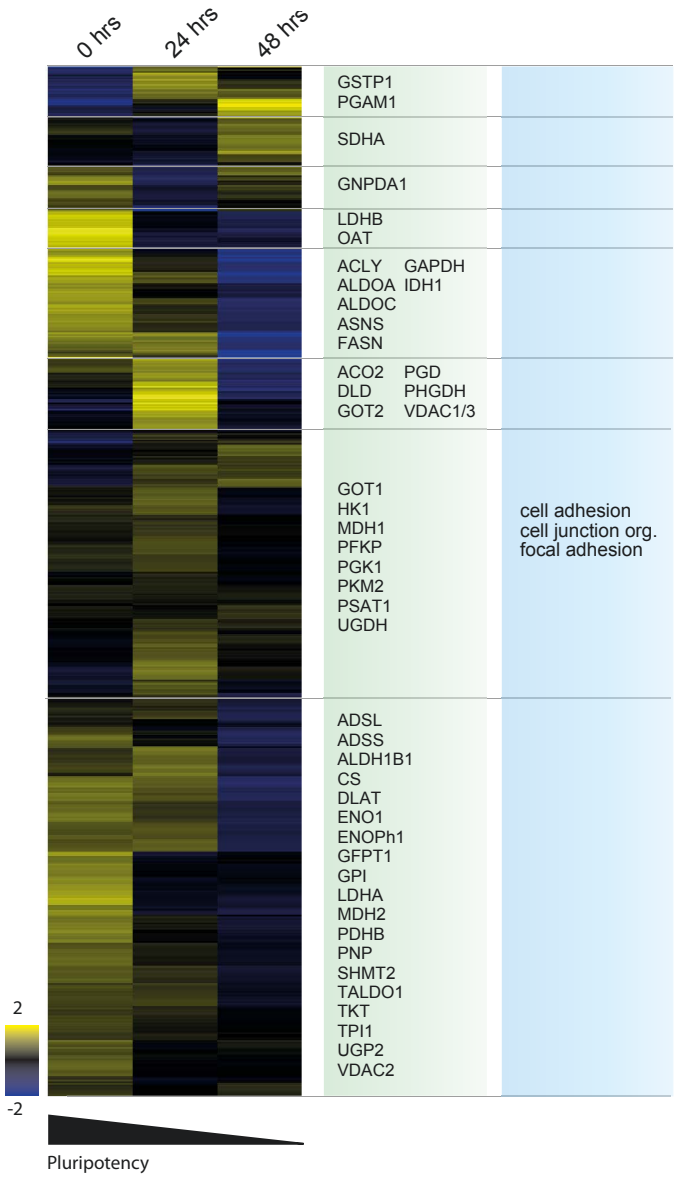


Figure 3.15.: Hierarchical cluster analysis of hESCs H1 during early differentiation. Metabolic enzymes are stated according to their cluster in the green box. Gene ontology enrichment analysis of GOBP are shown in the blue box.

Enzymes involved in glycolysis, TCA-cycle and one-carbon metabolism remained constantly expressed within early differentiation, e.g., ENO1, GPI, MDH2, MTHFD1, PSAT1 (Suppl. Figure B.1). At the same time ribosomal and glycolytic proteins (ALDOA, GAPDH) were enriched in the top50 scoring of proteins with the highest variance of expression during the first 48 hours of early differentiation (Suppl. Table B.12).

The protein expression of glutathione S-transferase P (GSTP1), phoshoglycerate mutase

(PGAM1), and succinate dehydrogenase A (SDHA) increased within the first 48 hours of differentiation. PGAM1 and GSTP1 expression levels were early up-regulated and reached their maximum level already after 24 hours. Protein levels of FASN, LDHB, and ornithine aminotransferase (OAT, m) diminished with onset of differentiation (Figure 3.16-A). The expression of FASN continuously decreased with proceeding differentiation (Figure 3.16-B and C).

The TCA-cycle enzyme IDH1 (c) as well as DUT[1] and NME1[2], two enzymes related to nucleotide and nucleoside triphosphate metabolism, showed significantly increased protein expression levels in hESC H1 before initiation of differentiation.

After 24 hours of differentiation enzyme level of glutaminase synthase raised (GLUL, c/m), catalysing the production of glutamine or 4-aminobutanoate[3] in the cytosol and mitochondria (Figure 3.16-A and C). The quantities of the PDHc subunit PDHA1 and GFPTS[4], a protein regulating the flux of glucose into hexosamine pathway, increased within 48 hours after induction of differentiation.

An intermediate maximum of protein expression has been detected for mitochondrial proteins ACO2, DLD, and GOT2, as well as for PGD, PHGDH, and VDAC1/3 after 24 hours of differentiation (Figure 3.15).

#### 3.1.3.2. Metabolic profile of hESC H1

The hESC H1 metabolic profile has been determined based on GC-MS derived quantities of nine biological replicates; three per $^{13}C$-substrate and experimental time point.

The profile shows a high abundance of amino acids, e.g. threonine, valine, glycine and glutamate (Figure 3.17-A). The pool size of Lac exceeds the quantity of Pyr in hESC H1 cells. Glycolytic phosphates, DHAP and FBP are present in similar concentrations as Lac. All intermediates of the TCA-cyle are low abundant, whereas quantities of Mal and Cit are slightly higher in comparison to the pool sizes of Fum and Suc.

The pool sizes of hESC H1 cells of this setup are in agreement with the previous shown

[1]Deoxyuridine 5'-triphosphate nucleotidohydralase, mitochondrial
[2]Nucleoside diphosphate kinase A, cytoplasm / nucleus
[3]GABA: gamma-aminobutyric acid
[4]Glutamine-fructose-6-phosphate aminotransferase isoenzyme 2

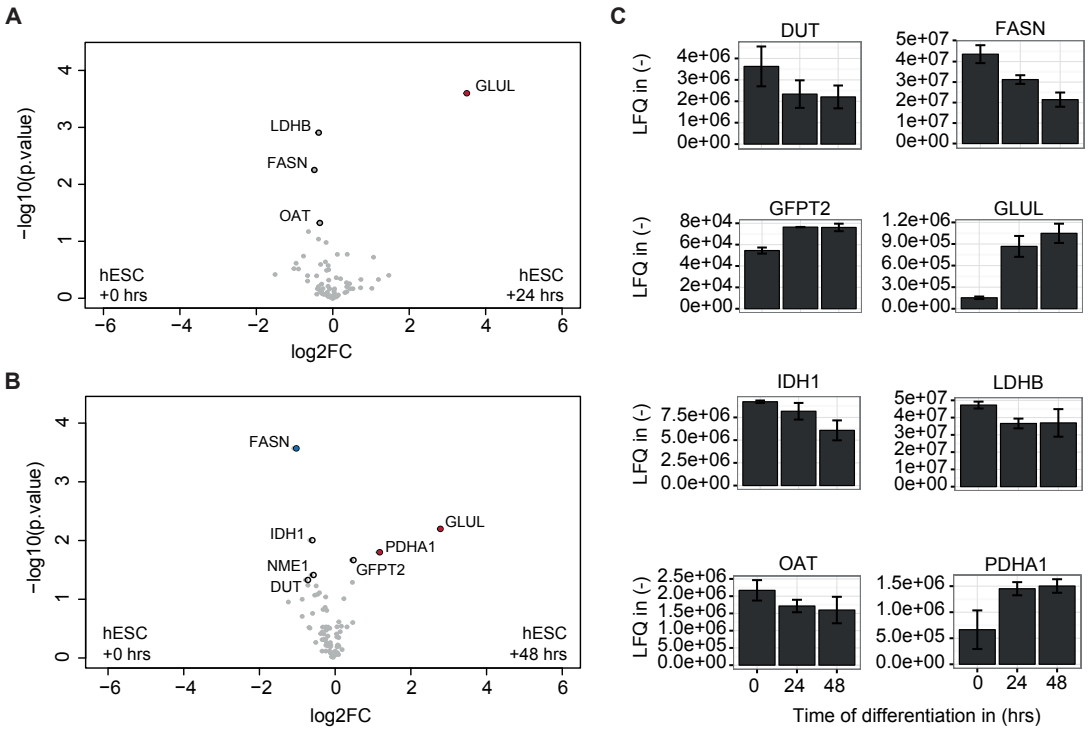


Figure 3.16.: Regulation of CCM-protein expression during early differentiation of hESC H1 cells. (A) Volcano-plot of CCM-associated proteins up-regulated within 24 hrs after induction of spontaneous differentiation of hESC H1 cells. (B) CCM protein expression in native hESC H1 cells and 48 hrs after induction of spontaneous differentiation compared in a volcano plot. (C) LFQ values of selected enzymes during early differentiation of hESCs.

metabolic profiles of pluripotent cells in Section 3.1.1.

#### 3.1.3.3. Regulation of carbon-usage in early differentiation of hESC H1

**$^{13}$C-Glucose** The onset of spontaneous differentiation results in a change of nutrient consumption in hESCs H1. The incorporation of $^{13}C$-Glc remained constant in glycolytic intermediates, e.g., Pyr (75%) and Lac (70%) (Figure 3.17-B).

The incorporation of $^{13}C$-Glc into amino acid and nucleotide synthesis has been reduced within the 48 hours of differentiation. The routing of $^{13}C$-Glc diminished in gluconic acid-6-phosphate (6PGA), and simultaneously increased in GA3P during differentiation (Supp. Table B.14). At the same time the transport of $^{13}C$-Glc into the TCA-cycle intermediates has been elevated with ongoing loss of pluripotency, here shown for Cit and Fum (Figure 3.17-B).

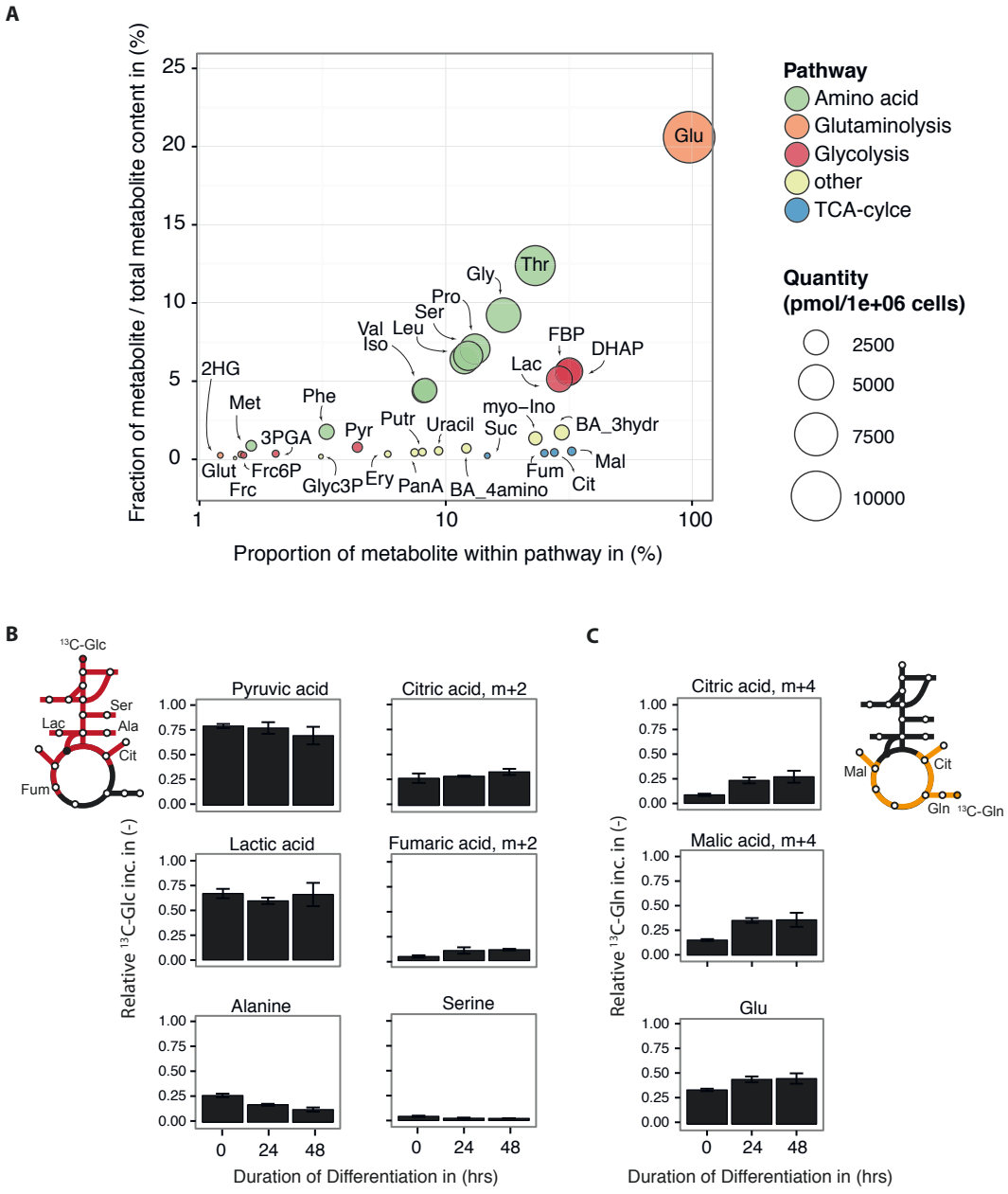


Figure 3.17.: Metabolic profile and nutrient consumption in hESCs H1. (A) Metabolite pool sizes are averaged quantities over the experiment. The area of the circle correlates with the absolute quantity of the metabolite. (B) The incorporation of $^{13}C$-Glc in Pyr and Lac remain constant during the first 48 hours of differentiation. The incorporation of glucose-derived carbons in amino acid synthesis decreases, whereas the import into the TCA-cycle elevates. (C) Differentiation induces an increased import of $^{13}C$-Gln and elevates the turn-over of the TCA-cycle.

**$^{13}$C-Glutamine** Side by side to the rearrangement of glycolysis the uptake and usage of $^{13}C$-Gln has been elevated within the first 48 hours of differentiation, shown by increased incorporation into glutamic acid of 45%. The canonical incorporation of four carbons raises in all TCA-cycle intermediates, shown for Cit and Mal, continuously from 22% to 35% (Figure 3.17-C). Simultaneously, the activity of the reductive TCA-cycle decreased. The incorporation of five carbons derived from $^{13}C$-Gln diminished from 25% to 16% in Cit (Supp. Table B.14). Altogether the induction of differentiation results in an early rearrangement in mitochondrial metabolism characterised by a raise of carbon transport towards oxidative phosphorylation.

### 3.1.4. Neuronal differentiation induced changes in proteome and metabolome

In 2005 Lotharius and colleagues established the LUHMES line (Lund human mesencephalic); a sub-clone of MESC2.10 to investigate dopamine related cell death mechanisms (Lotharius et al., 2005). Experiments in cell cultures provide the molecular manipulation and analysis of an almost homogenous cell population. The post-mitotic state of neurones and thus the absence of proliferation constitute a bottleneck in the molecular analysis of neurones.

The transformation of a proliferating, neuronal precursor cell with the myc oncogene allows the generation of a reasonable number of cells for experiments (Hoshimaru et al., 1996). The application of tetracycline (Tet) abolishes the expression of v-Myc and induces cell differentiation (Scholz et al., 2011). Proliferating, multi-potent Luhmes d0 alter with high conversion rate into post-mitotic neurones (Luhmes d6) (Figure 3.18-A). Within six days of differentiation these cells express markers of A9 dopaminergic neurones, e.g., tyrosine hydroxylase (TH), and dopamine transport (DAT). The loss of dopamine is associated with the progression of Parkinson disease (Figure 3.18-B).

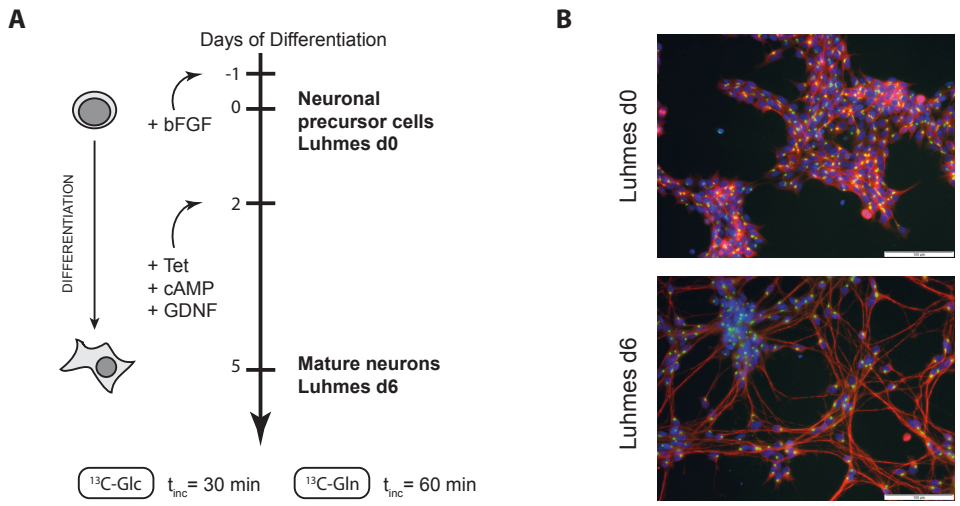


Figure 3.18.: Experimental setup of terminal neuronal differentiation of Luhmes cells. (A) Time line of cell cultivation for differentiation of Luhmes d0 cells into dopaminergic neurons Luhmes d6. (B) Fluorescence microscopy of Luhmes d0 and d6 cells. Green: giantin, blue: all nuclei, red: $\beta$-III-tubulin. Kindly provided by Simon Gutbier, Leist Lab University Konstanz.

Luhmes cells provide a cell culture based model to study the development, progression and biological mechanisms in neuronal cells. In the frame of the thesis both cell type, pluripotent precursor and mature neuronal progenitor, are studied to monitor metabolic reprogramming during terminal, neuronal differentiation. In time course experiments we collected quantitative information about protein expression, metabolite pool sizes and $^{13}C$-substrate incorporation of glucose and glutamine.

#### 3.1.4.1. Neuronal differentiation induced alterations of protein expression

The application of shotgun LFQ proteomics provided the quantification of approx. 6,400 proteins in Luhmes d0 and d6 cells. The hierarchical cluster analysis of four biological replicates revealed cell-line dependent expression of CCM proteins (Figure 3.19). Up-regulated protein levels related to the CCM are shown in the green box for both cell lines. The GOBP enrichment analysis of both cluster is summarised in the blue box.

As expected, expression of neuronal specific proteins associated with GOBP "Parkinson's disease" and "Alzheimer's disease" increased with differentiation in Luhmes d6 cells.

Side to side expression levels of proteins involved in cell proliferation (cyclins, cycline-dependent kinases, nucleotide synthesis) and one-carbon metabolism diminished with differentiation due to the pruning of the cell cycle in non-proliferating neuronal progenitor cells (Suppl. Figure B.2).

Proteins of GOBP classes "oxidative phosphorylation", "decarboxylate and fatty acid metabolism" were enriched in Luhmes d6 cells, e.g., IDH3G, MDH2, and subunits of the PDH complex (PDHc).

The abundance of glycolytic enzymes, e.g., LDHA or GPI, decreased with the differentiation of Luhmes d0 cells. The pluripotent precursor cells expressed high levels of ASNS and ASS1, two enzymes involved in the synthesis of aspartic acid.

Neuronal differentiation induced a switch of isoenzyme expression. Luhmes d0 cells showed high levels of hexokinase 2 (HK2, c), enolase 1 (ENO1, c) and aldolase A (ALDOA, c). With differentiation Luhmes cells acquired an increased protein expression of HK1, ENO2 and ENO3, as well as ALDOC (Figure 3.20-A and B).

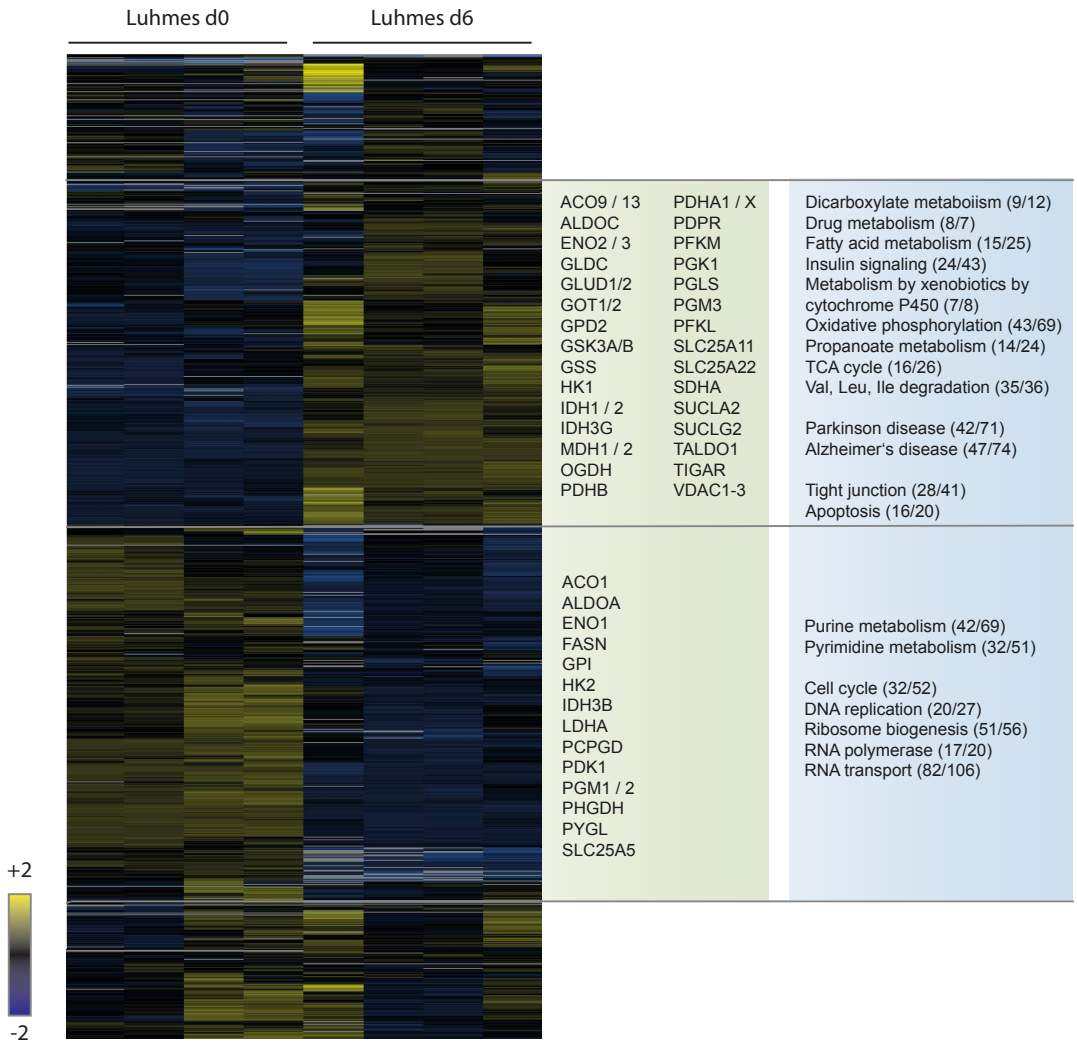


Figure 3.19.: Hierarchical clustering of shotgun proteomics data comparing Luhmes d0 and d6 cells. Green box highlights CCM enzyme expression regarding clustering. The enrichment analysis of GOBP is summarised in the blue box. Numbers in brackets represent number of proteins within the cluster in comparison to the total number of protein per GOBP class in the complete data set.

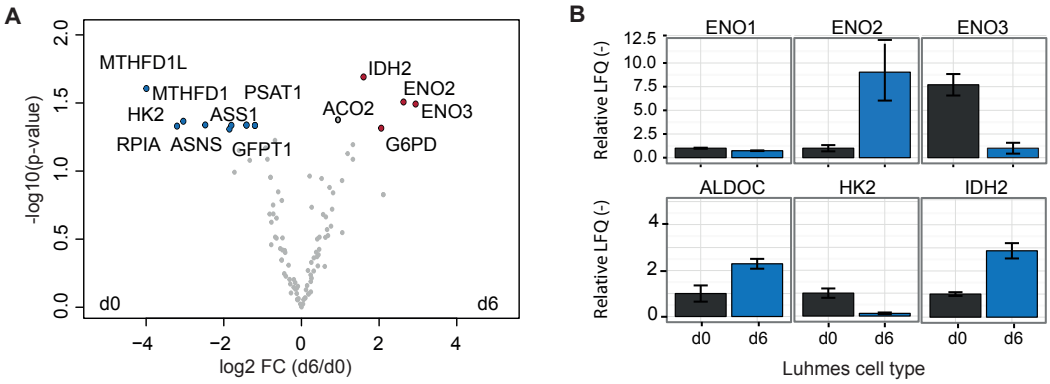


Figure 3.20.: Proteome analysis of CCM-related enzymes in Luhmes d0 and d6 cells. (A) Volcano plot of CCM-related proteins in Luhmes d0 and d6 cells. Protein names are shown for proteins with an absolute fold change $FC >= 2$ and $p - value < 0.05$. (B) LFQ values for selected CCM enzymes comparing protein expression in Luhmes d0 and d6 cells.

The expression of the transporter proteins SLC25A11 and SLC25A22 (mitochondrial glutamate carrier 1) increased in Luhmes d6 cells. SLC25A11 is part of the malate/aspartate shuttle and facilitates the exchange of reducing equivalents between the cytoplasm and mitochondria. Concurrently, levels of MDH1 and MDH2, driving the conversion of malate to oxaloacetate in both cellular compartments, raised with the loss of pluripotency in Luhmes d6 cells.

#### 3.1.4.2. Metabolic profiles of Luhmes d0 and d6 cells

The metabolic profile has been determined as described before. GC-MS derived quantitative measurements are summarised from a time course pSIRM experiment in both cell lines, assuming the metabolic steady state during the experiment. Pool sizes of central carbon metabolism metabolites slightly increased during differentiation from precursor cells into mature neurones (Figure 3.21). Glutamic acid is the most abundant metabolite independently from the cell type.

The metabolic reprogramming has been accompanied by switch in pool sizes of Lac and Pyr. In differentiated cells the pool of Pyr exceeded the quantity of Lac.

Intermediates of the TCA-cylce were low-abundant in precursor and progenitor cells. Their quantitative distribution has not been affected by differentiation, similarly to the compo-

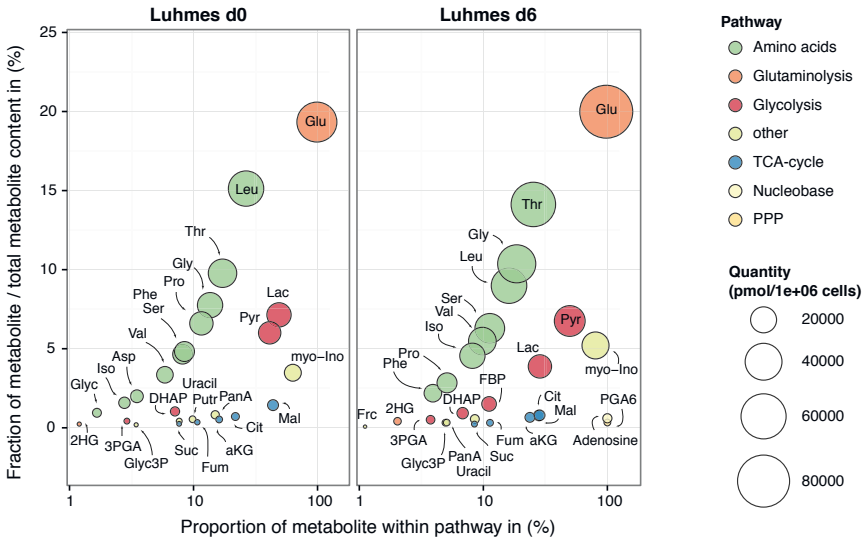


Figure 3.21.: Metabolic profiles of Luhmes d0 and d6 cells. Pool sizes of all metabolite classes slightly increased with differentiation. Metabolic priming reversed the ratio of Pyr and Lac quantities.

sition of amino acids. Threonine, leucine and glycine remained constant with the loss of pluripotency.

### 3.1.4.3. Routing of carbons in neuronal precursor cells and mature neurones

**$^{13}$C-Glucose** The differentiation of Luhmes d0 cells resulted in a reprogramming of substrate uptake. Herein the $^{13}C$-Glc incorporation is compared in both cell types after 30 min of incubation time.

The incorporation of $^{13}C$-Glc in Lac decreased from 20% to 3% with differentiation in Luhmes d6 cells (Figure 3.22-A). At the same time $^{13}C$-Glc incorporation dropped in Pyr and the amino acids Ala and Ser. Also the transport of glucose-derived carbons into mitochondria reduced with the loss of pluripotency, reflected by the decreased of level of two carbon-13 incorporated in citric acid.

The low incorporation levels of $^{13}C$-Glc in Fum did not provide clear information about the turnover of carbons in the TCA-cycle.

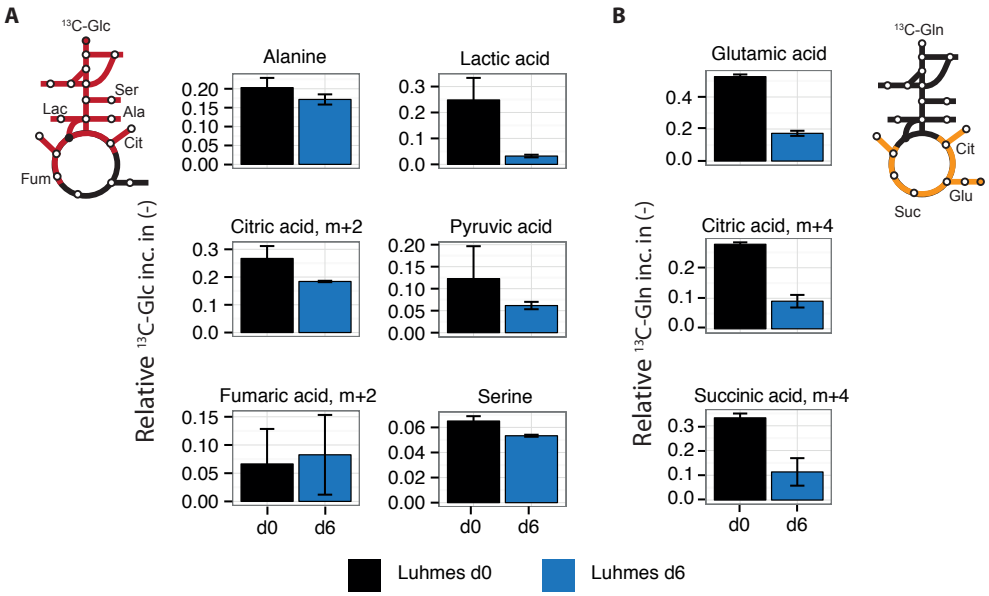


Figure 3.22.: Incorporation of u-$^{13}C$-substrates in Luhmes d0 and d6 cells. (A) The routing of u-$^{13}C$-Glc dropped in intermediates of the glycolysis and TCA-cycle with the acquisition of neuronal characteristics. (B) The utilisation of u-$^{13}C$-Gln decreased with differentiation of Luhmes cells.

**$^{13}$C-Glutamine** Data are shown for $^{13}C$-Gln incubation of 60 min in both cell lines. The uptake rate of glutamine in Luhmes d0 cells was almost twice as high as in Luhmes d6 cells (Figure 3.22-B).

The further canonical processing of $^{13}C$-Gln within the TCA-cylce decreased with differentiation, as shown for succinic and citric acid. Concurrently, the reductive incorporation of glutamine-derived carbons into Cit was reduced in Luhmes d6 cells.

## 3.2. Phenotype specific features of proteome and metabolome of pluripotent, cancer and differentiated cells

The previous section introduced the single projects and their results regarding protein expression, metabolite pool sizes and nutrient consumption. Every project focuses on an aspect of metabolic reprogramming induced by the gain or loss of pluripotency and how this transition affects the central carbon metabolism and its intermediates.
The following section summarises all obtained data. Cell lines are categorised regarding their phenotypic state into cancer cells, hESCs, iPS cells, fibroblasts and derived fibroblasts (DF). The integration of all data creates a powerful data matrix to identify cell status specific patterns in the proteome and metabolome. It also provides a comparison of native and reprogrammed CCM: hESCs vs. iPSCs, and fibroblasts vs. derived fibroblasts.
The separate analysis of protein expression (Section 3.2.1) and metabolite abundance (Section 3.2.2) follows the comparison of carbon routing into pyruvic acid and citric acid in Section 3.2.3. Both metabolites represent a hub of multiple pathways in the CCM. Ultimately, two aspects of pluripotent metabolism — one-carbon metabolism and the metabolite 2-hydroxyglutaric acid (2HG) — are summarised in Section 3.2.4.

### 3.2.1. Phenotype-dependent protein expression in cancer, hESCs, iPS cells and their derivates

Project-specific analysis of protein expression showed a phenotype dependent expression of enzymes and their isoforms. LFQ protein quantities were summarised regarding their phenotype for the identification of phenotype-specific expression of isoenzymes of cancer cells, hESCs, iPS cells, fibroblasts or derived fibroblasts (Supp. Table C.1). Therefore protein quantification derived from all introduced projects were summarised in a single matrix and z-score transformed within the experiments as described in Section 2.5.
Expression levels were classified regarding their z-score in up-regulated ($z-score > 0.5$) and down-regulated ($z-score > -0.5$) proteins. Individual and common proteins within

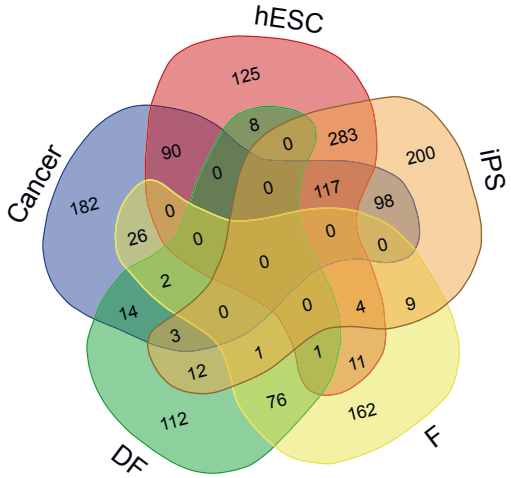


| hESC, iPS | 283 |
|---|---|
| Ribosome | 35 |
| Spliceosome | 26 |
| Metabolic pw | 34 |
| Purine metabolism | 13 |
| RNA degradation | 9 |
| Ribosome biogenesis | 8 |
| Pyrimidine metabolism | 8 |
| RNA transport | 9 |
| mRNA surveillance | 6 |
| aminoacyl-tRNA biosynthesis | 5 |

| Cancer, hESC, iPS | 117 |
|---|---|
| RNA transport | 17 |
| Spliceosome | 12 |
| DNA replication | 5 |
| Ribosome biogensis | 5 |
| Cell cycle | 5 |
| Purine metabolism | 5 |
| Nucleotide excision repai | 3 |
| Proteasome | 3 |
| Ub. mediated proteolysis | 4 |
| One carbon pool by folate | 2 |

| Cancer, iPS | 98 |
|---|---|
| Spliceosome | 10 |
| Proteasome | 7 |
| mRNA surveillance | 7 |
| RNA transport | 6 |
| Ribosome | 5 |
| Metabolic pw | 12 |
| TCA cycle | 3 |
| Protein proc. in ER | 4 |
| One carbon pool by folate | 2 |
| Ribosome biogenesis | 3 |

| Cancer, hESC | 90 |
|---|---|
| RNA transport | 11 |
| DNA replication | 7 |
| Ribosome bioge | 6 |
| Cell cycle | 6 |
| Mismatch repair | 3 |
| mRNA surveillance | 4 |
| Nucleotide excision repair | 3 |
| Spliceosome | 4 |
| Homologous recomb. | 2 |
| Ub. mediated proteolysis | 3 |

| Cancer, Fibroblast | 26 |
|---|---|
| Shigellosis | 3 |
| Leukocyte migration | 3 |
| Focal adhesion | 3 |
| Reg. actin cytoskeleton | 3 |
| Amino sugar and nucleoside sugar metabolism | 2 |
| Adherens junction | 2 |
| Ventr. cardiomyoitis | 2 |
| Axon guidance | 2 |
| Osteoblast differentiation | 2 |
| Wnt signaling pw | 2 |

| Fibroblast, Derived Fibroblast | 76 |
|---|---|
| Protein proc. in ER | 11 |
| Focal adhesion | 8 |
| Lysosome | 7 |
| Phagosome | 7 |
| Reg. of actin cytoskeleton | 6 |
| Path. e.coli infection | 4 |
| Fc-gamma R-med phagocytosis | 4 |
| Bac. invasion of epith. cells | 3 |
| Shigellosis | 3 |
| Antigen proc.and pres. | 3 |

Figure 3.23.: Venn diagram of protein expression comparing the data regarding the phenotype. LFQ data were normalised within each setup and combined after z-score transformation. The diagram shows the number of proteins with increased expression levels ($z-score\ > 0.5$) shared between the cell types. KEGG pathway analysis of intersections has been performed at www.webgestalt.org.

the five classes are shown in a Venn diagram[5] (Figure 3.23 and Suppl. Figure C.1). KEGG pathway analysis has been performed for each intersection[6].

The most notable overlaps are: (i) Cancer, hESCs and iPS cells share 117 proteins involved in cellular biosynthesis, e.g., proteins associated with RNA transport (17), spliceosome (12), cell cycle (5) and purine metabolism (13).

Furthermore, (ii) the intersection of hESCs and iPS cells is composed of 283 proteins that are related to, e.g., ribosome (35), spliceosome (26), metabolic pathways (34) and cell proliferation. The individual sections of both classes contain fewer proteins in comparison to their joint sections.

In contrast (iii) native and derived fibroblasts share less enzymes (76) indicating an in-

[5]VIB, www.bioinformatics.psb.ugent.be, Belgium
[6]www.webgestalt.org, Netherlands

dividual, phenotype specific protein expression. Shared proteins are related to protein processing in the endoplasmatic reticulum (11), focal adhesion (8), and regulation of actin cytoskeleton (6). Interestingly, whereas the intersections of hESCs and iPS cells or cancer and iPS cells share proteins associated with metabolic pathways, cancer and hESCs do not have proteins of this KEGG pathway in common.

Cancer, hESCs, and iPS cells grouped together in the hierarchical clustering of CCM-related proteins as well (Figure 3.24-A). The second cluster is composed of native fibroblast and derived fibroblasts. A list of proteins considered as CCM-specific, including details regarding pathway association, localisation and Uniprot ID, is provided in the supplemental material (Supp. Table B.1). The clustering has been performed on the basis of z-scores as described previously.

The expression in hESCs dominates the row clustering. The top cluster contains CCM isoenzymes that showed a reciprocal protein expression in pluripotent (hESCs, iPS cells) and differentiated cells (F, DF). The expression of glycolytic enzymes (LDHB, PFKM, ENO1, MDH1, GOT1, PGAM1), proteins of the TCA-cycle (IDH3A, ME2, OGDH, GOT2, DLAT and IDH1), and one-carbon metabolism associated enzymes (PHGDH, MTHFDL, PSAT1) were elevated in hESCs and iPS cells and reduced in native and derived fibroblasts.

The most distant cluster contains CCM proteins with increased levels in cancer cells, fibroblasts and reduced expression in hESCs and iPS cells, e.g., ALDOA, PKM1, ME1, and pentose phosphate pathway related protein G6PD. Also the isoform LDHA is part of this cluster; in contrast to the expression of the isoform LDHB (Figure 3.24-B).

A similar switch of isoenzyme expression has been shown for PKM1, PKM2 and for the isoenzymes MDH1 and MDH2. Pluripotent cells did not express a specific isoenzyme of PKM. Increased levels of PKM1 were detected in differentiated cell lines, whereas PKM2 levels were elevated across all cancer cell lines.

The mitochondrial enzyme MDH2 has been associated with a cluster of proteins that are up-regulated in iPS and cancer cells, but less expressed in hESCs and fibroblasts. Further TCA-cycle enzymes are located in this cluster, e.g., CS, SUCLA1, SUCLG1, ACO2,

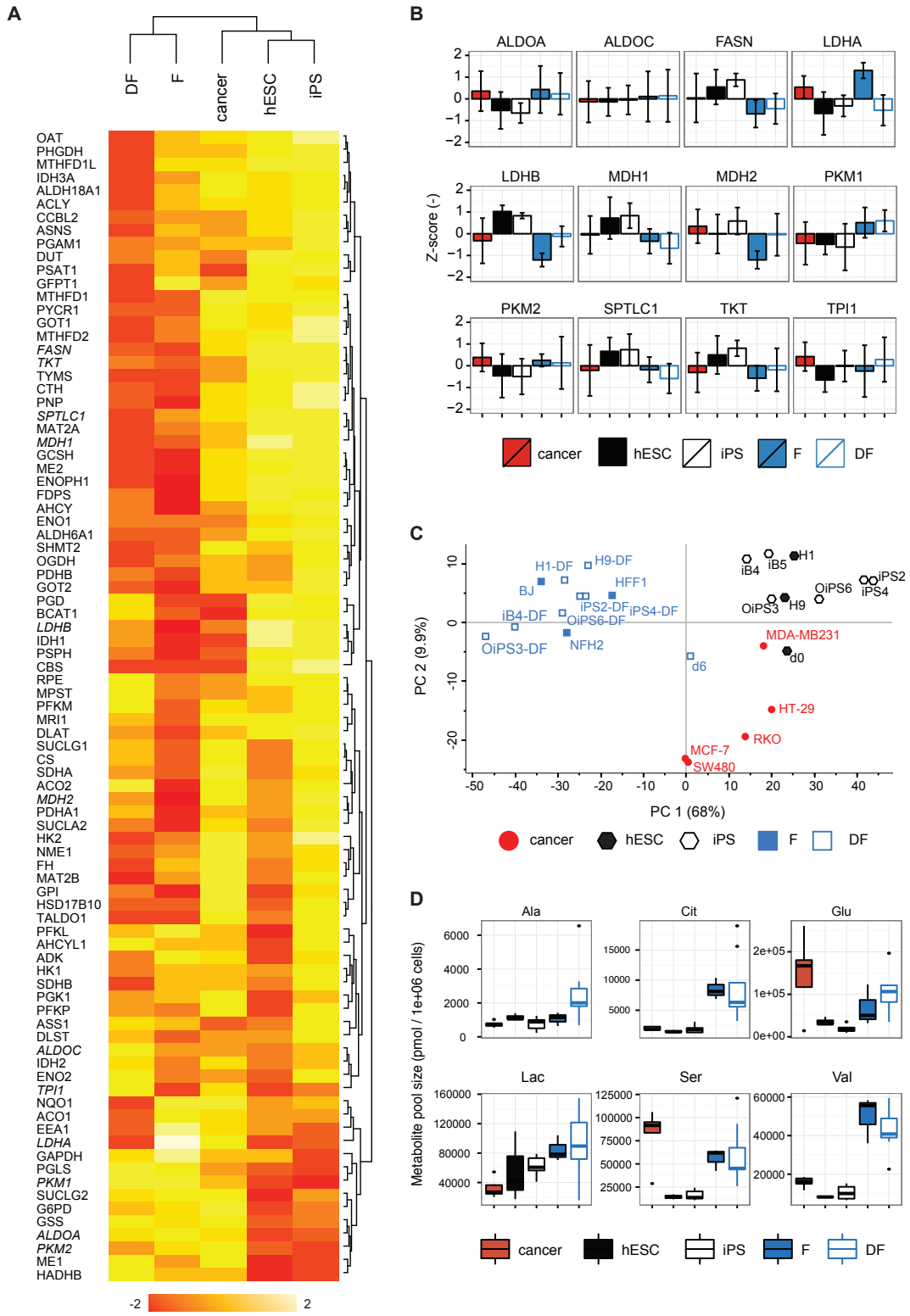


Figure 3.24.: Integrative analysis of cell-state specific protein expression and metabolite abundance. *Continued on next page.*

Figure 3.24.: *Continued from previous page.* (A) Hierarchical clustering of CCM protein expression averaged for cell states: cancer cells, human embryonic stem cells (hESCs), induced pluripotent (iPS) cells, fibroblasts (F), and derived fibroblasts (DF). Italic written protein names refers to proteins mentioned in the text. (B) Z-scores of selected proteins derived from the cluster analysis. (C) Phenotypes are distinguishable by principal component analysis (PCA) of 22 absolute quantified metabolite pools. (D) Quantities of selected metabolites that are contributing to the clustering in the PCA.

PDHA1, and FH. Also the levels of the mitochondrial associated isoenzyme HK2 and TALDO1 were increased in cancer and iPS cells only. A more detailed analysis of related reactions may gain new insights how to interfere with tumorigenesis.

### 3.2.2. Quantification of CCM metabolites

The integrative analysis of the proteomics data showed a clear separation between potent and differentiated cells. In a similar manner quantitative information of 27 metabolites have been combined for the integrative analysis of 24 cell lines. Absolute pool sizes were derived from the metabolic profile of each cell line and summarised multiple compound derivates. Only metabolites detected in every cell line have been considered and rank-normalised within all samples prior the analysis (Suppl. Tables C.2 and C.3).

The principal component analysis provided a clear separation of the samples according to their phenotype (Figure 3.24-C). The first principal component PC1 separates potent (cancer, hESCs, iPS cells) and differentiated cells (F, DF), and explains 68% the variance in the data. Only the Luhmes d6 cell line, the terminal dopaminergic neuronal cells, is not member of that cluster in the PCA.

Pool sizes of Lac, Ala and Val are responsible for the separation on the PC1, as shown in the loadings plot (Supp. Figure C.2). Cancer, hESCs and iPS cells are characterized by high levels of Lac and Ala, and differentiated cells contain high levels of Val, in relation to their general metabolic content (Figure 3.24-D).

Mainly the high levels of Ser and Glu in cancer cells cause the division of pluripotent cells and cancer cell on the second principal component PC2 and accounts for 10% of the data variance. The breast cancer cell line MDA-MB231 and Luhmes d0 cell line are located close to the border of the “pluripotent” and “cancer sector” in the PCA, indicating shared

features of both cells metabolic profile.

### 3.2.3. Regulation of hubs in the central carbon metabolism

#### 3.2.3.1. Routing of $^{13}C$-pyruvic acid — gluconeogenesis versus oxidative phosphorylation

Pyruvic acid (Pyr) is the end product and most "energy expensive" metabolite of glycolysis. It is either converted into lactic acid (LDH, c), transaminated into alanine (GPT, c), or transported into mitochondria. Two complexes facilitate the import of Pyr across the mitochondrial membrane (Figure 3.25-A). The voltage-dependent porin complex (VDAC1) transfers Pyr through the outer mitochondrial membrane (OMM); the heterotetrameric complex of mitochondrial pyruvate carrier (MPC1 / MPC2) enables the import across the

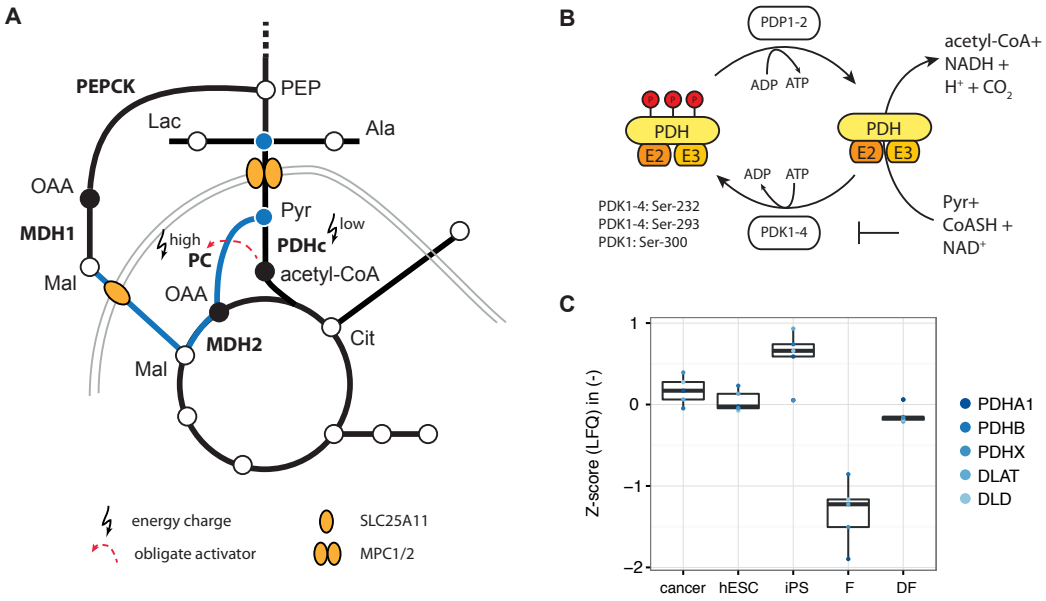


Figure 3.25.: Fate of pyruvic acid in central carbon metabolism. (A) Pyruvate enters the TCA-cycle via acetyl-CoA, facilitated by pyruvate dehydrogenase complex (PDHc). At high energy charge states Pyr fuels gluconeogenesis driven by pyruvate carboxylase (PC). (B) Regulation of the PDH complex by pyruvate dehydrogenase kinases (PDK) and phosphates (PDP). Accumulation of PDHc substrates inhibit the phosphorylation of PDKs. (C) Z-scores of PDHc subunits summarised for cell phenotypes. Z-scores have been determined as described before from the global analysis of LFQ protein expression.

inner mitochondrial matrix (IMM).

In the mitochondria Pyr is either directed into gluconeogenesis or enters the TCA-cycle depending on the energy charge of the cell. At high cellular energy charges the enzyme pyruvate carboxylase (PC) converts Pyr into oxaloacetate (OAA), respectively malic acid (Mal) that is transported into the cytoplasm by SLC25A11 and fuels gluconeogenesis. PC is a member of ABC proteins and requires ATP, Biotin, and $CO_2$ as cofactors for the synthesis of OAA. It is also one of two enzymes that requires an obligate activator — acetyl-CoA. Low energy charges, reflected in low acetyl-CoA levels, inactivate PC and Pyr is solely converted into acetyl-CoA by the Pyruvate dehydrogenase complex (PDHc) and subsequently into Cit by Citrate synthase (CS).

The regulation of the PDHc defines the transport of carbons in glycolysis, gluconeogenesis, fatty acid oxidation, and the TCA-cycle. The complex itself consists of multiple copies of three enzymes: Pyruvate dehydrogenase (PDH, E1, 30 subunits), Dihydrolipoyllysine-residue acetyltransferase (DLAT, E2, 60 subunits) and Dihydrolipoyl dehydrogenase (DLD, E3, 12 subunits). The synthesis of acetyl-CoA catalysed by PDHc requires the cofactors CoA, NAD+, FAD+, lipoic acid and thiamine pyrophosphate (TPP). Substrate and product level influence the activity of PDHc by the regulation of Pyruvate dehydrogenase kinases (PDK1–4).

High levels of NADH, ATP and acetyl-CoA activate PDKs, and decrease the PDHc activity by sustaining the phosphorylation at Ser-232, Ser-292, and Ser-300. Although the phosphorylation of a single residue results in the deactivation of PDHc, only the complete dephosphorylated protein resumes its catalytic activity. Substrate and products pools of PDHc allosterically inhibit or activate PDKs (Figure 3.25-B).

Shotgun proteomics provides quantitative information about PDHC subunits: PDHA, PDHB, PDHX, DLAT, and DLD. Native and derived fibroblasts express lower levels of all subunits in comparison to cancer, hESCs and iPS cells (Figure 3.25-C). Regulators of PDHc activity, i.e., PDKs and PDPs, were not detectable in the measurements. Solely, PDK1 has been detected in Luhmes d0 and d6 cells; with reduced levels in the neuronal progenitor cells after cell differentiation.

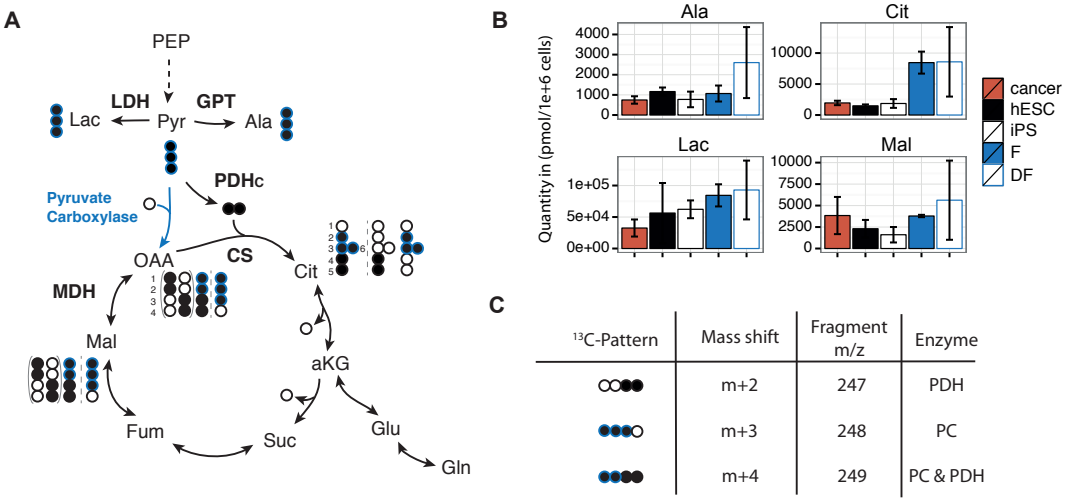


Figure 3.26.: Routing of pyruvate-derived carbons in central carbon metabolism. (A) Isotope pattern in TCA-cycle intermediates. (B) Pool sizes of intermediates derived from pyruvic acid. (C) Incorporation pattern of carbon-13 in malic acid reflects enzyme activities of PDHc and PC.

The application of stable isotope labeled substrates provided an indirect measurement of the metabolic flux. Depending on enzyme activities different numbers of carbons were directed into down-stream intermediates. The GC-MS based metabolomics approach enabled the carbon-resolved analysis and thereby the monitoring of carbon routing within the CCM (Figure 3.26-A).

The incubation of cell cultures with $^{13}C$-Glc and $^{13}C$-Pyr, itself a product of glucose breakdown, induces identical mass shifts in the GC-MS spectra of Lac, Ala, Mal, and Cit. An individual incorporation rate in these metabolites would point towards a nutrient-specific usage of carbons. The pattern of isotope incorporation gain first insights about enzyme activities contributing to the synthesis of malic acid (Figure 3.26-C).

As described before, metabolite pool sizes were cell type depend. Quantities of Ala, Cit, and Mal in differentiated cells were larger than in iPS, hES and cancer cells, although the data display a huge variance in all four intermediates in derived fibroblasts (Figure 3.26-B). Levels of Ala and Lac were lower in cancer cells in comparison to pluripotent cells, whereas the pool of Mal exceeded stem- and iPS cell quantities.

Radarcharts provide the visual comparison of fractions between different samples, i.e.,

different cell lines. Figure 3.27 summarises the $^{13}C$-incorporation in cancer vs. pluripotent cells, respectively native and derived fibroblasts vs. iPS cells. Each axis of the radar shows the fraction of $^{13}C$-Glc (Figure 3.27-A) or $^{13}C$-Pyr (Figure 3.27-B) incorporation per metabolite. Cross braces are equidistant and represent an increase of 0.1, respectively 0.02 units, while a value of 1 corresponds to 100% carbon-13 incorporation.

The incorporation of different numbers of carbon-13 in Mal reflects enzyme activities of PC and PDHc, giving a measure of the carbon routing towards TCA-cycle and gluconeogenesis (Figure 3.27-C).

The incorporation patterns have been almost overlapping in either hESCs and iPSCs, or fibroblasts and derived fibroblasts; independently from the $^{13}C$-substrate. Each cell type showed a specific routing of glucose- and pyruvate-derived carbons. The majority of both substrates were directed into the synthesis of lactic acid in pluripotent and cancer cells. Also differentiated cells directed the bulk of $^{13}C$-Pyr into lactic acid, whereas glucose-derived carbons fueled equally the aerobic glycolysis, alanine synthesis and mitochondrial metabolism. Cancer cells incorporated similar levels of $^{13}C$-Glc into citric acid, as well as of $^{13}C$-Pyr in Mal and Cit, to differentiated cells.

The comparison of $^{13}C$-Glc and $^{13}C$-Pyr labeled quantities demonstrated the nutrient-dependent contribution to the synthesis of down-stream intermediates (Figure 3.27-C). Especially the labeled quantities derived from $^{13}C$-Pyr increased in differentiated cells.

#### 3.2.3.2. Citric acid — integrating carbon routing in the mitochondria

The condensation of acetyl-CoA and oxaloacetic acid (OAA) to citric acid (Cit) by citrate synthase (CS, m) represents the first reaction of the TCA-cycle and is responsible for the strong forward orientation (clockwise) of the cycle (standard free energy -8 kcal/mol). The enzymes PDHc and PC are highly regulated as described in the Section (Section 3.2.3.1). Depending on the cell energy status either the gluconeogenic PC or the PDH complex shuttles carbons derived from pyruvic acid into citric acid (Figure 3.28-A). Two carbon-13 C#4–5 are incorporated in citric acid by the PDHc. Active PC transports four carbon-13 into citric acid — C#1–3,6 (Figure 3.28-C).

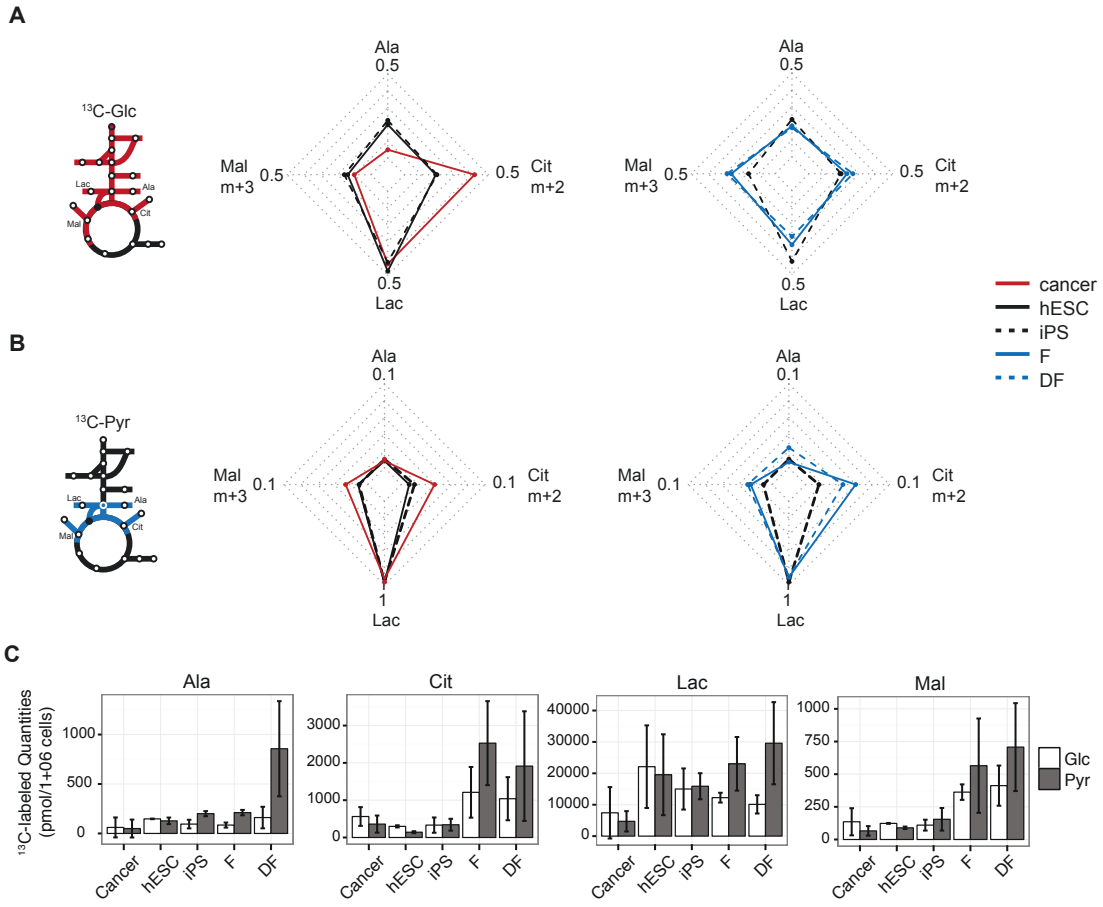


Figure 3.27.: Comparison of $^{13}C$-Glc and $^{13}C$-Pyr incorporation at the hub of glycolysis, TCA-cycle, and amino acid synthesis. (A) $^{13}C$-Glc incorporation is similar in native and their reprogrammed pluripotent or differentiated counterparts. Cancer cells show an increased incorporation of glucose-derived carbons into citric acid. (B) Conversion of $^{13}C$-Pyr is different in comparison to glucose incorporation in all cell types, but also reprogrammable. (C) $^{13}C$-Glc and $^{13}C$-Pyr contributed in a different manner to the synthesis of alanine, citric acid, lactic acid, and malic acid.

Besides glucose glutamine is used to replenish oxidative phosphorylation. After the conversion of glutamine into glutamic acid (Glu) carbons enter the TCA-cycle in form of alpha-ketoglutaric acid (aKG). Subsequently aKG is either further converted via the canonical oxidative way into succinic acid and fumaric acid or carboxylated into citric acid by the reverse action of isocitrate dehydrogenase (IDH) (Figure 3.28-B). The canonical way results in the incorporation of four carbon-13 (C#1–3,6) into citric acid, analogous to glucose-derived carbons via PC activity. The reductive synthesis of citric acid is accom-

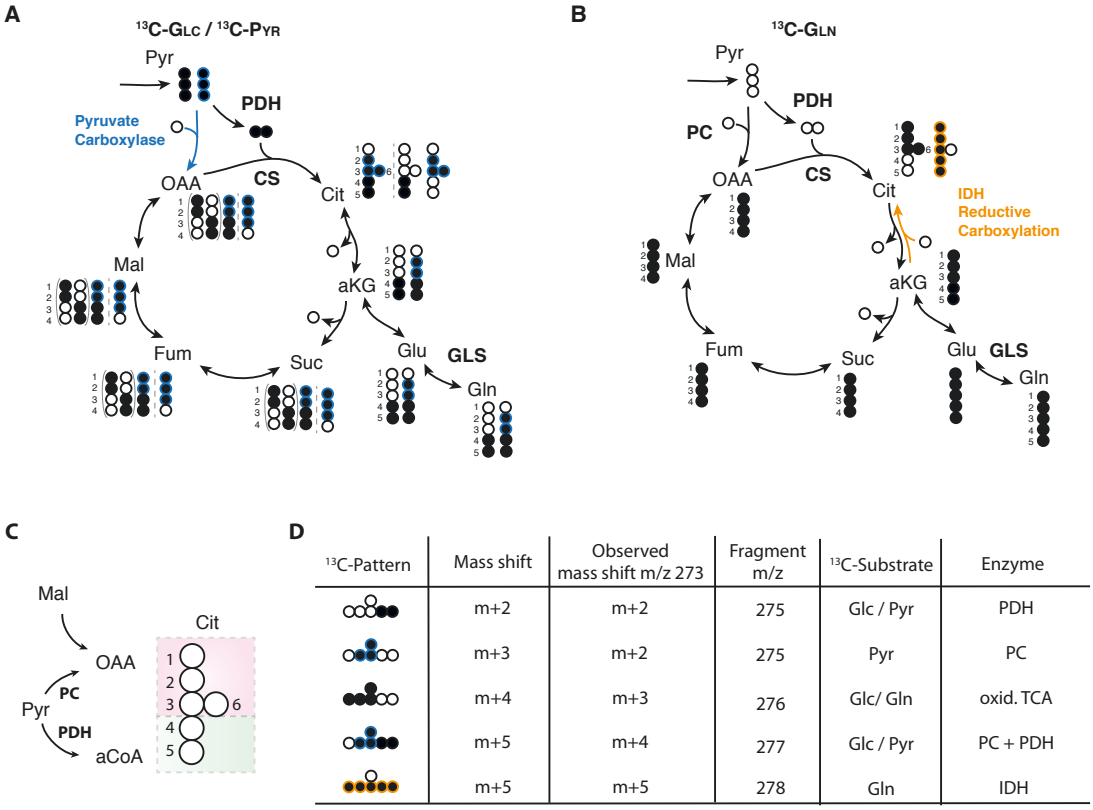


| 13C-Pattern | Mass shift | Observed mass shift m/z 273 | Fragment m/z | 13C-Substrate | Enzyme |
|---|---|---|---|---|---|
| | m+2 | m+2 | 275 | Glc / Pyr | PDH |
| | m+3 | m+2 | 275 | Pyr | PC |
| | m+4 | m+3 | 276 | Glc/ Gln | oxid. TCA |
| | m+5 | m+4 | 277 | Glc / Pyr | PC + PDH |
| | m+5 | m+5 | 278 | Gln | IDH |

Figure 3.28.: Stable isotope tracing of $^{13}C$-substrates in TCA-cycle intermediate citric acid. (A) Incorporation of glucose- or pyruvate-derived carbons in TCA-cylce intermediates via pyruvate carboxylase (PC) and pyruvate dehydrogenase complex (PDHc). (B) Oxidative and reductive incorporation of $^{13}C$-Glu. (C) Substrates of citric acid and their precursors. (D) Isotope pattern in citric acid after labelling with $^{13}C$-substrates and their corresponding mass shifts in the fragment m/z 273.

panied by the incorporation of five carbon-13 (C#1–5) in the carbon backbone.

The detectable isotope pattern in citric acid depends on the applied $^{13}C$-substrate and enzyme activity. Fragment information, mass shifts and corresponding enzymes are summarised in Figure 3.28-D.

The fragment m/z 273 of citric acid has been used for the determination of carbon-13 incorporation. The fragment contains the carbon C#1–5 and lacks C#6 as shown in the fragment analysis in Section 3.3. Therefore the observed mass shift differs from the actual incorporated carbons as shown in Figure 3.28.

The variety of pathways providing the synthesis of citric acid enables diverse regulatory

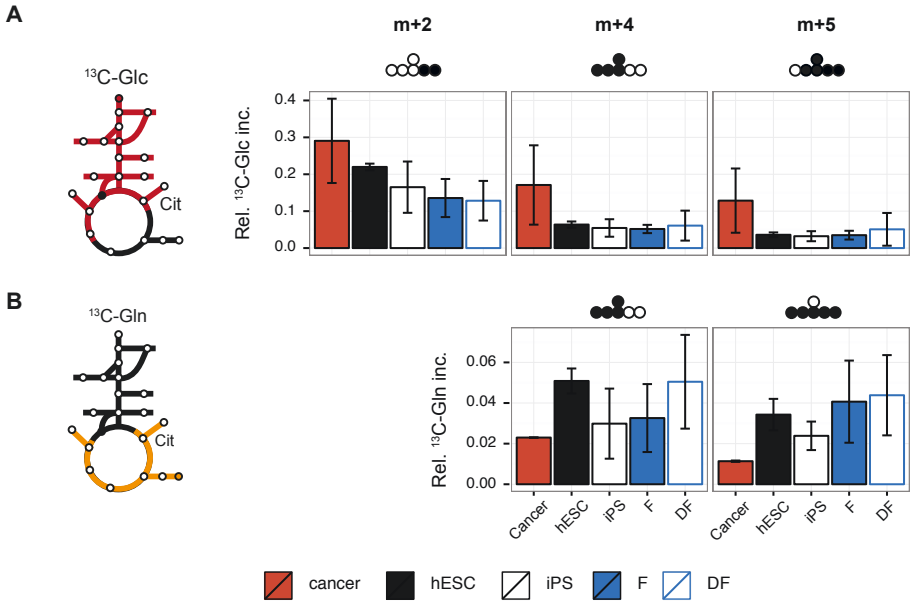


Figure 3.29.: Incorporation of $^{13}C$-substrates in citric acid in pluripotent, cancer and differentiated cells. Incorporation values are determined based on the intensities of fragment m/z 273, lacking the C6 of the carbon backbone. (A) Cancer cells show an increased routing of glucose-derived carbons via PDH complex (m+2) and a high turnover of carbons (m+4) within the TCA-cycle. In addition PC shuttles carbons into the cycle, reflected in the increased incorporation at m/z 273 (m+5). (B) Human ESCs and derived fibroblasts use glutamine to replenish the TCA-cycle in canonical (m+4) and reductive (m+5) manner.

mechanisms. Next to its role in the TCA-cylce citric acid is an important precursor for the synthesis of fatty acids. The citrate-malate shuttle (SLC25A1) transports citric acid across the mitochondrial membrane into the cytoplasm, where it is converted by the enzyme ATP-citrate synthase (ACLY) into OAA and acetyl-CoA. Increasing cytosolic pools of citric acid activates acetyl-CoA carboxylase (ACC) that produces manolyl-CoA, a required substrate of lipid synthesis. At the same time high cytosolic levels of citric acid inhibit the rate-limiting enzyme of glycolysis — phosphofructokinase (PFKM / PFKL).

The import of glucose-derived carbons via acetyl CoA into the mitochondria has been slightly higher in cancer and the pluripotent cells in comparison to differentiated cells (Figure 3.29-A). Although the incorporation at m/z 273 $m+2$ did not distinguish OAA- and acetyl-CoA-derived carbons *per se*. In the previous section it has been shown, that both cell types prefer to direct carbons into citric acid synthesis via PDHc. In additional

the PC reaction is only active on top of an active PDHc, due to obligatory acetyl-CoA level that activate PC. The cycling within the TCA-cycle has been elevated in cancer cells in comparison to hESCs, iPS cells and fibroblast (m+4). The simultaneous activity of PDHc and PC resulted in an increased incorporation of five carbon-13 (m+5), present in cancer cells and more variable in derived fibroblasts.

The consumption of glutamine and its oxidative conversion have been elevated in hESC cells and derived fibroblasts (Figure 3.29-B). Interestingly, the reductive routing of $^{13}C$-Gln has been low in cancer cells, and increased in hESCs, and as well as in native and derived fibroblasts. Though the incorporation rate in all cells was below 10%. The expansion of $^{13}C$-Gln labelling in further experiments may help to gain more insights how glutamine replenished the TCA-cycle.

### 3.2.4. Pluripotency specific aspects

#### 3.2.4.1. One-carbon metabolism

The central carbon metabolism provides in the first place building blocks for biosynthesis and cellular maintenance. Glycolysis, TCA-cycle and pentose phosphate pathway synthesise the majority of those precursors. The revival of the Warburg effect and the impact of tumour suppressors and oncogenes on metabolic enzymes provoked also a re-evaluation of the one-carbon metabolism.

Three interconnected cycles — folate, methionine, and transulfuration cycle — integrate the cellular nutrient status into the production of several compounds that are required for macromolecule synthesis, e.g., for the synthesis of proteins, lipids, nucleic acids and co-factors.

Serine, glycine and threonine provide the majority of carbons for the reactions based on chemical conversion of folate compounds that are highly available in western diets. The

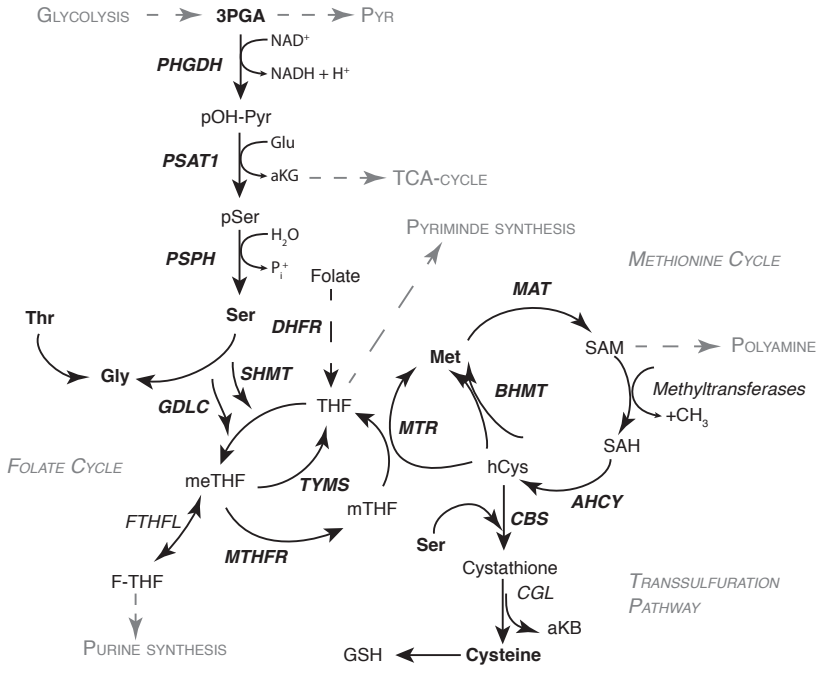


Figure 3.30.: Pathway scheme of one-carbon metabolism adapted from Locasale (2013). Bold intermediates have been quantified either by LC-MS/MS or GC-MS.

donation of single carbon units from one amino acid to another is the principle of the one-carbon metabolism, shown in Figure 3.30.

The imported folate is reduced to tetrahydrofolate (THF) and converted by serine hydroxymethyl transferases (SHMT) into me-THF. Subsequently me-THF[7] is either utilised by methylenetetrahydrofolate reductase (MTHFR) for the synthesis of mTHF[8], or transformed into F-THF[9], a precursor required for purine synthesis.

The demethylation of mTHF donates the carbon to the methionine cycle that starts with the condensation of homocysteine and mTHF into methionine. Methionine adenyltransferase (MAT) produces S-adenosylmethionine (SAM) that is subsequently demethylated by methyltransferases providing methyl-groups for the epigenetic modification of histones, DNA, and RNA. The third cycle, the transsulfuration pathway, is connected by the fusion of homocysteine and serine into cystathionine that can be converted by cystathionine lyase (CGL) to $\alpha$-ketobutyrate (KB) and cysteine. Latter one is an important substrate for the synthesis of glutathionine and taurine.

The *de novo* synthesis of serine derived from 3PGA connects glycolysis and the one-carbon metabolism. Three enzymes facilitate the conversion of 3PGA into serine — PHGDH, PSAT1, and PSPH. Studies have shown, that up to 10% of the 3PGA pool is used for the generation of serine in cancer cells (Amelio et al., 2014). The expression of PHGDH is up-regulated in triple-negative breast cancer cell lines and melanoma cells. The second enzyme PSAT1 requires glutamate as a cofactor and produces aKG, that replenishes the TCA-cycle. It has been shown that the synthesis of serine from 3PGA might be responsible for up to 50% of TCA-cycle intermediates (Amelio et al., 2014).

A one-step conversion from glycine into serine is facilitated by the enzyme serine hydroxymethyl transferase (SHMT). Two isoenzymes exist in mammalian cells: SHMT1 is located in the cytoplasm, SHMT2 in the mitochondria. A splice variant of SHMT2 lacking the peptide for the mitochondrial import remains in the cytoplasm and is capable to compensate SHMT1-deficiency. Imported glycine could also enter the one-carbon metabolism

[7] 5,10-methylene-tetrahydrofolate
[8] 5-methyltetrahydrofolate
[9] 10-Formyltetrahydrofolate

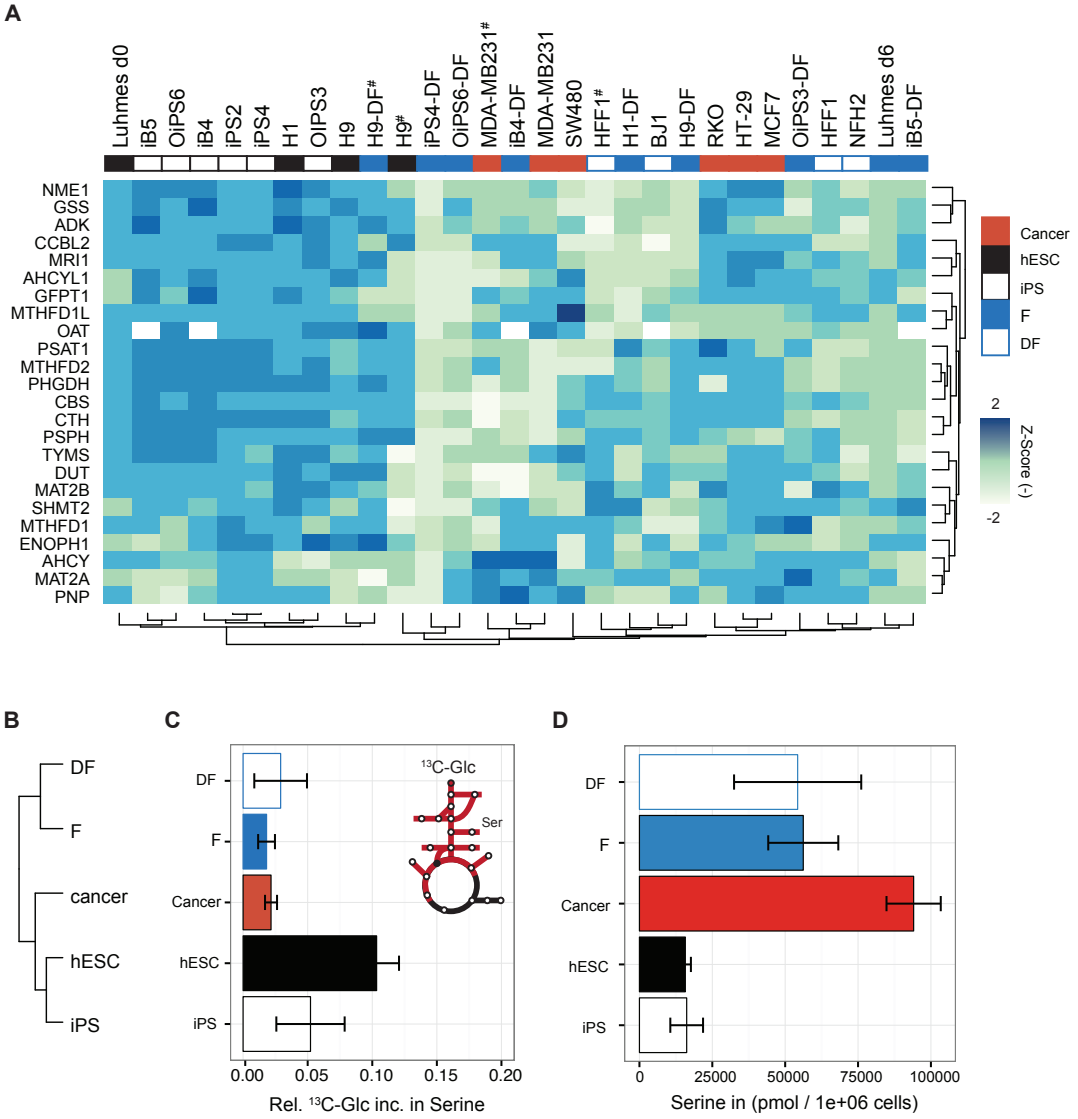


Figure 3.31.: Expression of one-carbon metabolism associates proteins and phenotype-dependent routing of nutrients into serine synthesis. (A) Native and reprogrammed pluripotent cells show an up-regulation of one-carbon protein expression in the hierarchical clustering. Levels in cancer cells increases only for smaller subgroup of proteins. Asterisks mark cell lines included derived from different experiments for data validation. (B) Dendrogram of the phenotype-dependent cluster analysis, averaging protein levels regarding the cellular status. (C) Comparison of $^{13}C$-Glc incorporation into serine reveals low levels in cancer and differentiated cells. (D) Absolute pool size of serine in hESCs, iPS, cancer and differentiated cells.

by glycine decarboxylase (GLDC). Threonine as a substrate for glycine synthesis has been shown in mammals including mice. The corresponding protein in human has not been identified so far. The fused proteomics data set of all projects has been filtered for enzymes related to the one-carbon metabolism. The hierarchical clustering identifies a main cluster with up-regulated expression levels covering almost exclusively all native and reprogrammed pluripotent cell lines (Figure 3.31-A). This cluster includes all enzymes of the *de novo* serine synthesis pathway — PHGDH, PSAT1, and PSPH — as well as the mitochondrial isoform SHMT2, and isoenzymes of MTHFD. A small subset of proteins show increased expression levels specifically in cancer cells, e.g., adenosylhomocysteinase (AHCY, c/er[10]), the subunit MAT2A (c) of the MAT complex, and purine nucleoside phosphorylase (PNP). In comparison to pluripotent and cancer cells, protein levels are decreased in native and derived fibroblasts.

The phenotype-specific clustering of one-carbon proteins shows the same dendrogram clustering as determined for the complete proteome (Figure 3.31-B).

The up-regulated protein expression of the *de novo* serine pathway is accompanied by an increased routing of glucose-derived carbons into serine in pluripotent cells in comparison to cancer and differentiated cells (Figure 3.31-C).

Glycine and threonine are two of the most abundant amino acids independent from the phenotype as shown in the metabolic profiles in Section 3.1. The high pool sizes of serine in cancer and differentiated cells point towards an increased uptake of extracellular serine, whereas hESCs and iPS cells rely on the *de novo* synthesis (Figure 3.31-D).

[10]endoplasmic reticulum

#### 3.2.4.2. 2HG – oncometabolite and driver of pluripotency

The metabolite 2-hydroxyglutaric acid (2HG) has been described in *E. coli* for the first time in 1968 (Wegener et al., 1968). A decade later Gregersen et al. identified the important role of 2HG in newborn urine (Gregersen et al., 1977). Since then the knowledge about the role and function of 2HG within the CCM is still incomplete.

Every cell produces small quantities of 2HG. The enzymes D- and L-hydroxyglutarate dehydrogenase (D2HGDH / L2HGDH) facilitate the oxidation of 2HG into $\alpha$KG and prevent the accumulation of the metabolite. Enzyme dysfunction results in 2HG aciduaries and is ongoing with the the development of severe pathological phenotypes and premature death (Struys, 2005).

In 2009 Dang et al proofed that a point mutation causing a gain-of-function mutation in the enzymes IDH1 and IDH2. Mutated IDH (mIDH) acquires the ability to produce 2HG from $\alpha$KG in glioblastoma cells, resulting in oxidative stress and reduced competitive inhibition of aKG-dependent enzymes (Dang et al., 2009). It was the first study claiming an oncogenic potential to a metabolite. Recently, it has been shown that mIDH is only responsible for the synthesis of the R-enantiomer D-2HG (Dang et al., 2009). The enzymes MDH1/2 and LDHA promiscuously catalyse the conversion of $\alpha$KG to L-2HG in different cell types (Figure3.32-A). A hypoxic environment even increases the production of L-2HG, independently from the activation of HIF1 (Oldham et al., 2015; Intlekofer et al., 2015). Both enantiomers act on different downstream targets. D-2HG contributes to cancer pathology via the inhibition of dioxygenases TET1/2. At the same time D-2HG activates PHD2 and thereby prevents the stabilisation of HIF1-$\alpha$. L-2HG suppresses TET1/2 and PHD2, and modifies the regulation downstream of HIF-1. L-2HG also influences the regulation of chromatin formation by inhibiting the activity of histone demethylase KDM4C (Oldham et al., 2015). The regulation of chromatin accessibility by histone methylation is the key for the maintenance of pluripotency.

2HG levels have been determined in all previously introduced projects. An absolute quantification of 2HG could not be performed due to the low levels of the metabolite. Instead of peak areas have been determined manually from the chromatograms. 2HG levels

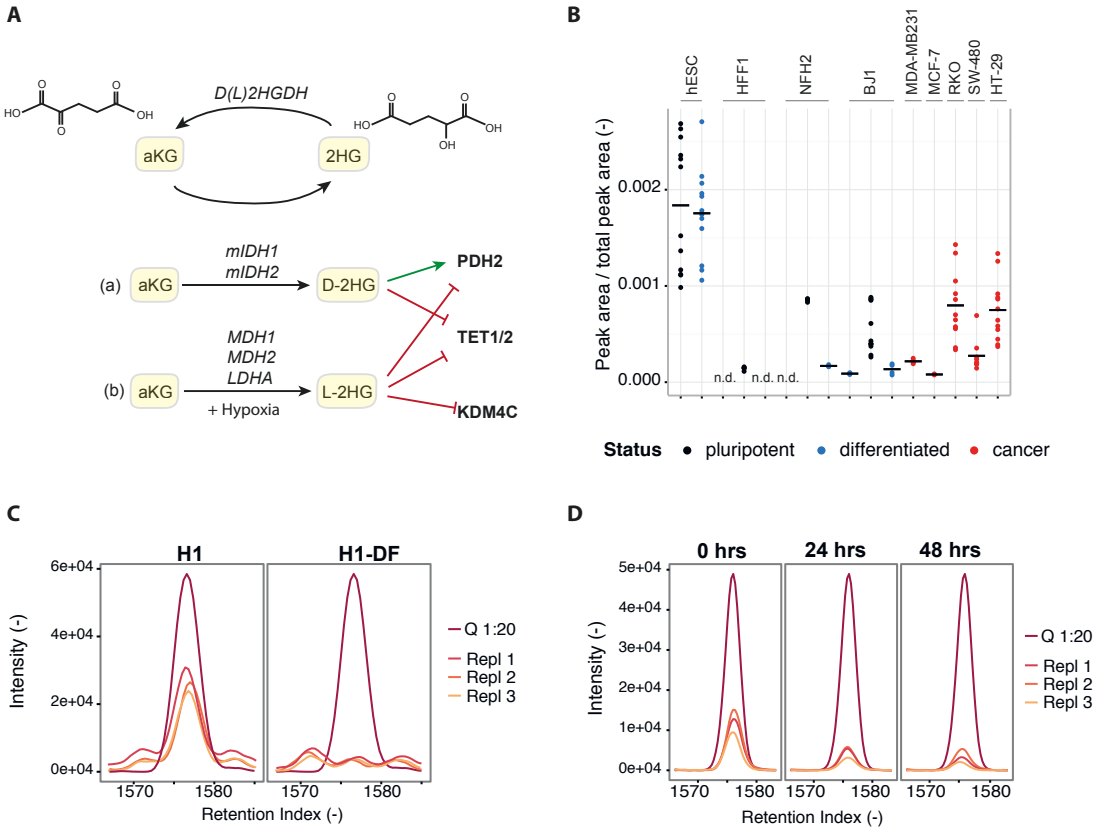


Figure 3.32.: 2HG levels in hESCs, iPS cells and their derivates. (A) The conversion of aKG into 2HG driven by CCM enzymes. (B) Levels of 2HG in hESCs, iPS cells, fibroblasts and cancer cells. 2HG levels are shown in the following order for each fibroblast cell lines: fibroblast, iPS cells, and iPS-DFs. (C) Differentiation of hESCs H1 results in a reduction of 2HG levels in H1-DFs. (D) 2HG levels drop in hESCs H1 cells during the first 48 hours of early differentiation.

have been normalised to the total peak area within each setup to provide comparability between the experiments. The GC-MS based metabolomics approach did not provide the differentiation of D- and L-enantiomer of 2HG. Determined quantities reflect the cumulated abundance of both enantiomer (Figure 3.32 - B). 2HG levels have been reduced with the differentiation of hESCs (Figure 3.32-C). The synthesis of 2HG has been also reversibly affected during reprogramming and re-differentiation of fibroblasts. 2HG levels increased in iPS cells after reprogramming pluripotency and diminished in iPS-DF cells. Its production has been also affected early during differentiation. We observed a depletion of 2HG in hESCs after 24 hrs of induction of differentiation (Figure 3.32-D).

The enzymes D- or L2HGDH have not been detected by shotgun LC-MS in any of the data sets. As shown before protein levels of cytosolic MDH1 were increased in hESCs and iPS cells, whereas the expression of mitochondrial MDH2 was up-regulated in cancer and iPS cells (Figure 3.24-B). High levels of LDHA has been detected in cancer and native fibroblasts only, whereas LDHB quantities has been elevated in pluripotent cell types. So far, the additional ability to convert L-2HG has only be shown for LDHA, not for LDHB. Summarising, MDH1 might be the responsible enzyme converting aKG into the pluripotency-driving L-2HG; LDHA and MDH2 the oncometabolite L-2HG.

## 3.3. From pSIRM to INST-MFA – methodical developments for the metabolic flux analysis in mammalian cells

The herein summarised work is a group effort achieved in the frame of the BMBF financed project "Dynametox". Experiments were conducted in the Kempa lab and performed in cooperation with Simon Gutbier, Leist Lab at the University of Konstanz. The processing and measurement of samples and data analysis has been performed in the Kempa lab. The mathematical modelling including the establishment of the network and data integration has been performed in co-work with Sebastian Niedenführ and Martin Cerff of the lab of Katharina Nöh at Forschungszentrum Jülich.

The metabolic flux of a cell is the readout of the interaction of metabolites and proteins. It mirrors the cellular function and describes all rates contributing to cellular maintenance and cell growth. During the last decade different approaches have been developed to determine absolute metabolic fluxes in cellular systems. Mainly this development was driven by the white biotechnology aiming to optimise the yield of small substances in bacteria and fungi. In their latest review Niedenführ and colleagues compare the required input parameter and the gain of knowledge of different MFA approaches (Niedenführ et al., 2015).

The herein applied approach of in-stationary metabolic flux (INST-MFA) analysis strictly assumes the metabolic steady state of the cell system. The only time-variant component is the incorporation of stable isotopes, e.g., $^{13}C$-glucose. In comparison to other approaches the INST-MFA requires a high number of input parameters. INST-MFA demands absolute pool sizes, extracellular rates and sufficient sampling to detect the dynamics of isotope incorporation, besides the definition of atom transitions and carbon balancing. The outcome of INST-MFA are the absolute quantification of forward and backward fluxes as well as the estimation of unknown pool sizes, energy and reducing equivalents characterising the functional status of a cell.

One of the aims of the present work here has been the establishment of a workflow start-

ing from cell culture tracing experiments and resulting in a metabolic flux map comparing pluripotent and differentiated cell metabolism.

This chapter summarises the flux maps of pluripotent Luhmes d0 and terminal differentiated, neuronal Luhmes d6 cell. Such a complex data analysis could have been carried out mainly by the introduction of a semi-automated quality control tool for GC-MS derived data (MTXQC, summarised in Section 3.3.3.2) and the further development of GC-MS fragment mapping (Section 3.3.3.1).

### 3.3.1. Mathematical model of the central carbon metabolism for INST-MFA

Absolute pool sizes of metabolites do not explain the contribution of nutrients to synthesise building blocks and energy equivalents. A model of the central carbon metabolism covering the main pathways has to be created for the metabolic flux analysis (Figure 3.33-A). The network covers the pathways of the central carbon metabolism contributing to biosynthesis and energy production: Glycolysis, TCA-cycle, pentose phosphate pathway, amino acid synthesis and degradation as well as glutaminolysis. In total the network includes 60 metabolites, 66 reactions, 32 intracellular fluxes (15 net, 17 exchange fluxes). Each reaction is defined with its substrates, products and required cofactors. Omix visualisation provides the creation of the network and its export for 13CFlux (Nöh et al., 2015).

The compartmentalisation of metabolic pathways is the main difference between prokaryotic and eukaryotic cells and increases the complexity for MFA. GC-MS determined absolute quantities reflect the total abundance of the intermediate in the cell only. So far methods providing a compartment specific quantification of metabolites are not available. Any manipulation or disconnection of compartments would immediately result in a change of the metabolic state. Shared pool sizes between compartments, e.g., of pyruvic acid, are incorporated as two separate pools but defined as a lump pool and balanced in the mathematical network. Uptake and export rates are defined for each substrate and exported product, e.g., glucose uptake, and lactic acid secretion. The quantification of the supernatant intermediates provides the determination of extracellular rates.

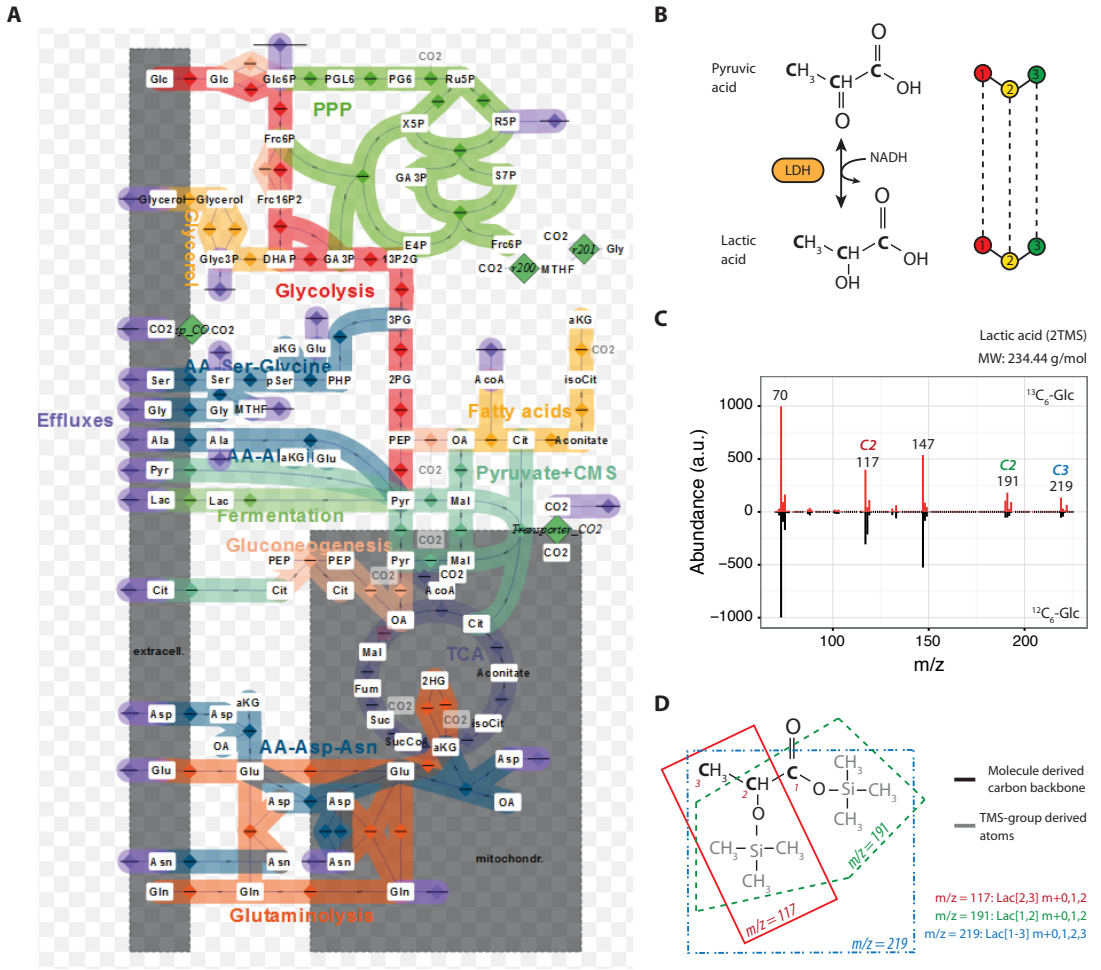


Figure 3.33.: Network of the central carbon metabolism for in-stationary metabolic flux analysis. (A) 60 metabolites, 66 reactions and 5 rates are integrated in the network created in OMIX visualisation(Nöh et al., 2015). (B) The routing of carbons are defined for each reaction as carbon transition, e.g., between pyruvic and lactic acid. (C) The mass spectra of a molecule summarises all molecule derived fragments and functions as a fingerprint. The evaluation of the mass isotopomer distribution (MID) of different fragments provides the determination of isotope incorporation, shown here for lactic acid comparing $^{13}C_6$-Glc labeled (red) and the natural, $^{12}C_6$-Glc labeled (black), mass spectra. (D) Mapping of GC-MS derived fragments to the molecule structure is required for the integration of MIDs in the mathematical framework for MFA. The fragments m/z 117, 191, 219 of lactic acid cover different parts of the molecule and differ in their atomic composition. Section 3.3.3.1 summarises the applied approaches for the mapping of GC-MS fragments.

Intracellular fluxes, meaning *in vivo* reaction rates, are the result of the interaction between the catalytic protein and its substrate(s). These fluxes are fine-tuned by "regulatory interactions at the genetic, protein modification, allosteric, and kinetic level" (Sauer, 2006). Tracing the fate of stable isotopes provides an indirect measurement of intracellular

fluxes. The exchange of carbons of each reaction in the network has to be defined prior the MFA. For each reaction carbon transitions have been defined between substrates and products, an example is shown for pyruvic and lactic acid in Figure 3.33-B.

Electron impact (EI) ionisation during GC-MS measurement induces the robust fragmentation of the molecule and enables detection in the mass spectrometer. The "breaking points" are mainly defined by the molecule structure, and thereby highly reproducible and unique for each compound. The incorporation of stable isotopes, like $^{13}C$-Glc, induces mass shifts in the mass isotopomer distribution (MID) in each fragment depending on the number of replaced carbon-12. Each fragment represents only a segment of the molecule and differs regarding its atomic composition. The derivatisation procedure introduces functional groups to increase the volatility and detectability of compounds in GC-MS measurements. These groups introduce molecule-independent atoms, e.g., each TMS group ($Si(CH_3)_3$) introduces three carbons, that are not affected by the incorporation of stable isotopes.

Lactic acid fragments m/z 117, 191, and 219 cover different molecule-related and TMS-derived carbons as shown in Figure 3.33-D. Fragment m/z 117 and 191 contain two carbons derived from the molecule backbone of lactic acid: m/z 117 — Lac[2,3] and m/z 191 — Lac[1,2], whereas m/z 219 recovers the complete carbon backbone. Each metabolic intermediate of the network has been implemented with at least one fragment and its detailed measurement specifications. Only the complete knowledge about the atomic composition of each fragment provides the correction for the natural abundance of each molecule and the correct interpretation of the MIDs for MFA. So far only a low number of GC-MS derived fragments are identified and classified in the literature. Section 3.3.3.1 outlines the experimental and theoretical approaches to further develop and refine the mapping of GC-MS derived fragments.

### 3.3.2. pSIRM time series experiments in Luhmes cells

Extensive time course pSIRM experiments have been performed for the generation of the metabolic flux map in Luhmes d0 and d6 cells. Comprehensive summaries about protein

expression and the metabolic profiles are outlined in Section 3.1.4.

The INST-MFA strictly requires the metabolic steady state; meaning constant pool sizes of metabolites throughout the labelling experiment. The only time-variant component is the incorporation of the stable isotopes in the intermediates of the CCM. The developed protocol of pSIRM experiments (see 2.3) fulfills the experimental criteria of MFA. According to the pSIRM protocol cells were seeded in appropriate manner to avoid contact induced growth inhibition during the experiment. The cell culture media has been replaced 24 and 4 hours prior the labelling experiment to prevent the deprivation of nutrients. Luhmes d0 and d6 cells were incubated for up to 24 hours with $^{13}C$-glucose and $^{13}C$-glutamine at 37 $\circ$ $C$, ambient oxygen level and 5% $CO_2$. Independent 6-well plates were harvested at 2, 3, 4, 6, 8, 12, and 30 minutes, as well as 1, 6 and 24 hours after the application of labelling media, containing either $^{13}C$-Glc or $^{13}C$-Gln. The tight sampling in the first experimental period covers the detection of the incorporation dynamics of both isotopic labeled substrates in CCM intermediates (Figure 3.34-A). Sampling of supernatant prior

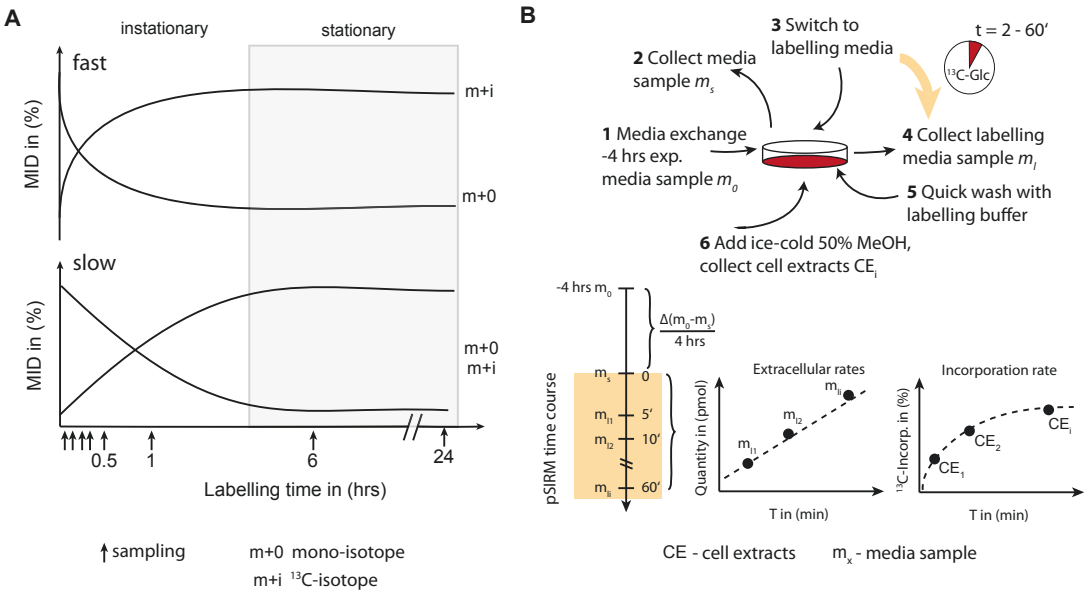


Figure 3.34.: Sampling scheme for INST-MFA in Luhmes cells. (A) Extensive sampling scheme of $^{13}C$-substrate labelling to monitor the different dynamics of isotope incorporation. (B) Time scheme and sampling procedure of a pSIRM time course experiment. The collection of media samples at different time points during the pSIRM labelling experiment provides the determination of extracellular rates and of the incorporation of stable isotopes in intracellular metabolites.

and throughout the experiment enables the determination of extracellular uptake and production rates (Figure 3.34- B).

The comparison of metabolite pool sizes of the plain cultivation media ($m_0$) and after four hours of cultivation $m_s$ result in a rough estimation of metabolite import and export. The quantification of extracellular metabolites in the supernatant during the labelling experiment at different time points ($m_{li}$) allows the determination of production and consumption rates, complementing the intracellular pool sizes determined in cell extract ($CE_i$) samples.

## 3.3.3. Methodical developments

### 3.3.3.1. GC-MS fragmentation mapping

The preprocessing of biological samples for GC-MS measurement includes the derivatisation. The chemical replacement of active hydrogens by functional groups improves the chromatographic behaviour, thermal and chemical stability, volatility, tailing and detectability of compounds, but also introduces molecule-independent carbons in the mass spectra. The choice of derivatisation reagents depends on the compounds of interest. Three groups of derivatisation reagents are classified upon their chemical modification: acylation, alkylation or methylation, and silylation. The latter two are applied in the lab routine for metabolomics analysis and result in the introduction of trimethylsilyl (TMS, $Si(CH_3)_3$) groups, thereby the addition of three molecule-independent carbons.

The exact mapping of GC-MS derived fragments to the molecule structure is important because of two reasons: (i) Only carbons related to the molecule itself provide information about the metabolic flux by incorporation stable isotopes and (ii) the correction of natural isotopes has to be performed based on fragment atomic composition, including the molecule-independent atoms introduced by derivatisation.

Therefore the mapping of the molecule structure and GC-MS derived fragments is a prerequisite for the reliable determination of metabolic fluxes. Misaligned atoms would result in an incorrect correction for the natural abundance of all atom isotopes, and thus to incorrect fluxes.

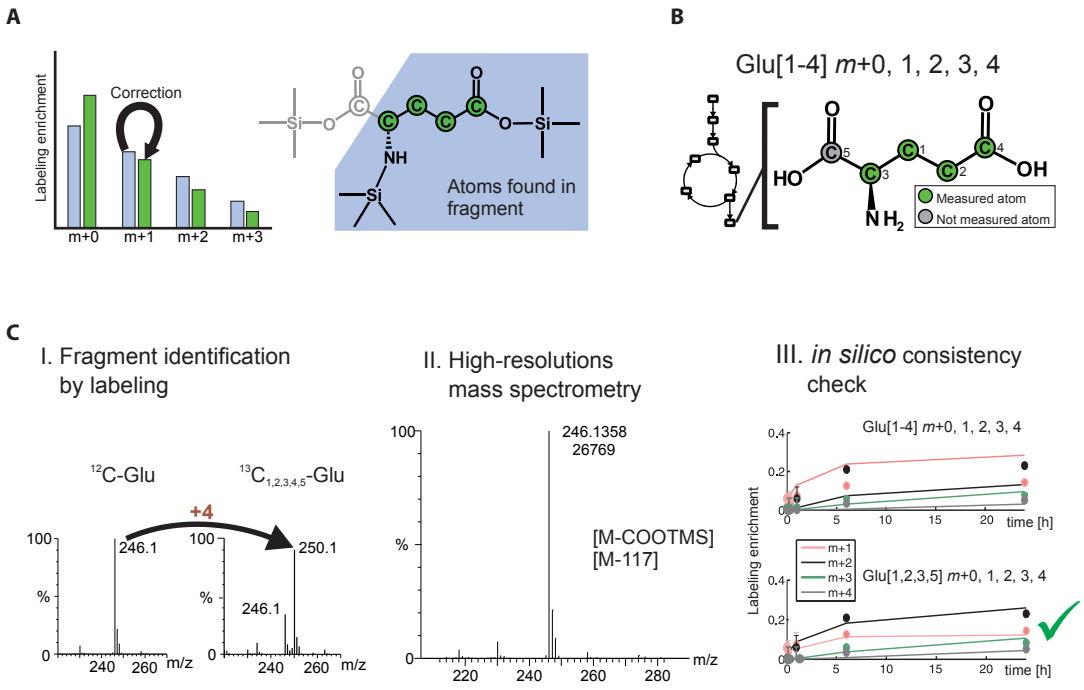


Figure 3.35.: Strategies for the structural analysis of GC-MS derived fragments. (A) The correct mapping of the fragment affects the correction for natural abundance of isotopes. (B) Measurement specifications have to be included for each compound including the carbon composition in the mathematical network. (C) (I) Position-specific labelling with isotopes provides the identification of molecule-specific carbons. (II) High-resolution mass spectrometry give an exact mass of each GC-MS fragment. (III) The consistency of fragment mapping is checked by the application of the mathematical model of the CCM. Figures are adapted from S. Niedenführ, former member of the Nöh lab.

We combined three approaches for the structural mapping of GC-MS fragments of CCM-related metabolites (Figure 3.35 C). The application of position-specific labeled substrates, e.g., $^{13}C_{12}$-Glc provides the structural identification of molecule-dependent fragments and the analysis of their carbon atom composition. High-resolution GC-ToF-MS measurements provide the determination of an exact mass for each fragment. The measurements were performed at the Forschungszentrum Jülich, Germany. At long least a carbon-resolved mathematical model of the central carbon metabolism has been applied checking the consistency of theoretical and experimental derived carbon mappings.

A number of position-specific labeled variants of glucose and glutamine were applied for the structural analysis of GC-MS derived fragments in a cell culture experiment (Supp. Ta-

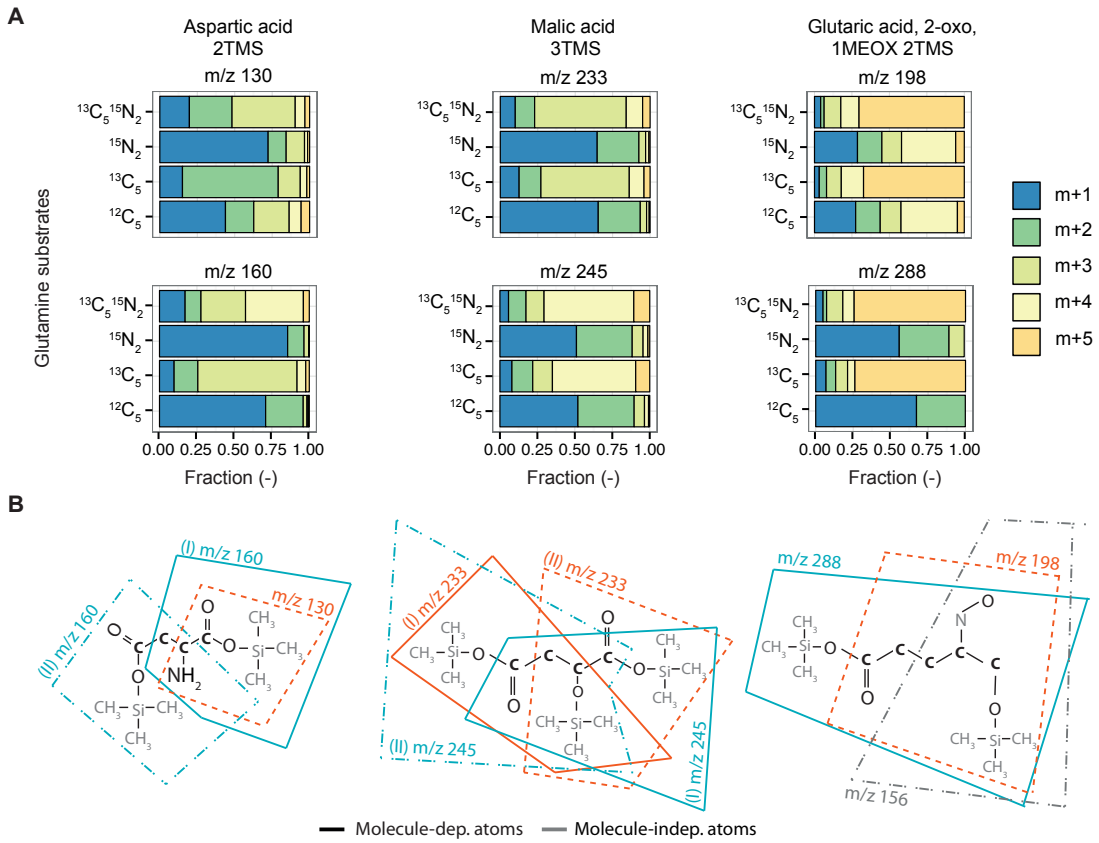


Figure 3.36.: GC-MS fragment analysis by the application of differently isotopic labeled glutamine species. (A) Mass isotopomer distributions (MIDs) of selected metabolite-specific fragments after the application of different labeled species of glutamine. (B) Mapping of GC-MS fragment to the molecule structure based on the combination of high-resolution GC-ToF-MS, application of stable isotopes and computational validation. Chemical compositions of the fragments are summarised in Table E.6.

ble 2.4.4). Samples were collected, processed and annotated as described before. The plugin "SpectraExport" in MAUI-SILVA enables the export of MIDs for predefined fragments in GC-MS measurements. Metabolite-specific fragments are selected based on insights from previous pSIRM experiments and complemented with additional high-abundant, metabolite-specific fragments (Pietzke et al., 2014).

Isotope incorporation induces a shift in MIDs regarding the number of replaced atoms. Figure 3.36-A summarises the MIDs in two selected fragments of aspartic, malic and $\alpha$–ketoglutaric acid after the application of glutamine isotopes. In combination with an exact mass of the fragments we are able to map the GC-MS fragment to the structure of

the metabolite (Figure 3.36-B). In the general run of things fragments cover only a part of the molecules carbon backbone. Often the symmetrical nature of the molecule does not provide an exact determination of the carbons that are mirrored in the fragment, i.e., Asp 2TMS: m/z 160 or Mal 3TMS: m/z 233. Smaller, but positionally defined (Asp 2TMS m/z 130), fragments should be included in the analysis to increase the robustness of the interpretation of the incorporation dynamics.

Fragments containing the complete carbon backbone of the molecule but suit due to the symmetry of the molecule to more than one combination are useful and should be implemented, e.g., Mal 3TMS m/z 245. Not the position but the exact composition of these kind of fragments are required for a correct consideration of natural isotope abundance. We determined the exact mass, the carbon-body or c-body and its atomic composition for each metabolite including different derivates and fragments. The results are summarised in the Table E.6. An extended summary of fragment mapping and a graphical illustration are shown in the Supplement E. The extension of fragment mappings enables the implementation of multiple isotope information for several metabolites or even its consideration in MFA for the first time.

Table 3.1.: GC-MS derived fragment mapping.

| **Metabolite** | **Derivate** | **m+0** | **Exact mass** | **C-body** | **Carbons** | **Formula** |
|---|---|---|---|---|---|---|
| Ala | (2TMS) | 116 | 116.0890 | C2 | [2,3] | C5H14NSi |
| Ala | (3TMS) | 188 | 188.1285 | C2 | [2,3] | C8H22NSi2 |
| Ala | (3TMS) | 262 | 262.1473 | C2 | [1,2] | C10H28NOSi3 |
| Asp | (2TMS) | 130 | 130.0319 | C2 | [1,2] | C4H8NO2Si |
| Asp | (2TMS) | 160 | 160.0788 | C3 | [1-3]/[2-4] | C6H14NO2Si |
| Asp | (3TMS) | 218 | 218.1027 | C2 | [1,2] | C8H20NO2Si2 |
| Asp | (3TMS) | 232 | 232.1184 | C3 | [2,3,4] | C9H22NO2Si2 |
| Cit | (4TMS) | 273 | 273.0973 | C5 | [1,2,3,4,5] | C11H21O4Si2 |
| Cit | (4TMS) | 347 | 347.1161 | C4 | symmetry | C13H27O5Si3 |
| Cit | (4TMS) | 465 | 465.1611 | C6 | [1-6] | C17H37O7Si4 |
| DHAP | (1MEOX)(3TMS) | 400 | 400.1191 | C3 | [1-3] | C12H31NO6PSi3 |
| Fru | (1MEOX)(5TMS) | 205 | 205.1075 | C2 | [5,6] | C8H21O2Si2 |
| Fru | (1MEOX)(5TMS) | 217 | 217.1075 | C3 | [4,5,6] | C9H21O2Si2 |

Continued on next page

**Table 3.1 – continued from previous page**

| Metabolite | Derivate | m+0 | Exact mass | C-body | Carbons | Formula |
|---|---|---|---|---|---|---|
| FBP | (1MEOX)(7TMS) | 217 | 217.1075 | C3 | [4,5,6] | C9H21O2Si2 |
| F6P | (1MEOX)(6TMS) | 217 | 217.1075 | C3 | symmetry | C9H21O2Si2 |
| Fum | (2TMS) | 245 | 245.0660 | C4 | [1-4] | C9H17O4Si2 |
| PG6 | (7TMS) | 217 | 217.1075 | C3 | | C9H21O2Si2 |
| Glc | (1MEOX)(5TMS) | 160 | 160.27 | C2 | [1,2] | C6H14NO2Si |
| Glc | (1MEOX)(5TMS) | 205 | 205.1075 | C2 | [5,6] | C8H21O2Si2 |
| Glc | (1MEOX)(5TMS) | 217 | 217.1075 | C3 | [4,5,6] | C9H21O2Si2 |
| G1/6P | (1MEOX)(6TMS) | 217 | 217.1075 | C3 | [4,5,6] | C9H21O2Si2 |
| G1/6P | (1MEOX)(6TMS) | 357 | 357.1133 | C2 | | C11H30O5PSi3 |
| Glu | (2TMS) | 230 | 230.1027 | C3 | [1-3] | C9H20NO2Si2 |
| Glu | (2TMS) | 276 | 276.1082 | C5 | [1-5] | C10H22NO4Si2 |
| Glu | (3TMS) | 230 | 230.1027 | C3 | [1-3] | C9H20NO2Si2 |
| Glu | (3TMS) | 246 | 246.1340 | C4 | [1,2,3,5] | C10H24NO2Si2 |
| Glu | (3TMS) | 348 | 348.1477 | C5 | [1-5] | C13H30NO4Si3 |
| Gln | (3TMS) | 156 | 156.0839 | C4 | [2,3,4,5] | C7H14NOSi |
| Gln | (3TMS) | 245 | 245.1500 | C4 | [1-4] | C10H25N2OSi2 |
| 2HG | (3TMS) | 231 | 231.0867 | C3 | [1-3] | C9H19O3Si2 |
| 2HG | (3TMS) | 247 | 247.1180 | C4 | symmetry | C10H23O3Si2 |
| 2HG | (3TMS) | 349 | 349.1317 | C5 | [1-5] | C13H29O5Si3 |
| aKG | (1MEOX)(2TMS) | 156 | 156.0475 | C3 | [3-5] | C6H10NO2Si |
| aKG | (1MEOX)(2TMS) | 198 | 198.0581 | C5 | symmetry | C8H12NO3Si |
| aKG | (1MEOX)(2TMS) | 288 | 288.1082 | C5 | [1-5] | C11H22NO4Si2 |
| GA3P | (1MEOX)(3TMS) | 217 | 217.1075 | C3 | [1-3] | C9H21O2Si2 |
| 3PGA | (4TMS) | 357 | 357.1133 | C2 | [2,3] | C11H30O5PSi3 |
| Glyc | (3TMS) | 218 | 218.1153 | C3 | [1-3] | C9H22O2Si2 |
| Glyc | (3TMS) | 293 | 293.1419 | C3 | [1-3] | C11H29O3Si3 |
| Glyc3P | (4TMS) | 357 | 357.1133 | C2 | [2,3] | C11H30O5PSi3 |
| Gly | (2TMS) | 204 | 204.0871 | C2 | [1,2] | C7H18NO2Si2 |
| Gly | (3TMS) | 276 | 276.1266 | C2 | [1,2] | C10H26NO2Si3 |
| Lac | (2TMS) | 117 | 117.0730 | C2 | [2,3] | C5H13OSi |
| Lac | (2TMS) | 191 | 191.0918 | C2 | [1,2] | C7H19O2Si2 |
| Lac | (2TMS) | 219 | 219.0867 | C3 | [1-3] | C8H19O3Si2 |
| Mal | (3TMS) | 233 | 233.1024 | C3 | symmetry | C9H21O3Si2 |

Continued on next page

**Table 3.1 – continued from previous page**

| Metabolite | Derivate | m+0 | Exact mass | C-body | Carbons | Formula |
|---|---|---|---|---|---|---|
| Mal | (3TMS) | 245 | 245.0660 | C4 | [1-4] | C9H17O4Si2 |
| Mal | (3TMS) | 335 | 335.1161 | C4 | [1-4] | C12H27O5Si3 |
| PEP | (3TMS) | 369 | 369.0769 | C3 | [1-3] | C11H26O6PSi3 |
| Pyr | (1MEOX)(1TMS) | 158 | 158.0632 | C3 | [1-3] | C6H12NO2Si |
| Pyr | (1MEOX)(1TMS) | 174 | 174.0581 | C3 | [1-3] | C6H12NO3Si |
| Pyr | (1MEOX)(1TMS) | 189 | 189.0816 | C3 | [1-3] | C7H15NO3Si |
| R5P | (1MEOX)(5TMS) | 217 | 217.1075 | C3 | | C9H21O2Si2 |
| R5P | (1MEOX)(5TMS) | 357 | 357.1133 | C2 | | C11H30O5PSi3 |
| Ser | (2TMS) | 116 | 116.0526 | C2 | [2,3] | C4H10NOSi |
| Ser | (2TMS) | 132 | 132.0839 | C2 | [2,3] | C5H14NOSi |
| Ser | (3TMS) | 188 | 188.0921 | C2 | [2,3] | C7H18NOSi2 |
| Ser | (3TMS) | 204 | 204.1234 | C2 | [2,3] | C8H22NOSi2 |
| Ser | (3TMS) | 218 | 218.1027 | C2 | [1,2] | C8H20NO2Si2 |
| Suc | (2TMS) | 172 | 172.0550 | C4 | | C7H12O3Si |
| Suc | (2TMS) | 247 | 247.0816 | C4 | all | C9H19O4Si2 |

#### 3.3.3.2. MTXQC — A quality control tool for GC-MS derived metabolomics data

Manual data processing and analysis still represent the major bottlenecks of high-throughput omics-technologies. The in-house developed software MAUI-SILVIA improves GC-MS derived metabolomics data analysis regarding the handling of large-scale data sets and time requirements. It simplifies the complexity of data analysis. But a reduction on the one hand always comes along with a loss of insights on the other hand - in particular the chromatography providing the information about the peak shape and therefore the reliability of compound quantification.

The metabolomics quality control (MTXQC) has been developed to redeem this information. MTXQC is a R-script based tool which is optimised to use the output of MAUI-SILVIA. In total the tool uses 14 criteria for assessing the data quality regarding (i) GC-MS performance, (ii) absolute quantification and (iii) stable isotope incorporation (Table 3.2). Outcomes of each metric are visualised in heat-maps for all annotated CCM-intermediates and their derivates (Figure 3.37). Every score is determined in a way that a scoring of 1 reflects the perfect, a scoring of zero the worse outcome.

Furthermore MTXQC includes first steps of data post-processing. It performs the absolute quantification and combines all data outcomes into one spreadsheet-file that can be filtered regarding individual quality requirements in a subsequent independent analysis. R code, generated statistics and graphical outputs are reported in a PDF-file and serves as data analysis documentation.

The herein described version of MTXQC evaluates GC-MS data derived from a pSIRM

Table 3.2.: Metrics for the metabolomics data quality control (MTXQC)

| Class | Criteria | Description |
|---|---|---|
| GC-performance | G.1 | Alkane profile |
| | G.2 | Derivatisation efficiency |
| | G.3 | Internal extraction standard: cinnamic acid |
| | G.4 | Total peak detection |
| Quantification | Q.1, Q.2 | Calibration curve (linearity, number of data points) |
| | Q.3 | Experimental data points within linear range of calibration |
| | Q.4, Q.5 | Metabolite pool $Q_{ss}$ (number of data points, $sd(Q_{ss})$) |
| | Q.6 | Correlation of cinnamic acid and total peak area normalisation |
| Isotope incorporation | I.1, I.2 | Quality of MID (count of missing values, low intensity) |
| | I.3 | Natural isotopic incorporation at $t = 0$ |
| | I.4 | Variance of isotope incorporation between biological replicates within the experiment |

time series experiment. A shortened version of MTXQC is available for solely absolute quantification, excluding the evaluation of isotope incorporation.

The commented R code, an overview of input- and output-files, and generated figures are shown exemplarily for one experiment in the Supplement E.

**QC GC-MS performance** A consistent GC-MS performance is essential for a reliable identification and quantification of metabolites. Even sample extraction, uniform injection, and a homogenous derivatisation are mirrored in the four scores of GC-MS performance metric. The scores are determined for the entire experimental setup.

**G.1 – Alkane profile** Kováts et al. introduced the application of alkane mixtures for the determination of the retention indices (Kováts, 1958). A mixture of nine alkanes

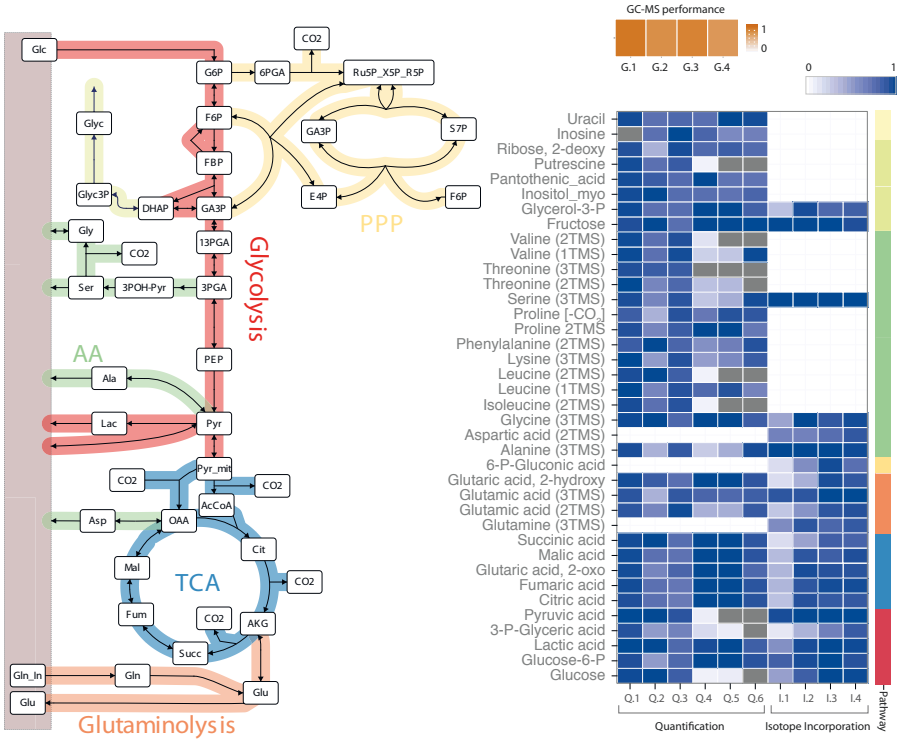


Figure 3.37.: Quality control for GC-MS based metabolomics data analysis (MTXQC) for the analysis of pSIRM experiments. Heatmaps visualise the metrics for the GC-MS performance, absolute quantification and isotope incorporation for all annotated CCM-intermediates and their derivates.

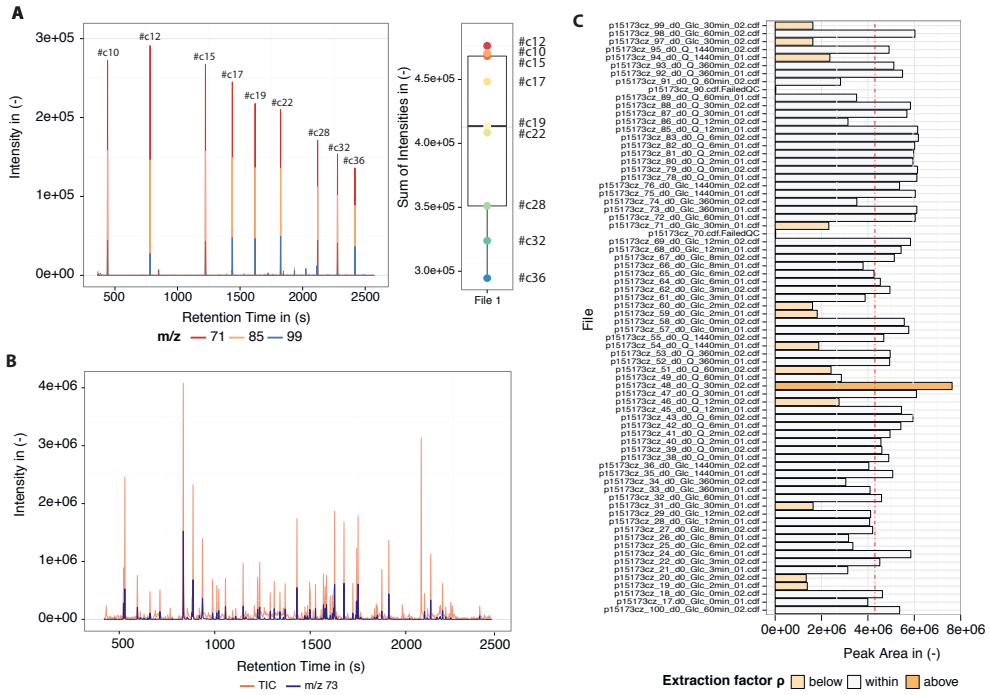


Figure 3.38.: Profile of retention index standard alkanes c10 – c36. (A) The distribution of the intensities of the characteristic ions (m/z: 71, 85, 99) for each alkane is compared within the setup. (B) Derivatisation increases volatility of each compound by chemically modification, e.g., addition of TMS-groups (m/z 73). (C) The profile of the internal extraction standard cinnamic acid is shown for one experimental batch.

(c10 - c36) is supplemented during derivatisation to each sample. The number of carbons defines the retention time of each alkane within the chromatogram (Figure 3.38 - A). The retention times and intensities of the alkanes remain constant over the entire batch.

MTXQC summarises the intensities for each alkane per file and determines the total variance within the experimental setup. An increase of variance between measurements results in a reduction of the G.1 scoring.

**G.2 – Derivatisation efficiency** A sufficient derivatisation is a prerequisite for GC-MS based metabolomics. The chemical modification of the compounds by the substitution of hydrogen bonds by oxamination (MeOx) or trimethylsilyation (TMS, $-[Si(CH3)_3]$, $m/z = 73$) increases the volatility and enables the detection by GC-MS. Minimum requirement for compound detectability is the addition of at least one TMS-group.

The Electron-Impact (EI) ionisation induces the molecule-dependent fragmentation and

leads to a fingerprint-like, compound specific mass spectra. Every mass spectra contains the ion $m/z = 73$ because of its ubiquitous presence in each compound (Figure 3.38 - B). A drop of the total intensity of $m/z = 73$ per file points towards an inefficient derivatisation. The G.2 scoring is calculated based on the total variance of the TMS-specific ion abundance within the setup. Variations due to a reduced number of identified peaks are taken into account by the normalisation of the score to the sum of total peak intensities per file.

**G.3 – Internal standard cinnamic acid** The metabolite extraction is an essential step during the sample preparation. Fluctuations of extraction solvent introduce quantity changes of intermediates, that may incorrectly be connected to the biological phenotype. The quantification of the internal standard cinnamic acid, supplemented to the solvent prior to the extraction, corrects for sampling inaccuracies.
The correction factor $\rho$ considers the quantity of cinnamic acid in a single measurement normalised to the average of all cinnamic acid quantities of the setup. Files with a cinnamic acid factor beyond $\rho\ \epsilon[0.65; 1.45]$ should be excluded from the analysis, due to enormous errors in sample preparation, injection and derivatisation.

**G.4 – Total peak detection** The normalisation according to the total intensity of a file is yet another data normalisation strategy. The sum of all peak intensities persists independently from the biological variation and may occur due to a variance of extraction, derivatisation or injection.
The corresponding normalisation factor $\eta$ is an analogue to the internal extraction factor $\rho$. It is defined as the ratio of the sum of all peak areas per file, and normalised to the average of all peak areas within the experimental batch. Out of scope are experiments targeting central pathways of the metabolism, e.g., inhibition of a glycolytic enzyme that may lead to an extreme reduction of detectable compounds. In that case the applicability of the normalisation strategy has to be evaluated by the experimentalist.

**QC Absolute quantification** Absolute quantification of compounds provides a batch and machine independent evaluation of a metabolomic experiment. The measurement of an

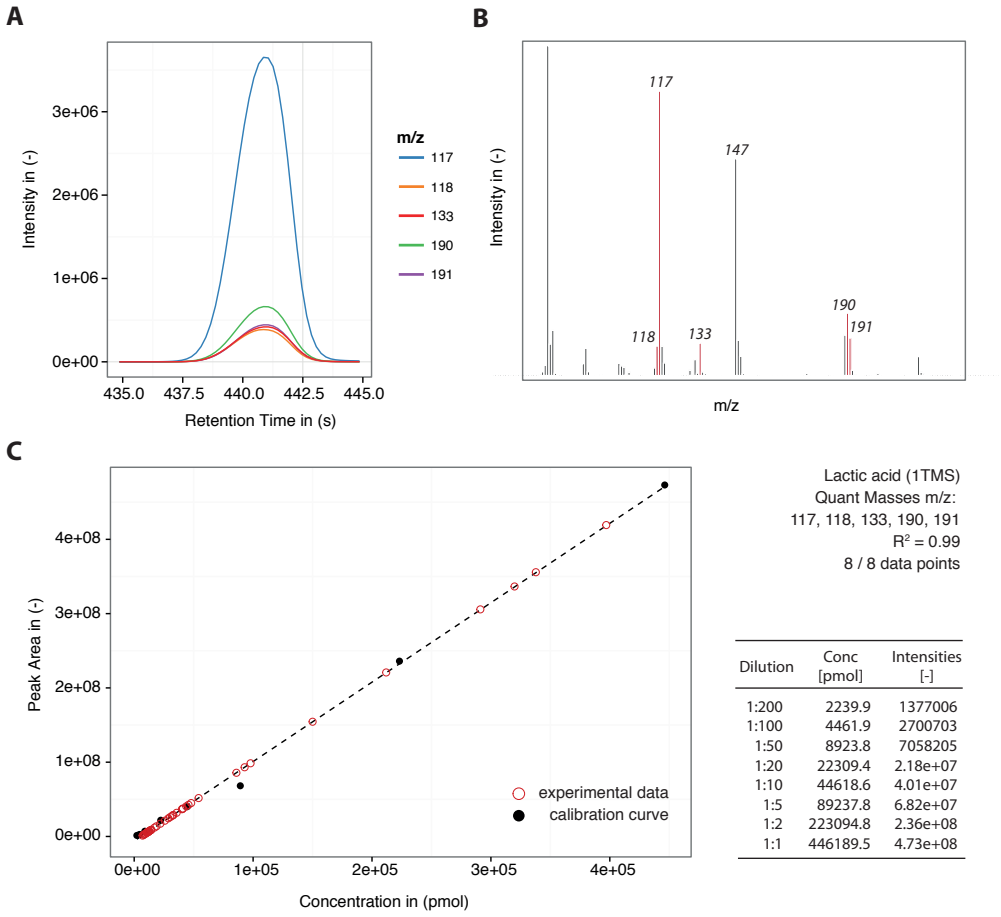


| Dilution | Conc [pmol] | Intensities [-] |
|---|---|---|
| 1:200 | 2239.9 | 1377006 |
| 1:100 | 4461.9 | 2700703 |
| 1:50 | 8923.8 | 7058205 |
| 1:20 | 22309.4 | 2.18e+07 |
| 1:10 | 44618.6 | 4.01e+07 |
| 1:5 | 89237.8 | 6.82e+07 |
| 1:2 | 223094.8 | 2.36e+08 |
| 1:1 | 446189.5 | 4.73e+08 |

Figure 3.39.: Absolute metabolite quantification by external calibration. (A) The Top5 intense masses are depicted from the detected mass spectra, here shown for lactic acid, for the determination of the calibration curve. (B) In pSIRM experiments carbon-dependent masses are supplemented with mass-shift induced counterparts, called (pTop5) approach. Peak areas of those masses are summed up and correlated with the known amount of the corresponding dilution of the quantification mixture. (C) Visualisation of experimental data within the range of the calibration curve for lactic acid, including data of calibration curve considering pTop5-quantification approach.

in-house developed quantification mixture enables the absolute quantification of around 50 intermediates by external calibration. MTXQC calls six parameters evaluating the quality of the calibration curve and resulting absolute quantities (Figure 3.39 - A, B).

**Q.1 – Linearity of calibration curve** Reliable absolute quantification is only facilitated within the linear range of the calibration curve. Extrapolation outside this range may lead to an over- or underestimation of the quantity due to the unpredictable relation of quantity

and detector response. The regression coefficient $R^2$ mirrors the linearity of the calibration curve.

**Q.2 – Data points of calibration curve** In an optimal case, the calibration curve summarises the information of eight data points according to the dilutions of the quantification mixture. A reduction of data points at the upper and lower border results in the limitation of the quantification range of the samples.

**Q.3 – Range of experimental data points according to calibration curve** Experimental data points have to be evaluated regarding their position within the linear range of the calibration as explained before (Figure 3.39 - C).
Data points out of the range of the calibration curve should be neglected from absolute quantification, but still may be analysed in a relative manner using peak areas within the experimental setup.

**Q.4 – Metabolite pool size $Q_{ss}$** The quasi-stationary metabolic state is a unalterable requirement for non-stationary MFA. Pool sizes remain constant within the experiment. The only time-variant of the system is the isotope incorporation. All pool measurements over the time course are summarised into one stationary pool $Q_{ss}$ per metabolite and derivate.
The Q.4 criteria reflects the number of data points contributing to $Q_{ss}$ and matching the quality requirements in relation to the total number of available measurements per each metabolite.

**Q.5 – Variation of $Q_{ss}$** The certainty of $Q_{ss}$ is reflected by the variation of the metabolite pool size within the complete setup.

**Q.6 – Correlation between normalisation factors $\rho$ and $\eta$** This parameter describes the correlation of the quantities normalised with the cinnamic acid factor $\rho$ and quantities corrected for cinnamic acid and the total peak intensity. It has been shown, that in particular quantities determined in a sample with a cinnamic acid factor beyond the predefined

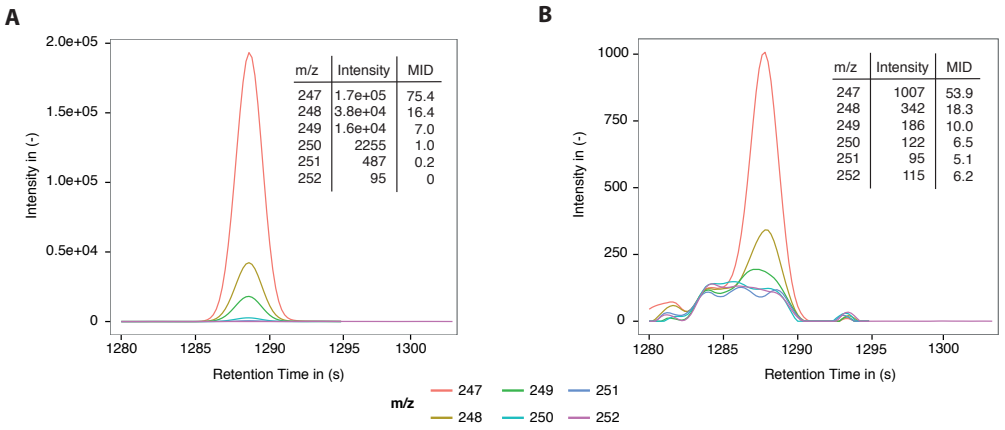


Figure 3.40.: Influence of metabolite abundance on peak shape shown for 2-Hydroxyglutaric acid - (A) ultimate peak shape and mass isotopomer distribution (MID) and (B) low abundant peak and misleading MID.

range do not correlate with total peak normalised quantities.

**QC Stable isotope incorporation** The incorporation of stable labeled isotopes leads to a shift of intensity in the mass spectra in every fragment that contains an atom of the carbon backbone of the molecule. The incorporation of carbon-13 therefore affects the mass isotopomer distribution (MID) of the fragment. Low peak abundances and an insufficient chromatography leads to noisy data and has to be evaluated prior to the MFA analysis. MAUI-SILVIA provides a tool for the automated export of all MIDs for pre-defined fragments for each metabolite. MIDs that require manual validation are highlighted with "low quality" regarding the scores of the metrics for isotope incorporation. MIDs have to be corrected also for the natural abundance of carbon-13. Therefore it is necessary to know which part of the molecule is covered in the actual fragment. The outcomes of the combined approaches of fragment mapping are summarised in Section 3.3.3.1.

**I.1 – NA count in mass isotopomer distribution (MID)** Overlapping peaks in the chromatography or low peak intensities often introduce missing values in the MID. Gaps in the MID may introduce misleading isotopomer patterns and a false determination of metabolic fluxes.

The first criteria of isotope QC compares the MID of a sample to a non-labeled refer-

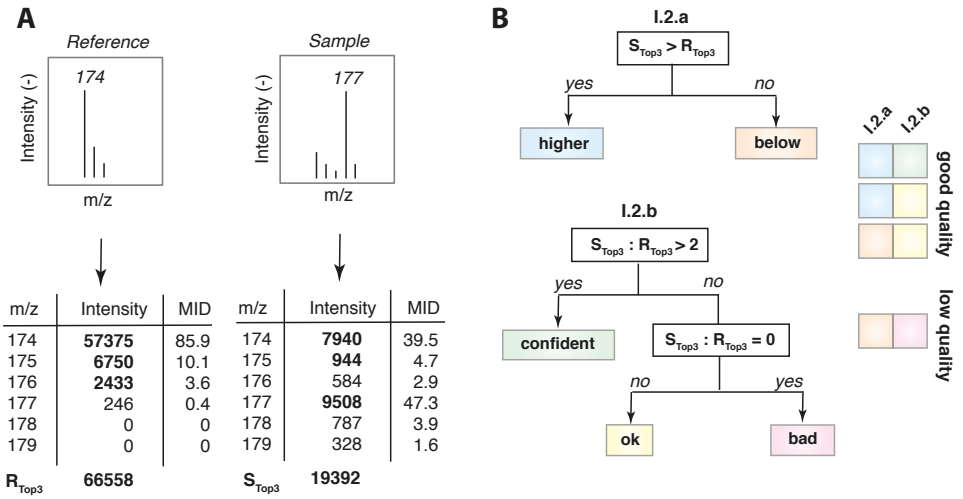


Figure 3.41.: Evaluation of the mass isotopomer distribution. (A) $R_{Top3}$ and sample $S_{Top3}$ are calculated based on the top3 intensities within a defined fragment. (B) Relative and rational comparison of the parameters enable the classification in low and good quality MIDs.

ence distribution, that is either selected from a measurement of a quantification mixture matching the intensity range of sample, or if not possible, from a manually defined backup reference.

**I.2 – MID quality** Minor increases of intensities within the MID may lead to an overestimation of isotope incorporation in low abundant peaks as shown exemplarily for 2-hydroxy glutaric acid in Figure 3.40.

A combination of absolute (I.2.a) and relative comparison (I.2.b) of the summation of the top3 intensities of a sample to a reference MID provides a distinct identification of good and low quality MIDs (Figure 3.41).

The absolute comparison of $S_{Top3}$ and $R_{Top3}$ evaluates the general intensity range between sample and reference. The ratio of $S_{Top3} : R_{Top3}$ pinpoints MIDs that have to be evaluated manually. Ratios $\varepsilon[0;1]$ are classified as "low quality" MID. The score calculates the fraction of good quality MIDs per metabolite.

**I.3 – Isotope incorporation** $LI(t=0)$ The measurement of a non-labeled control sample is included in every pSIRM time course experiment. MAUI-SILVIA itself calculates the

$^{13}C$-incorporation in each metabolite based on the targeted approach published by Pietzke et al. (2014). The isotopic incorporation of all metabolites in the control sample should be close to the natural abundance of carbon-13. Low peak abundance may lead to a higher isotope incorporation rate as described before. The I.3 scoring decreases with increasing isotope incorporation.

**I.4 – Variance of isotope incorporation** $LI$ The final score tests the variance of isotope incorporation between biological replicates at each time point within the pSIRM experiment. A huge variation decreases the value of I.4 and indicates the need of manual validation of the data. Misaligned peaks may lead to a imprecise determination of isotope incorporation and cause big variation between biological replicates.

### 3.3.4. Metabolic flux maps of pluripotent and neuronal Luhmes cells

The differentiation of Luhmes d0 into mature neurons Luhmes d6 is accompanied by a rearrangement of the CCM. The metabolic reprogramming is reflected in the distinct routing of $^{13}C$-glucose and $^{13}C$-glutamine derived carbons to fuel pathways providing reducing equivalents or building blocks for biosynthesis, as outlined in Section 3.1.4.

The herein presented flux maps for both cell lines illustrate the readout of the interaction of proteins and metabolites. The applied mathematical technology of 13CFlux is well documented in numerous publication of the lab (Nöh et al., 2006, 2007; Weitzel et al., 2013). At this point the description of the results is limited to the biology, processing and integration of the data, and the description of the resulting flux maps for Luhmes d0 and d6 cells.

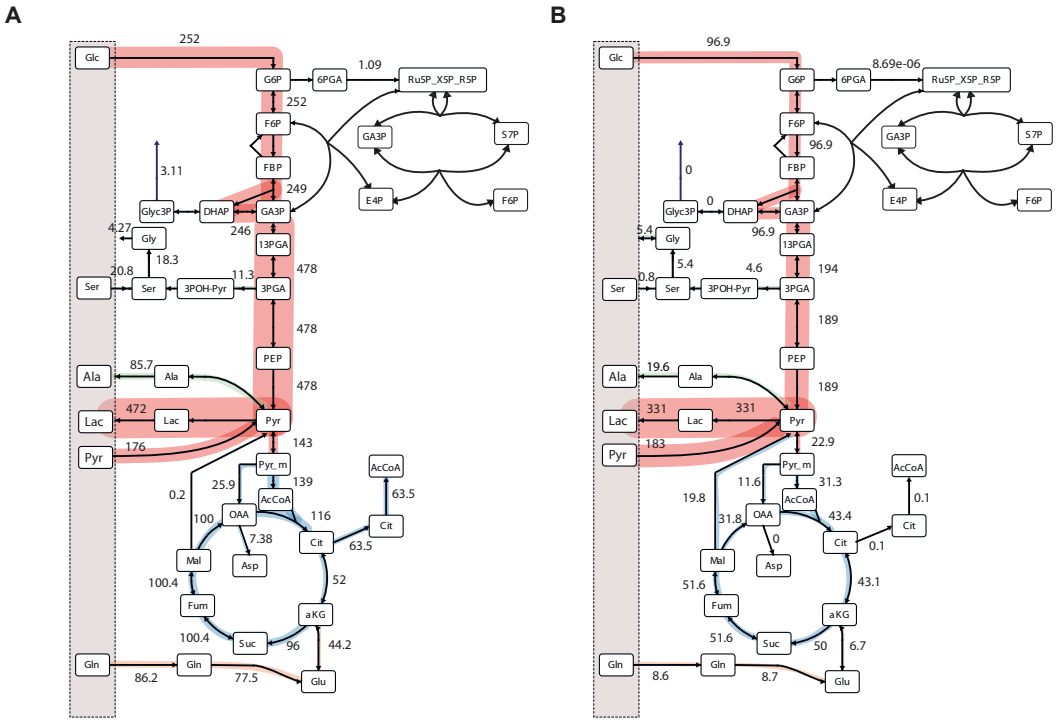


Figure 3.42.: Instationary metabolic flux analysis in Luhmes cells. (A) Metabolic flux map of Luhmes d0, neuronal precursor cells. (B) Metabolic flux map of terminal, neuronal Luhmes d6 cells. Absolute flux values are shown in $nmol/(10^6\ cells\ x\ h)$. Thickness of pathway lines corresponds to the metabolic flux and is normalised to the highest flux within each cell line.

In comprehensive time course pSIRM experiments (0–24 hrs) we determined absolute intracellular and extracellular metabolite pool sizes as well as the incorporation of both stable isotopes $^{13}C$-Glc and $^{13}C$-Gln in Luhmes d0 and d6 cells. The substrate uptake and production rates are examined in an independent experiment covering a longer time frame than the pSIRM time course. Input for the modelling the dynamics of isotope incorporation are mass isotopomer distributions (MIDs) of metabolite specific fragments. A pSIRM-experiment specific plug-in in MAUI-SILVIA provides the export of MIDs for predefined fragments from each measurement. The quality of the exported MIDs is validated regarding multiple parameters in MTXQC, as described in Section 3.3.3.2. The correction of natural isotope abundance of the MIDs has been performed following the published method by Wahl et al. (2004) in the Nöh lab (Jülich). Additional material complementing the INST-MFA are collected in Supplemental D.

The absolute fluxes in Luhmes d0 and d6 cells are illustrated in a simplified network in Figure 3.42. The thickness of each pathway is normalised to the highest absolute flux within one cell line. Absolute fluxes are stated in $nmol/(10^6\ cell\ x\ h)$ and are shown next to the pathway.

In the following the metabolic activities are characterized by comparing ratios of absolute fluxes, summarised in Table 3.3.

As shown before both cell types differ regarding their nutrient consumption and carbon-routing in the CCM. Luhmes d0 cells utilise 2.6-times more glucose, and 10-times more

Table 3.3.: Comparison of CCM pathway activity by flux ratio analysis in Luhmes d0 and d6 cells. Ratios are calculated based on absolute flux values in $nmol/(10^6\ cells\ x\ h)$.

| **Nb.** | **Description** | **Flux ratios** | **d0** | **d6** | **FC d6 / d0** |
|---|---|---|---|---|---|
| FR1 | Aerobic glycolysis | $Lac_{out} : Glc_{in}$ | 1.87 | 3.42 | 1.8 |
| FR2 | Contribution of Pyr to W | $Pyr_{glyc} : Pyr_{in}$ | 2.7 | 1.03 | 0.38 |
| FR3 | Mitochondrial Import of Pyr | $Pyr_{PDHc} : Pyr_{PC}$ | 5.4 | 2.7 | 0.5 |
| FR4 | Mitochondr. Respr. vs. WE | $Cit : Lac$ | 0.25 | 1.3 | 5.2 |
| FR5 | Fate of citric acid | $Cit_c : Cit_m$ | 1.2 | 0 | n.def. |
| FR6 | $\alpha$-ketoglutaric acid synthesis | $aKG_{Cit} : aKG_{Glu}$ | 1.17 | 6.4 | 5.47 |
| FR7 | ETC activity | $Fum : (aCoA + aKG)$ | 0.55 | 1.36 | 2.47 |
| FR8 | Malic acid production | $Mal_{MDH} : Mal_{ME}$ | 500 | 1.6 | 0 |
| FR9 | Serine synthesis | $Ser : 3PGA$ | 0.05 | 0.02 | 0.4 |
| FR10 | Alanine synthesis | $Ala : Pyr$ | 0.18 | 0.1 | 0.55 |

glutamine in comparison to their neuronal counterparts.

Almost all glucose-derived carbons are shuttled into the synthesis of lactic acid in the precursor cell line. One molecule of glucose is converted into two molecules of Lac based on the stoichiometry of the glycolysis. The ratio of $Lac_{out} : Glc_{in} = 1.87$ reflects the predominant conversion of Glc into Lac (Table 3.3-FR1). In mature neurons the ratio exceeds this limit, pointing towards an additional source of carbon that contributes to the production of Lac.

In Luhmes d6 cells the uptake of extracellular Pyr is almost in the same proportion of the glycolytic flux into the Pyr pool; whereas in the pluripotent precursor cells this flux only contributes to one-third to the intracellular pool (Table 3.3-FR2). In general the metabolic flux into Lac is the dominating pathway of both cell lines. The routing of Pyr into mitochondria is facilitated by two enzymes — the pyruvate dehydrogenase complex (PDHc) and pyruvate carboxylase (PC). The regulation of this central hub has been described in Section 3.2.3.1. In Luhmes d0 cells the mitochondrial import of Pyr is mainly driven by the PDHc (Table 3.3-FR3). With differentiation the activity of PC increases and facilitates one-third of the mitochondrial import of Pyr in Luhmes d6 cells.

The enzyme citrate synthase (CS), first enzyme of the TCA-cycle and solely expressed in the mitochondria, catalyses the fusion of oxalic acid (OAA) and acetyl-CoA (AcCoA) in citric acid (Cit). This intermediate either fuels mitochondrial oxidative phosphorylation or the synthesis of fatty acids in the cytosol by its export via the citrate/malate-pyruvate shuttle. Latter pathway shows an high metabolic flux in Luhmes d0 cells that almost vanishes with neuronal differentiation (Table 3.3-FR5).

Glutamine (Gln) is an alternative carbon source to replenish the TCA-cycle. Converted into glutamic acid (Glu) the nutrient enters in form of $\alpha$-ketoglutaric acid (aKG) the TCA-cylce. In Luhmes d0 cells glucose and glutamine contribute in an equal manner carbons for the synthesis of the aKG (Table 3.3-FR6). The differentiation in Luhmes d6 results in a reduced uptake of glutamine and mainly glycolysis-derived carbons are shuttled into the TCA-cycle and aKG. The comparison of the sum of metabolic influxes in the mitochondria (Glc: aCoA, Gln: aKG) to the metabolic flux into fumaric acid (Fum) reveals the impact

of mitochondrial oxidation in Luhmes d6 cells (Table 3.3-FR7). The activity of the ETC increases up to 2.5-fold in mature neurons. The metabolic flux further diverges at the following metabolite malic acid (Mal) that is converted into OAA by MDH or into Pyr by the mitochondrial or cytosolic variant of malic enzyme (ME). Herein the metabolic flux via the ME increases with neuronal differentiation in Luhmes d6 cells (Table 3.3-FR8). Luhmes d0 cells solely use malic acid for the synthesis of OAA, closing the TCA-cylce.
The metabolic pathways glycolysis, TCA-cycle and glutaminolysis maintain cellular homeostasis and provide the majority of reducing equivalents, substrates for adjacent pathways and building blocks. The pentose phosphate pathway could not been evaluated due to an inefficient quantification of its intermediates. Lower pathway activities but present in both cell lines are the routing of carbons into the synthesis of serine (Ser), alanine (Ala), and glycerol-3-phosphate (Glyc3P).

# 4 Discussion

## 4.1. The Warburg effect in cancer and stem cells

Cancer cells represent an extreme cellular phenotype — resistance to cell death signals and activation of invasion and metastasis are only two of the main characteristics that have been summarised by Hanahan and Weinberg (Hanahan and Weinberg, 2000, 2011). The events causing genomic aberrations and leading to oncogene activation or tumor suppressor inhibition, and subsequently inducing tumorigenesis, are complex, random and rarely shared among different cancer types, or even among patients suffering from the same disease.

Quite in contrary is the phenotype of stem cells. Each single event, e.g., cell duplication, is tightly controlled by a complex interaction of check-points that are defined right from the "beginning" and are not acquired during a complex process like tumorigenesis. The restrictive fate of a stem cell is in direct contrast to the random nature of cancer cells.

Despite their divergent phenotype both cell systems share the metabolic modus named Warburg effect or aerobic glycolysis postulated by Otto Warburg in the early 1930s. Since then a number of studies have been published proposing explanations how the alteration of glycolysis outperforms the supply of energy equivalents by mitochondrial respiration in cancer cells (Vander Heiden et al., 2009; Hsu and Sabatini, 2008). It has been demonstrated that glycolytic enzymes are targeted by transcription factors and oncogenes, e.g., HIF-1$\alpha$ or c-Myc (Yeung et al., 2008; Albihn et al., 2010). The latter one is also required for the reprogramming of pluripotency. The combined application of Kfl4, Sox2, Oct4 and c-Myc induces the gain of pluripotency in somatic cells; a finding that has been decorated with

the Nobel price of medicine in 2012 (Takahashi and Yamanaka, 2006). The work presented here provides data to compare both cell types glycolysis on the level of the proteome and metabolome and to identify common and cell type specific aspects of the Warburg effect.

Quantitative proteomics and metabolomics approaches have been applied in the frame of four experiments addressing the metabolic reprogramming in cancer, stem and reprogrammed iPS cells, as well as in native and derived fibroblasts. The integrative analysis of all these projects confirms the increased routing of glucose-derived carbons into lactic acid in pluripotent and cancerous cell types in comparison to somatic cells as described in the literature (Zhang et al., 2012).

The Warburg effect, namely the increased routing of glucose into lactic acid, is reversible and programmable as shown during the induction of pluripotency in fibroblast cell lines, resulting in an increased transport of carbon-13 into the synthesis of lactic acid in iPS cells (Figure 4.1). With differentiation into iPS-DFs the rate of $^{13}C$-Glc incorporation in Lac decreases to a similar level as seen in the native fibroblasts before. Also the differentiation of pluripotent Luhmes d0 cells into mature, dopaminergic neurons (Luhmes d6) induces a reduction of $^{13}C$-Glc incorporation in Lac and goes along with an elevated trafficking of carbons into the TCA-cycle.

The rearrangement of carbon routing is not an event during the early differentiation of

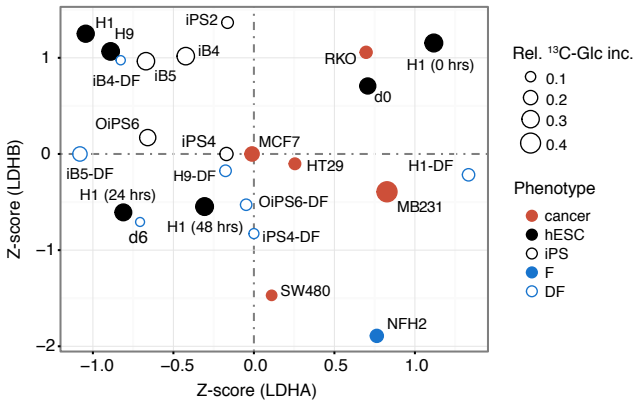


Figure 4.1.: Expression of LDH isoenzymes in pluripotent, cancer and differentiated cells in relation to $^{13}C$-Glc incorporation in lactic acid. Details of the analysis are summarised in Section 2.5. $^{13}C$-Glc incorporation in lactic acid is shown as scaled area size of each data point.

stem cells. The incorporation of $^{13}C$-Glc remains constant during the first 48 hours of differentiation in hESC H1 cells.

The integrative illustration of protein levels, metabolite quantities and $^{13}C$-Glc incorporation demonstrates a huge variance of isoenzyme expression and carbon routing (Figure 4.2). The box for each metabolite merges the information of the pool sizes (box height) and the incorporation rate of $^{13}C$ - Glc (scaled, coloured bar within the box). Protein expression levels are shown as averaged z-scores in the heatmap separating stem cell and cancer cell derived data.

The comparison reveals that hESCs contain almost twice the amount of Lac in comparison to the analysed cancer cell lines. As shown earlier, Lac discriminants the quantitative metabolic profiles of cancer and stem cells in the principal component analysis (see Figure 3.24-C and Supp. Figure C.2). The quantities of $^{13}C$-Lac are within the range from $8 - 35\ nmol/1 \times 10^6$ cells in both cell types; whereas markedly higher levels have been determined in late stage breast cancer MDA-MB231 and hESCs H1 cells.

Interestingly, the levels of LDH isoforms, the enzyme catalysing the conversion from pyruvic into lactic acid, differ between both cell types. The enzyme is composed of two dimeric subunits of its isoenzymes LDHA and LDHB.

The first-mentioned one is a known target of oncogenes and in the focus in studies addressing the regulation of the glycolytic enzymes in cancer. In comparison little is known about LDHB. It has been shown that the loss of LDHB alter cell growth of triple negative breast cancer cells *in vitro* and reduce tumor growth *in vivo* (McCleland et al., 2012).

Pluripotent cells, hESC as well as iPS cells, are characterised by high levels of LDHB, whereas cancer cells predominantly express LDHA (Figure 4.1 and Figure 4.2).

The abundance of LDHB drops significantly after 24 hrs of stem cell differentiation in contrast to the constant carbon-13 incorporation in Lac.

Lactic acid is only one product of glycolysis. Upstream intermediates link glycolysis with amino acid and lipid synthesis, the pentose phosphate pathway, and the one-carbon metabolism providing precursors and building blocks for biosynthesis. Though the expression of enzymes is quite different, hESCs and cancer cells incorporate glucose-derived

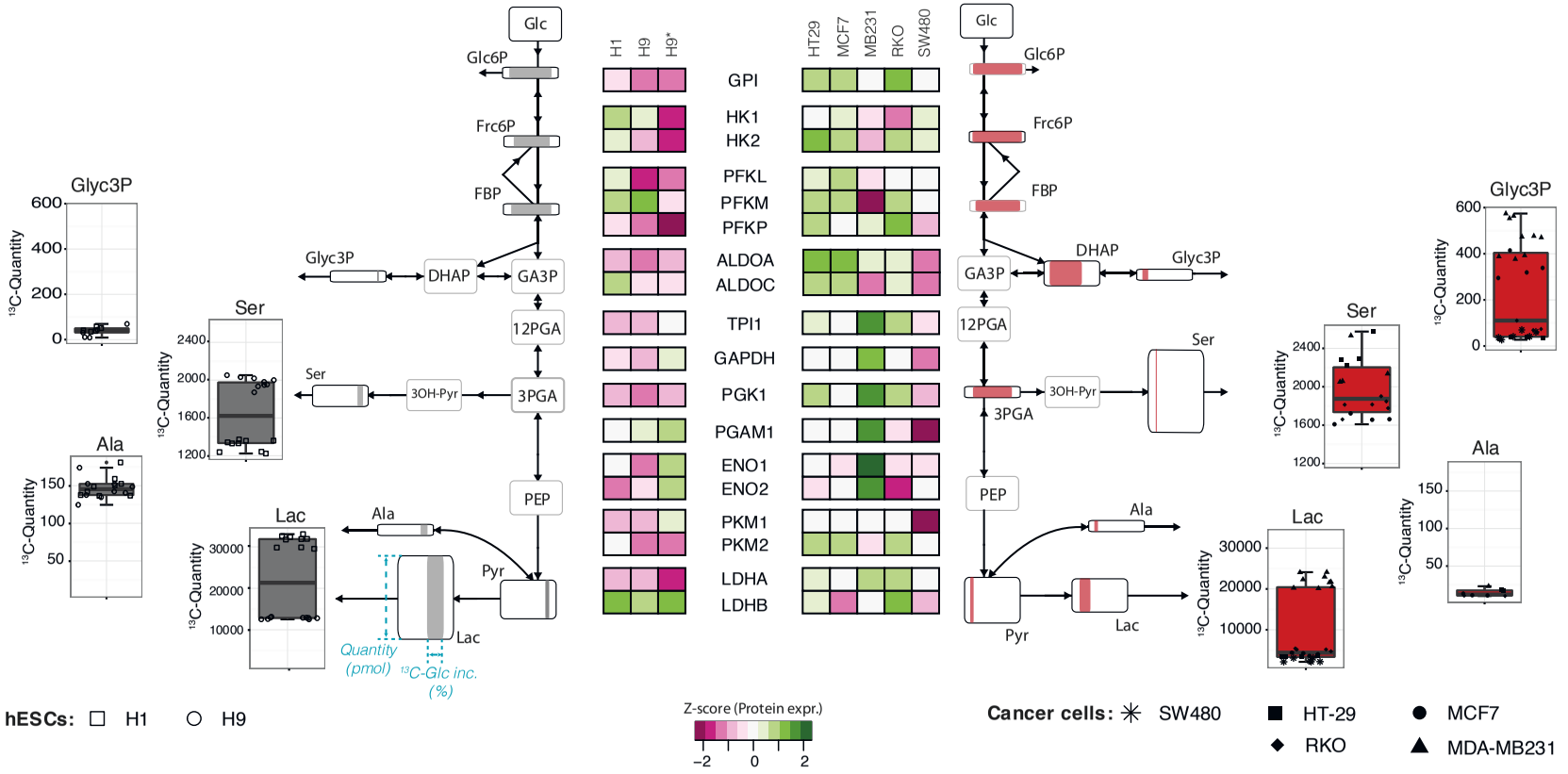


Figure 4.2.: Integrative analysis of glycolysis: protein expression, metabolite pool sizes, and $^{13}C$-Glc incorporation show multiple routes leading to the Warburg effect in hESCs (black, left side) and cancer cells (red, right side). Metabolite quantities are reflected in the height of the boxes. The width of the coloured bar inside the box represents the averaged incorporation rate of $^{13}C$-Glc in the respective intermediate. Labelled quantities of selected outputs of glycolysis are shown in boxplots for both cell types. Expression levels of glycolytic enzymes are summarised in the heatmap located in the center of the figure.

carbons in a similar manner. Variations between both phenotypes are shown in glycolytic products, e.g., serine (Figure 4.2). The amino acid links the CCM and the one-carbon metabolism providing functional groups that are required for histone and DNA methylation, a prerequisite to maintain cellular pluripotency. Expression levels of proteins associated with the one-carbon metabolism are raised in hESCs and reprogrammed iPS cells. Also the transport of glucose-derived carbons into the serine synthesis is elevated in pluripotent cells and, analogue to carbon-routing into lactic acid, reversible during the induction of pluripotency and re-differentiation.
Though the incorporation rate of $^{13}C$-Glc is lower in cancer cells, the $^{13}C$-labeled quantities of serine is within a range of $1.2 - 2\ nmol/1 \times 10^6$ cells in both cell types.

In the literature the predominantly usage of glucose for the synthesis of lactic acid is described as a metabolic phenomenon in proliferating cells like cancer cells (Vander Heiden et al., 2009). Recently, we showed that this metabolic mode also occurs in senescent lymphoma cells. In co-operation with Jan Doerr (C.A. Schmitt lab, Charité, Germany) we contributed to the investigation of metabolic reprogramming in senescent lymphoma cells (Doerr et al., 2013). The experiments demonstrated that the metabolic phenomenon "Warburg effect" is not an exclusive property of dividing cells. Primary E$\mu - myc$ lymphoma mice are an established mouse model to study therapy-induced senescence (TIS), a terminal growth arrest of viable cells caused by histone 3 lysine 9 trimethylation (H3K9me3) blocking the entry into cell cycle S-phase (Narita et al., 2003; Braig et al., 2005; Schmitt et al., 2002). These cells lack any apoptotic response due to the transduction with the apoptosis regulating protein Bcl2. The induction of TIS in E$\mu - myc$; Bcl2 cells depends on the expression of SUV39h1, a H3K9 histone methyltransferase. The application of the chemotherapeutic agent adriamycin (ADR) results in a terminal growth arrest in SUV39h1 proficient (control) lymphoma cells. In contrast E$\mu - myc$;Bcl2 SUV39h1-deficient (SUV-) cells maintain their cell proliferation independently from the ADR treatment (Figure 4.3-A).
Interestingly, the senescent control cells show an increased uptake of glucose in the FDG-PET scan. SUV- lymphoma cells are not affected by the treatment with ADR and do not alter the consumption rate of glucose. Tracing the fate of glucose reveals that the induc-

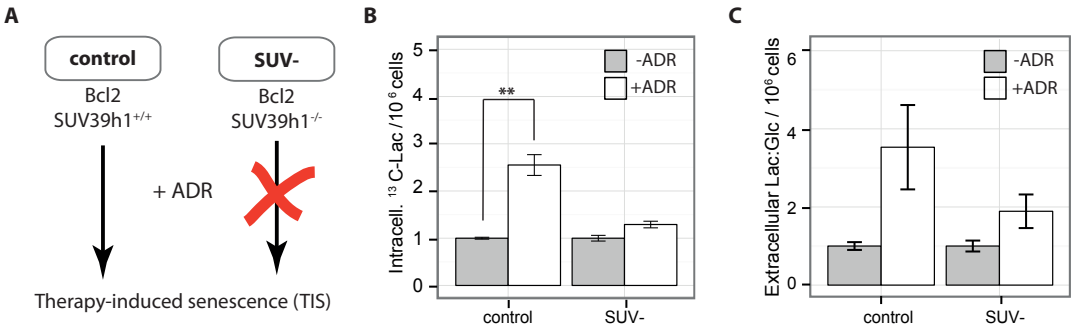


Figure 4.3.: Proliferation-independent Warburg effect in E$\mu - myc$;Bcl2 transduced mouse lymphoma cells. (A) Adriamycin (ADR) treatment induces senescence (TIS) in SUV39h1-proficient (control) cells. A lack of SUV39h1 (SUV-) expression does not alter the cell growth independently from the treatment. (B) Incorporation of $^{13}C$ - Glc increases in intracellular lactic acid (Lac) after the induction of senescence in control cells. (C) Lactic acid accumulates in the media after ADR treatment in control cells. Shown are mean values of three biological replicates.

tion of senescence in control cells is accompanied by the reprogramming of metabolism. The incorporation of $^{13}C$-Glc in Lac and the extracellular export of Lac increases after ADR treatment in control cells; two main characteristics of aerobic glycolysis (Figure 4.3-B and C). At the same time these cells also accelerate their TCA-cycle activity and fatty acid synthesis. This hyper-metabolic mode creates the possibility to drive E$\mu - myc$ mouse lymphoma cells into synthetic lethality. An additional block of glycolysis induced by the inhibition of the glucose transporter (phloretin), a stable knockdown of HK2, or the inhibition of LDH (sodium oxamate) results in decreased viability of lymphoma cells.

In summary, cancer and stem cells share the metabolic mode of an increased transport of glucose-derived carbons into lactic acid, described as aerobic glycolysis or Warburg effect. This metabolic mode is reversible as shown in reprogrammed iPS cells and their derived fibroblasts. Nevertheless the executing proteins are different in stem and cancer cells. A multitude of alterations in glycolytic isoenzyme expression lead to the increased routing of glucose into the synthesis of lactic acid. The integrative analysis of proteomics and metabolomics data has demonstrated, that only the measurement of the intracellular intermediates provides information to decipher how cells meet their phenotype-specific demands regarding cellular maintenance and proliferation.

## 4.2. Global analysis of cancer, pluripotent cells and fibroblasts.

The quantitative characterisation of protein expression, metabolite abundance and carbon routing in the CCM have been performed in a panel of pluripotent, cancer and differentiated cell lines. Phenotype-specific characteristics have been identified in the integrative analysis in Section 3.2. For this purpose cell lines were grouped regarding their phenotype into cancer, pluripotent, iPS cells, native and derived fibroblasts. Protein levels, metabolite quantities and isotopic incorporation rates were averaged across all cell lines for each phenotype. Similarities in protein expression have been detected in cancer, stem and iPS cells, and respectively for native and derived fibroblasts. The phenotype specific mean values of protein levels are suprisingly consistent and show a low variance, e.g., isoenzymes of LDH and MDH.

Proteins with raised expression levels in cancer and iPS cells, but not in hESCs cells, are of special interest. These enzymes are not affected by the natural pluripotency machinery, but vulnerable for external stimuli leading to an acquired, potent cell state.
Eighteen out of ninety-eight shared proteins between cancer and iPS cells are associated with metabolic pathways and in particular related to the TCA-cycle, e.g., SDHA, MDH2, FH (Figure 3.23). Protein levels of these enzymes are shown in Figure 3.24-A and B. The isoenzymes SDHA and FH have been described as tumor suppressor genes involved in familiar paraganglioma, leiomyoma and renal cancer (Burnichon et al., 2010; Levine and Puzio-Kuter, 2012). The role of both proteins in reprogramming pluripotency has not been addressed so far.

Protein levels, metabolite quantities and isotope incorporation rates are combined for each cell line in a global, multi-omics profile. For the integrative analysis all global profiles have been merged into a comprehensive data matrix summarising the quantities of 41 isoenzymes, 41 absolute pool sizes and in total 68 isotope incorporation rates derived from three $^{13}C$-substrates and resolved regarding the number of incorporated carbons.
Data derived from the neuronal differentiation of Luhmes cells and the analysis of early differentiation have been excluded due to the missing application $^{13}C$-Pyr in those setups.

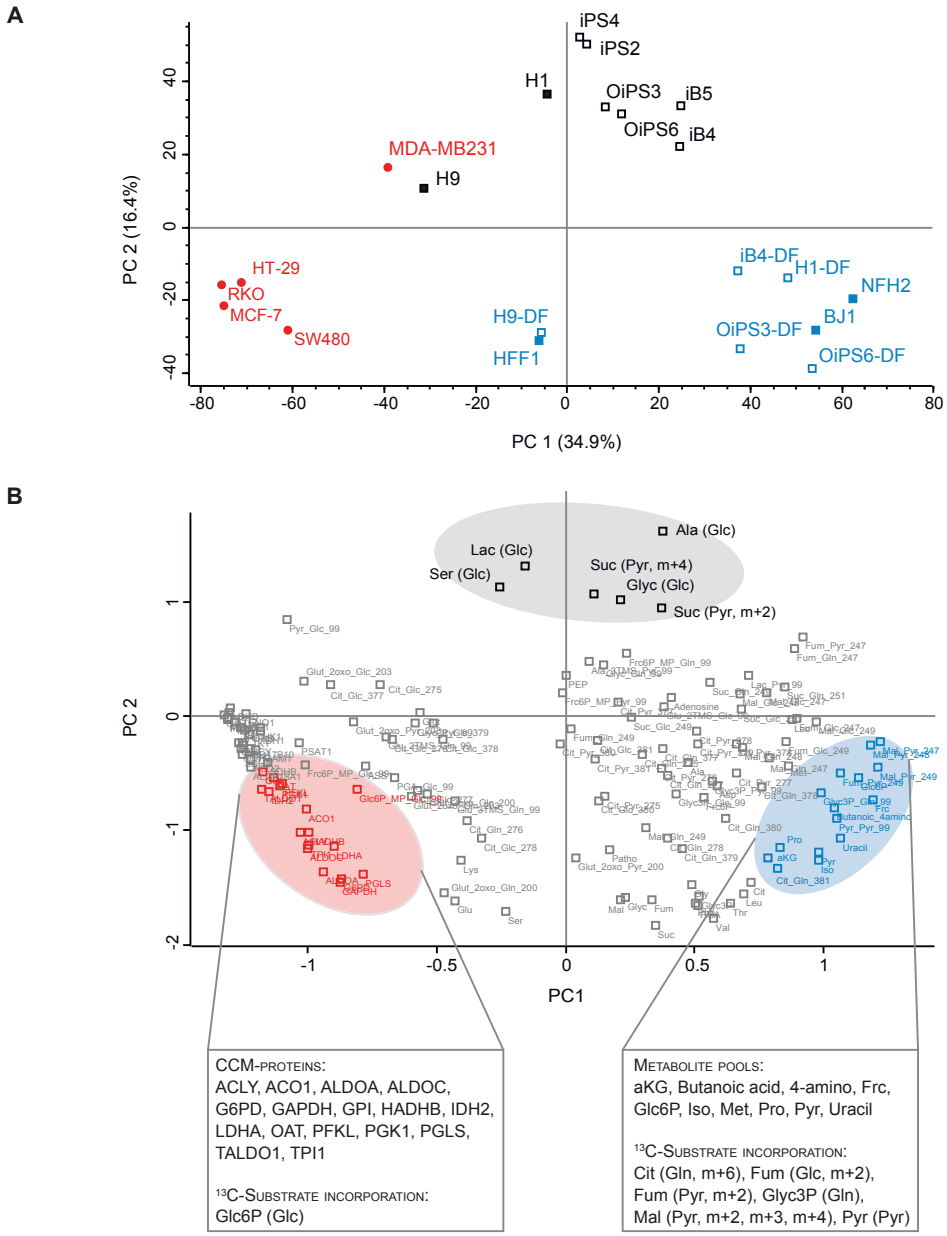


Figure 4.4.: Principal component analysis of quantitative isoenzyme levels, metabolite abundances, and incorporation of three $^{13}C$-substrates (Glc, Gln, Pyr) in hESCs, iPS and cancer cells, as well as native and derived fibroblasts. (A) The score plot shows the principal components PC1 and PC2. Both components discriminate three clusters composed of pluripotent (black: hESCs, iPS cells), cancer (red), and differentiated (blue; native and derived fibroblasts) cell lines. (B) Corresponding loading vectors of the PCA. Major contributing vectors are selected manually and highlighted in corresponding phenotype color.

The principal component analysis ascertains a separation of the global cell profiles regarding their phenotype based on the quantitative information of 150 intermediates (Figure 4.4-A).

The principal components PC1 and PC2 describe approximately 50% of the variance of the data and provide the distinction of three clusters covering almost exclusively a specific cellular phenotype. PC1 discriminates cancer, pluripotent and differentiated cells, whereas PC2 distinguishes further between the pluripotent cells from cancer and fibroblasts. With few exceptions the global profile of reprogrammed iPS cells or derived fibroblasts cluster together with their native equivalents hESCs or fibroblasts. The late breast cancer cell line MDA-MB231 and hESCs H9 show differences in the global profile in comparison to their counterparts.

Most influential loadings are coloured regarding their corresponding phenotype in the scoring plot (Figure 4.4-B). Interestingly, each cluster is defined by a specific kind of data of the global profile. The incorporation of $^{13}C$-Glc in lactic acid, serine, alanine and glycerol and of $^{13}C$-Pyr in succinic acid distinguish hESCs and iPS cells from cancer cells and fibroblasts. The expression levels of CCM-related isoenzymes determine the clustering of cancer cell lines. Contributing loading vectors are central enzymes e.g., GAPDH, GPI, LDHA, PFKM, ACO1, IDH2 and G6PD[1]. All these enzymes are known to be affected by oncogenic activation and as targets of transcription factors that are altered during tumorigenesis. Indeed, high and medium increased levels of GPI and G6PD have been detected in breast and colorectal cancer cell lines (Uhlén et al., 2015). Furthermore the enzyme GAPDH is involved prostate cancer, mutated IDH2 acquire the ability to produce 2HG in glioblastoma cells and LDHA in general os known as target of oncogenes, e.g., c-Myc (Sirover, 1999; Dang et al., 2009; Qing et al., 2010).

Absolute pool sizes of CCM intermediates specify differentiated cells, e.g., $\alpha$KG, Glc6P, Pyr, as well as amino acid levels of Iso, Met, and Pro. The somatic cells shows an unique incorporation of $^{13}C$-Glc into TCA-cycle intermediates citric and malic acid. Both metabolites render important hubs in the CCM. The isotopic pattern in citric acid gives

[1]Glucose-6-phosphate-1-dehydrogenase, cytoplasm

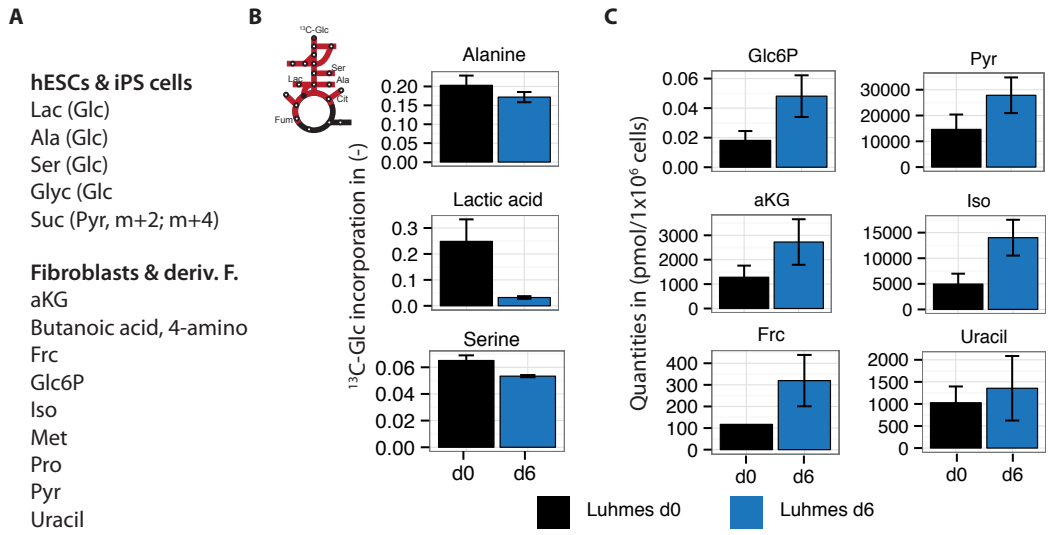


Figure 4.5.: Luhmes d0 and d6 cells confirm phenotype-specific features derived from the global profile analysis. (A) Phenotype-defining parameters for pluripotent and differentiated cells. (B) Pluripotent Luhmes d0 cells show increased 13C-Glc incorporation in comparison to differentiated counterparts. (C) Pool sizes of CCM-intermediates are raised in differentiated Luhmes d6 cells.

an indirect measure of the cycling of carbons through the TCA-cycle. Differentiated cells shows an increased turnover of carbons in the TCA-cycle fueling ATP-synthesis. In cancer and pluripotent cells the elevated incorporation of $^{13}C$-Glc in citric acid is not further processed towards subsequent downstream intermediates pointing towards an increased export of citric acid into the cytosol. Cytosolic citric acid provides precursors for fatty acid synthesis and post-translational modification of proteins. The acetyl-CoA-dependent acetylation of proteins provides the crosstalk regulating transcription and translation, nutrient sensing, control cell cycle and cell fate (Folmes et al., 2012). Glutaminolysis provides carbon to replenish the oxidative and reductive part of the TCA-cycle driving the synthesis of ATP and provides nitrogen for nucleotide synthesis in hESCs and cancer cells.

Not only the routing within the TCA-cycle, also the entry of carbons into the TCA-cycle is specifically regulated. The isotope pattern in malic acid emphasises the entry of pyruvate at the point of OAA into the TCA-cylce via OAA in differentiated cells. The reaction is catalysed by the pyruvate carboxylase (PC) that requires an obligatory activator: acetyl-

CoA. Carbons entering the cycle via PC are transported anticlockwise within the TCA-cycle into malic acid, that is exported into the cytosol fueling gluconeogenesis.

Indeed, the clustering analysis of the solitary omics-data revealed the cell phenotype specific regulated of protein expression, the abundance of metabolite pools or nutrient uptake. The comparison of the global profiles enables the identification of the essential features of the CCM characterising a cellular phenotype. Protein levels describe cancer cells, carbon routing into glycolysis pluripotent cells and metabolite pool sizes and incorporation rates in mitochondrial metabolites characterise differentiated cells. The experimental setup addressing terminal, neuronal differentiation in Luhmes cells has been excluded from the global profile analysis, due to missing application of $^{13}C$-Pyr. The comparison of pool sizes and $^{13}C$-Glc incorporation in pluripotent Luhmes d0 cells and their differentiated counterparts is in agreement with the defined phenotype-specific features (Figure 4.5). The routing of glucose-derived carbons is increased in lactic acid, alanine and serine in Luhmes d0 cells. On the other hand pool sizes of amino acids are raised in terminal differentiated neurons Luhmes d6.

## 4.3. INST-MFA cells shows rearrangement of mitochondrial metabolism after terminal, neuronal differentiation in Luhmes cells

The analysis of metabolic fluxes complements the molecular characterisation of a cell. Though expression profiles of genes, proteins and metabolite pool sizes gain worthwhile insights, only the determination of metabolic fluxes provides a functional readout (Niedenführ et al., 2015; Weindl et al., 2015). The distribution of metabolic fluxes reflect the summary of post-transcriptional and post-translational regulation.
In the 1970s established concepts of MFA have been revised and further refined during the last decade. Most commonly, metabolic flux rates have been determined to unravel the structure of genetic modified organisms to optimise the yield of a bacterial-derived products (Nocon et al., 2014; Coze et al., 2013).
Recently, eukaryotic cells gain a greater visibility in metabolic flux analysis, e.g., monitoring the regulation of cancer metabolism (Murphy et al., 2013). The determination of metabolic fluxes in eukaryotic cells is challenging due to compartment-separated pathways, the complex cell cultivation media containing several carbon-sources and the aim for genome-wide networks (Zamboni, 2011). The interpretation of enzyme activities based solely on isotope incorporation are limited when it comes to complex pivots in biochemical networks, e.g., the conversion of pyruvate inside the mitochondria combining reversible reactions. Only the determination of absolute fluxes using computational power allows a proper analysis of the direction and therefore the activity of enzymes.

Non-stationary MFA (INST-MFA) approaches overcome the limitations of stationary MFA and can provide the investigation of transient processes. Major advantages are the independence of the analysis from cofactor balance, reduced amount of required substrates, an improved information of flux identification and estimation of intracellular metabolite levels, that are not possible to measure (Amaral, 2011). But with the gain of knowledge the complexity of the required input data increases. INST-MFA requires (i) a model

of the metabolic network, (ii) a closed carbon-balance given by substrate uptake and products export, and (iii) isotope incorporation pattern and (iv) the absolute pool sizes of intermediates located in the metabolic network (Zamboni, 2011; Niedenführ et al., 2015). The neuronal cell model Luhmes has been used to determine and compare the metabolic flux maps of pluripotent and differentiated cells. The deactivation of v-myc initiates the differentiation of Luhmes d0 cells into neuronal cells within six days (Luhmes d6). The quantitative profiles of the metabolome and proteome, as well as the individual flux maps of both cell types have been described in Section 3.1.4 and Section 3.3.4. Herein the combined analysis of transcriptome, proteome and fluxome data of the CCM illustrates a multi-omix perspective of metabolic reprogramming during terminal, neuronal differentiation.

The terminal, neuronal differentiation induces a rearrangement of fluxome, proteome and transcriptome as shown in the comparison of Luhmes d6 relatively to Luhmes d0 cells (Figure 4.6).

With the loss of pluripotency Luhmes d6 cells reduce the uptake of nutrients and their turnover within the CCM. Notably, neuronal cells maintain a high metabolic flux into lactic acid, independently from the low glycolytic rate. Differentiation induces a switch of carbon sources contributing to the synthesis of Lac. Whereas Luhmes d0 cells predominantly use glucose-derived carbons to fuel Lac synthesis, differentiated Luhmes d6 cells maintain their high synthesis rate by the uptake of extracellular pyruvic acid that is supplemented in the cell culture media.

Also mitochondria fluxes are affected by the loss of pluripotency. The uptake of glutamine and the metabolic flux of glutaminolysis into the TCA-cycle decreases with differentiation. It is known that glutaminolysis is under the direct control of the oncogene *myc* and a reduction of the metabolic flux has been expected due to the induction of differentiation by the deactivation of *v-myc* (Dang, 2010; Gao et al., 2009).

Luhmes d6 cells solely uses glycolysis and pyruvic acid derived carbons to fuel mitochondrial respiration. The activity of pyruvate carboxylase (PC) raises in Luhmes d6 cells and provides an alternative pathway to replenish the TCA-cycle, a phenomenon that has been described by Duarte et al. (2011), in one of the few INST-MFA studies in mam-

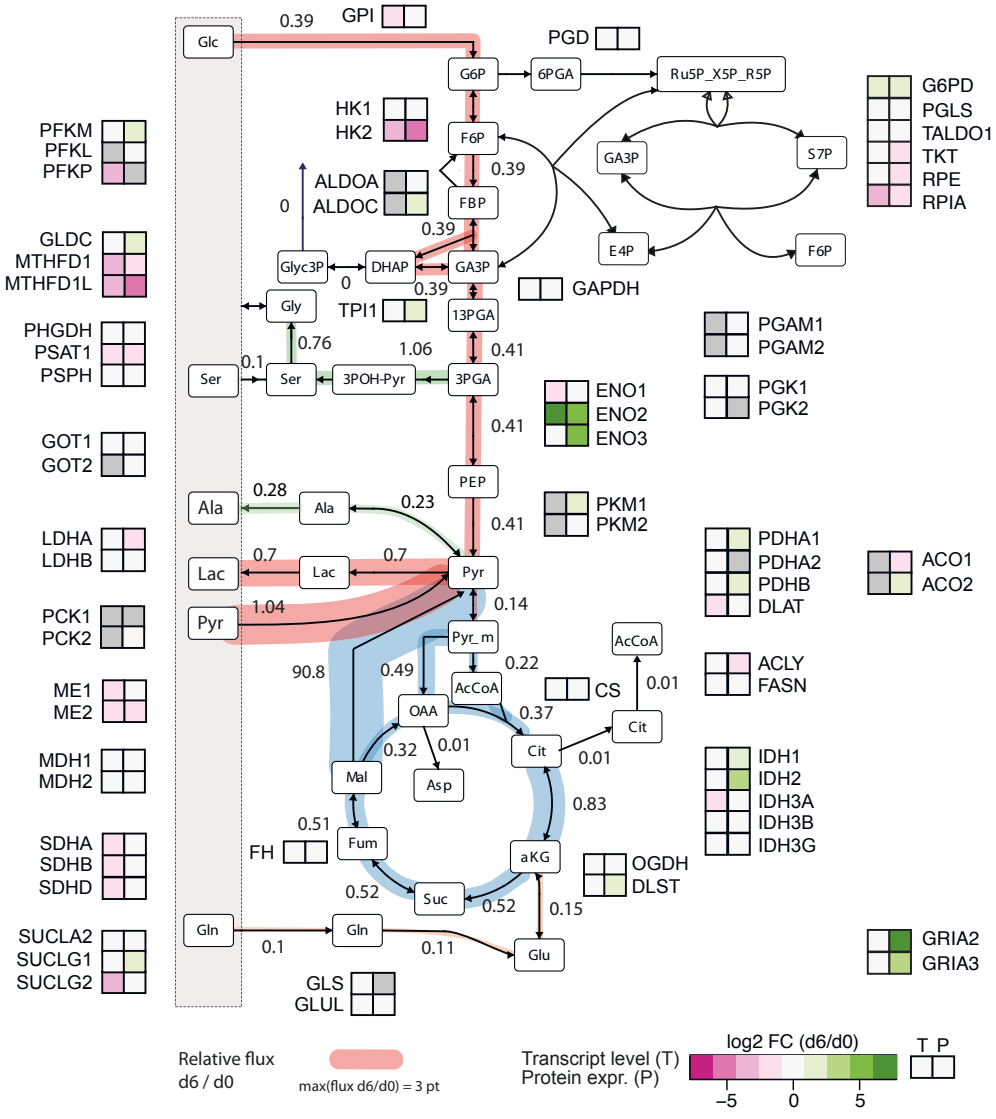


Figure 4.6.: Terminal, neurone differentiation induces a rearrangement of metabolic fluxes in Luhmes cells. The flux maps shows flux ratios of Luhmes d6 / d0 cells in glycolysis, TCA-cycle and amino acid synthesis. Ratios of absolute fluxes are shown next to the reactions. Thickness of pathways is scaled regarding the fluxes with the exception of the flux of Mal into Pyr. This reaction has to be scaled separately because of the absence of any flux in Luhmes d0 cells. Transcriptome and protein levels are integrated for central enzymes in form of heatmaps showing log2 fold changes Luhmes d6 / d0 cells. Not determined transcript and protein levels or not quantified metabolite pools are shown in grey.

Table 4.1.: Key parameters of published INST-MFA studies in mammalian cells. Pool sizes are distinguished in measures / assumed ones.
*n.s. — not shown; * — questionable, no exact statements*

| Reference | Organism | Cell type | Comp. | Substrate | Intracell. Pools | Reactions | Technology |
|---|---|---|---|---|---|---|---|
| Luhmes model | human | Luhmes | 2 | Glc, Gln | 22/60 | 66 | GC-MS |
| Bagga et al. (2014) | mice | neurons | 3 | Gln | 2/10 | 13 | NMR |
| Shlomi et al. (2014) | human | fibrosarcoma | 1 | Met | 6/8 | 9 | LC-MS |
| Jeffrey et al. (2013) | rat | neurons | 2 | Glc | 3/5 | 7 | NMR |
| Murphy et al. (2013) | human | B-cells | 2 | Glc | n.s./35 | 54 | GC-MS |
| Duarte and Gruetter (2013) | rat | neurons | 3 | Glc | 8/12 | 24 | NMR |
| Duarte et al. (2011) | rat | neurons | 2 | Glc | 3/12 | 16 | NMR |
| Amaral (2011) | mice | neurons | 1 | Glc | 2/32 | 47 | GC-MS |
| Ahn and Antoniewicz (2011) | hamster | ovary cells | Glc | 2 | n.s./77* | 73 | GC-MS |
| Maier et al. (2009) | rat | hepatocytes | Gln | 3 | 11/47 | 73 | GC-MS |
| Hofmann et al. (2008) | human | hepatocytes | Glc | 2 | 14/25 | 40 | GC/LC-MS |
| Munger et al. (2008) | human | lung fibroblasts | Glc | | 4/17 | 12 | LC-MS |

malian, neuronal cells. Furthermore the export of mitochondrial malic acid and citric acid is adjusted to the metabolic needs of neuronal cells. The export of malic acid increases, whereas the export of citric acid decreases in differentiated cells.
Luhmes d0 cells show a nutrient-specific fuelling of metabolic pathways. While pyruvate-derived carbons fuel the oxygen-independent part of the TCA-cycle providing citric acid for the synthesis of fatty acids and precursors for protein-acetylation in the cytosol, glutamine is used to run the oxygen-dependent reactions and the synthesis of ATP. Interestingly, the alterations of the metabolic fluxes are not predictable by the quantification of either the transcriptome, nor the proteome. Transcript and protein expression levels of the main enzymes are not affected by the differentiation in Luhmes cells. In particular the protein expression of TCA-cycle isoenzymes remain constant and do not mirror any alterations of the metabolic fluxes. Only the low expression levels of ACLY, the enzyme converting citric acid into its precursors acetyl-CoA and OAA in the cytosol, indicate a reduction of the metabolic flux.

The complexity of INST-MFA requires an extensive sampling, an increased demand of measurement and data analysis time. So far only few studies have been published performing INST-MFA in mammalian cells, predominantly in neuronal cells, as summarised by Niedenführ et al. (2015). Main parameters of published INST-MFA studies are collected in Table 4.1. The majority of studies have been performed in neuronal cells to understand the metabolic fluxes between glial and neuronal cells. These studies have been limited to

small subnetworks and include only a few absolutely quantified pool sizes (Bagga et al., 2014; Jeffrey et al., 2013; Duarte and Gruetter, 2013; Duarte et al., 2011). Maier et al. (2009) and Ahn and Antoniewicz (2011) set up the first networks covering the central carbon metabolism including glycolysis, TCA-cylce and amino acid synthesis. Murphy and colleagues performed a comparison of different MFA strategies in B-cells. They concluded that INST-MFA provides the most robust approach to determine metabolic fluxes (Murphy et al., 2013). The integration of multiple time points of isotope incorporation and the least restrictive modelling assumptions results in a highly precise flux determination free from bias introduced e.g., by isotopic steady-state assumptions.

In a novel approach the INST-MFA analysis in Luhmes cells incorporates simultaneously the isotope incorporation of two $^{13}C$-substrates and covers several pathways of the central carbon metabolism. The majority of pool sizes have been supplemented with absolute values determined in both cell types. The determination of metabolic fluxes in the pentose phosphate pathway are limited by the inefficient detection of its intermediates.

In summary, the herein established workflow — starting from the cell culture and ending at the development of computational tools — results in the determination of metabolic flux maps providing the evaluation of metabolic reprogramming in pluripotent and differentiated cells. Further time course experiments in hESCs, iPS and cancer cells can be implemented in the present framework. The experimental handling as well as the data analysis strategies are setup and ready for further developments.

Though the work provides only a partial comparison of the metabolic flux maps of two phenotypes in the context of all determined data it provides novel insights in metabolic reprogramming. Similarties in isotope incorporation, metabolite abundance and protein expression levels between pluripotent Luhmes d0 cells and hESCs or iPS cells, or respectively Luhmes d6 and somatic cells, might point towards a related metabolic flux map. Applying the criteria defining a pluripotent state based on a global cell profile as outlined in the section before, Luhmes d0 cells full-fill the determined characteristics of a pluripotent cell. In that way the conclusions might be drawn also the other way around — from shared phenotype-specific characteristics towards similarities in metabolic flux maps.

# 5 Outlook

The herein presented workflow — starting with the cell culture dish and ending at the metabolic flux maps — provides new targets to interfere with metabolic reprogramming in cancer and stem cells. Only INST-MFA allows to monitor the short-term effects of applied small molecules, e.g., protein kinase inhibitors or toxins, on the level of the metabolome. In the frame of the cooperation project between Jülich, Konstanz and Berlin (BMBF Dynametox) we analysed the different affects of toxins to neuronal Luhmes d6 cells. The mode of operation of a toxin can be defined in three phases: early, adaptive and terminal. We applied isotopic-labeled nutrients ($^{13}C$-Glc, $^{13}C$-Gln) in extensive time course experiments to monitor the dynamics of stable isotope incorporation in each phase after the application of a toxin.
The implementation of the data in the established INST-MFA network for Luhmes d6 cells may result in metabolic flux maps reflecting the metabolic mode of action of the compound. Determining the point of action may help to identify new targets addressing metabolic disorders.

So far, INST-MFA requires a dense sampling and the generation of high numbers of samples during a time course application of stable isotopes, resulting in an increased demand of measurement and data analysis time. Isotope incorporation data, as well as intra- and extracellular metabolite levels have to be evaluated and incorporated into the complex computational framework. In addition, for the determination of substrate uptake and production rates, a different time window of sampling has to be chosen. Whereas intracellular dynamics have to be determined within seconds up to minutes or an hour, the accumulation or uptake of metabolites in the media requires a sampling up to several

hours.

The limitation of the analysis to a few key points mirroring specific pathways activity may provide the adaption of the present workflow and to focus on the screening of small molecules in cell culture experiments. Though the absolute quantification of metabolic fluxes may result in the determination of exact numbers, e.g., produced reducing equivalents, a rather rough readout, e.g., pathway on or off, may be sufficient enough to develop new strategies to interfere with a specific pathway.

Based on the present data, particularly the evaluation of the function of the metabolite 2HG in cancer and stem cells will be in the focus of follow-up experiments. The identification of the catalysing enzymes as well as the quantification of both stereoisomers are challenging tasks for the future. The confirmation of the mixed blessing of 2HG would provide an interesting target to balance the metabolic characteristics of cancer and stem cells.

At the same time the introduced tool for GC-MS derived data analysis (MTXQC) is going to be implemented in a R package, providing the platform-independent evaluation of data quality. Although the field of metabolomics is still in its infancy, an increasing number of labs implement their metabolomics platforms and contribute to the analysis of different cell system. An interchangeable evaluation of metabolomics data may nourish the fruitful exchange and interaction between laboratories.

# 6 Publication list

## 6.1. Publication

### Published

Zasada, Christin, and Stefan Kempa. 2016. Quantitative Analysis of Cancer Metabolism: From pSIRM to MFA. Inbook. In Metabolism in Cancer, edited by Thorsten Cramer and Clemens A. Schmitt, 20720. Cham: Springer International Publishing. doi:10.1007/978-3-319-42118-6-9.

Pietzke, Matthias*, Christin Zasada*, Susann Mudrich, and Stefan Kempa. 2014. Decoding the Dynamics of Cellular Metabolism and the Action of 3-Bromopyruvate and 2-Deoxyglucose Using Pulsed Stable Isotope-Resolved Metabolomics. Cancer & Metabolism 2 (1): 9. doi:10.1186/2049-3002-2-9. *First authors with equal contribution

Mastrobuoni, Guido, Christin Zasada, Fabian Bindel, Lukas Aeberhard, and Stefan Kempa. 2014. Rapid Peptide in-Solution Isoelectric Focusing Fractionation for Deep Proteome Analysis. Journal of Chromatography Separation Techniques 5 (5). OMICS International. doi:10.4172/2157-7064.1000240.

Doerr, Jan R, Yong Yu, Maja Milanovic, Gregor Beuster, Christin Zasada, J Henry M Däbritz, Jan Lisec, et al. 2013. Synthetic Lethal Metabolic Targeting of Cellular Senescence in Cancer Therapy. Nature 501 (7467): 42125. doi:10.1038/nature12437.

Rohwer, Nadine, Christin Zasada, Stefan Kempa, and Thorsten Cramer. 2012. The Growing Complexity of HIF-1$\alpha$s Role in Tumorigenesis: DNA Repair and Beyond. Oncogene, no. September (November): 18. doi:10.1038/onc.2012.510.

### In discussion for correct authorship

Moussaieff, Arieh, Matthieu Rouleau, Daniel Kitsberg, Merav Cohen, Gahl Levy, Dinorah Barasch, Alina Nemirovski, et al. 2015. Glycolysis-Mediated Changes in Acetyl-CoA and Histone Acetylation Control the Early Differentiation of Embryonic Stem Cells. Cell Metabolism 21 (3): 392402. doi:10.1016/j.cmet.2015.02.002.

### In revision

Varano, Gabriele, Simon Raffel, Martina Sormani et. al. The B-cell receptor confers super competitor status to lymphoma cells via GSK3 inhibition. Nature

Thomas J. Park, Jane Reznick, Bethany L. Peterson , Gregory Blass , Damir Omerbasic, Nigel C. Bennett, P. Henning J.L. Kuich, Christin Zasada, Brigitte M. Browe, Wiebke Hamann et. al. "Fructose driven glycolysis supports anoxia resistance in the naked mole-rat" Science

### In preparation

Zasada, Christin, Chris Bielow, and Stefan Kempa MTXQC - quality control for GC-MS metabolomics data.

Zasada, Christin, Simon Gutbier, Johannes Delp, Martin Cerff, Katharina Nöh, Marcel Leist, and Stefan Kempa INST-MFA in LUHMES cells

Zasada, Christin, and Stefan Kempa Strategies to implement multi-omics data analysis to gain insights in the metabolic reprogramming of the CCM.

Zasada, Christin, Katharina Nöh, and Stefan Kempa GC-MS fragment mapping for presicion in metabolic flux studies.

## 6.2. Patents

Short term isotope pulse labeling method for analysing metabolic products in biological samples; United States Patent Application 20150330969

Short term isotope pulse labeling method for analysing metabolic products in biological samples; European Patent EP2944963

# 7 Bibliography


W. S. Ahn and M. R. Antoniewicz. Metabolic flux analysis of CHO cells at growth and non-growth phases using isotopic tracers and mass spectrometry. *Metabolic engineering*, 13(5):598–609, sep 2011. ISSN 1096-7184. doi: 10.1016/j.ymben.2011.07.002. URL http://www.ncbi.nlm.nih.gov/pubmed/21821143.

A. Albihn, J. I. Johnsen, and M. Arsenian Henriksson. MYC in Oncogenesis and as a Target for Cancer Therapies. *Advances in Cancer Research*, 107(10):163–224, 2010. doi: 10.1016/S0065-230X(10)07006-5. URL http://linkinghub.elsevier.com/retrieve/pii/S0065230X10070065.

A. Amaral. A comprehensive metabolic profile of cultured astrocytes using isotopic transient metabolic flux analysis and 13C-labeled glucose. *Frontiers in Neuroenergetics*, 3, 2011. ISSN 16626427. doi: 10.3389/fnene.2011.00005. URL http://journal.frontiersin.org/article/10.3389/fnene.2011.00005/abstract.

A. I. Amaral, A. P. Teixeira, U. Sonnewald, and P. M. Alves. Estimation of Intracellular Fluxes in Cerebellar Neurons After Hypoglycemia : Importance of the Pyruvate Recycling Pathway and Glutamine Oxidation. *Journal of Neuroscience Research*, 710:700–710, 2011. doi: 10.1002/jnr.22571.

I. Amelio, F. Cutruzzolá, A. Antonov, M. Agostini, and G. Melino. Serine and glycine metabolism in cancer. *Trends in biochemical sciences*, 39(4):191–8, apr 2014. ISSN 0968-0004. doi: 10.1016/j.tibs.2014.02.004. URL http://www.ncbi.nlm.nih.gov/pubmed/24657017http://www.pubmedcentral.nih.gov/articlerender.fcgi?artid=PMC3989988http://linkinghub.elsevier.com/retrieve/pii/S0968000414000280.

L. Armstrong, K. Tilgner, G. Saretzki, S. P. Atkinson, M. Stojkovic, R. Moreno, S. Przyborski, and M. Lako. Human Induced Pluripotent Stem Cell Lines Show Stress Defense Mechanisms and Mitochondrial Regulation Similar to Those of Human Embryonic Stem Cells. *STEM CELLS*, 28(4):661–673, jan 2010. ISSN 10665099. doi: 10.1002/stem.307. URL http://doi.wiley.com/10.1002/stem.307.

P. Bagga, K. L. Behar, G. F. Mason, H. M. De Feyter, D. L. Rothman, and A. B. Patel. Characterization of cerebral glutamine uptake from blood in the mouse brain: implications for metabolic modeling of 13C NMR data. *Journal of Cerebral Blood Flow & Metabolism*, 34(10):1666–1672, oct 2014. ISSN 0271-678X. doi: 10.1038/jcbfm.2014.129. URL http://jcb.sagepub.com/lookup/doi/10.1038/jcbfm.2014.129.

G. W. Beadle and E. L. Tatum. Genetic Control of Biochemical Reactions in Neurospora. *Proceedings of the National Academy of Sciences of the United States of America*, 27(11):499–506, 1941. ISSN 0003-0147. doi: 10.1086/281267.

S. A. Beausoleil, J. Villén, S. A. Gerber, J. Rush, and S. P. Gygi. A probability-based approach for high-throughput protein phosphorylation analysis and site localization. *Nature biotechnology*, 24 (10):1285–92, oct 2006. ISSN 1087-0156. doi: 10.1038/nbt1240. URL `http://www.ncbi.nlm.nih.gov/pubmed/16964243`.

C. Bielow, G. Mastrobuoni, and S. Kempa. Proteomics Quality Control: Quality Control Software for MaxQuant Results. *Journal of Proteome Research*, 15(3):777–787, mar 2016. ISSN 15353907. doi: 10.1021/acs.jproteome.5b00780. URL `http://pubs.acs.org/doi/abs/10.1021/acs.jproteome.5b00780`.

M. J. Birket, A. L. Orr, A. A. Gerencser, D. T. Madden, C. Vitelli, A. Swistowski, M. D. Brand, and X. Zeng. A reduction in ATP demand and mitochondrial activity with neural differentiation of human embryonic stem cells. *Journal of Cell Science*, 124(3):348–358, feb 2011. ISSN 0021-9533. doi: 10.1242/jcs.072272. URL `http://jcs.biologists.org/cgi/doi/10.1242/jcs.072272`.

M. Braig, S. Lee, C. Loddenkemper, C. Rudolph, A. H. F. M. Peters, B. Schlegelberger, H. Stein, B. Dörken, T. Jenuwein, and C. A. Schmitt. Oncogene-induced senescence as an initial barrier in lymphoma development. *Nature*, 436(7051):660–5, aug 2005. ISSN 1476-4687. doi: 10.1038/nature03841. URL `http://www.ncbi.nlm.nih.gov/pubmed/16079837`.

J. M. Buescher, M. R. Antoniewicz, L. G. Boros, S. C. Burgess, H. Brunengraber, C. B. Clish, R. J. DeBerardinis, O. Feron, C. Frezza, B. Ghesquiere, E. Gottlieb, K. Hiller, R. G. Jones, J. J. Kamphorst, R. G. Kibbey, A. C. Kimmelman, J. W. Locasale, S. Y. Lunt, O. D. Maddocks, C. Malloy, C. M. Metallo, E. J. Meuillet, J. Munger, K. Nöh, J. D. Rabinowitz, M. Ralser, U. Sauer, G. Stephanopoulos, J. St-Pierre, D. a. Tennant, C. Wittmann, M. G. Vander Heiden, A. Vazquez, K. Vousden, J. D. Young, N. Zamboni, and S.-M. Fendt. A roadmap for interpreting 13C metabolite labeling patterns from cells. *Current Opinion in Biotechnology*, 34:189–201, 2015. ISSN 09581669. doi: 10.1016/j.copbio.2015.02.003. URL `http://linkinghub.elsevier.com/retrieve/pii/S0958166915000221`.

N. Burnichon, J.-j. Brie, R. Libe, L. Vescovo, J. Riviere, F. Tissier, E. Jouanno, X. Jeunemaitre, P. Benit, A. Tzagoloff, P. Rustin, J. Bertherat, J. Favier, and A.-P. Gimenez-Roqueplo. SDHA is a tumor suppressor gene causing paraganglioma. 19(15):3011–3020, 2010. doi: 10.1093/hmg/ddq206.

B. W. Carey, L. W. S. Finley, J. R. Cross, C. D. Allis, and C. B. Thompson. Intracellular $\alpha$-ketoglutarate maintains the pluripotency of embryonic stem cells. *Nature*, dec 2014. ISSN 1476-4687. doi: 10.1038/nature13981. URL `http://www.nature.com/nature/journal/vaop/ncurrent/full/nature13981.html?WT.ec{_}id=NATURE-20141211`.

J. Cox and M. Mann. MaxQuant enables high peptide identification rates, individualized p.p.b.-range mass accuracies and proteome-wide protein quantification. *Nature Biotechnology*, 26(12): 1367–1372, dec 2008. ISSN 1087-0156. doi: 10.1038/nbt.1511. URL `http://www.nature.com/doifinder/10.1038/nbt.1511`.

F. Coze, F. Gilard, G. Tcherkez, M.-J. Virolle, A. Guyonvarch, G. Mahajan, L. Balachandran, S. Bentley, K. Chater, A. Cerdeño-Tárraga, G. Challis, and E. Al. Carbon-Flux Distribution within Streptomyces coelicolor Metabolism: A Comparison between the Actinorhodin-Producing Strain M145 and Its Non-Producing Derivative M1146. *PLoS ONE*, 8(12):e84151, dec 2013. ISSN 1932-6203. doi: 10.1371/journal.pone.0084151. URL `http://dx.plos.org/10.1371/journal.pone.0084151`.

C. V. Dang. Enigmatic MYC Conducts an Unfolding Systems Biology Symphony. *Genes Cancer*, 1(6):526 –531, 2010. ISSN 19476027. doi: 10.1177/1947601910378742. URL `http://gan.sagepub.com/content/1/6/526.abstract`.

L. Dang, D. W. White, S. Gross, B. D. Bennett, M. a. Bittinger, E. M. Driggers, V. R. Fantin, H. G. Jang, S. Jin, M. C. Keenan, K. M. Marks, R. M. Prins, P. S. Ward, K. E. Yen, L. M. Liau, J. D. Rabinowitz, L. C. Cantley, C. B. Thompson, M. G. Vander Heiden, and S. M. Su. Cancer-associated IDH1 mutations produce 2-hydroxyglutarate. Technical Report 7274, 2009. URL `http://dx.doi.org/10.1038/nature08617`.

L. M. F. de Godoy, J. V. Olsen, J. Cox, M. L. Nielsen, N. C. Hubner, F. Fröhlich, T. C. Walther, and M. Mann. Comprehensive mass-spectrometry-based proteome quantification of haploid versus diploid yeast. *Nature*, 455(7217):1251–4, oct 2008. ISSN 1476-4687. doi: 10.1038/nature07341. URL `http://www.ncbi.nlm.nih.gov/pubmed/18820680`.

J. Deprez, D. Vertommen, D. R. Alessi, L. Hue, and M. H. Rider. Phosphorylation and Activation of Heart 6-Phosphofructo-2-kinase by Protein Kinase B and Other Protein Kinases of the Insulin Signaling Cascades. *Journal of Biological Chemistry*, 272(28):17269–17275, jul 1997. ISSN 0021-9258. doi: 10.1074/jbc.272.28.17269. URL `http://www.jbc.org/cgi/doi/10.1074/jbc.272.28.17269`.

J. R. Doerr, Y. Yu, M. Milanovic, G. Beuster, C. Zasada, J. H. M. Däbritz, J. Lisec, D. Lenze, A. Gerhardt, K. Schleicher, S. Kratzat, B. Purfürst, S. Walenta, W. Mueller-Klieser, M. Gräler, M. Hummel, U. Keller, A. K. Buck, B. Dörken, L. Willmitzer, M. Reimann, S. Kempa, S. Lee, and C. A. Schmitt. Synthetic lethal metabolic targeting of cellular senescence in cancer therapy. *Nature*, 501(7467):421–5, sep 2013. ISSN 1476-4687. doi: 10.1038/nature12437. URL `http://www.ncbi.nlm.nih.gov/pubmed/23945590`.

B. Domon and R. Aebersold. Options and considerations when selecting a quantitative proteomics strategy. *Nature biotechnology*, 28(7):710–721, 2010. ISSN 1087-0156. doi: 10.1038/nbt.1661. URL `http://dx.doi.org/10.1038/nbt.1661`.

J. M. N. Duarte and R. Gruetter. Glutamatergic and GABAergic energy metabolism measured in the rat brain by 13C NMR spectroscopy at 14.1 T. *Journal of Neurochemistry*, 126(5):579–590, 2013. ISSN 00223042. doi: 10.1111/jnc.12333.

J. M. N. Duarte, B. Lanz, and R. Gruetter. Compartmentalized Cerebral Metabolism of [1,6-13C]Glucose Determined by in vivo13C NMR Spectroscopy at 14.1 T. *Frontiers in Neuroenergetics*, 3, 2011. ISSN 1662-6427. doi: 10.3389/fnene.2011.00003. URL `http://journal.frontiersin.org/article/10.3389/fnene.2011.00003/abstract`.

T. Ezashi, P. Das, and R. M. Roberts. Low O2 tensions and the prevention of differentiation of hES cells. *Proceedings of the National Academy of Sciences*, 102(13):4783–4788, mar 2005. ISSN 0027-8424. doi: 10.1073/pnas.0501283102. URL http://www.pnas.org/cgi/doi/10.1073/pnas.0501283102.

T. W. M. Fan, A. N. Lane, R. M. Higashi, M. A. Farag, H. Gao, M. Bousamra, and D. M. Miller. Altered regulation of metabolic pathways in human lung cancer discerned by (13)C stable isotope-resolved metabolomics (SIRM). *Molecular cancer*, 8:41, 2009. ISSN 1476-4598. doi: 10.1186/1476-4598-8-41.

J. D. Fassett and J. Paul. Isotope Dilution Mass Spectrometry for Accurate Elemental Analysis. *Analytical chemistry*, 61(10):643–649, 1989. ISSN 0003-2700. doi: 10.1021/ac00185a715.

C. D. L. Folmes, T. J. Nelson, A. Martinez-Fernandez, D. K. Arrell, J. Z. Lindor, P. P. Dzeja, Y. Ikeda, C. Perez-Terzic, and A. Terzic. Somatic oxidative bioenergetics transitions into pluripotency-dependent glycolysis to facilitate nuclear reprogramming. *Cell metabolism*, 14(2):264–71, aug 2011. ISSN 1932-7420. doi: 10.1016/j.cmet.2011.06.011. URL http://www.ncbi.nlm.nih.gov/pubmed/21803296http://www.pubmedcentral.nih.gov/articlerender.fcgi?artid=PMC3156138.

C. D. L. Folmes, P. P. Dzeja, T. J. Nelson, and A. Terzic. Metabolic Plasticity in Stem Cell Homeostasis and Differentiation. *Cell Stem Cell*, 11(5):596–606, nov 2012. ISSN 19345909. doi: 10.1016/j.stem.2012.10.002. URL http://www.ncbi.nlm.nih.gov/pubmed/23122287http://www.pubmedcentral.nih.gov/articlerender.fcgi?artid=PMC3593051http://linkinghub.elsevier.com/retrieve/pii/S1934590912005838http://www.cell.com/cell-stem-cell/fulltext/S1934-5909(12)00583-8.

P. Gao, I. Tchernyshyov, T.-C. Chang, Y.-S. Lee, K. Kita, T. Ochi, K. I. Zeller, A. M. De Marzo, J. E. Van Eyk, J. T. Mendell, and C. V. Dang. c-Myc suppression of miR-23a/b enhances mitochondrial glutaminase expression and glutamine metabolism. *Nature*, 458(7239):762–765, 2009. ISSN 0028-0836. doi: 10.1038/nature07823. URL http://dx.doi.org/10.1038/nature07823.

K. Gottlob, N. Majewski, S. Kennedy, E. Kandel, R. B. Robey, and N. Hay. Inhibition of early apoptotic events by Akt/PKB is dependent on the first committed step of glycolysis and mitochondrial hexokinase. *Genes & development*, 15(11):1406–18, jun 2001. ISSN 0890-9369. doi: 10.1101/gad.889901. URL http://www.ncbi.nlm.nih.gov/pubmed/11390360http://www.pubmedcentral.nih.gov/articlerender.fcgi?artid=PMC312709.

N. Gregersen, J. Ingerslev, and K. Rasmussen. Low molecular weight organic acids in the urine of the newbown. *Acta Paediatrica*, 66(1):85–89, jan 1977. ISSN 0803-5253. doi: 10.1111/j.1651-2227.1977.tb07812.x. URL http://doi.wiley.com/10.1111/j.1651-2227.1977.tb07812.x.

S. P. Gygi, B. Rist, S. a. Gerber, F. Turecek, M. H. Gelb, and R. Aebersold. Quantitative analysis of complex protein mixtures using isotope-coded affinity tags. *Nature biotechnology*, 17(10):994–999, 1999. ISSN 1087-0156. doi: 10.1038/13690.

D. Hanahan and R. A. Weinberg. The hallmarks of cancer. *Cell*, 100(1):57–70, jan 2000. ISSN 0092-8674. URL http://www.ncbi.nlm.nih.gov/pubmed/10647931.

D. Hanahan and R. A. Weinberg. Hallmarks of cancer: the next generation. *Cell*, 144(5):646–674, 2011. ISSN 00928674. doi: 10.1016/j.cell.2011.02.013. URL http://dx.doi.org/10.1016/j.cell.2011.02.013http://www.ncbi.nlm.nih.gov/pubmed/21376230.

C. S. Henry, L. J. Broadbelt, and V. Hatzimanikatis. Thermodynamics-based metabolic flux analysis. *Biophysical journal*, 92(5):1792–805, mar 2007. ISSN 1542-0086. doi: 10.1529/biophysj.106.093138. URL http://www.pubmedcentral.nih.gov/articlerender.fcgi?artid=1796839{&}tool=pmcentrez{&}rendertype=abstracthttp://www.sciencedirect.com/science/article/pii/S0006349507709876.

K. G. Heumann. Isotope dilution mass spectrometry. *International Journal of Mass Spectrometry and Ion Processes*, 118-119(August 1991):575–592, 1992. ISSN 01681176. doi: 10.1016/0168-1176(92)85076-C.

U. Hofmann, K. Maier, A. Niebel, G. Vacun, M. Reuss, and K. Mauch. Identification of metabolic fluxes in hepatic cells from transient13C-labeling experiments: Part I. Experimental observations. *Biotechnology and Bioengineering*, 100(2):344–354, jun 2008. ISSN 00063592. doi: 10.1002/bit.21747. URL http://doi.wiley.com/10.1002/bit.21747.

M. Hoshimaru, J. Ray, D. W. Sah, and F. H. Gage. Differentiation of the immortalized adult neuronal progenitor cell line HC2S2 into neurons by regulatable suppression of the v-myc oncogene. *Proceedings of the National Academy of Sciences of the United States of America*, 93(February): 1518–1523, 1996. ISSN 00278424. doi: 10.1073/pnas.93.4.1518.

P. P. Hsu and D. M. Sabatini. Cancer cell metabolism: Warburg and beyond. *Cell*, 134(5):703–7, sep 2008. ISSN 1097-4172. doi: 10.1016/j.cell.2008.08.021. URL http://www.ncbi.nlm.nih.gov/pubmed/18775299.

A. M. Intlekofer, R. G. DeMatteo, S. Venneti, L. W. S. Finley, C. Lu, A. R. Judkins, A. S. Rustenburg, P. B. Grinaway, J. D. Chodera, J. R. Cross, and C. B. Thompson. Hypoxia Induces Production of L-2-Hydroxyglutarate. *Cell Metabolism*, 22(2):304–311, 2015. ISSN 19327420. doi: 10.1016/j.cmet.2015.06.023.

Y. Ishihama, Y. Oda, T. Tabata, T. Sato, T. Nagasu, J. Rappsilber, and M. Mann. Exponentially modified protein abundance index (emPAI) for estimation of absolute protein amount in proteomics by the number of sequenced peptides per protein. *Molecular & cellular proteomics : MCP*, 4(9):1265–1272, 2005. ISSN 1535-9476. doi: 10.1074/mcp.M500061-MCP200.

K. Ito and T. Suda. Metabolic requirements for the maintenance of self-renewing stem cells. *Nature reviews. Molecular cell biology*, 15(4):243–56, 2014a. ISSN 1471-0080. doi: 10.1038/nrm3772. URL http://www.ncbi.nlm.nih.gov/pubmed/24651542.

K. Ito and T. Suda. Metabolic requirements for the maintenance of self-renewing stem cells. *Nature reviews. Molecular cell biology*, 15(4):243–56, apr 2014b. doi: 10.1038/nrm3772. URL http://www.ncbi.nlm.nih.gov/pubmed/24651542.

F. M. Jeffrey, I. Marin-Valencia, L. B. Good, A. A. Shestov, P.-G. Henry, J. M. Pascual, and C. R. Malloy. Modeling of brain metabolism and pyruvate compartmentation using 13C NMR in vivo: caution required. *Journal of Cerebral Blood Flow & Metabolism*, 33(8):1160–1167, aug 2013. ISSN 0271-678X. doi: 10.1038/jcbfm.2013.67. URL http://jcb.sagepub.com/lookup/doi/10.1038/jcbfm.2013.67.

P. A. Jones and S. B. Baylin. The fundamental role of epigenetic events in cancer. *Nature Reviews Genetics, Published online: 01 June 2002; — doi:10.1038/nrg816*, 3(6):415, 2002. doi: 10.1038/nrg816.

A. Joyce and B. Palsson. The model organism as a system: integrating'omics' data sets. *Nature Reviews Molecular Cell Biology*, 7(3):198–210, 2006. URL http://www.nature.com/nrm/journal/v7/n3/abs/nrm1857.html.

S. Kempa, W. Rozhon, J. Samaj, A. Erban, F. Baluska, T. Becker, J. Haselmayer, E. Schleiff, J. Kopka, H. Hirt, and C. Jonak. A plastid-localized glycogen synthase kinase 3 modulates stress tolerance and carbohydrate metabolism. *The Plant journal : for cell and molecular biology*, 49(6):1076–90, mar 2007. ISSN 0960-7412. doi: 10.1111/j.1365-313X.2006.03025.x. URL http://www.pubmedcentral.nih.gov/articlerender.fcgi?artid=1865003{&}tool=pmcentrez{&}rendertype=abstract.

S. Kempa, J. Hummel, T. Schwemmer, M. Pietzke, N. Strehmel, S. Wienkoop, J. Kopka, and W. Weckwerth. An automated GCxGC-TOF-MS protocol for batch-wise extraction and alignment of mass isotopomer matrixes from differential 13 C-labelling experiments: a case study for photoautotrophic-mixotrophic grown Chlamydomonas reinhardtii cells. *Journal of Basic Microbiology*, 49(1):82–91, feb 2009. ISSN 0233111X. doi: 10.1002/jobm.200800337. URL http://doi.wiley.com/10.1002/jobm.200800337.

M. C. Kerr and R. D. Teasdale. Defining Macropinocytosis. *Traffic*, 10(4):364–371, apr 2009. ISSN 13989219. doi: 10.1111/j.1600-0854.2009.00878.x. URL http://doi.wiley.com/10.1111/j.1600-0854.2009.00878.x.

H. Kondoh, M. E. Lleonart, Y. Nakashima, M. Yokode, M. Tanaka, D. Bernard, J. Gil, and D. Beach. A High Glycolytic Flux Supports the Proliferative Potential of Murine Embryonic Stem Cells. *Antioxidants & Redox Signaling*, 9(3):293–299, mar 2007. ISSN 1523-0864. doi: 10.1089/ars.2006.1467. URL http://www.liebertonline.com/doi/abs/10.1089/ars.2006.1467.

E. Kováts. Gas-chromatographische Charakterisierung organischer Verbindungen. Teil 1: Retentionsindices aliphatischer Halogenide, Alkohole, Aldehyde und Ketone. *Helvetica Chimica Acta*, 41(7):1915–1932, 1958. ISSN 0018-019X. doi: 10.1002/hlca.19580410703. URL http://dx.doi.org/10.1002/hlca.19580410703$\delimiter"026E30F$nhttp://onlinelibrary.wiley.com/doi/10.1002/hlca.19580410703/abstract$\delimiter"026E30F$nhttp://onlinelibrary.wiley.com/store/10.1002/hlca.19580410703/asset/19580410703{_}ftp.pdf?v=1{&}t=hdq0x5mu{&}s=d7c44ebbbeb663bfa7a7cad25a424cc2a087.

M. Krajcovic, S. Krishna, L. Akkari, J. A. Joyce, and M. Overholtzer. mTOR regulates phagosome and entotic vacuole fission. *Molecular biology of the cell*, 24(23):3736–45, dec 2013. ISSN

1939-4586. doi: 10.1091/mbc.E13-07-0408. URL http://www.ncbi.nlm.nih.gov/pubmed/24088573http://www.pubmedcentral.nih.gov/articlerender.fcgi?artid=PMC3842999.

P. H. J. L. Kuich, N. Hoffmann, and S. Kempa. Maui-VIA: A User-Friendly Software for Visual Identification, Alignment, Correction, and Quantification of Gas Chromatography-Mass Spectrometry Data. *Frontiers in bioengineering and biotechnology*, 2(January):84, 2014. ISSN 2296-4185. doi: 10.3389/fbioe.2014.00084. URL http://journal.frontiersin.org/article/10.3389/fbioe.2014.00084/abstract.

A. J. Levine and A. M. Puzio-Kuter. The Control of the Metabolic Switch in Cancers by Oncogenes and Tumor. *Science*, 330:1340–1344, 2012.

J. W. Locasale. Serine, glycine and one-carbon units: cancer metabolism in full circle. *Nature reviews. Cancer*, 13(8):572–83, aug 2013. ISSN 1474-1768. doi: 10.1038/nrc3557. URL http://dx.doi.org/10.1038/nrc3557.

G. Löffler and J. Schölmerich. *Basiswissen Biochemie : mit Pathobiochemie ; mit 139 Tabellen ; [jetzt mit Fällen]*. Springer, 2008. ISBN 9783540765110.

J. Lotharius, J. Falsig, J. van Beek, S. Payne, R. Dringen, P. Brundin, and M. Leist. Progressive degeneration of human mesencephalic neuron-derived cells triggered by dopamine-dependent oxidative stress is dependent on the mixed-lineage kinase pathway. *The Journal of neuroscience : the official journal of the Society for Neuroscience*, 25(27):6329–42, 2005. ISSN 1529-2401. doi: 10.1523/JNEUROSCI.1746-05.2005. URL http://www.ncbi.nlm.nih.gov/pubmed/16000623.

J. J. Lum, D. E. Bauer, M. Kong, M. H. Harris, C. Li, T. Lindsten, and C. B. Thompson. Growth Factor Regulation of Autophagy and Cell Survival in the Absence of Apoptosis. *Cell*, 120(2):237–248, 2005. ISSN 00928674. doi: 10.1016/j.cell.2004.11.046.

K. Maier, U. Hofmann, A. Bauer, A. Niebel, G. Vacun, M. Reuss, and K. Mauch. Quantification of statin effects on hepatic cholesterol synthesis by transient 13C-flux analysis. *Metabolic Engineering*, 11(4-5):292–309, 2009. ISSN 10967176. doi: 10.1016/j.ymben.2009.06.001. URL http://dx.doi.org/10.1016/j.ymben.2009.06.001.

M. L. McCleland, A. S. Adler, Y. Shang, T. Hunsaker, T. Truong, D. Peterson, E. Torres, L. Li, B. Haley, J.-P. Stephan, M. Belvin, G. Hatzivassiliou, E. M. Blackwood, L. Corson, M. Evangelista, J. Zha, and R. Firestein. An integrated genomic screen identifies LDHB as an essential gene for triple-negative breast cancer. *Cancer research*, 72(22):5812–23, nov 2012. ISSN 1538-7445. doi: 10.1158/0008-5472.CAN-12-1098. URL http://www.ncbi.nlm.nih.gov/pubmed/23139210.

J. Munger, B. D. Bennett, A. Parikh, X.-J. Feng, J. McArdle, H. A. Rabitz, T. Shenk, and J. D. Rabinowitz. Systems-level metabolic flux profiling identifies fatty acid synthesis as a target for antiviral therapy. *Nature Biotechnology*, 26(10):1179–1186, oct 2008. ISSN 1087-0156. doi: 10.1038/nbt.1500. URL http://www.nature.com/doifinder/10.1038/nbt.1500.

T. a. Murphy, C. V. Dang, and J. D. Young. Isotopically nonstationary 13C flux analysis of Myc-induced metabolic reprogramming in B-cells. *Metabolic Engineering*, 15(1):206–217, 2013. ISSN

10967176. doi: 10.1016/j.ymben.2012.07.008. URL http://dx.doi.org/10.1016/j.ymben.2012.07.008.

M. Narita, S. Nnez, E. Heard, M. Narita, A. W. Lin, S. A. Hearn, D. L. Spector, G. J. Hannon, and S. W. Lowe. Rb-mediated heterochromatin formation and silencing of E2F target genes during cellular senescence. *Cell*, 113(6):703–16, jun 2003. ISSN 0092-8674. URL http://www.ncbi.nlm.nih.gov/pubmed/12809602.

D. L. Nelson, M. M. Cox, and A. L. Lehninger. *Lehninger Biochemie : mit 131 Tabellen*. Springer, 2009. ISBN 9783540686378.

S. Niedenführ, W. Wiechert, K. Nöh, I. Biotechnology, F. J. Gmbh, and K. Noeh. How to Measure Metabolic Fluxes : A Taxonomic Guide for 13 C Fluxomics Supplementary Table S . 1 :. *Current opinion in biotechnology*, 34:82–90, 2015. ISSN 1879-0429. doi: 10.1016/j.copbio.2014.12.003.

J. Nocon, M. G. Steiger, M. Pfeffer, S. B. Sohn, T. Y. Kim, M. Maurer, H. Rußmayer, S. Pflügl, M. Ask, C. Haberhauer-Troyer, K. Ortmayr, S. Hann, G. Koellensperger, B. Gasser, S. Y. Lee, and D. Mattanovich. Model based engineering of Pichia pastoris central metabolism enhances recombinant protein production. *Metabolic engineering*, 24:129–38, jul 2014. ISSN 1096-7184. doi: 10.1016/j.ymben.2014.05.011. URL http://www.ncbi.nlm.nih.gov/pubmed/24853352http://www.pubmedcentral.nih.gov/articlerender.fcgi?artid=PMC4094982.

K. Nöh and W. Wiechert. The benefits of being transient: isotope-based metabolic flux analysis at the short time scale. *Applied Microbiology and Biotechnology*, 91(5):1247–65, sep 2011. ISSN 01757598. doi: 10.1007/s00253-011-3390-4. URL http://www.ncbi.nlm.nih.gov/pubmed/21732247.

K. Nöh, A. Wahl, and W. Wiechert. Computational tools for isotopically instationary 13C labeling experiments under metabolic steady state conditions. *Metabolic engineering*, 8(6):554–77, nov 2006. ISSN 1096-7176. doi: 10.1016/j.ymben.2006.05.006. URL http://www.ncbi.nlm.nih.gov/pubmed/16890470.

K. Nöh, K. Grönke, B. Luo, R. Takors, M. Oldiges, and W. Wiechert. Metabolic flux analysis at ultra short time scale: isotopically non-stationary 13C labeling experiments. *Journal of biotechnology*, 129(2):249–67, apr 2007. ISSN 0168-1656. doi: 10.1016/j.jbiotec.2006.11.015. URL http://www.sciencedirect.com/science/article/pii/S0168165606009722http://www.ncbi.nlm.nih.gov/pubmed/17207877.

K. Nöh, P. Droste, and W. Wiechert. Visual workflows for 13C-metabolic flux analysis. *Bioinformatics*, 31(3):346–354, feb 2015. ISSN 1367-4803. doi: 10.1093/bioinformatics/btu585. URL http://www.ncbi.nlm.nih.gov/pubmed/25297067http://bioinformatics.oxfordjournals.org/cgi/doi/10.1093/bioinformatics/btu585.

W. M. Old, K. Meyer-Arendt, L. Aveline-Wolf, K. G. Pierce, A. Mendoza, J. R. Sevinsky, K. a. Resing, and N. G. Ahn. Comparison of label-free methods for quantifying human proteins by shotgun proteomics. *Molecular & cellular proteomics : MCP*, 4(10):1487–1502, 2005. ISSN 1535-9476. doi: 10.1074/mcp.M500084-MCP200.

W. M. Oldham, C. B. Clish, Y. Yang, and J. Loscalzo. Hypoxia-Mediated Increases in l-2-hydroxyglutarate Coordinate the Metabolic Response to Reductive Stress. *Cell Metabolism*, 22(2):291–303, 2015. ISSN 19327420. doi: 10.1016/j.cmet.2015.06.021. URL http://dx.doi.org/10.1016/j.cmet.2015.06.021.

S.-E. Ong, B. Blagoev, I. Kratchmarova, D. B. Kristensen, H. Steen, A. Pandey, and M. Mann. Stable isotope labeling by amino acids in cell culture, SILAC, as a simple and accurate approach to expression proteomics. *Molecular & cellular proteomics : MCP*, 1(5):376–386, 2002. ISSN 15359476. doi: 10.1074/mcp.M200025-MCP200.

M. Ono, M. Shitashige, K. Honda, T. Isobe, H. Kuwabara, H. Matsuzuki, S. Hirohashi, and T. Yamada. Label-free quantitative proteomics using large peptide data sets generated by nanoflow liquid chromatography and mass spectrometry. *Molecular & cellular proteomics : MCP*, 5(7):1338–1347, 2006. ISSN 1535-9476. doi: 10.1074/mcp.T500039-MCP200.

J. D. Orth, I. Thiele, and B. Ø. Palsson. What is flux balance analysis? *Nature biotechnology*, 28(3):245–248, 2010. ISSN 1087-0156. doi: 10.1038/nbt.1614. URL http://dx.doi.org/10.1038/nbt.1614.

Z. Pan and D. Raftery. Comparing and combining NMR spectroscopy and mass spectrometry in metabolomics. *Analytical and Bioanalytical Chemistry*, 387(2):525–527, 2007. ISSN 16182642. doi: 10.1007/s00216-006-0687-8.

A. D. Panopoulos and J. C. Izpisua Belmonte. Anaerobicizing into Pluripotency. *Cell Metabolism*, 14:143–144, 2011. doi: 10.1016/j.cmet.2011.07.003.

N. N. Pavlova and C. B. Thompson. The Emerging Hallmarks of Cancer Metabolism. *Cell Metabolism*, 23(1):27–47, jan 2016. ISSN 15504131. doi: 10.1016/j.cmet.2015.12.006. URL http://linkinghub.elsevier.com/retrieve/pii/S155041311500621X.

M. Pietzke and S. Kempa. *Pulsed stable isotope-resolved metabolomic studies of cancer cells*, volume 543. Elsevier Inc., 1 edition, 2014. ISBN 9780128013298. doi: 10.1016/B978-0-12-801329-8.00009-X. URL http://dx.doi.org/10.1016/B978-0-12-801329-8.00009-X.

M. Pietzke, C. Zasada, S. Mudrich, and S. Kempa. Decoding the dynamics of cellular metabolism and the action of 3-bromopyruvate and 2-deoxyglucose using pulsed stable isotope-resolved metabolomics. *Cancer & metabolism*, 2(1):9, jan 2014. ISSN 2049-3002. doi: 10.1186/2049-3002-2-9. URL http://www.pubmedcentral.nih.gov/articlerender.fcgi?artid=4101711{&}tool=pmcentrez{&}rendertype=abstract.

A. Prigione, B. Fauler, R. Lurz, H. Lehrach, and J. Adjaye. The senescence-related mitochondrial/oxidative stress pathway is repressed in human induced pluripotent stem cells. *Stem cells (Dayton, Ohio)*, 28(4):721–33, apr 2010. ISSN 1549-4918. doi: 10.1002/stem.404. URL http://www.ncbi.nlm.nih.gov/pubmed/20201066http://doi.wiley.com/10.1002/stem.404.

A. Prigione, B. Lichtner, H. Kuhl, E. A. Struys, M. Wamelink, H. Lehrach, M. Ralser, B. Timmermann, and J. Adjaye. Human Induced Pluripotent Stem Cells Harbor Homoplasmic and Heteroplasmic Mitochondrial DNA Mutations While Maintaining Human Embryonic Stem Cell-like

Metabolic Reprogramming. *Stem cells (Dayton, Ohio)*, 29:1338–1348, apr 2011. ISSN 1549-4918. doi: 10.1002/stem.15. URL http://www.ncbi.nlm.nih.gov/pubmed/19353526.

G. Qing, N. Skuli, P. A. Mayes, B. Pawel, D. Martinez, J. M. Maris, and M. C. Simon. Combinatorial regulation of neuroblastoma tumor progression by N-Myc and hypoxia inducible factor HIF-1alpha. *Cancer Research*, 70(24):10351–10361, 2010. URL http://www.pubmedcentral.nih.gov/articlerender.fcgi?artid=3005134{&}tool=pmcentrez{&}rendertype=abstract.

K. Raman and N. Chandra. Flux balance analysis of biological systems: Applications and challenges. *Briefings in Bioinformatics*, 10(4):435–449, 2009. ISSN 14675463. doi: 10.1093/bib/bbp011.

P. L. Ross. Multiplexed Protein Quantitation in Saccharomyces cerevisiae Using Amine-reactive Isobaric Tagging Reagents. *Molecular & Cellular Proteomics*, 3(12):1154–1169, sep 2004. ISSN 1535-9476. doi: 10.1074/mcp.M400129-MCP200. URL http://www.mcponline.org/cgi/doi/10.1074/mcp.M400129-MCP200.

J. G. Ryall, T. Cliff, S. Dalton, V. Sartorelli, F. Arai, A. Hirao, M. Ohmura, H. Sato, S. Matsuoka, K. Takubo, K. Ito, G. Koh, T. Suda, K. Blaschke, K. Ebata, M. Karimi, J. Zepeda-Martínez, P. Goyal, S. Mahapatra, A. Tam, D. Laird, M. Hirst, A. Rao, E. Al., A. Brack, T. Rando, R. Brinster, D. Troike, I. Brons, L. Smithers, M. Trotter, P. Rugg-Gunn, B. Sun, S. C. d. S. Lopes, S. Howlett, A. Clarkson, L. Ahrlund-Richter, R. Pedersen, L. Vallier, S. Buczacki, H. Zecchini, A. Nicholson, R. Russell, L. Vermeulen, R. Kemp, and Et.al. Metabolic Reprogramming of Stem Cell Epigenetics. *Cell Stem Cell*, 17(6):651–662, dec 2015. ISSN 19345909. doi: 10.1016/j.stem.2015.11.012. URL http://linkinghub.elsevier.com/retrieve/pii/S193459091500510X.

U. Sauer. Metabolic networks in motion: 13C-based flux analysis. *Molecular Systems Biology*, 2:1–10, jan 2006. ISSN 1744-4292. doi: 10.1038/msb4100109. URL http://www.pubmedcentral.nih.gov/articlerender.fcgi?artid=1682028{&}tool=pmcentrez{&}rendertype=abstracthttp://msb.embopress.org/cgi/doi/10.1038/msb4100109.

C. A. Schmitt, J. S. Fridman, M. Yang, S. Lee, E. Baranov, R. M. Hoffman, and S. W. Lowe. A senescence program controlled by p53 and p16INK4a contributes to the outcome of cancer therapy. *Cell*, 109(3):335–46, may 2002. ISSN 0092-8674. URL http://www.ncbi.nlm.nih.gov/pubmed/12015983.

D. Scholz, D. Pöltl, A. Genewsky, M. Weng, T. Waldmann, S. Schildknecht, and M. Leist. Rapid, complete and large-scale generation of post-mitotic neurons from the human LUHMES cell line. *Journal of Neurochemistry*, 119(5):957–971, 2011. ISSN 00223042. doi: 10.1111/j.1471-4159.2011.07255.x.

A. Schulze and A. L. Harris. How cancer metabolism is tuned for proliferation and vulnerable to disruption. *Nature*, 491(7424):364–373, nov 2012a. ISSN 0028-0836. doi: 10.1038/nature11706. URL http://dx.doi.org/10.1038/nature11706http://www.nature.com/doifinder/10.1038/nature11706.

A. Schulze and A. L. Harris. How cancer metabolism is tuned for proliferation and vulnerable to disruption. *Nature*, 491(7424):364–373, nov 2012b. ISSN 0028-0836. doi: 10.1038/nature11706. URL http://www.nature.com/doifinder/10.1038/nature11706.

K. Sheikh, J. Förster, and L. K. Nielsen. Modeling Hybridoma Cell Metabolism Using a Generic Genome-Scale Metabolic Model of Mus musculus. *Biotechnology Progress*, 21(1):112–121, sep 2008. doi: 10.1021/bp0498138. URL http://doi.wiley.com/10.1021/bp0498138.

T. Shlomi, J. Fan, B. Tang, W. D. Kruger, and J. D. Rabinowitz. Quantitation of Cellular Metabolic Fluxes of Methionine. *Analytical chemistry*, 86(3):1583–1591, feb 2014. ISSN 15378276. doi: 10.1016/j.biotechadv.2011.08.021.Secreted. URL http://pubs.acs.org/doi/abs/10.1021/ac4032093.

M. a. Sirover. New insights into an old protein: the functional diversity of mammalian glyceraldehyde-3-phosphate dehydrogenase. *Biochimica et biophysica acta*, 1432(2):159–184, 1999. ISSN 0006-3002. doi: 10.1016/S0167-4838(99)00119-3.

E. Struys. Mutations in the D-2-hydroxyglutarate dehydrogenase gene cause D-2-hydroxyglutaric aciduria. *Am J Hum Genet*, 76:358–360, 2005.

S. T. Suhr, E. A. Chang, J. Tjong, N. Alcasid, G. A. Perkins, M. D. Goissis, M. H. Ellisman, G. I. Perez, and J. B. Cibelli. Mitochondrial Rejuvenation After Induced Pluripotency. *PLoS ONE*, 5(11):e14095, nov 2010. ISSN 1932-6203. doi: 10.1371/journal.pone.0014095. URL http://dx.plos.org/10.1371/journal.pone.0014095.

T. Szyperski. Biosynthetically directed fractional 13C-labeling of proteinogenic amino acids. An efficient analytical tool to investigate intermediary metabolism. *European Journal of Biochemistry*, 232(2):433–448, 1995. ISSN 00142956. doi: 10.1111/j.1432-1033.1995.tb20829.x.

K. Takahashi and S. Yamanaka. Induction of Pluripotent Stem Cells from Mouse Embryonic and Adult Fibroblast Cultures by Defined Factors. *Cell*, 126(4):663–676, 2006. ISSN 00928674. doi: 10.1016/j.cell.2006.07.024.

S. Tyanova, T. Temu, P. Sinitcyn, A. Carlson, M. Y. Hein, T. Geiger, M. Mann, and J. Cox. The Perseus computational platform for comprehensive analysis of (prote)omics data. *Nature Methods*, jun 2016. ISSN 1548-7091. doi: 10.1038/nmeth.3901. URL http://www.nature.com/doifinder/10.1038/nmeth.3901.

M. Uhlén, L. Fagerberg, B. M. Hallström, C. Lindskog, P. Oksvold, A. Mardinoglu, Å. Sivertsson, C. Kampf, E. Sjöstedt, A. Asplund, I. Olsson, K. Edlund, E. Lundberg, S. Navani, C. A.-K. Szigyarto, J. Odeberg, D. Djureinovic, J. O. Takanen, S. Hober, T. Alm, P.-H. Edqvist, H. Berling, H. Tegel, J. Mulder, J. Rockberg, P. Nilsson, J. M. Schwenk, M. Hamsten, K. von Feilitzen, M. Forsberg, L. Persson, F. Johansson, M. Zwahlen, G. von Heijne, J. Nielsen, and F. Pontén. Proteomics. Tissue-based map of the human proteome. *Science (New York, N.Y.)*, 347(6220):1260419, jan 2015. doi: 10.1126/science.1260419. URL http://www.ncbi.nlm.nih.gov/pubmed/25613900.

M. G. Vander Heiden. Targeting cancer metabolism: a therapeutic window opens. *Nature reviews. Drug discovery*, 10(9):671–84, sep 2011. ISSN 1474-1784. doi: 10.1038/nrd3504. URL http://www.ncbi.nlm.nih.gov/pubmed/21878982http://dx.doi.org/10.1038/nrd3504.

M. G. Vander Heiden, L. C. Cantley, and C. B. Thompson. Understanding the Warburg effect: the metabolic requirements of cell proliferation. *Science (New York, N.Y.)*, 324(5930):1029–33, may 2009. ISSN 1095-9203. doi: 10.1126/science.1160809. URL http://www.pubmedcentral.nih.gov/articlerender.fcgi?artid=2849637{&}tool=pmcentrez{&}rendertype=abstract.

A. Varma and B. O. Palsson. Metabolic Flux Balancing: Basic concepts, scientific and practical use. *Nature biotechnology*, 12:994–998, 1994.

S. Varum, O. Momčilović, C. Castro, A. Ben-Yehudah, J. Ramalho-Santos, and C. Navara. Enhancement of human embryonic stem cell pluripotency through inhibition of the mitochondrial respiratory chain. *Stem Cell Research*, 3(2-3):142–156, sep 2009. ISSN 18735061. doi: 10.1016/j.scr.2009.07.002. URL http://linkinghub.elsevier.com/retrieve/pii/S1873506109000853.

S. Varum, A. S. Rodrigues, M. B. Moura, O. Momcilovic, C. a. Easley, J. Ramalho-Santos, B. Van Houten, and G. Schatten. Energy Metabolism in Human Pluripotent Stem Cells and Their Differentiated Counterparts. *PLoS ONE*, 6(6):e20914, jun 2011. ISSN 1932-6203. doi: 10.1371/journal.pone.0020914. URL http://dx.plos.org/10.1371/journal.pone.0020914.

P. Vaupel, F. Kallinowski, and P. Okunieff. Blood flow, oxygen and nutrient supply, and metabolic microenvironment of human tumors: a review. *Cancer research*, 49(23):6449–65, dec 1989. ISSN 0008-5472. URL http://www.ncbi.nlm.nih.gov/pubmed/2684393.

S. A. Wahl, M. Dauner, and W. Wiechert. New Tools for Mass Isotopomer Data Evaluation in 13C Flux Analysis: Mass Isotope Correction, Data Consistency Checking, and Precursor Relationships. *Biotechnology and Bioengineering*, 85(3):259–268, 2004. ISSN 00063592. doi: 10.1002/bit.10909.

S. A. Wahl, K. Nöh, and W. Wiechert. 13C labeling experiments at metabolic nonstationary conditions: an exploratory study. *BMC bioinformatics*, 9:152, jan 2008. ISSN 1471-2105. doi: 10.1186/1471-2105-9-152. URL http://www.pubmedcentral.nih.gov/articlerender.fcgi?artid=2373788{&}tool=pmcentrez{&}rendertype=abstract.

C. Wang, K. Guo, D. Gao, X. Kang, K. Jiang, Y. Li, L. Sun, S. Zhang, C. Sun, X. Liu, W. Wu, P. Yang, and Y. Liu. Identification of transaldolase as a novel serum biomarker for hepatocellular carcinoma metastasis using xenografted mouse model and clinic samples. *Cancer Letters*, 313 (2):154–166, dec 2011a. ISSN 03043835. doi: 10.1016/j.canlet.2011.08.031. URL http://linkinghub.elsevier.com/retrieve/pii/S0304383511005283.

R. Wang, C. P. Dillon, L. Z. Shi, S. Milasta, R. Carter, D. Finkelstein, L. L. McCormick, P. Fitzgerald, H. Chi, J. Munger, and D. R. Green. The transcription factor Myc controls metabolic reprogramming upon T lymphocyte activation. *Immunity*, 35(6):871–82, dec 2011b. ISSN 1097-4180. doi: 10.1016/j.immuni.2011.09.021. URL http://www.ncbi.nlm.nih.gov/pubmed/22195744http://www.pubmedcentral.nih.gov/articlerender.fcgi?artid=PMC3248798.

O. Warburg, K. Posener, and E. Negelein. Über den Stoffwechsel der Carcinomzelle. *Biochemische Zeitschrift*, 152:319–344, 1924.

O. Warburg, F. Wind, and E. Negelein. The Metabolism of tumors in the body. *The Journal of general physiology*, 8(6):519–530, 1927. URL http://www.pubmedcentral.nih.gov/articlerender.fcgi?artid=2140820{&}tool=pmcentrez{&}rendertype=abstract.

S. W. Wegener, H. C. Reeves, and S. J. AJL. Propionate Metabolism. *Archives of Biochemistry and Biophysics*, 123:62–65, 1968.

D. Weindl, A. Wegner, and K. Hiller. Metabolome-Wide Analysis of Stable Isotope Labeling-Is It Worth the Effort? *Frontiers in physiology*, 6:344, jan 2015. ISSN 1664-042X. doi: 10.3389/fphys.2015.00344. URL http://www.pubmedcentral.nih.gov/articlerender.fcgi?artid=4653307{&}tool=pmcentrez{&}rendertype=abstract.

M. Weitzel, K. Nöh, T. Dalman, S. Niedenführ, B. Stute, and W. Wiechert. 13CFLUX2–high-performance software suite for (13)C-metabolic flux analysis. *Bioinformatics (Oxford, England)*, 29(1):143–5, jan 2013. ISSN 1367-4811. doi: 10.1093/bioinformatics/bts646. URL http://www.pubmedcentral.nih.gov/articlerender.fcgi?artid=3530911{&}tool=pmcentrez{&}rendertype=abstract.

M. Wenzel, I. Joel, and W. Oelkers. Application of double isotope labeling to the study of the metabolism of ascites tumor cells under the influence of glyceraldehyde. *Advanced Tracer Methodology*, 3:223–31, 1966. URL http://www.ncbi.nlm.nih.gov/pubmed/5919828.

W. Wiechert. 13C Metabolic Flux Analysis. *Metabolic engineering*, 206:195–206, 2001.

W. Wiechert, M. Mo, S. Petersen, and A. A. D. Graaf. A Universal Framework for ... Metabolic Flux Analysis. *Metabolic engineering*, 283:265–283, 2001.

S. Wiese, K. a. Reidegeld, H. E. Meyer, and B. Warscheid. Protein labeling by iTRAQ: A new tool for quantitative mass spectrometry in proteome research. *Proteomics*, 7(3):340–350, 2007. ISSN 16159853. doi: 10.1002/pmic.200600422.

D. R. Wise, R. J. DeBerardinis, A. Mancuso, N. Sayed, X.-Y. Zhang, H. K. Pfeiffer, I. Nissim, E. Daikhin, M. Yudkoff, S. B. McMahon, and C. B. Thompson. Myc regulates a transcriptional program that stimulates mitochondrial glutaminolysis and leads to glutamine addiction. *Proceedings of the National Academy of Sciences of the United States of America*, 105(48):18782–7, dec 2008. ISSN 1091-6490. doi: 10.1073/pnas.0810199105. URL http://www.ncbi.nlm.nih.gov/pubmed/19033189http://www.pubmedcentral.nih.gov/articlerender.fcgi?artid=PMC2596212.

X. Xu, A. zur Hausen, J. F. Coy, and M. Löchelt. Transketolase-like protein 1 (TKTL1) is required for rapid cell growth and full viability of human tumor cells. *International Journal of Cancer*, 124(6):1330–1337, mar 2009. ISSN 00207136. doi: 10.1002/ijc.24078. URL http://doi.wiley.com/10.1002/ijc.24078.

S. J. Yeung, J. Pan, and M. H. Lee. Roles of p53, MYC and HIF-1 in regulating glycolysis - The seventh hallmark of cancer. *Cellular and Molecular Life Sciences*, 65(24):3981–3999, 2008. ISSN 1420682X. doi: 10.1007/s00018-008-8224-x.

J. D. Young, J. L. Walther, M. R. Antoniewicz, H. Yoo, and G. Stephanopoulos. An Elementary Metabolite Unit (EMU) based method of isotpocially nonstationary flux analysis. *Biotechnology and bioengineering*, 99(3):686–699, 2007. ISSN 0021-8782. doi: 10.1002/bit.

N. Zamboni. 13C metabolic flux analysis in complex systems. *Current opinion in biotechnology*, 22(1):103–8, feb 2011. ISSN 09581669. doi: 10.1016/j.copbio.2010.08.009. URL `http://www.sciencedirect.com/science/article/pii/S0958166910001394`.

C. Zasada and S. Kempa. *Quantitative Analysis of Cancer Metabolism: From pSIRM to MFA*, pages 207–220. Springer International Publishing, Cham, 2016. ISBN 978-3-319-42118-6. doi: 10.1007/978-3-319-42118-6_9. URL `http://dx.doi.org/10.1007/978-3-319-42118-6{_}9`.

J. Zhang, I. Khvorostov, J. S. Hong, Y. Oktay, L. Vergnes, E. Nuebel, P. N. Wahjudi, K. Setoguchi, G. Wang, A. Do, H.-J. Jung, J. M. McCaffery, I. J. Kurland, K. Reue, W.-N. P. Lee, C. M. Koehler, and E. Al. UCP2 regulates energy metabolism and differentiation potential of human pluripotent stem cells. *The EMBO Journal*, 30(24):4860–4873, dec 2011. ISSN 02614189. doi: 10.1038/emboj.2011.401. URL `http://emboj.embopress.org/cgi/doi/10.1038/emboj.2011.401`.

J. Zhang, E. Nuebel, G. Q. Q. Daley, C. M. M. Koehler, and M. A. A. Teitell. Metabolic Regulation in Pluripotent Stem Cells during Reprogramming and Self-Renewal. *Cell Stem Cell*, 11(5):589–595, nov 2012. ISSN 19345909. doi: 10.1016/j.stem.2012.10.005. URL `http://www.cell.com/cell-stem-cell/fulltext/S1934-5909(12)00586-3http://linkinghub.elsevier.com/retrieve/pii/S1934590912005863http://dx.doi.org/10.1016/j.stem.2012.10.005`.

# A Supplementary: Chemicals, solutions and equipment

Table A.1.: Chemicals

| **Name** | **Formula** | **Supplier** |
|---|---|---|
| $^{13}$C-Glucose | $^{13}C_5H_{12}O_6$ | Campro Scientific, D - Berlin |
| $^{13}$C-Glutamine | $^{13}C_4H_{10}N_2O_3$ | Campro Scientific, D - Berlin |
| $\beta$-Mercaptoethanol | $C_2H_6OS$ | Sigma-Aldrich, D - München |
| Chloroform | $CHC_{13}$ | Sigma-Aldrich, D - München |
| Cinnamic acid | $C_9H_8O_2$ | Sigma-Aldrich, D - München |
| DMEM | w/o Glc, Gln, Pyr, Phenolred | Life Technologies, D - Darmstadt |
| FBS | - | Life Technologies, D - Darmstadt |
| Glucose | $C_6H_{12}O_6$ | Sigma-Aldrich, D - München |
| Glutamine | $C_5H_{10}N_2O_3$ | Life Technologies, D - Darmstadt |
| Glycerol | $C_3H_8O_3$ | Life Technologies, D - Darmstadt |
| Glycine | $C_2H_5NO_2$ | Life Technologies, D - Darmstadt |
| HEPES | $C_8H_{18}N_2O_4$S | Carl Roth, D - Karlsruhe |
| Isopropanol | $C_3H_8O$ | Carl Roth, D - Karlsruhe |
| Kaliumchlorid | $KCl$ | Carl Roth, D - Karlsruhe |
| MeOH | $CH_4O$ | Merck, D - Darmstadt |
| MeOx | $C_{11}H_{17}NO_3$ * HCl | Sigma-Aldrich, D - München |
| MSTFA | $CF_3CON(CH_3)Si(CH_3)_3$ | VWR, USA - Radnor |
| PenStrep | - | Life Technologies, D - Darmstadt |
| Pyridine | $C_5H_5N$ | Sigma-Aldrich, D - München |
| Sodium chloride | $NaCl$ | Carl Roth, D - Karlsruhe |
| Sodium hydroxide | $NaOH$ | Carl Roth, D - Karlsruhe |
| Sodium phosphate dibasic | $Na_2HPO_4$ | CARL ROTH, D - Karlsruhe |
| Tris Base | $C_4H_{11}NO_3$ | Carl Roth, D - Karlsruhe |
| Tris-HCl | $C_4H_{11}NO_3$ * HCl | Carl Roth, D - Karlsruhe |
| Trypan blue | - | Life Technologies, D - Darmstadt |
| TrypLE Express | - | Life Technologies, D - Darmstadt |
| Urea | $CH_4N_2O$ | Carl Roth, D - Karlsruhe |

Table A.2.: Solutions

| **Solution** | **Composition** |
|---|---|
| Dissolver | 40 mg MeOx<br>+ 1 mL Pyridine |
| Labelling buffer | 140 mM NaCl<br>+ 5 mM HEPES<br>+ x g/L $^{12/13}$C-Glc<br>+ x g/L $^{12/13}$C-Gln<br>in bi-dest. $H_2O$<br>pH 7.4 |
| MCW | 50 mL MEOH<br>+ 20 mL Chloroform<br>+ 2 ug/ml cinnamic acid<br>+ 10 mL bi-dest. $H_2O$ |
| MeOH (50 %) | 100 mL MeOH<br>+ 2 ug/ml cinnamic acid<br>adjust volume to 200 mL with bi-dest. $H_2O$ |
| MSTFA | 1 mL MSTFA<br>+ 10 ug/ml alkane standard |
| Urea buffer (8 M) | 2.4 g Urea<br>+ 3.2 mL 100 mM Tris |

Table A.3.: Consumables

| **Name** | **Supplier** |
|---|---|
| Gas liner, CI34 | Gerstel, D - Mühlheim an der Ruhr |
| Petridish, 10 cm | Greiner, D - Frickenhausen |
| Cell lifter | Sarstedt, D - Nümbrecht |
| Counting slides | Biorad, D - München |
| Safe-lock Tubes | Eppendorf, D - Hamburg |
| 96-well plate | Greiner, D - Frickenhausen |
| Falcon tubes (15 mL) | Greiner, D - Frickenhausen |
| Falcon tubes (50 mL) | Greiner, D - Frickenhausen |
| Filter paper | Biorad, D - München |
| Nitrocellulose membrane (0.2 um) | Biorad, D - München |

Table A.4.: Equipment

| **Name** | **Manufacturer** |
|---|---|
| Autosampler, MPS2XL-Twister | Gerstel, D - Mühlheim an der Ruhr |
| Balance, CP2202S | Satorius, D - Göttigen |
| Blotting device, TransBlot Turbo | Biorad, D - München |
| Cell culture incubator, CB 210 | Binder, D - Tuttlingen |
| Cellcounter, TC10 automated | Biorad, D - München |
| Centrifuge, 5417R | Eppendorf, D - Hamburg |
| Centrifuges, 5430 | Eppendorf, D - Hamburg |
| Electrophoresis system, Protean Tetra cell | Biorad, D - München |
| Gas chromatograph, Agilent 6890N | Leco, USA - St. Joseph |
| Infrared Imaging System, Odyssey | Licor, USA - Lincoln |
| Microplate reader, Infinite M200 | Tecan, CH - Männedorf |
| pH meter, VMS C7 | VWR, USA- Radnor |
| Power supply, PowerPac Universal | Biorad, D - München |
| Rotational-Vacuum-Concentrator, 2-33 CD plus | Christ, D - Osterode |
| Sonicator, Sonorex Digitech | Bandelin electronic, D - Berlin |
| Thermomixer, comfort | Eppendorf, D - Hamburg |
| MS-TOF, Pegasus IV | Leco, USA - St. Joseph |
| Tube roller, SRT6D | Stuart, UK - Staffordshire |
| Tube rotator, SB2 | Stuart, UK - Staffordshire |
| Vacuum chamber, Alpha L-4 LD plus | Christ, D - Osterode |

Table A.5.: Range of quantification standard in pmol. Maximum value corresponds to quantification standard 1:1

| **Compound** | **min(Quantity)** | **max(Quantity)** |
|---|---|---|
| Adenine | 37 | 7400 |
| Adenosine | 94 | 18709 |
| Alanine | 673 | 134695 |
| Alanine, beta | 56 | 11225 |
| Arginine | 57 | 11481 |
| Asparagine | 114 | 22707 |
| Aspartic acid | 75 | 15025 |
| Butyric acid, 3-hydroxy | 144 | 28818 |
| Butyric acid, 4-amino | 48 | 9697 |
| Citric acid | 260 | 52051 |
| Creatinine | 221 | 44201 |
| Cysteine | 41 | 8254 |
| Cytosine | 45 | 9001 |
| Dihydroxyacetone phosphate | 441 | 88183 |
| Erythritol, meso | 409 | 81887 |

Continued on next page

**Table A.5 – continued from previous page**

| Compound | min(Quantity) | max(Quantity) |
|---|---|---|
| Fructose | 416 | 83259 |
| Fructose-1,6-bisphosphate | 271 | 54288 |
| Fructose-6-phosphate | 66 | 13154 |
| Fumaric acid | 172 | 34462 |
| Gluconic acid-6-phosphate | 73 | 14616 |
| Glucosamine | 23 | 4638 |
| Glucose | 1943 | 388544 |
| Glucose 1-phosphate | 59 | 11894 |
| Glucose-6-phosphate | 164 | 32884 |
| Glutamic acid | 680 | 135934 |
| Glutamine | 684 | 136855 |
| Glutaric acid | 151 | 30278 |
| Glutaric acid, 2-hydroxy | 286 | 57268 |
| Glutaric acid, 2-oxo | 171 | 34223 |
| Glyceraldehyde-3-phosphate | 323 | 64668 |
| Glyceric acid | 80 | 15987 |
| Glyceric acid-3-phosphate | 217 | 43478 |
| Glycerol | 326 | 65154 |
| Glycerol-3-phosphate | 135 | 26996 |
| Glycine | 333 | 66605 |
| GMP | 101 | 20113 |
| Hypotaurine | 92 | 18323 |
| Inosine | 56 | 11184 |
| Inositol, myo | 278 | 55506 |
| Isoleucine | 191 | 38116 |
| Lactic Acid | 2231 | 446190 |
| Leucine | 457 | 91484 |
| Lysine | 103 | 20531 |
| Malic acid | 224 | 44746 |
| Methionine | 34 | 6702 |
| Pantothenic acid | 84 | 16788 |
| Phenylalanine | 242 | 48429 |
| Phosphoenolpyruvic acid | 75 | 15036 |
| Proline | 304 | 60801 |
| Putrescine | 31 | 6208 |
| Pyroglutamic acid | 465 | 92937 |
| Pyruvate | 1454 | 290803 |
| Ribose | 100 | 19983 |
| Ribose, 2-deoxy | 37 | 7455 |
| Ribose 5-phosphate | 456 | 91208 |
| Serine | 571 | 114188 |

Continued on next page

**Table A.5 – continued from previous page**

| **Compound** | **min(Quantity)** | **max(Quantity)** |
|---|---|---|
| Succinic acid | 212 | 42341 |
| Threonine | 839 | 167898 |
| Tryptophan | 49 | 9793 |
| Tyrosine | 55 | 11038 |
| Uracil | 134 | 26764 |
| Uridine 5-monophosphate | 407 | 81489 |
| Valine | 213 | 42680 |

# B Supplementary: Project-related data

### Uniprot identifier list

Table B.1.: Protein stuff

| Gene name | Uniprot-ID | Protein name | Synonyms | Mass | Length | E.C. |
|---|---|---|---|---|---|---|
| ADK | P55263 | Adenosine kinase (AK) | ADK | 40,545 | 362 | 2.7.1.20 |
| AADAT | Q8N5Z0 | Kynurenine/alpha-aminoadipate aminotransferase | AADAT KAT2 | 47,352 | 425 | 2.6.1.39; 2.6.1.7 |
| ABAT | P80404 | 4-aminobutyrate aminotransferase | ABAT GABAT | 56,439 | 500 | 2.6.1.19; 2.6.1.22 |
| SOAT1 | P35610 | Sterol O-acyltransferase 1 | SOAT1 ACACT ACACT1 ACAT ACAT1 SOAT STAT | 64,735 | 550 | 2.3.1.26 |
| ACCS | Q96QU6 | 1-aminocyclopropane-1-carboxylate synthase-like protein 1 (ACC synthase-like protein 1) | ACCS PHACS | 57,324 | 501 | |
| ACCSL | Q4AC99 | Probable inactive 1-aminocyclopropane-1-carboxylate synthase-like protein 2 (ACC synthase-like protein 2) | ACCSL | 65,249 | 568 | |
| ACLY | P53396 | ATP-citrate synthase | ACLY | 120,839 | 1101 | 2.3.3.8 |
| ACO1 | P21399 | Cytoplasmic aconitate hydratase (Aconitase) | ACO1 IREB1 | 98,399 | 889 | 4.2.1.3 |
| ACO2 | Q99798 | Aconitate hydratase | ACO2 | 85,425 | 780 | 4.2.1.3 |
| ADI1 | Q9BV57 | 1,2-dihydroxy-3-keto-5-methylthiopentene dioxygenase | ADI1 MTCBP1 HMFT1638 | 21,498 | 179 | 1.13.11.54 |
| ADPGK | Q9BRR6 | ADP-dependent glucokinase | ADPGK PSEC0260 | 54,089 | 497 | 2.7.1.147 |
| AGXT | P21549 | Serine–pyruvate aminotransferase (SPT) | AGXT AGT1 SPAT | 43,010 | 392 | 2.6.1.51; 2.6.1.44 |
| AGXT2 | Q9BYV1 | Alanine–glyoxylate aminotransferase 2 | AGXT2 AGT2 | 57,156 | 514 | 2.6.1.44; 2.6.1.40 |
| AHCY | P23526 | Adenosylhomocysteinase (AdoHcyase) | AHCY SAHH | 47,716 | 432 | 3.3.1.1 |
| AHCYL1 | O43865 | Adenosylhomocysteinase 2 (AdoHcyase 2) | AHCYL1 DCAL IRBIT XPVKONA | 58,951 | 530 | 3.3.1.1 |

Continued on next page

**Table B.1 – continued from previous page**

| Gene name | Uniprot-ID | Protein name | Synonyms | Mass | Length | E.C. |
|---|---|---|---|---|---|---|
| AHCYL2 | Q96HN2 | Adenosylhomocysteinase 3 (AdoHcyase 3) | AHCYL2 KIAA0828 | 66,721 | 611 | 3.3.1.1 |
| ALAS1 | P13196 | 5-aminolevulinate synthase, nonspecific | ALAS1 ALAS3 ALASH OK/SW-cl.121 | 70,581 | 640 | 2.3.1.37 |
| ALAS2 | P22557 | 5-aminolevulinate synthase, erythroid-specific | ALAS2 ALASE ASB | 64,633 | 587 | 2.3.1.37 |
| ALDH18A1 | P54886 | Delta-1-pyrroline-5-carboxylate synthase | ALDH18A1 GSAS P5CS PYCS | 87,302 | 795 | 2.7.2.11; 1.2.1.41 |
| ALDH6A1 | Q02252 | Methylmalonate-semialdehyde dehydrogenase [acylating] | ALDH6A1 MMSDH | 57,840 | 535 | 1.2.1.18; 1.2.1.27 |
| ALDH1L1 | O75891 | Cytosolic 10-formyltetrahydrofolate dehydrogenase | ALDH1L1 FTHFD | 98,829 | 902 | 1.5.1.6 |
| ALDH1L2 | Q3SY69 | Mitochondrial 10-formyltetrahydrofolate dehydrogenase | ALDH1L2 | 101,746 | 923 | 1.5.1.6 |
| ALDOA | P04075 | Fructose-bisphosphate aldolase A | ALDOA ALDA | 39,420 | 364 | 4.1.2.13 |
| ALDOB | P05062 | Fructose-bisphosphate aldolase B | ALDOB ALDB | 39,473 | 364 | 4.1.2.13 |
| ALDOC | P09972 | Fructose-bisphosphate aldolase C | ALDOC ALDC | 39,456 | 364 | 4.1.2.13 |
| AMT | P48728 | Aminomethyltransferase | AMT GCST | 43,946 | 403 | 2.1.2.10 |
| APIP | Q96GX9 | Methylthioribulose-1-phosphate dehydratase (MTRu-1-P dehydratase) | APIP CGI-29 | 27,125 | 242 | 4.2.1.109 |
| ASL | P04424 | Argininosuccinate lyase (ASAL) | ASL | 51,658 | 464 | 4.3.2.1 |
| ASNS | P08243 | Asparagine synthetase [glutamine-hydrolyzing] | ASNS TS11 | 64,370 | 561 | 6.3.5.4 |
| ASNSD1 | Q9NWL6 | Asparagine synthetase domain-containing protein 1 (HCV NS3-transactivated protein 1) | ASNSD1 NS3TP1 Nbla00058 | 72,080 | 643 | |
| ASS1 | P00966 | Argininosuccinate synthase | ASS1 ASS | 46,530 | 412 | 6.3.4.5 |

Continued on next page

**Table B.1 – continued from previous page**

| Gene name | Uniprot-ID | Protein name | Synonyms | Mass | Length | E.C. |
|---|---|---|---|---|---|---|
| BCAT1 | P54687 | Branched-chain-amino-acid amino-transferase, cytosolic (BCAT(c)) | BCAT1 BCT1 ECA39 | 42,966 | 386 | 2.6.1.42 |
| BCAT2 | O15382 | Branched-chain-amino-acid amino-transferase | BCAT2 BCATM BCT2 ECA40 | 44,288 | 392 | 2.6.1.42 |
| BHMT | Q93088 | Betaine–homocysteine S-methyltransferase 1 | BHMT | 44,998 | 406 | 2.1.1.5 |
| BHMT2 | Q9H2M3 | S-methylmethionine–homocysteine S-methyltransferase BHMT2 (SMM-hcy methyltransferase) | BHMT2 | 40,354 | 363 | 2.1.1.10 |
| BPGM | P07738 | Bisphosphoglycerate mutase (BPGM) | BPGM | 30,005 | 259 | 5.4.2.4; 3.1.3.13; 5.4.2.11 |
| CA1 | P00915 | Carbonic anhydrase 1 | CA1 | 28,870 | 261 | 4.2.1.1 |
| CA12 | O43570 | Carbonic anhydrase 12 | CA12 | 39,451 | 354 | 4.2.1.1 |
| CA13 | Q8N1Q1 | Carbonic anhydrase 13 | CA13 | 29,443 | 262 | 4.2.1.1 |
| CA2 | P00918 | Carbonic anhydrase 2 | CA2 | 29,246 | 260 | 4.2.1.1 |
| CA3 | P07451 | Carbonic anhydrase 3 | CA3 | 29,557 | 260 | 4.2.1.1 |
| CA4 | P22748 | Carbonic anhydrase 4 | CA4 | 35,032 | 312 | 4.2.1.1 |
| CA5A | P35218 | Carbonic anhydrase 5A | CA5A CA5 | 34,750 | 305 | 4.2.1.1 |
| CA5BP1 | Q8WTZ4 | Putative inactive carbonic anhydrase 5B-like protein (CA-VB-like protein) | CA5BP1 CA5B CA5BL | 22,622 | 195 | |
| CA5B | Q9Y2D0 | Carbonic anhydrase 5B | CA5B | 36,434 | 317 | 4.2.1.1 |
| CA6 | P23280 | Carbonic anhydrase 6 | CA6 | 35,367 | 308 | 4.2.1.1 |
| CA7 | P43166 | Carbonic anhydrase 7 | CA7 | 29,658 | 264 | 4.2.1.1 |
| CA8 | P35219 | Carbonic anhydrase-related protein | CA8 CALS | 32,973 | 290 | |
| CA9 | Q16790 | Carbonic anhydrase 9 | CA9 G250 MN | 49,698 | 459 | 4.2.1.1 |
| CBS | P35520 | Cystathionine beta-synthase | CBS | 60,587 | 551 | 4.2.1.22 |

Continued on next page

**Table B.1 – continued from previous page**

| Gene name | Uniprot-ID | Protein name | Synonyms | Mass | Length | E.C. |
|---|---|---|---|---|---|---|
| KYAT1 | Q16773 | Kynurenine–oxoglutarate transaminase 1 | KYAT1 CCBL1 | 47,875 | 422 | 2.6.1.7; 4.4.1.13; 2.6.1.64 |
| KYAT3 | Q6YP21 | Kynurenine–oxoglutarate transaminase 3 | KYAT3 CCBL2 KAT3 | 51,400 | 454 | 2.6.1.7; 4.4.1.13; 2.6.1.63 |
| CFTR | P13569 | Cystic fibrosis transmembrane conductance regulator | CFTR ABCC7 | 168,142 | 1480 | 3.6.3.49 |
| CS | O75390 | Citrate synthase | CS | 51,712 | 466 | 2.3.3.1 |
| CTH | P32929 | Cystathionine gamma-lyase | CTH | 44,508 | 405 | 4.4.1.1 |
| VSIG2 | Q96IQ7 | V-set and immunoglobulin domain-containing protein 2 | VSIG2 CTH CTXL UNQ2770/PRO7154 | 34,348 | 327 | |
| DHFR | P00374 | Dihydrofolate reductase | DHFR | 21,453 | 187 | 1.5.1.3 |
| DHFRL1 | Q86XF0 | Dihydrofolate reductase | DHFRL1 DHFRP4 | 21,620 | 187 | 1.5.1.3 |
| DHTKD1 | Q96HY7 | Probable 2-oxoglutarate dehydrogenase E1 component DHKTD1 | DHTKD1 KIAA1630 | 103,077 | 919 | 1.2.4.2 |
| DUT | P33316 | Deoxyuridine 5'-triphosphate nucleotidohydrolase | DUT | 26,563 | 252 | 3.6.1.23 |
| DLAT | P10515 | Dihydrolipoyllysine-residue acetyltransferase component of pyruvate dehydrogenase complex | DLAT DLTA | 68,997 | 647 | 2.3.1.12 |
| DLST | P36957 | Dihydrolipoyllysine-residue succinyltransferase component of 2-oxoglutarate dehydrogenase complex | DLST DLTS | 48,755 | 453 | 2.3.1.61 |
| EEA1 | Q15075 | Early endosome antigen 1 | EEA1 ZFYVE2 | 162,466 | 1411 | |
| ENO1 | P06733 | Alpha-enolase | ENO1 ENO1L1 MBPB1 MPB1 | 47,169 | 434 | 4.2.1.11 |
| ENO2 | P09104 | Gamma-enolase | ENO2 | 47,269 | 434 | 4.2.1.11 |

Continued on next page

**Table B.1 – continued from previous page**

| Gene name | Uniprot-ID | Protein name | Synonyms | Mass | Length | E.C. |
|---|---|---|---|---|---|---|
| ENO3 | P13929 | Beta-enolase | ENO3 | 46,987 | 434 | 4.2.1.11 |
| ENOPH1 | Q9UHY7 | Enolase-phosphatase E1 | ENOPH1 MASA MSTP145 | 28,933 | 261 | 3.1.3.77 |
| ETNPPL | Q8TBG4 | Ethanolamine-phosphate phospho-lyase | ETNPPL AGXT2L1 | 55,671 | 499 | 4.2.3.2 |
| FASN | P49327 | Fatty acid synthase | FASN FAS | 273,427 | 2511 | 2.3.1.85; 2.3.1.38; 2.3.1.39; 2.3.1.41; 1.1.1.100 |
| FDPS | P14324 | Farnesyl pyrophosphate synthase | FDPS FPS KIAA1293 | 48,275 | 419 | 2.5.1.10; 2.5.1.1 |
| FH | P07954 | Fumarate hydratase | FH | 54,637 | 510 | 4.2.1.2 |
| FOXA1 | P55317 | Hepatocyte nuclear factor 3-alpha | FOXA1 HNF3A TCF3A | 49,148 | 472 | |
| FOXA2 | Q9Y261 | Hepatocyte nuclear factor 3-beta | FOXA2 HNF3B TCF3B | 48,306 | 457 | |
| FOXA3 | P55318 | Hepatocyte nuclear factor 3-gamma | FOXA3 HNF3G TCF3G | 37,140 | 350 | |
| FPGS | Q05932 | Folylpolyglutamate synthase | FPGS | 64,609 | 587 | 6.3.2.17 |
| FTCD | O95954 | Formimidoyltransferase-cyclodeaminase | FTCD | 58,927 | 541 | 2.1.2.5; 4.3.1.4 |
| G6PD | P11413 | Glucose-6-phosphate 1-dehydrogenase (G6PD) | G6PD | 59,257 | 515 | 1.1.1.49 |
| GAD1 | Q99259 | Glutamate decarboxylase 1 | GAD1 GAD GAD67 | 66,897 | 594 | 4.1.1.15 |
| GAD2 | Q05329 | Glutamate decarboxylase 2 | GAD2 GAD65 | 65,411 | 585 | 4.1.1.15 |
| GAPDH | P04406 | Glyceraldehyde-3-phosphate dehydro-genase (GAPDH) | GAPDH GAPD CDABP0047 OK/SW-cl.12 | 36,053 | 335 | 1.2.1.12; 2.6.99.- |
| GAPDHS | O14556 | Glyceraldehyde-3-phosphate dehydro-genase, testis-specific | GAPDHS GAPD2 GAPDH2 GAPDS HSD-35 HSD35 | 44,501 | 408 | 1.2.1.12 |

Continued on next page

**Table B.1 – continued from previous page**

| Gene name | Uniprot-ID | Protein name | Synonyms | Mass | Length | E.C. |
|---|---|---|---|---|---|---|
| GCAT | O75600 | 2-amino-3-ketobutyrate coenzyme A ligase | GCAT KBL | 45,285 | 419 | 2.3.1.29 |
| GCK | P35557 | Glucokinase | GCK | 52,191 | 465 | 2.7.1.2 |
| MAP4K2 | Q12851 | Mitogen-activated protein kinase kinase kinase kinase 2 | MAP4K2 GCK RAB8IP | 91,556 | 820 | 2.7.11.1 |
| GCLC | P48506 | Glutamate–cysteine ligase catalytic subunit | GCLC GLCL GLCLC | 72,766 | 637 | 6.3.2.2 |
| GCLM | P48507 | Glutamate–cysteine ligase regulatory subunit | GCLM GLCLR | 30,727 | 274 | |
| GCSH | P23434 | Glycine cleavage system H protein | GCSH | 18,885 | 173 | |
| GFPT1 | Q06210 | Glutamine–fructose-6-phosphate aminotransferase [isomerizing] 1 | GFPT1 GFAT GFPT | 78,806 | 699 | 2.6.1.16 |
| GFPT2 | O94808 | Glutamine–fructose-6-phosphate aminotransferase [isomerizing] 2 | GFPT2 | 76,931 | 682 | 2.6.1.16 |
| GLDC | P23378 | Glycine dehydrogenase (decarboxylating) | GLDC GCSP | 112,730 | 1020 | 1.4.4.2 |
| GLS | O94925 | Glutaminase kidney isoform | GLS GLS1 KIAA0838 | 73,461 | 669 | 3.5.1.2 |
| GLS2 | Q9UI32 | Glutaminase liver isoform | GLS2 GA | 66,323 | 602 | 3.5.1.2 |
| GLUD1 | P00367 | Glutamate dehydrogenase 1 | GLUD1 GLUD | 61,398 | 558 | 1.4.1.3 |
| GLUD2 | P49448 | Glutamate dehydrogenase 2 | GLUD2 GLUDP1 | 61,434 | 558 | 1.4.1.3 |
| GLUL | P15104 | Glutamine synthetase (GS) | GLUL GLNS | 42,064 | 373 | 6.3.1.2; 4.1.1.15 |
| GMEB1 | Q9Y692 | Glucocorticoid modulatory element-binding protein 1 | GMEB1 | 62,591 | 573 | |
| GMEB2 | Q9UKD1 | Glucocorticoid modulatory element-binding protein 2 | GMEB2 KIAA1269 | 56,421 | 530 | |
| GNMT | Q14749 | Glycine N-methyltransferase | GNMT | 32,742 | 295 | 2.1.1.20 |

Continued on next page

**Table B.1 – continued from previous page**

| Gene name | Uniprot-ID | Protein name | Synonyms | Mass | Length | E.C. |
|---|---|---|---|---|---|---|
| GOT1 | P17174 | Aspartate aminotransferase, cytoplasmic (cAspAT) | GOT1 | 46,248 | 413 | 2.6.1.1; 2.6.1.3 |
| GOT1L1 | Q8NHS2 | Putative aspartate aminotransferase, cytoplasmic 2 | GOT1L1 | 47,305 | 421 | 2.6.1.- |
| GOT2 | P00505 | Aspartate aminotransferase | GOT2 | 47,518 | 430 | 2.6.1.1; 2.6.1.7 |
| GPI | P06744 | Glucose-6-phosphate isomerase (GPI) | GPI | 63,147 | 558 | 5.3.1.9 |
| GPT | P24298 | Alanine aminotransferase 1 (ALT1) | GPT AAT1 GPT1 | 54,637 | 496 | 2.6.1.2 |
| GPT2 | Q8TD30 | Alanine aminotransferase 2 (ALT2) | GPT2 AAT2 ALT2 | 57,904 | 523 | 2.6.1.2 |
| GRIA1 | P42261 | Glutamate receptor 1 | GRIA1 GLUH1 GLUR1 | 101,506 | 906 | |
| GRIA2 | P42262 | Glutamate receptor 2 | GRIA2 GLUR2 | 98,821 | 883 | |
| GRIA3 | P42263 | Glutamate receptor 3 | GRIA3 GLUR3 GLURC | 101,157 | 894 | |
| GRIA4 | P48058 | Glutamate receptor 4 | GRIA4 GLUR4 | 100,871 | 902 | |
| GSS | P48637 | Glutathione synthetase | GSS | 52,385 | 474 | 6.3.2.3 |
| HADHB | P55084 | Trifunctional enzyme subunit beta | HADHB MSTP029 | 51,294 | 474 | 2.3.1.16 |
| HK1 | P19367 | Hexokinase-1 | HK1 | 102,486 | 917 | 2.7.1.1 |
| HK2 | P52789 | Hexokinase-2 | HK2 | 102,380 | 917 | 2.7.1.1 |
| HK3 | P52790 | Hexokinase-3 | HK3 | 99,025 | 923 | 2.7.1.1 |
| HKDC1 | Q2TB90 | Putative hexokinase HKDC1 | HKDC1 | 102,545 | 917 | 2.7.1.1 |
| HSD17B10 | Q99714 | 3-hydroxyacyl-CoA dehydrogenase type-2 | HSD17B10 ERAB HADH2 MRPP2 SCHAD SDR5C1 XH98G2 | 26,923 | 261 | 1.1.1.35; 1.1.1.51; 1.1.1.178 |
| IDH1 | O75874 | Isocitrate dehydrogenase [NADP] cytoplasmic (IDH) | IDH1 PICD | 46,659 | 414 | 1.1.1.42 |
| IDH2 | P48735 | Isocitrate dehydrogenase [NADP] | IDH2 | 50,909 | 452 | 1.1.1.42 |
| IDH3A | P50213 | Isocitrate dehydrogenase [NAD] subunit alpha | IDH3A | 39,592 | 366 | 1.1.1.41 |

Continued on next page

**Table B.1 – continued from previous page**

| Gene name | Uniprot-ID | Protein name | Synonyms | Mass | Length | E.C. |
|---|---|---|---|---|---|---|
| IDH3B | O43837 | Isocitrate dehydrogenase [NAD] subunit beta | IDH3B | 42,184 | 385 | 1.1.1.41 |
| IDH3G | P51553 | Isocitrate dehydrogenase [NAD] subunit gamma | IDH3G | 42,794 | 393 | 1.1.1.41 |
| LDHA | P00338 | L-lactate dehydrogenase A chain (LDH-A) | LDHA PIG19 | 36,689 | 332 | 1.1.1.27 |
| LDHB | P07195 | L-lactate dehydrogenase B chain (LDH-B) | LDHB | 36,638 | 334 | 1.1.1.27 |
| ACAT1 | P24752 | Acetyl-CoA acetyltransferase | ACAT1 ACAT MAT | 45,200 | 427 | 2.3.1.9 |
| MAT1A | Q00266 | S-adenosylmethionine synthase isoform type-1 (AdoMet synthase 1) | MAT1A AMS1 MATA1 | 43,648 | 395 | 2.5.1.6 |
| MAT2A | P31153 | S-adenosylmethionine synthase isoform type-2 (AdoMet synthase 2) | MAT2A AMS2 MATA2 | 43,661 | 395 | 2.5.1.6 |
| MAT2B | Q9NZL9 | Methionine adenosyltransferase 2 subunit beta | MAT2B TGR MSTP045 Nbla02999 UNQ2435/PRO4995 | 37,552 | 334 | |
| MDH1 | P40925 | Malate dehydrogenase, cytoplasmic | MDH1 MDHA | 36,426 | 334 | 1.1.1.37; 1.1.1.96 |
| MDH1B | Q5I0G3 | Putative malate dehydrogenase 1B | MDH1B | 58,651 | 518 | 1.1.1.- |
| MDH2 | P40926 | Malate dehydrogenase | MDH2 | 35,503 | 338 | 1.1.1.37 |
| ME1 | P48163 | NADP-dependent malic enzyme (NADP-ME) | ME1 | 64,150 | 572 | 1.1.1.40 |
| ME2 | P23368 | NAD-dependent malic enzyme | ME2 | 65,444 | 584 | 1.1.1.38 |
| ME3 | Q16798 | NADP-dependent malic enzyme | ME3 | 67,068 | 604 | 1.1.1.40 |
| MPST | P25325 | 3-mercaptopyruvate sulfurtransferase (MST) | MPST TST2 | 33,178 | 297 | 2.8.1.2 |
| MRI1 | Q9BV20 | Methylthioribose-1-phosphate isomerase | MRI1 MRDI UNQ6390/PRO21135 | 39,150 | 369 | 5.3.1.23 |

Continued on next page

**Table B.1 – continued from previous page**

| Gene name | Uniprot-ID | Protein name | Synonyms | Mass | Length | E.C. |
|---|---|---|---|---|---|---|
| MTHFD1 | P11586 | C-1-tetrahydrofolate synthase, cytoplasmic (C1-THF synthase) [Cleaved into: C-1-tetrahydrofolate synthase, cytoplasmic, N-terminally processed] [Includes: Methylenetetrahydrofolate dehydrogenase | MTHFD1 MTHFC MTHFD | 101,559 | 935 | 1.5.1.5; 3.5.4.9; 6.3.4.3 |
| MTHFD1L | Q6UB35 | Monofunctional C1-tetrahydrofolate synthase | MTHFD1L FTHFSDC1 | 105,790 | 978 | 6.3.4.3 |
| MTHFD2 | P13995 | Bifunctional methylenetetrahydrofolate dehydrogenase/cyclohydrolase | MTHFD2 NMDMC | 37,895 | 350 | 1.5.1.15; 3.5.4.9 |
| MTHFD2L | Q9H903 | Probable bifunctional methylenetetrahydrofolate dehydrogenase/cyclohydrolase 2 | MTHFD2L | 37,315 | 347 | 1.5.1.15; 3.5.4.9 |
| MTHFR | P42898 | Methylenetetrahydrofolate reductase | MTHFR | 74,597 | 656 | 1.5.1.20 |
| MTHFS | P49914 | 5-formyltetrahydrofolate cyclo-ligase | MTHFS | 23,256 | 203 | 6.3.3.2 |
| MTOR | P42345 | Serine/threonine-protein kinase mTOR | MTOR FRAP FRAP1 FRAP2 RAFT1 RAPT1 | 288,892 | 2549 | 2.7.11.1 |
| MTR | Q99707 | Methionine synthase | MTR | 140,527 | 1265 | 2.1.1.13 |
| MTRR | Q9UBK8 | Methionine synthase reductase (MSR) | MTRR | 80,410 | 725 | 1.16.1.8 |
| NAGS | Q8N159 | N-acetylglutamate synthase | NAGS | 58,156 | 534 | 2.3.1.1 |
| NFS1 | Q9Y697 | Cysteine desulfurase | NFS1 NIFS HUSSY-08 | 50,196 | 457 | 2.8.1.7 |
| NME1 | P15531 | Nucleoside diphosphate kinase A | NME1 NDPKA NM23 | 17,149 | 152 | 2.7.4.6 |
| NQO1 | P15559 | NAD(P)H dehydrogenase [quinone] 1 | NQO1 DIA4 NMOR1 | 30,868 | 274 | 1.6.5.2 |
| OAT | P04181 | Ornithine aminotransferase | OAT | 48,535 | 439 | 2.6.1.13 |
| OGDH | Q02218 | 2-oxoglutarate dehydrogenase | OGDH | 115,935 | 1023 | 1.2.4.2 |
| OGDHL | Q9ULD0 | 2-oxoglutarate dehydrogenase-like | OGDHL KIAA1290 | 114,481 | 1010 | 1.2.4.- |
| OTC | P00480 | Ornithine carbamoyltransferase | OTC | 39,935 | 354 | 2.1.3.3 |

Continued on next page

**Table B.1 – continued from previous page**

| Gene name | Uniprot-ID | Protein name | Synonyms | Mass | Length | E.C. |
|---|---|---|---|---|---|---|
| PDHA1 | P08559 | Pyruvate dehydrogenase E1 component subunit alpha, somatic form | PDHA1 PHE1A | 43,296 | 390 | 1.2.4.1 |
| PDHA2 | P29803 | Pyruvate dehydrogenase E1 component subunit alpha, testis-specific form | PDHA2 PDHAL | 42,933 | 388 | 1.2.4.1 |
| PDHB | P11177 | Pyruvate dehydrogenase E1 component subunit beta | PDHB PHE1B | 39,233 | 359 | 1.2.4.1 |
| PFKL | P17858 | ATP-dependent 6-phosphofructokinase, liver type | PFKL | 85,018 | 780 | 2.7.1.11 |
| PFKM | P08237 | ATP-dependent 6-phosphofructokinase | PFKM PFKX | 85,183 | 780 | 2.7.1.11 |
| PFKP | Q01813 | ATP-dependent 6-phosphofructokinase, platelet type | PFKP PFKF | 85,596 | 784 | 2.7.1.11 |
| PGAM1 | P18669 | Phosphoglycerate mutase 1 | PGAM1 PGAMA CDABP0006 | 28,804 | 254 | 3.1.3.13; 5.4.2.11; 5.4.2.4 |
| PGAM2 | P15259 | Phosphoglycerate mutase 2 | PGAM2 PGAMM | 28,766 | 253 | 3.1.3.13; 5.4.2.11; 5.4.2.4 |
| PGAM4 | Q8N0Y7 | Probable phosphoglycerate mutase 4 | PGAM4 PGAM3 | 28,777 | 254 | 3.1.3.13; 5.4.2.11; 5.4.2.4 |
| PGD | P52209 | 6-phosphogluconate dehydrogenase, decarboxylating | PGD PGDH | 53,140 | 483 | 1.1.1.44 |
| PGK1 | P00558 | Phosphoglycerate kinase 1 | PGK1 PGKA MIG10 OK/SW-cl.110 | 44,615 | 417 | 2.7.2.3 |
| PGK2 | P07205 | Phosphoglycerate kinase 2 | PGK2 PGKB | 44,796 | 417 | 2.7.2.3 |
| PGLS | O95336 | 6-phosphogluconolactonase (6PGL) | PGLS | 27,547 | 258 | 3.1.1.31 |
| PHGDH | O43175 | D-3-phosphoglycerate dehydrogenase (3-PGDH) | PHGDH PGDH3 | 56,651 | 533 | 1.1.1.95 |

Continued on next page

**Table B.1 – continued from previous page**

| Gene name | Uniprot-ID | Protein name | Synonyms | Mass | Length | E.C. |
|---|---|---|---|---|---|---|
| PHYKPL | Q8IUZ5 | 5-phosphohydroxy-L-lysine phospho-lyase | PHYKPL AGXT2L2 PP9286 | 49,711 | 450 | 4.2.3.134 |
| PKLR | P30613 | Pyruvate kinase PKLR | PKLR PK1 PKL | 61,830 | 574 | 2.7.1.40 |
| PKM | P14618 | Pyruvate kinase PKM | PKM OIP3 PK2 PK3 PKM2 | 57,937 | 531 | 2.7.1.40 |
| PNP | P00491 | Purine nucleoside phosphorylase (PNP) | PNP NP | 32,118 | 289 | 2.4.2.1 |
| PPY | P01298 | Pancreatic prohormone | PPY PNP | 10,445 | 95 | |
| PNPLA3 | Q9NST1 | Patatin-like phospholipase domain-containing protein 3 | PNPLA3 ADPN C22orf20 | 52,865 | 481 | 3.1.1.3; 2.3.1.- |
| PPP1CC | P36873 | Serine/threonine-protein phosphatase PP1-gamma catalytic subunit (PP-1G) | PPP1CC | 36,984 | 323 | 3.1.3.16 |
| PRODH | O43272 | Proline dehydrogenase 1 | PRODH PIG6 POX2 | 68,002 | 600 | 1.5.5.2 |
| PSAT1 | Q9Y617 | Phosphoserine aminotransferase | PSAT1 PSA | 40,423 | 370 | 2.6.1.52 |
| PSPH | P78330 | Phosphoserine phosphatase | PSPH | 25,008 | 225 | 3.1.3.3 |
| PYCR1 | P32322 | Pyrroline-5-carboxylate reductase 1 | PYCR1 | 33,361 | 319 | 1.5.1.2 |
| PYCR2 | Q96C36 | Pyrroline-5-carboxylate reductase 2 | PYCR2 | 33,637 | 320 | 1.5.1.2 |
| PYCRL | Q53H96 | Pyrroline-5-carboxylate reductase 3 | PYCRL | 28,663 | 274 | 1.5.1.2 |
| RPE | Q96AT9 | Ribulose-phosphate 3-epimerase | RPE HUSSY-17 | 24,928 | 228 | 5.1.3.1 |
| RPIA | P49247 | Ribose-5-phosphate isomerase | RPIA RPI | 33,269 | 311 | 5.3.1.6 |
| SARDH | Q9UL12 | Sarcosine dehydrogenase | SARDH DMGDHL1 | 101,037 | 918 | 1.5.8.3 |
| SCLY | Q96I15 | Selenocysteine lyase (hSCL) | SCLY SCL | 48,149 | 445 | 4.4.1.16 |
| SDHA | P31040 | Succinate dehydrogenase [ubiquinone] flavoprotein subunit | SDHA SDH2 SDHF | 72,692 | 664 | 1.3.5.1 |
| SDHB | P21912 | Succinate dehydrogenase [ubiquinone] iron-sulfur subunit | SDHB SDH SDH1 | 31,630 | 280 | 1.3.5.1 |
| SDHC | Q99643 | Succinate dehydrogenase cytochrome b560 subunit | SDHC CYB560 SDH3 | 18,610 | 169 | |

Continued on next page

**Table B.1 – continued from previous page**

| Gene name | Uniprot-ID | Protein name | Synonyms | Mass | Length | E.C. |
|---|---|---|---|---|---|---|
| SDHD | O14521 | Succinate dehydrogenase [ubiquinone] cytochrome b small subunit | SDHD SDH4 | 17,043 | 159 | |
| SHMT1 | P34896 | Serine hydroxymethyltransferase, cytosolic (SHMT) | SHMT1 | 53,083 | 483 | 2.1.2.1 |
| SHMT2 | P34897 | Serine hydroxymethyltransferase | SHMT2 | 55,993 | 504 | 2.1.2.1 |
| SIRT2 | Q8IXJ6 | NAD-dependent protein deacetylase sirtuin-2 | SIRT2 SIR2L SIR2L2 | 43,182 | 389 | 3.5.1.- |
| SLC1A1 | P43005 | Excitatory amino acid transporter 3 | SLC1A1 EAAC1 EAAT3 | 57,100 | 524 | |
| SLC1A2 | P43004 | Excitatory amino acid transporter 2 | SLC1A2 EAAT2 GLT1 | 62,104 | 574 | |
| SLC1A3 | P43003 | Excitatory amino acid transporter 1 | SLC1A3 EAAT1 GLAST GLAST1 | 59,572 | 542 | |
| SLC25A18 | Q9H1K4 | Mitochondrial glutamate carrier 2 | SLC25A18 GC2 | 33,849 | 315 | |
| SLC25A22 | Q9H936 | Mitochondrial glutamate carrier 1 | SLC25A22 GC1 | 34,470 | 323 | |
| SLC38A1 | Q9H2H9 | Sodium-coupled neutral amino acid transporter 1 | SLC38A1 ATA1 NAT2 SAT1 SNAT1 | 54,048 | 487 | |
| SLC38A3 | Q99624 | Sodium-coupled neutral amino acid transporter 3 | SLC38A3 G17 NAT1 SN1 SNAT3 | 55,773 | 504 | |
| SLC7A11 | Q9UPY5 | Cystine/glutamate transporter | SLC7A11 | 55,423 | 501 | |
| SPTLC1 | O15269 | Serine palmitoyltransferase 1 | SPTLC1 LCB1 | 52,744 | 473 | 2.3.1.50 |
| SPTLC2 | O15270 | Serine palmitoyltransferase 2 | SPTLC2 KIAA0526 LCB2 | 62,924 | 562 | 2.3.1.50 |
| SPTLC3 | Q9NUV7 | Serine palmitoyltransferase 3 | SPTLC3 C20orf38 SPTLC2L | 62,049 | 552 | 2.3.1.50 |
| SUCLA2 | Q9P2R7 | Succinyl-CoA ligase [ADP-forming] subunit beta | SUCLA2 | 50,317 | 463 | 6.2.1.5 |
| SUCLG1 | P53597 | Succinyl-CoA ligase [ADP/GDP-forming] subunit alpha | SUCLG1 | 36,250 | 346 | 6.2.1.4; 6.2.1.5 |
| SUCLG2 | Q96I99 | Succinyl-CoA ligase [GDP-forming] subunit beta | SUCLG2 | 46,511 | 432 | 6.2.1.4 |

Continued on next page

**Table B.1 – continued from previous page**

| Gene name | Uniprot-ID | Protein name | Synonyms | Mass | Length | E.C. |
|---|---|---|---|---|---|---|
| TALDO1 | P37837 | Transaldolase | TALDO1 TAL TALDO TALDOR | 37,540 | 337 | 2.2.1.2 |
| TAT | P17735 | Tyrosine aminotransferase (TAT) | TAT | 50,399 | 454 | 2.6.1.5 |
| TKT | P29401 | Transketolase (TK) | TKT | 67,878 | 623 | 2.2.1.1 |
| DDR2 | Q16832 | Discoidin domain-containing receptor 2 (Discoidin domain receptor 2) | DDR2 NTRKR3 TKT TYRO10 | 96,736 | 855 | 2.7.10.1 |
| TPI1 | P60174 | Triosephosphate isomerase (TIM) | TPI1 TPI | 30,791 | 286 | 5.3.1.1 |
| TYMS | P04818 | Thymidylate synthase | TYMS TS OK/SW-cl.29 | 35,716 | 313 | 2.1.1.45 |

## hESCs, hESC-DFs and cancer cells

Additional tables summarising the metabolic profiles of the analysed cells can be found on the attached CD.

Table B.2.: Stable isotope incorporation of $^{13}$C-glucose glucose in cancer cells, hESCs and hESC-DF cells of selected metabolites.

| Metabolite | SubGroup | State | N | Inc.mean | Inc.sd |
|---|---|---|---|---|---|
| Ala_3TMS | RKO | Cancer | 1 | 0.03 | NA |
| Ala_3TMS | SW480 | Cancer | 2 | 0.02 | 0.00 |
| Ala_3TMS | HT29 | Cancer | 2 | 0.03 | 0.00 |
| Ala_3TMS | MCF | Cancer | 2 | 0.02 | 0.00 |
| Ala_3TMS | MDA | Cancer | 1 | 0.24 | NA |
| Ala_3TMS | H9 | DF | 3 | 0.08 | 0.03 |
| Ala_3TMS | H1 | DF | 3 | 0.11 | 0.04 |
| Ala_3TMS | H1 | hESC | 3 | 0.14 | 0.01 |
| Ala_3TMS | H9 | hESC | 3 | 0.10 | 0.01 |
| Cit | MCF | Cancer | 3 | 0.42 | 0.08 |
| Cit | HT29 | Cancer | 3 | 0.19 | 0.08 |
| Cit | SW480 | Cancer | 3 | 0.20 | 0.01 |
| Cit | MDA | Cancer | 3 | 0.24 | 0.01 |
| Cit | RKO | Cancer | 3 | 0.40 | 0.14 |
| Cit | H9 | DF | 2 | 0.14 | 0.01 |
| Cit | H1 | DF | 1 | 0.16 | NA |
| Cit | H9 | hESC | 3 | 0.21 | 0.00 |
| Cit | H1 | hESC | 3 | 0.23 | 0.02 |
| Lac | HT29 | Cancer | 3 | 0.13 | 0.00 |
| Lac | MCF | Cancer | 2 | 0.20 | 0.02 |
| Lac | MDA | Cancer | 3 | 0.40 | 0.03 |
| Lac | RKO | Cancer | 3 | 0.14 | 0.01 |
| Lac | SW480 | Cancer | 3 | 0.10 | 0.02 |
| Lac | H1 | DF | 3 | 0.15 | 0.00 |
| Lac | H9 | DF | 3 | 0.13 | 0.02 |
| Lac | H1 | hESC | 3 | 0.29 | 0.01 |
| Lac | H9 | hESC | 3 | 0.30 | 0.00 |
| Pyr | HT29 | Cancer | 3 | 0.05 | 0.01 |
| Pyr | MCF | Cancer | 2 | 0.04 | 0.02 |
| Pyr | MDA | Cancer | 3 | 0.02 | 0.00 |
| Pyr | RKO | Cancer | 3 | 0.16 | 0.07 |
| Pyr | SW480 | Cancer | 3 | 0.04 | 0.01 |
| Pyr | H1 | DF | 3 | 0.01 | 0.00 |
| Pyr | H9 | DF | 3 | 0.01 | 0.00 |
| Pyr | H1 | hESC | 3 | 0.06 | 0.01 |
| Pyr | H9 | hESC | 3 | 0.07 | 0.01 |

Continued on next page

**Table B.2 – continued from previous page**

| Metabolite | SubGroup | State | N | Inc.mean | Inc.sd |
|---|---|---|---|---|---|
| Ser_3TMS | HT29 | Cancer | 3 | 0.03 | 0.00 |
| Ser_3TMS | MCF | Cancer | 2 | 0.02 | 0.00 |
| Ser_3TMS | RKO | Cancer | 3 | 0.02 | 0.00 |
| Ser_3TMS | SW480 | Cancer | 3 | 0.02 | 0.00 |
| Ser_3TMS | H1 | DF | 3 | 0.02 | 0.00 |
| Ser_3TMS | H9 | DF | 3 | 0.05 | 0.01 |
| Ser_3TMS | H1 | hESC | 3 | 0.09 | 0.00 |
| Ser_3TMS | H9 | hESC | 3 | 0.12 | 0.00 |

Table B.3.: Stable isotope incorporation of $^{13}$C-glutamine in cancer cells, hESCs and hESC-DF cells of selected metabolites.

| Metabolite | SubGroup | State | N | Inc.mean | Inc.sd |
|---|---|---|---|---|---|
| Cit | RKO | Cancer | 3 | 0.05 | 0.01 |
| Cit | SW480 | Cancer | 3 | 0.07 | 0.01 |
| Cit | HT29 | Cancer | 3 | 0.09 | 0.01 |
| Cit | MCF | Cancer | 3 | 0.03 | 0.00 |
| Cit | MDA | Cancer | 2 | 0.02 | 0.00 |
| Cit | H1 | DF | 1 | 0.02 | NA |
| Cit | H1 | hESC | 2 | 0.05 | 0.01 |
| Cit | H9 | DF | 2 | 0.06 | 0.01 |
| Cit | H9 | hESC | 2 | 0.06 | 0.01 |
| Glu_3TMS | H1 | DF | 2 | 0.13 | 0.01 |
| Glu_3TMS | H1 | hESC | 2 | 0.15 | 0.01 |
| Glu_3TMS | H9 | DF | 2 | 0.13 | 0.00 |
| Glu_3TMS | H9 | hESC | 2 | 0.15 | 0.00 |
| Glu_3TMS | HT29 | Cancer | 3 | 0.34 | 0.03 |
| Glu_3TMS | MCF | Cancer | 3 | 0.13 | 0.03 |
| Glu_3TMS | MDA | Cancer | 2 | 0.15 | 0.02 |
| Glu_3TMS | RKO | Cancer | 3 | 0.20 | 0.01 |
| Glu_3TMS | SW480 | Cancer | 3 | 0.37 | 0.01 |
| Suc | H1 | hESC | 2 | 0.09 | 0.02 |
| Suc | H9 | hESC | 2 | 0.17 | 0.02 |
| Suc | HT29 | Cancer | 2 | 0.01 | 0.00 |
| Suc | MCF | Cancer | 3 | 0.09 | 0.00 |
| Suc | MDA | Cancer | 1 | 0.09 | NA |
| Suc | RKO | Cancer | 1 | 0.02 | NA |
| Suc | SW480 | Cancer | 3 | 0.08 | 0.01 |
| Suc | H1 | hESC | 2 | 0.20 | 0.01 |
| Suc | H9 | hESC | 2 | 0.18 | 0.02 |
| Suc | HT29 | Cancer | 3 | 0.15 | 0.03 |
| Suc | MCF | Cancer | 3 | 0.08 | 0.00 |

Continued on next page

**Table B.3 – continued from previous page**

| Metabolite | SubGroup | State | N | Inc.mean | Inc.sd |
|---|---|---|---|---|---|
| Suc | MDA | Cancer | 2 | 0.21 | 0.11 |
| Suc | RKO | Cancer | 3 | 0.07 | 0.01 |
| Suc | SW480 | Cancer | 3 | 0.19 | 0.01 |

Table B.4.: Stable isotope incorporation of $^{13}$C-pyruvic acid in cancer cells, hESCs and hESC-DF cells of selected metabolites.

| Metabolite | SubGroup | State | N | Inc.mean | Inc.sd |
|---|---|---|---|---|---|
| Ala_3TMS | H1 | DF | 2 | 0.27 | 0.02 |
| Ala_3TMS | H1 | hESC | 2 | 0.10 | 0.01 |
| Ala_3TMS | H9 | hESC | 2 | 0.11 | 0.00 |
| Ala_3TMS | H9 | DF | 2 | 0.28 | 0.02 |
| Ala_3TMS | HT29 | Cancer | 2 | 0.01 | 0.00 |
| Ala_3TMS | MCF | Cancer | 1 | 0.02 | NA |
| Ala_3TMS | MDA | Cancer | 2 | 0.17 | 0.09 |
| Ala_3TMS | RKO | Cancer | 2 | 0.01 | 0.00 |
| Ala_3TMS | SW480 | Cancer | 2 | 0.01 | 0.00 |
| Cit | H1 | DF | 2 | 0.06 | 0.01 |
| Cit | H1 | hESC | 2 | 0.11 | 0.01 |
| Cit | H9 | hESC | 2 | 0.10 | 0.01 |
| Cit | H9 | DF | 2 | 0.05 | 0.02 |
| Cit | HT29 | Cancer | 1 | 0.36 | NA |
| Cit | MCF | Cancer | 2 | 0.17 | 0.05 |
| Cit | MDA | Cancer | 2 | 0.01 | 0.00 |
| Cit | RKO | Cancer | 2 | 0.18 | 0.06 |
| Cit | SW480 | Cancer | 2 | 0.25 | 0.01 |
| Lac | H1 | DF | 2 | 0.25 | 0.01 |
| Lac | H1 | hESC | 2 | 0.26 | 0.00 |
| Lac | H9 | DF | 2 | 0.30 | 0.03 |
| Lac | H9 | hESC | 2 | 0.25 | 0.02 |
| Lac | HT29 | Cancer | 2 | 0.12 | 0.00 |
| Lac | MCF | Cancer | 2 | 0.13 | 0.07 |
| Lac | MDA | Cancer | 2 | 0.19 | 0.01 |
| Lac | RKO | Cancer | 2 | 0.09 | 0.01 |
| Lac | SW480 | Cancer | 2 | 0.16 | 0.01 |

## Reprogramming pluripotency in fibroblasts and re-differentiation

Additional tables summarising the metabolic profiles of the analysed cells can be found on the attached CD.

Table B.5.: Stable isotope incorporation of $^{13}$C-glucose in HFF1 and derived iPS and iPS-DF cells of selected metabolites.

| **Metabolite** | **SubGroup** | **State** | **N** | **Inc.mean** | **Inc.sd** |
|---|---|---|---|---|---|
| Alanine_(3TMS)_MP | HFF1 | F | 3 | 0.07 | 0.02 |
| Alanine_(3TMS)_MP | iPS2 | DF | 3 | 0.07 | 0.00 |
| Alanine_(3TMS)_MP | iPS2 | iPS | 3 | 0.14 | 0.00 |
| Alanine_(3TMS)_MP | iPS4 | DF | 3 | 0.08 | 0.00 |
| Alanine_(3TMS)_MP | iPS4 | iPS | 3 | 0.12 | 0.01 |
| Citric acid 275_(4TMS)_MP | HFF1 | F | 3 | 0.08 | 0.01 |
| Citric acid 275_(4TMS)_MP | iPS2 | DF | 3 | 0.08 | 0.02 |
| Citric acid 275_(4TMS)_MP | iPS2 | iPS | 3 | 0.08 | 0.01 |
| Citric acid 275_(4TMS)_MP | iPS4 | DF | 3 | 0.15 | 0.01 |
| Citric acid 275_(4TMS)_MP | iPS4 | iPS | 3 | 0.07 | 0.02 |
| Fumaric acid 247_(2TMS)_MP | HFF1 | F | 3 | 0.12 | 0.03 |
| Fumaric acid 247_(2TMS)_MP | iPS2 | DF | 3 | 0.08 | 0.02 |
| Fumaric acid 247_(2TMS)_MP | iPS2 | iPS | 3 | 0.09 | 0.01 |
| Fumaric acid 247_(2TMS)_MP | iPS4 | DF | 3 | 0.12 | 0.03 |
| Fumaric acid 247_(2TMS)_MP | iPS4 | iPS | 3 | 0.09 | 0.02 |
| Lactic acid_(2TMS)_MP | HFF1 | F | 3 | 0.13 | 0.02 |
| Lactic acid_(2TMS)_MP | iPS2 | DF | 3 | 0.06 | 0.01 |
| Lactic acid_(2TMS)_MP | iPS2 | iPS | 3 | 0.13 | 0.02 |
| Lactic acid_(2TMS)_MP | iPS4 | DF | 3 | 0.09 | 0.03 |
| Lactic acid_(2TMS)_MP | iPS4 | iPS | 3 | 0.17 | 0.00 |
| Pyruvic acid_(1MEOX)(1TMS)_MP | HFF1 | F | 3 | 0.01 | 0.00 |
| Pyruvic acid_(1MEOX)(1TMS)_MP | iPS2 | DF | 3 | 0.01 | 0.00 |
| Pyruvic acid_(1MEOX)(1TMS)_MP | iPS2 | iPS | 3 | 0.04 | 0.00 |
| Pyruvic acid_(1MEOX)(1TMS)_MP | iPS4 | DF | 3 | 0.01 | 0.00 |
| Pyruvic acid_(1MEOX)(1TMS)_MP | iPS4 | iPS | 3 | 0.04 | 0.00 |
| Serine_(3TMS)_MP | HFF1 | F | 3 | 0.03 | 0.01 |
| Serine_(3TMS)_MP | iPS2 | DF | 3 | 0.02 | 0.00 |
| Serine_(3TMS)_MP | iPS2 | iPS | 3 | 0.06 | 0.00 |
| Serine_(3TMS)_MP | iPS4 | DF | 3 | 0.01 | 0.00 |
| Serine_(3TMS)_MP | iPS4 | iPS | 3 | 0.05 | 0.00 |

Table B.6.: Stable isotope incorporation of $^{13}$C-glucose in BJ1 and derived iPS and iPS-DF cells of selected metabolites.

| **Metabolite** | **SubGroup** | **State** | **N** | **Inc.mean** | **Inc.sd** |
|---|---|---|---|---|---|
| Alanine_(3TMS)_MP | BJ | F | 3 | 0.08 | 0.02 |
| Alanine_(3TMS)_MP | iB4 | DF | 3 | 0.00 | 0.00 |
| Alanine_(3TMS)_MP | iB4 | iPS | 3 | 0.12 | 0.01 |
| Alanine_(3TMS)_MP | iB5 | DF | 3 | 0.09 | 0.03 |
| Alanine_(3TMS)_MP | iB5 | iPS | 2 | 0.11 | 0.00 |
| Citric acid 275_(4TMS)_MP | BJ | F | 3 | 0.14 | 0.01 |
| Citric acid 275_(4TMS)_MP | iB4 | DF | 3 | 0.04 | 0.04 |
| Citric acid 275_(4TMS)_MP | iB4 | iPS | 3 | 0.21 | 0.01 |
| Citric acid 275_(4TMS)_MP | iB5 | DF | 3 | 0.19 | 0.04 |
| Citric acid 275_(4TMS)_MP | iB5 | iPS | 2 | 0.22 | 0.00 |
| Fumaric acid 247_(2TMS)_MP | BJ | F | 3 | 0.15 | 0.03 |
| Fumaric acid 247_(2TMS)_MP | iB4 | DF | 3 | 0.00 | 0.00 |
| Fumaric acid 247_(2TMS)_MP | iB4 | iPS | 3 | 0.09 | 0.02 |
| Fumaric acid 247_(2TMS)_MP | iB5 | DF | 3 | 0.00 | 0.00 |
| Fumaric acid 247_(2TMS)_MP | iB5 | iPS | 2 | 0.11 | 0.01 |
| Lactic acid_(2TMS)_MP | BJ | F | 3 | 0.14 | 0.02 |
| Lactic acid_(2TMS)_MP | iB4 | DF | 3 | 0.08 | 0.01 |
| Lactic acid_(2TMS)_MP | iB4 | iPS | 3 | 0.30 | 0.01 |
| Lactic acid_(2TMS)_MP | iB5 | DF | 3 | 0.20 | 0.07 |
| Lactic acid_(2TMS)_MP | iB5 | iPS | 2 | 0.30 | 0.02 |
| Pyruvic acid_(1MEOX)(1TMS)_MP | BJ | F | 3 | 0.00 | 0.00 |
| Pyruvic acid_(1MEOX)(1TMS)_MP | iB4 | DF | 3 | 0.01 | 0.00 |
| Pyruvic acid_(1MEOX)(1TMS)_MP | iB4 | iPS | 3 | 0.03 | 0.01 |
| Pyruvic acid_(1MEOX)(1TMS)_MP | iB5 | DF | 3 | 0.00 | 0.00 |
| Pyruvic acid_(1MEOX)(1TMS)_MP | iB5 | iPS | 2 | 0.03 | 0.00 |
| Serine_(3TMS)_MP | BJ | F | 3 | 0.02 | 0.00 |
| Serine_(3TMS)_MP | iB4 | DF | 3 | 0.01 | 0.00 |
| Serine_(3TMS)_MP | iB4 | iPS | 3 | 0.08 | 0.00 |
| Serine_(3TMS)_MP | iB5 | DF | 3 | 0.00 | 0.00 |
| Serine_(3TMS)_MP | iB5 | iPS | 2 | 0.08 | 0.01 |

Table B.7.: Stable isotope incorporation of $^{13}$C-glucose in NFH2 and derived iPS and iPS-DF cells of selected metabolites.

| **Metabolite** | **SubGroup** | **State** | **N** | **Inc.mean** | **Inc.sd** |
|---|---|---|---|---|---|
| Alanine_(3TMS)_MP | NFH2 | F | 3 | 0.10 | 0.03 |
| Alanine_(3TMS)_MP | OiPS3 | DF | 3 | 0.04 | 0.01 |
| Alanine_(3TMS)_MP | OiPS3 | iPS | 3 | 0.15 | 0.02 |
| Alanine_(3TMS)_MP | OiPS6 | DF | 3 | 0.04 | 0.02 |
| Alanine_(3TMS)_MP | OiPS6 | iPS | 3 | 0.10 | 0.02 |
| Citric acid 275_(4TMS)_MP | NFH2 | F | 3 | 0.19 | 0.01 |
| Citric acid 275_(4TMS)_MP | OiPS3 | DF | 3 | 0.12 | 0.00 |
| Citric acid 275_(4TMS)_MP | OiPS3 | iPS | 3 | 0.20 | 0.01 |
| Citric acid 275_(4TMS)_MP | OiPS6 | DF | 3 | 0.18 | 0.02 |
| Citric acid 275_(4TMS)_MP | OiPS6 | iPS | 3 | 0.21 | 0.01 |
| Fumaric acid 247_(2TMS)_MP | NFH2 | F | 3 | 0.09 | 0.00 |
| Fumaric acid 247_(2TMS)_MP | OiPS3 | DF | 3 | 0.09 | 0.01 |
| Fumaric acid 247_(2TMS)_MP | OiPS3 | iPS | 3 | 0.01 | 0.00 |
| Fumaric acid 247_(2TMS)_MP | OiPS6 | DF | 3 | 0.12 | 0.01 |
| Fumaric acid 247_(2TMS)_MP | OiPS6 | iPS | 3 | 0.03 | 0.02 |
| Lactic acid_(2TMS)_MP | NFH2 | F | 3 | 0.17 | 0.02 |
| Lactic acid_(2TMS)_MP | OiPS3 | DF | 3 | 0.09 | 0.01 |
| Lactic acid_(2TMS)_MP | OiPS3 | iPS | 3 | 0.26 | 0.00 |
| Lactic acid_(2TMS)_MP | OiPS6 | DF | 3 | 0.12 | 0.01 |
| Lactic acid_(2TMS)_MP | OiPS6 | iPS | 3 | 0.26 | 0.00 |
| Pyruvic acid_(1MEOX)(1TMS)_MP | NFH2 | F | 3 | 0.00 | 0.00 |
| Pyruvic acid_(1MEOX)(1TMS)_MP | OiPS3 | DF | 3 | 0.01 | 0.00 |
| Pyruvic acid_(1MEOX)(1TMS)_MP | OiPS3 | iPS | 3 | 0.04 | 0.00 |
| Pyruvic acid_(1MEOX)(1TMS)_MP | OiPS6 | DF | 3 | 0.00 | 0.00 |
| Pyruvic acid_(1MEOX)(1TMS)_MP | OiPS6 | iPS | 3 | 0.02 | 0.00 |
| Serine_(3TMS)_MP | NFH2 | F | 3 | 0.01 | 0.00 |
| Serine_(3TMS)_MP | OiPS3 | DF | 3 | 0.00 | 0.00 |
| Serine_(3TMS)_MP | OiPS3 | iPS | 3 | 0.03 | 0.00 |
| Serine_(3TMS)_MP | OiPS6 | DF | 3 | 0.00 | 0.00 |
| Serine_(3TMS)_MP | OiPS6 | iPS | 3 | 0.01 | 0.00 |

Table B.8.: Stable isotope incorporation of $^{13}$C-glutamine in all fibroblasts and derived iPS and iPS-DF cells of selected metabolites.

| **Metabolite** | **SubGroup** | **State** | **N** | **Inc.mean** | **Inc.sd** |
|---|---|---|---|---|---|
| Citric acid 276_(4TMS)_MP | BJ | F | 2 | 0.04 | 0.02 |
| Citric acid 276_(4TMS)_MP | HFF1 | F | 2 | 0.01 | 0.01 |
| Citric acid 276_(4TMS)_MP | iB5 | F | 1 | 0.02 | NA |
| Citric acid 276_(4TMS)_MP | NFH2 | F | 2 | 0.02 | 0.00 |
| Glutamic acid_(3TMS)_MP | BJ | F | 2 | 0.32 | 0.03 |
| Glutamic acid_(3TMS)_MP | HFF1 | F | 2 | 0.16 | 0.00 |
| Glutamic acid_(3TMS)_MP | iB5 | F | 1 | 0.24 | NA |
| Glutamic acid_(3TMS)_MP | NFH2 | F | 2 | 0.22 | 0.03 |
| Succinic acid 251_(2TMS)_MP | BJ | F | 2 | 0.56 | 0.22 |
| Succinic acid 251_(2TMS)_MP | HFF1 | F | 2 | 0.53 | 0.11 |
| Succinic acid 251_(2TMS)_MP | iB5 | F | 1 | 0.66 | NA |
| Succinic acid 251_(2TMS)_MP | NFH2 | F | 2 | 0.55 | 0.01 |
| Citric acid 276_(4TMS)_MP | iB4 | iPS | 2 | 0.06 | 0.02 |
| Citric acid 276_(4TMS)_MP | iB5 | iPS | 2 | 0.04 | 0.00 |
| Citric acid 276_(4TMS)_MP | iPS2 | iPS | 2 | 0.02 | 0.01 |
| Citric acid 276_(4TMS)_MP | iPS4 | iPS | 2 | 0.01 | 0.01 |
| Citric acid 276_(4TMS)_MP | OiPS3 | iPS | 2 | 0.01 | 0.01 |
| Citric acid 276_(4TMS)_MP | OiPS6 | iPS | 2 | 0.01 | 0.01 |
| Glutamic acid_(3TMS)_MP | iB4 | iPS | 2 | 0.07 | 0.09 |
| Glutamic acid_(3TMS)_MP | iB5 | iPS | 2 | 0.14 | 0.01 |
| Glutamic acid_(3TMS)_MP | iPS2 | iPS | 2 | 0.14 | 0.00 |
| Glutamic acid_(3TMS)_MP | iPS4 | iPS | 2 | 0.11 | 0.02 |
| Glutamic acid_(3TMS)_MP | OiPS3 | iPS | 2 | 0.10 | 0.01 |
| Glutamic acid_(3TMS)_MP | OiPS6 | iPS | 2 | 0.13 | 0.00 |
| Succinic acid 251_(2TMS)_MP | iB4 | iPS | 2 | 0.33 | 0.00 |
| Succinic acid 251_(2TMS)_MP | iB5 | iPS | 2 | 0.45 | 0.09 |
| Succinic acid 251_(2TMS)_MP | iPS2 | iPS | 2 | 0.46 | 0.01 |
| Succinic acid 251_(2TMS)_MP | iPS4 | iPS | 2 | 0.47 | 0.11 |
| Succinic acid 251_(2TMS)_MP | OiPS3 | iPS | 2 | 0.32 | 0.02 |
| Succinic acid 251_(2TMS)_MP | OiPS6 | iPS | 2 | 0.36 | 0.10 |
| Citric acid 276_(4TMS)_MP | iB4 | DF | 2 | 0.02 | 0.00 |
| Citric acid 276_(4TMS)_MP | iPS2 | DF | 2 | 0.04 | 0.00 |
| Citric acid 276_(4TMS)_MP | iPS4 | DF | 2 | 0.03 | 0.01 |
| Citric acid 276_(4TMS)_MP | OiPS3 | DF | 2 | 0.07 | 0.00 |
| Citric acid 276_(4TMS)_MP | OiPS6 | DF | 2 | 0.08 | 0.01 |
| Glutamic acid_(3TMS)_MP | iB4 | DF | 2 | 0.03 | 0.02 |
| Glutamic acid_(3TMS)_MP | iPS2 | DF | 2 | 0.09 | 0.01 |
| Glutamic acid_(3TMS)_MP | iPS4 | DF | 2 | 0.14 | 0.02 |
| Glutamic acid_(3TMS)_MP | OiPS3 | DF | 2 | 0.11 | 0.01 |
| Glutamic acid_(3TMS)_MP | OiPS6 | DF | 2 | 0.15 | 0.03 |

Continued on next page

**Table B.8 – continued from previous page**

| Metabolite | SubGroup | State | N | Inc.mean | Inc.sd |
|---|---|---|---|---|---|
| Succinic acid 251_(2TMS)_MP | iB4 | DF | 2 | 0.30 | 0.01 |
| Succinic acid 251_(2TMS)_MP | iPS2 | DF | 2 | 0.45 | 0.01 |
| Succinic acid 251_(2TMS)_MP | iPS4 | DF | 2 | 0.35 | 0.05 |
| Succinic acid 251_(2TMS)_MP | OiPS3 | DF | 2 | 0.34 | 0.06 |
| Succinic acid 251_(2TMS)_MP | OiPS6 | DF | 2 | 0.50 | 0.01 |

Table B.9.: Stable isotope incorporation of $^{13}$C-pyruvic acid in all fibroblasts and derived iPS and iPS-DF cells of selected metabolites.

| Metabolite | SubGroup | State | N | Inc.mean | Inc.sd |
|---|---|---|---|---|---|
| Alanine_(3TMS)_MP | HFF1 | F | 2 | 0.15 | 0.07 |
| Alanine_(3TMS)_MP | NFH2 | F | 2 | 0.12 | 0.03 |
| Citric acid 275_(4TMS)_MP | BJ | F | 2 | 0.22 | 0.01 |
| Citric acid 275_(4TMS)_MP | HFF1 | F | 2 | 0.29 | 0.00 |
| Citric acid 275_(4TMS)_MP | NFH2 | F | 2 | 0.37 | 0.01 |
| Lactic acid_(2TMS)_MP | BJ | F | 2 | 0.23 | 0.01 |
| Lactic acid_(2TMS)_MP | HFF1 | F | 2 | 0.32 | 0.04 |
| Lactic acid_(2TMS)_MP | NFH2 | F | 2 | 0.25 | 0.07 |
| Lactic acid_(2TMS)_MP | iB4 | DF | 2 | 0.36 | 0.06 |
| Lactic acid_(2TMS)_MP | iPS2 | DF | 2 | 0.23 | 0.10 |
| Lactic acid_(2TMS)_MP | iPS4 | DF | 2 | 0.35 | 0.04 |
| Lactic acid_(2TMS)_MP | OiPS3 | DF | 2 | 0.26 | 0.02 |
| Lactic acid_(2TMS)_MP | OiPS6 | DF | 2 | 0.21 | 0.09 |
| Alanine_(3TMS)_MP | iB4 | iPS | 2 | 0.09 | 0.11 |
| Alanine_(3TMS)_MP | iB5 | iPS | 2 | 0.17 | 0.01 |
| Alanine_(3TMS)_MP | iPS2 | iPS | 2 | 0.21 | 0.02 |
| Alanine_(3TMS)_MP | iPS4 | iPS | 2 | 0.26 | 0.02 |
| Citric acid 275_(4TMS)_MP | iB4 | iPS | 2 | 0.15 | 0.03 |
| Citric acid 275_(4TMS)_MP | iB5 | iPS | 2 | 0.19 | 0.01 |
| Citric acid 275_(4TMS)_MP | iPS2 | iPS | 2 | 0.16 | 0.07 |
| Citric acid 275_(4TMS)_MP | iPS4 | iPS | 2 | 0.15 | 0.03 |
| Citric acid 275_(4TMS)_MP | OiPS3 | iPS | 2 | 0.19 | 0.01 |
| Citric acid 275_(4TMS)_MP | OiPS6 | iPS | 2 | 0.24 | 0.01 |
| Lactic acid_(2TMS)_MP | iB4 | iPS | 2 | 0.14 | 0.14 |
| Lactic acid_(2TMS)_MP | iB5 | iPS | 2 | 0.23 | 0.00 |
| Lactic acid_(2TMS)_MP | iPS2 | iPS | 2 | 0.31 | 0.00 |
| Lactic acid_(2TMS)_MP | iPS4 | iPS | 2 | 0.36 | 0.00 |
| Lactic acid_(2TMS)_MP | OiPS3 | iPS | 2 | 0.23 | 0.01 |
| Lactic acid_(2TMS)_MP | OiPS6 | iPS | 2 | 0.24 | 0.01 |
| Alanine_(3TMS)_MP | iB4 | DF | 2 | 0.25 | 0.01 |
| Alanine_(3TMS)_MP | iPS2 | DF | 2 | 0.25 | 0.05 |

Continued on next page

**Table B.9 – continued from previous page**

| Metabolite | SubGroup | State | N | Inc.mean | Inc.sd |
|---|---|---|---|---|---|
| Alanine_(3TMS)_MP | iPS4 | DF | 2 | 0.28 | 0.01 |
| Citric acid 275_(4TMS)_MP | iB4 | DF | 2 | 0.28 | 0.01 |
| Citric acid 275_(4TMS)_MP | iPS2 | DF | 2 | 0.29 | 0.03 |
| Citric acid 275_(4TMS)_MP | iPS4 | DF | 2 | 0.24 | 0.01 |
| Citric acid 275_(4TMS)_MP | OiPS3 | DF | 2 | 0.16 | 0.02 |
| Citric acid 275_(4TMS)_MP | OiPS6 | DF | 2 | 0.27 | 0.00 |

## Reprogramming in early differentiation of hESC H1

Table B.10.: Media composition for the cultivation of hESC H1 cells

| | **Stem cell media** SM | **Differentiation media** SpDiff |
|---|---|---|
| Basal media | DMEM/F12 | DMEM/F12 |
| Glc (g/L) | 4.5 | 4.5 |
| Gln (mM) | 2 | 2 |
| Supplements | 15 % KO-serum<br>2-ME<br>10 $ng/ml$ bFGF<br>100 $pg/ml$ IL6RIL6 | 15 % KO-serum<br>2-ME |

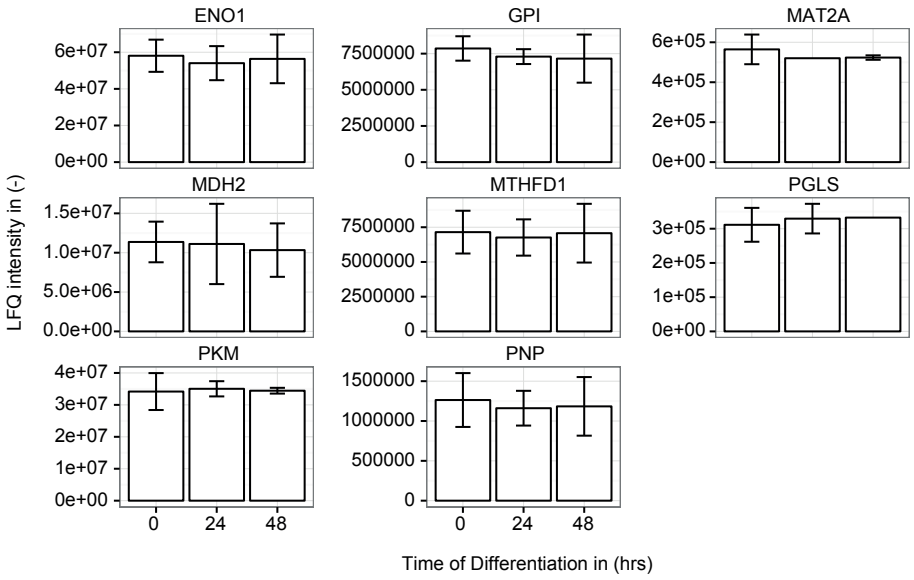


Figure B.1.: CCM related proteins with less than 5% variance of protein expression within 48 hrs of differentiation.

Table B.11.: Top50 proteins shown the highest variance within 48 hours of early differentiation in hESCs H1.

| **Gene names** | **0 hrs** | **24 hrs** | **48 hrs** | **var(LFQ)** |
|---|---|---|---|---|
| ALB | 1.00E+04 | 3.88E+07 | 1.00E+04 | 2.24E+07 |
| HIST1H4A | 6.43E+07 | 9.27E+07 | 5.49E+07 | 1.97E+07 |
| JMJD1C | 1.00E+04 | 1.00E+04 | 3.42E+07 | 1.97E+07 |

Continued on next page

**Table B.11 – continued from previous page**

| Gene names | 0 hrs | 24 hrs | 48 hrs | var(LFQ) |
|---|---|---|---|---|
| FASN | 4.36E+07 | 3.12E+07 | 2.14E+07 | 1.11E+07 |
| TF | 1.70E+07 | 7.25E+05 | 1.00E+04 | 9.60E+06 |
| RBP4 | 1.00E+04 | 1.09E+07 | 1.48E+07 | 7.67E+06 |
| EEF2 | 7.07E+07 | 5.80E+07 | 6.03E+07 | 6.77E+06 |
| PPIA | 5.19E+07 | 4.05E+07 | 4.04E+07 | 6.62E+06 |
| PTMA | 1.51E+07 | 2.43E+07 | 2.74E+07 | 6.38E+06 |
| RPL29 | 1.87E+07 | 7.19E+06 | 9.07E+06 | 6.19E+06 |
| LDHB | 4.73E+07 | 3.66E+07 | 3.69E+07 | 6.06E+06 |
| HSPD1 | 5.59E+07 | 5.42E+07 | 4.50E+07 | 5.90E+06 |
| BPIFB1 | 1.00E+04 | 9.99E+06 | 1.00E+04 | 5.76E+06 |
| RPL6 | 3.43E+07 | 2.86E+07 | 2.30E+07 | 5.65E+06 |
| GAPDH | 6.86E+07 | 6.83E+07 | 5.95E+07 | 5.18E+06 |
| NPM1 | 4.98E+07 | 4.09E+07 | 4.14E+07 | 4.98E+06 |
| HSPA8 | 5.18E+07 | 4.38E+07 | 4.29E+07 | 4.88E+06 |
| VIM | 7.87E+06 | 1.08E+07 | 1.68E+07 | 4.54E+06 |
| FLNC | 3.07E+05 | 4.28E+06 | 8.59E+06 | 4.14E+06 |
| HMGCS1 | 1.06E+07 | 5.48E+06 | 2.50E+06 | 4.12E+06 |
| C3orf56 | 1.00E+04 | 1.00E+04 | 6.77E+06 | 3.90E+06 |
| EEF1A1;EEF1A1P5 | 3.18E+07 | 2.57E+07 | 2.47E+07 | 3.84E+06 |
| INS | 2.10E+07 | 1.34E+07 | 1.74E+07 | 3.81E+06 |
| TAGLN | 1.81E+06 | 4.34E+06 | 9.25E+06 | 3.78E+06 |
| RPL8 | 2.01E+07 | 1.64E+07 | 1.27E+07 | 3.74E+06 |
| KRT1 | 5.34E+05 | 7.26E+06 | 1.51E+06 | 3.63E+06 |
| SPINT2 | 1.00E+04 | 5.94E+06 | 1.00E+04 | 3.42E+06 |
| RPL3 | 2.11E+07 | 1.84E+07 | 1.44E+07 | 3.40E+06 |
| FGF2 | 9.05E+06 | 5.44E+06 | 2.40E+06 | 3.33E+06 |
| YWHAE | 3.05E+07 | 2.57E+07 | 2.42E+07 | 3.30E+06 |
| RPS14 | 1.74E+07 | 1.41E+07 | 1.09E+07 | 3.24E+06 |
| UFL1 | 5.40E+06 | 5.47E+06 | 1.00E+04 | 3.13E+06 |
| HSPA5 | 2.13E+07 | 2.34E+07 | 1.73E+07 | 3.09E+06 |
| MUC5B | 1.00E+04 | 5.32E+06 | 1.00E+04 | 3.07E+06 |
| BPIFA1 | 3.92E+04 | 5.30E+06 | 1.00E+04 | 3.05E+06 |
| KRT9 | 4.00E+05 | 5.16E+06 | 1.40E+05 | 2.83E+06 |
| TPT1 | 7.33E+06 | 3.25E+06 | 2.07E+06 | 2.76E+06 |
| KRT10 | 1.13E+05 | 5.50E+06 | 2.01E+06 | 2.73E+06 |
| HSP90AB1 | 3.96E+07 | 3.61E+07 | 3.43E+07 | 2.68E+06 |
| RPL28 | 1.62E+07 | 1.43E+07 | 1.09E+07 | 2.66E+06 |
| GNB2L1 | 1.96E+07 | 1.47E+07 | 1.54E+07 | 2.64E+06 |
| HSP90B1 | 2.54E+07 | 2.91E+07 | 2.40E+07 | 2.64E+06 |
| NCL | 3.90E+07 | 3.47E+07 | 3.44E+07 | 2.57E+06 |
| PGAM1 | 2.04E+07 | 2.04E+07 | 2.48E+07 | 2.56E+06 |

Continued on next page

**Table B.11 – continued from previous page**

| Gene names | 0 hrs | 24 hrs | 48 hrs | var(LFQ) |
|---|---|---|---|---|
| ALDOA | 3.98E+07 | 4.00E+07 | 3.55E+07 | 2.55E+06 |
| RPS3A | 1.63E+07 | 1.33E+07 | 1.13E+07 | 2.53E+06 |
| CFL1 | 1.88E+07 | 1.45E+07 | 1.46E+07 | 2.43E+06 |
| HIST1H1B | 1.92E+07 | 1.87E+07 | 1.48E+07 | 2.42E+06 |
| RPS18 | 1.66E+07 | 1.37E+07 | 1.20E+07 | 2.34E+06 |

Table B.12.: KEGG pathway enrichment analysis of top50 varying proteins. Analysis has been performed with WEBGESTALT

| **KEGG pathway** | **adj. p-value** | **Nb. of proteins** |
|---|---|---|
| Ribosome | $2.35e-12$ | 8 |
| Glycolysis / Gluconeogenesis | 7.72e-06 | 4 |
| Protein processing in endoplasm. reticulum | 0.0002 | 4 |
| Antigen processing and presentation | 0.0004 | 3 |
| Prostate cancer | 0.0006 | 3 |
| Type I diabetes mellitus | 0.003 | 2 |
| NOD-like receptor signalling pathway | 0.0035 | 2 |
| Regulation of actin cytoskeleton | 0.0035 | 3 |
| Metabolic pathways | 0.0035 | 6 |
| MAPK signalling pathway | 0.0056 | 3 |

Table B.13.: Metabolic profile of hESC H1 cells. Quantities are shown in pmol/1e+6 cells

| **Metabolite** | **Pathway** | **Nb. of Derivates** | **mean(Quantity)** | **sd(Quantity)** |
|---|---|---|---|---|
| 2HG | glut | 1 | 163.05 | 56.75 |
| 3PGA | glyc | 1 | 188.61 | 95.1 |
| Ala | aa | 2 | 125.3 | 51.55 |
| Butanoic acid, 3-hydroxy | other | 1 | 896.14 | 1406.42 |
| Butanoic acid, 4-amino | other | 1 | 367.31 | 336.5 |
| Cit | tca | 1 | 228.7 | 117.5 |
| DHAP | glyc | 2 | 2905.59 | 108.96 |
| Ery | other | 1 | 176.18 | 59.38 |
| FBP | glyc | 1 | 2933.9 | 1143.21 |
| Frc | other | 1 | 42.23 | 21.31 |
| Frc6P | glyc | 1 | 139.74 | 59.93 |
| Fum | tca | 1 | 208.36 | 122.8 |
| Glu | glut | 2 | 10741.67 | 1686.97 |
| Glut | glut | 1 | 134.13 | 128.62 |
| Gly | aa | 2 | 4805.46 | 802 |
| Glyc | aa | 1 | 179.94 | 125.21 |
| Glyc3P | other | 1 | 94.31 | 65.52 |
| Iso | aa | 2 | 2282.17 | 730.1 |
| Lac | glyc | 1 | 2677.45 | 948.31 |
| Leu | aa | 2 | 3331.48 | 873.19 |
| Mal | tca | 1 | 269.02 | 102.03 |
| Met | aa | 1 | 454.08 | 196.87 |
| myo-Ino | other | 1 | 700.42 | 213.87 |
| Patho | other | 1 | 226.52 | 113.91 |
| Phe | aa | 1 | 918.93 | 359.76 |
| Pro | aa | 1 | 3677.95 | 2524.1 |
| Putr | other | 1 | 243.51 | 170.52 |
| Pyr | glyc | 1 | 404.81 | 199.84 |
| Ser | aa | 2 | 3452.17 | 626.07 |
| Suc | tca | 1 | 122.15 | 60.68 |
| Thr | aa | 2 | 6459.83 | 714.39 |
| Uracil | other | 1 | 283.39 | 131.06 |
| Val | aa | 2 | 2305.78 | 27.22 |

Table B.14.: $^{13}C$-substrate incorporation in hESC H1 during early differentiation (1 equals to 100 %).

| **Metabolite** | $^{13}C$**-Substrate** | **Time of differentiation** | | |
|---|---|---|---|---|
| | | **0 hrs** | textbf24 hrs | textbf48 hrs |
| Alanine_(3TMS)_MP | Glc | 0.27 | 0.19 | 0.14 |
| Citric acid, m+2 | Glc | 0.27 | 0.29 | 0.34 |
| Citric acid, m+4 | Gln | 0.09 | 0.23 | 0.27 |
| DHAP_(1MEOX)(3TMS)_BP | Glc | 0.22 | 0.53 | 0.29 |
| DHAP_(1MEOX)(3TMS)_MP | Glc | 0.65 | 0.83 | 0.75 |
| Fructose_(1MEOX)(5TMS)_BP | Glc | 0.74 | 0.84 | 0.79 |
| Fructose_(1MEOX)(5TMS)_MP | Glc | 0.84 | 0.98 | 0.91 |
| FBP_(1MEOX)(7TMS)_BP | Glc | 0.95 | 0.93 | 0.87 |
| FBP_(1MEOX)(7TMS)_MP | Glc | 0.97 | 0.94 | 0.91 |
| Frc6P_(1MEOX)(6TMS)_MP | Glc | 0.95 | 0.91 | 0.91 |
| Fumaric acid_(2TMS)_MP, m+2 | Glc | 0.04 | 0.1 | 0.11 |
| Fumaric acid_(2TMS)_MP, m+4 | Gln | 0.14 | 0.3 | 0.31 |
| 6PGA_(7TMS)_MP | Glc | 0.48 | 0.22 | 0.12 |
| Glutamic acid_(3TMS)_MP | Gln | 0.35 | 0.45 | 0.46 |
| Glutamine [-H2O]_(3TMS)_BP | Gln | 0.73 | 0.73 | 0.73 |
| Glutaric acid, 2-oxo | Glc | 0.05 | 0.11 | 0.11 |
| Glutaric acid, 2-oxo | Gln | 0.17 | 0.36 | 0.4 |
| GA3P | Glc | 0.19 | 0.34 | 0.39 |
| 3PGA_(4TMS)_MP | Glc | 0.75 | 0.78 | 0.64 |
| Glycerol_(3TMS)_MP | Glc | 0.15 | 0.12 | 0.17 |
| Glyc3P_(4TMS)_MP | Glc | 0.13 | 0.15 | 0.06 |
| Lactic acid_(2TMS)_MP | Glc | 0.67 | 0.59 | 0.66 |
| Malic acid_(3TMS)_MP, m+2 | Glc | 0.03 | 0.07 | 0.08 |
| Malic acid_(3TMS)_MP, m+4 | Gln | 0.15 | 0.35 | 0.36 |
| Pyruvic acid_(1MEOX)(1TMS)_MP | Glc | 0.8 | 0.78 | 0.7 |
| Serine_(3TMS)_MP | Glc | 0.04 | 0.02 | 0.02 |
| Succinic acid, m+2 | Glc | 0.04 | 0.04 | 0.07 |
| Succinic acid, m+4 | Gln | 0.15 | 0.29 | 0.35 |

## Terminal neuronal differentiation of LUHMES cells

Table B.15.: Composition of cell culture media for Luhmes d0 and d6 cells.

| | **Proliferation media** PM | **Differentiation media** DM |
|---|---|---|
| Basal media | adv. DMEM/F12 | adv. DMEM/F12 |
| Glc | | |
| Gln | 2 $mM$ | 2 $mM$ |
| Supplements | 1x N2 | 1x N2 |
| | 40 $ng/ml$ FGF-2 | 2.25 $uM$ Tetracycline |
| | | 1 $mM$ cAMP |
| | | 2 $ng/ml$ GNDF |

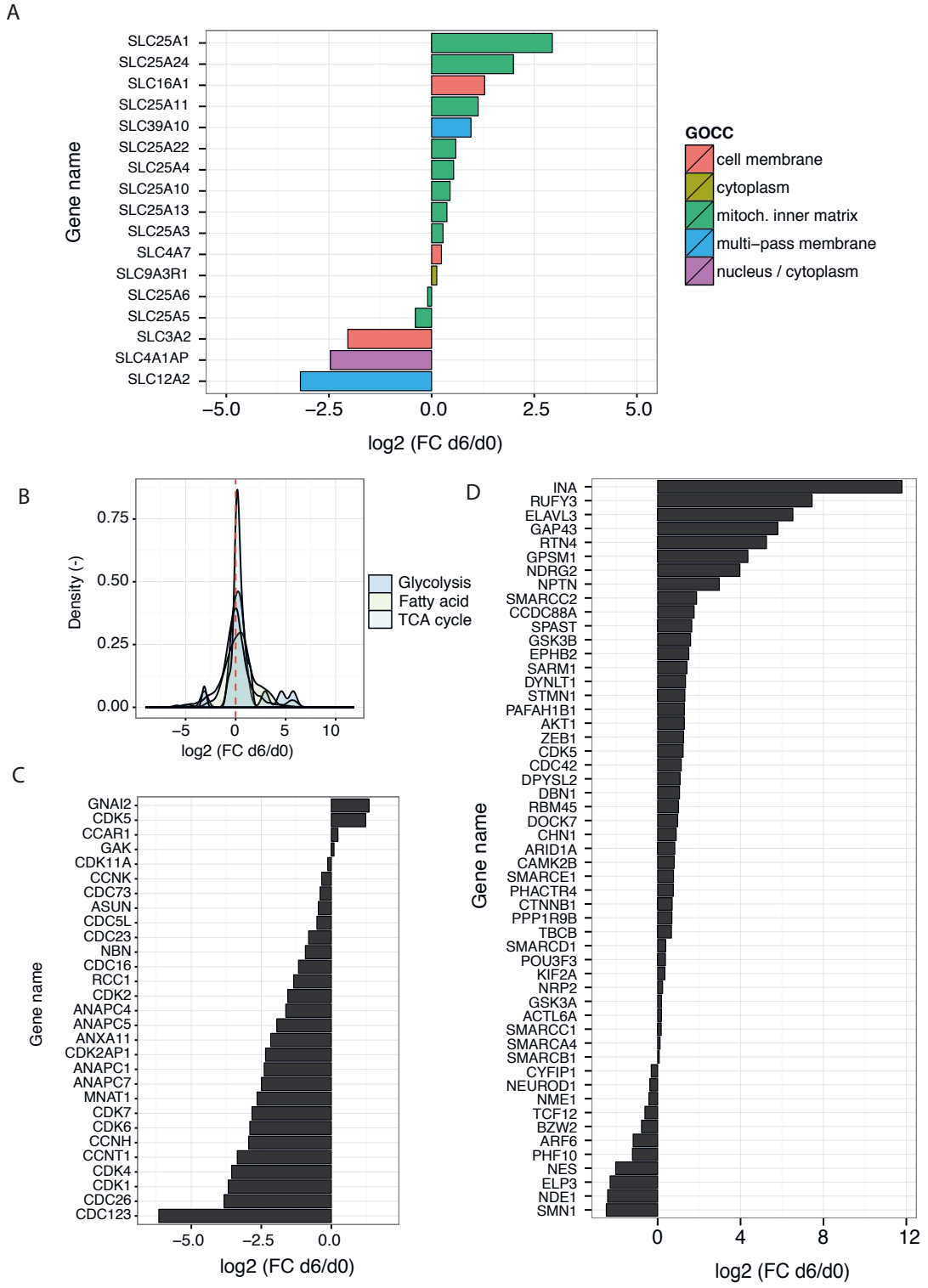


Figure B.2.: Proteomics analysis of Luhmes d0 and d6 cells. (A) Fold changes of transporter proteins comparing neuronal cells with their pluripotent progenitor cells. (B) Fold changes of central carbon metabolism enzymes. (C) Fold changes of proteins associated with cell cycle control. (D) Fold changes of proteins related to neuronal differentiation.

Table B.16.: Metabolic profile of Luhmes d0 cells. Quantities are shown in pmol/1e+6 cells.

| **Metabolite** | **Pathway** | **Nb. of Derivates** | **mean(Quantity)** | **sd(Quantity)** |
|---|---|---|---|---|
| 2HG | glut | 1 | 570.35 | 222.6985517 |
| aKG | tca | 1 | 1282.18 | 474.6242095 |
| Ala | aa | 1 | 1054.893833 | 425.2620849 |
| Asp | aa | 1 | 4849.848378 | 1816.495199 |
| Cit | tca | 1 | 1733.893476 | 614.6390913 |
| DHAP | glyc | 1 | 2519.353371 | 1176.545118 |
| Frc | other | 1 | 117.0629086 | NA |
| Fum | tca | 1 | 854.7557545 | 289.5679398 |
| Glc6P | glyc | 1 | 0.018163991 | 0.006327474 |
| Glu | glut | 1 | 47025.75569 | 27234.1175 |
| Gly | aa | 2 | 18862.66187 | 10542.18186 |
| Glyc | aa | 1 | 2308.640526 | 538.6346661 |
| Glyc3P | other | 1 | 461.6339077 | 166.800206 |
| Iso | aa | 2 | 3846.066929 | 1570.732905 |
| Lac | glyc | 1 | 17372.94361 | 13927.79232 |
| Leu | aa | 2 | 36795.79741 | 34850.6715 |
| Mal | tca | 1 | 3486.391367 | 1303.390282 |
| myo-Ino | other | 1 | 8468.120459 | 2713.062521 |
| Patho | other | 1 | 2003.571872 | 715.9522992 |
| PGA | glyc | 1 | 1031.394362 | 589.3240068 |
| Phe | aa | 1 | 11319.39234 | 5479.049817 |
| Pro | aa | 1 | 16060.98195 | 7181.314327 |
| Putr | other | 1 | 1315.854294 | 1029.572037 |
| Pyr | glyc | 1 | 14607.60072 | 5774.892468 |
| Ser | aa | 2 | 11730.70935 | 2762.655108 |
| Suc | tca | 1 | 609.7753253 | 216.4348563 |
| Thr | aa | 2 | 23772.10598 | 1182.478843 |
| Uracil | other | 1 | 1026.993724 | 369.1737849 |
| Val | aa | 2 | 8157.068954 | 1799.16568 |

Table B.17.: Metabolic profile of Luhmes d6 cells

| **Metabolite** | **Pathway** | **Nb. of Derivates** | **mean(Quantity)** | **sd(Quantity)** |
|---|---|---|---|---|
| 2HG | glut | 1 | 1709.57091 | 292.2885356 |
| Adenosine | nucleobase | 1 | 2485.625354 | 899.2015617 |
| aKG | tca | 1 | 2724.368988 | 933.1704082 |
| Ala | aa | 2 | 2069.509732 | 1642.613415 |
| Cit | tca | 1 | 3220.424837 | 980.5661789 |
| DHAP | glyc | 1 | 3812.587898 | 610.5648773 |
| FBP | glyc | 1 | 6226.411252 | NA |
| Frc | other | 1 | 319.6138291 | 118.8464703 |
| Fum | tca | 1 | 1298.84658 | 410.340008 |
| Glc6P | glyc | 1 | 0.04810577 | 0.014104223 |
| Glu | glut | 1 | 82428.89493 | 26172.16618 |
| Gly | aa | 2 | 42757.2963 | 4825.85418 |
| Glyc | aa | 1 | 1953.297761 | 530.8118958 |
| Glyc3P | other | 1 | 1324.740365 | 402.6150715 |
| Iso | aa | 2 | 18784.33659 | 6746.228249 |
| Lac | glyc | 1 | 16006.84151 | 4574.118745 |
| Leu | aa | 2 | 37061.49277 | 9196.222485 |
| Mal | tca | 1 | 3264.116351 | 1027.152832 |
| myo-Ino | other | 1 | 21474.28349 | 2373.354192 |
| Patho | other | 1 | 2284.790664 | 533.8188468 |
| PGA | glyc | 1 | 2101.58651 | 466.6203702 |
| PGA6 | ppp | 1 | 1379.512056 | NA |
| Phe | aa | 1 | 9017.038791 | 2512.286758 |
| Pro | aa | 1 | 11722.08673 | 2657.259621 |
| Pyr | glyc | 1 | 27849.17691 | 6920.896252 |
| Ser | aa | 2 | 25941.02329 | 7060.67849 |
| Suc | tca | 1 | 973.1476566 | 275.1102318 |
| Thr | aa | 2 | 58244.65947 | 13243.28567 |
| Uracil | other | 1 | 1355.098635 | 731.2035675 |
| Val | aa | 2 | 22599.5992 | 1176.72557 |

Table B.18.: Incorporation of $^{13}C$-Glucose in CCM intermediates of Luhmes d0 cells. A value of 1 corresponds to 100%.

| Lettercode | m/z | $^{13}C$-Glucose incubation in (min) | | | | | | | | | | |
|---|---|---|---|---|---|---|---|---|---|---|---|---|
| | | 0 | 2 | 3 | 6 | 8 | 12 | 30 | 60 | 360 | 1440 | |
| Ala_3TMS | 190 | 0.09+/-0.03 | 0.11+/-0.01 | 0.12+/-0.01 | 0.13+/-0.03 | 0.18+/-0.04 | 0.2+/-NA | 0.2+/-0.03 | 0.26+/-NA | 0.54+/-0.07 | 0.8+/-0 | |
| Cit | 275 | | 0.14+/-0.01 | 0.18+/-0.05 | 0.19+/-0.08 | 0.19+/-0.1 | 0.2+/-0.04 | 0.27+/-0.04 | 0.26+/-0.06 | 0.57+/-0.01 | 0.73+/-0.02 | |
| Cit | 276 | | 0.04+/-0.01 | 0.06+/-0.01 | 0.05+/-0.06 | 0.08+/-NA | 0.05+/-0 | 0.1+/-0.01 | 0.07+/-0.05 | 0.32+/-0.01 | 0.61+/-0.01 | |
| Cit | 277 | | 0.02+/-0.01 | 0.04+/-0 | 0.03+/-0.04 | 0.02+/-0.02 | 0.03+/-0.01 | 0.04+/-0.02 | 0.03+/-0.03 | 0.26+/-0.01 | 0.6+/-0.02 | |
| Cit | 278 | | 0.02+/-0.02 | 0.01+/-0 | 0.02+/-NA | 0.02+/-NA | 0.04+/-0.02 | 0.03+/-0.02 | 0+/-NA | 0.12+/-0.01 | 0.46+/-0 | |
| DHAP_MP | 403 | 0.66+/-0.05 | 0.29+/-0.2 | 0.51+/-0.22 | 0.49+/-0.16 | 0.31+/-0.09 | 0.58+/-0.06 | 0.29+/-0.23 | 0.31+/-NA | 0.56+/-0.16 | 0.25+/-0.04 | |
| Frc_MP | 220 | 0.49+/-0.06 | 0.67+/-0.09 | 0.62+/-0.08 | 0.75+/-0.08 | 0.76+/-0.02 | 0.77+/-0.03 | 0.77+/-0.01 | 0.73+/-0.02 | 0.74+/-0.07 | 0.62+/-NA | |
| Fum | 247 | 0.04+/-0.03 | 0.11+/-0.01 | 0.08+/-NA | 0.07+/-0 | 0.07+/-0.03 | 0.07+/-0.06 | 0.07+/-0.06 | 0.1+/-0.05 | 0.11+/-0.01 | 0.33+/-0.01 | |
| Fum | 249 | 0.02+/-0.03 | 0.05+/-0.02 | 0.01+/-0.02 | 0.01+/-0.01 | 0.02+/-0.02 | 0.04+/-0.02 | 0.04+/-0.01 | 0.04+/-0 | 0.05+/-0.01 | 0.17+/-0.01 | |
| Glc BP | 220 | 0.69+/-0.04 | 0.95+/-0.01 | 0.95+/-0 | 0.95+/-0 | 0.96+/-0 | 0.96+/-0 | 0.96+/-0 | 0.95+/-0.01 | 0.96+/-0 | 0.96+/-0 | |
| Glc6P_MP | 220 | 0.51+/-0.06 | 0.69+/-0.03 | 0.77+/-0.07 | 0.73+/-0.01 | 0.7+/-0.06 | 0.75+/-0.01 | 0.67+/-0.02 | 0.72+/-0 | 0.83+/-0.17 | 0.93+/-NA | |
| Gln_3TMS | NA | | | | 0.01+/-NA | 0.06+/-0.07 | 0.02+/-NA | | | 0.05+/-0.05 | NA | |
| Glu_3TMS | NA | 0.01+/-0.02 | 0+/-0 | 0+/-0 | 0+/-0 | 0.01+/-0.01 | 0+/-0 | 0.01+/-0 | 0.02+/-0 | 0.05+/-0 | 0.21+/-0.03 | |
| Glut_2oxo | 200 | 0.06+/-0 | 0.11+/-0.08 | 0.17+/-0.03 | 0.19+/-0.02 | 0.2+/-0 | 0.17+/-0 | 0.31+/-0.06 | 0.22+/-0.07 | 0.24+/-0 | 0.36+/-0 | |
| Glut_2oxo | 203 | 0.15+/-0.1 | 0.09+/-0.01 | 0.2+/-0.03 | 0.19+/-0.04 | 0.18+/-0.07 | 0.18+/-0.03 | 0.17+/-0.04 | 0.14+/-0.02 | 0.15+/-0.03 | 0.29+/-0.04 | |
| Gly_3TMS | NA | | 0.01+/-0.01 | 0.04+/-0.04 | 0.01+/-NA | 0.01+/-NA | 0.05+/-NA | 0.02+/-0.01 | 0.01+/-0.01 | 0.02+/-0.01 | 0.07+/-0 | |
| Glyc | 359 | 0.22+/-0.05 | 0.16+/-0.02 | 0.18+/-0.02 | 0.18+/-0.02 | 0.17+/-0 | 0.18+/-0.03 | 0.18+/-0.05 | 0.24+/-0.04 | 0.24+/-0.09 | 0.51+/-0.07 | |
| Glyc3P | 359 | | | | | | | | 0.21+/-NA | 0.4+/-NA | 0.71+/-0.01 | |
| Lac | 222 | 0.03+/-0.02 | 0.23+/-0.05 | 0.23+/-0.05 | 0.24+/-0.02 | 0.25+/-0.04 | 0.27+/-0.05 | 0.25+/-0.08 | 0.31+/-0.09 | 0.66+/-0.05 | 0.82+/-0.01 | |
| Mal | 247 | 0.12+/-0.02 | 0.14+/-0.01 | 0.11+/-0.01 | 0.15+/-0.02 | 0.11+/-0 | 0.15+/-0.04 | 0.14+/-0.03 | 0.17+/-0.02 | 0.23+/-0.01 | 0.35+/-0.01 | |
| Mal | 248 | 0.05+/-0.05 | 0.07+/-0.03 | 0.05+/-0.01 | 0.06+/-0.01 | 0.06+/-0.02 | 0.08+/-0 | 0.08+/-0.05 | 0.1+/-0 | 0.19+/-0.03 | 0.33+/-0.01 | |
| Mal | 249 | 0.04+/-0.04 | 0.03+/-0.02 | 0.03+/-0.01 | 0.04+/-0.03 | 0.04+/-0.01 | 0.04+/-0.02 | 0.05+/-0.01 | 0.06+/-0.01 | 0.07+/-0 | 0.22+/-0.01 | |
| PGA | 359 | 0.17+/-0.04 | | | | | | | 0.75+/-NA | 0.73+/-NA | 0.85+/-0.05 | |
| Pyr | 177 | 0.01+/-0 | 0.04+/-0.03 | 0.06+/-0.03 | 0.05+/-0.02 | 0.07+/-0.04 | 0.08+/-0.04 | 0.12+/-0.07 | 0.25+/-0.08 | 0.72+/-0.04 | 0.84+/-0 | |
| Ser_3TMS | 206 | 0.03+/-0.04 | 0.02+/-0.02 | 0.03+/-0.02 | 0.03+/-0 | 0.07+/-0.03 | 0.05+/-0.02 | 0.07+/-0 | 0.08+/-0.01 | 0.17+/-0.04 | 0.36+/-NA | |
| Suc | 249 | 0.16+/-0 | 0.18+/-0.01 | 0.13+/-0.04 | 0.2+/-0.17 | 0.15+/-0.1 | 0.18+/-0.05 | 0.16+/-0 | 0.17+/-0 | 0.23+/-0.03 | 0.33+/-0.02 | |
| Suc | 251 | 0.22+/-0.09 | 0.16+/-0.03 | 0.11+/-0.07 | 0.12+/-0.09 | 0.09+/-0.05 | 0.12+/-0.07 | 0.1+/-0.01 | 0.01+/-0.01 | 0.09+/-0.03 | 0.2+/-0.05 | |

Table B.19.: Incorporation of $^{13}C$-Glutamine in CCM intermediates of Luhmes d0 cells. A value of 1 corresponds to 100%.

| | | $^{13}C$-Glutamine incubation in (min) | | | | | | | |
|---|---|---|---|---|---|---|---|---|---|
| Lettercode | m/z | 0 | 2 | 6 | 12 | 30 | 60 | 360 | 1440 |
| Ala_3TMS | 190 | 0.05+/-0 | 0.04+/-0.01 | 0.05+/-0.01 | 0.06+/-0 | 0.05+/-0 | 0.11+/-0.03 | 0.07+/-0.03 | 0.08+/-0.01 |
| Cit | 275 | 0.08+/-NA | 0.09+/-0 | 0.05+/-0.06 | 0.1+/-NA | 0.08+/-0.02 | 0.17+/-0.03 | 0.17+/-0.01 | 0.35+/-0.07 |
| Cit | 276 | 0.02+/-NA | 0.03+/-0 | 0.04+/-NA | 0.04+/-0.04 | 0.08+/-0.02 | 0.28+/-0.01 | 0.42+/-0.02 | 0.52+/-0.09 |
| Cit | 277 | 0.01+/-NA | 0.01+/-0.01 | 0.01+/-NA | 0.02+/-NA | 0.06+/-0.05 | 0.11+/-0.01 | 0.15+/-0 | 0.22+/-0.05 |
| Cit | 278 | 0.01+/-NA | 0.01+/-0.01 | 0.03+/-0.01 | 0.03+/-NA | 0.02+/-NA | 0.11+/-0.02 | 0.16+/-0.01 | 0.17+/-0.05 |
| Fum | 247 | 0.04+/-0.01 | 0.07+/-0.01 | 0.09+/-0.03 | 0.04+/-0.02 | 0.1+/-0.04 | 0.11+/-0.03 | 0.19+/-NA | 0.39+/-0.06 |
| Fum | 249 | 0.02+/-0 | 0.02+/-0 | 0.03+/-0.01 | 0.07+/-0.01 | 0.14+/-0.01 | 0.27+/-0.04 | 0.44+/-NA | 0.53+/-0.09 |
| Glu_2TMS | NA | | 0.01+/-NA | 0.04+/-0.03 | 0.12+/-0 | 0.24+/-0.04 | 0.49+/-0.02 | 0.69+/-0.05 | 0.69+/-0.1 |
| Glu_3TMS | NA | 0.02+/-0 | 0.05+/-0.01 | 0.09+/-0.01 | 0.2+/-0.02 | 0.33+/-0.01 | 0.53+/-0.01 | 0.73+/-0.02 | 0.7+/-0.08 |
| Glut_2oxo | 200 | 0.11+/-0.02 | 0.13+/-0.03 | 0.12+/-0.03 | 0.19+/-0 | 0.22+/-0.13 | 0.16+/-0.01 | 0.29+/-0 | 0.39+/-0.03 |
| Glut_2oxo | 203 | 0.14+/-0.03 | 0.15+/-0 | 0.21+/-0.03 | 0.31+/-0.02 | 0.42+/-0.05 | 0.56+/-0.03 | 0.74+/-0.01 | 0.75+/-0.08 |
| Gly_3TMS | NA | 0.03+/-NA | NA+/-NA | 0+/-NA | 0.02+/-0.02 | 0.21+/-NA | 0.01+/-0 | 0.01+/-0 | 0.02+/-0 |
| Glyc | 359 | 0.25+/-0.02 | 0.23+/-0.01 | 0.21+/-0.01 | 0.2+/-0.09 | 0.22+/-0.08 | 0.18+/-0.02 | 0.2+/-0.01 | 0.41+/-0.08 |
| Lac | 222 | 0.03+/-0 | 0.03+/-0.02 | 0.04+/-0.02 | 0.03+/-0.01 | 0.03+/-0.01 | 0.03+/-0.01 | 0.01+/-0 | 0.03+/-0 |
| Mal | 247 | 0.12+/-0.02 | 0.13+/-0.01 | 0.12+/-0 | 0.14+/-0.01 | 0.18+/-0.01 | 0.21+/-0.01 | 0.31+/-0.02 | 0.43+/-0.02 |
| Mal | 248 | 0.07+/-0.06 | 0.06+/-0.03 | 0.05+/-0.02 | 0.07+/-0.01 | 0.08+/-0.04 | 0.13+/-0.05 | 0.24+/-0.02 | 0.3+/-0.02 |
| Mal | 249 | 0.03+/-0.01 | 0.03+/-0.01 | 0.03+/-0.02 | 0.09+/-0.04 | 0.18+/-0.09 | 0.32+/-0.02 | 0.49+/-0.02 | 0.55+/-0.08 |
| Pyr | 177 | 0+/-0 | 0+/-0 | 0+/-0 | 0.01+/-NA | 0+/-0 | 0+/-0 | 0.02+/-0.01 | 0.05+/-0.01 |
| Ser_3TMS | 206 | 0.04+/-0.03 | 0.01+/-0 | 0.07+/-NA | 0.03+/-0.02 | 0.01+/-0.01 | 0.05+/-0.04 | 0.03+/-NA | 0.01+/-0.01 |
| Suc | 249 | 0.16+/-0.04 | 0.18+/-0.07 | 0.07+/-0.04 | 0.22+/-0.06 | 0.2+/-0.06 | 0.12+/-0.02 | 0.3+/-0.06 | 0.39+/-0.02 |
| Suc | 251 | 0.1+/-0.05 | 0.06+/-0.05 | 0.06+/-0.04 | 0.16+/-0.05 | 0.22+/-0.05 | 0.33+/-0.02 | 0.43+/-0.05 | 0.47+/-0.09 |

# C Supplementary: Integrative analysis

Table C.1.: Classification of cell lines for the integrative analysis of omics-data.

| **Phenotype** | **Cell lines** |
|---|---|
| Cancer cells | HT-29, MCF-7, MDA-MB231, RKO, SW480 |
| hESCs | H1, H9, Luhmes d0 |
| iPSCs | iPS2, iPS4, OiPS3, OiPS6, iB4, iB5 |
| Fibroblast (F) | HFF1, NFH2, BJ1 |
| Derived fibroblast (DF) | H1-DF, H9-DF, iPS2-DF, iPS4-DF, OiPS3-DF, OiPS6-DF, iB4-DF, iB5-DF, Luhmes d6 |

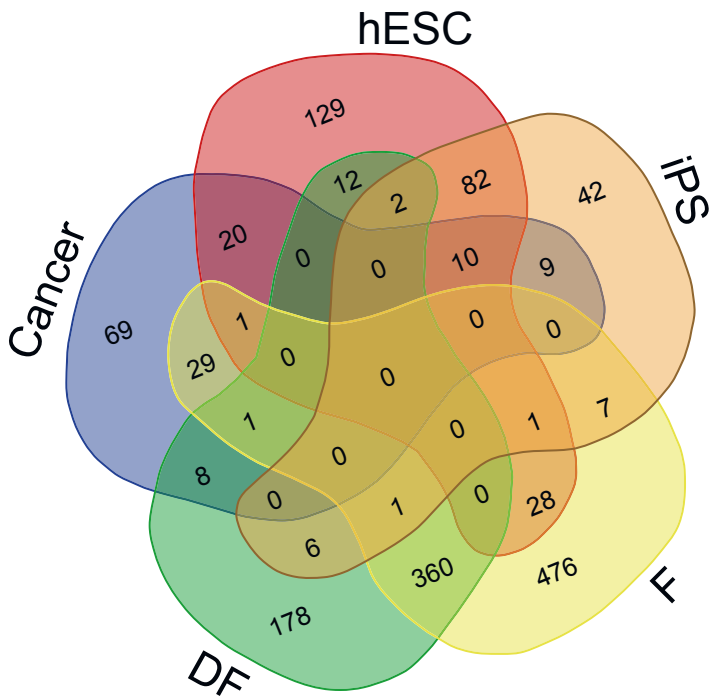


Figure C.1.: Venn diagramm of protein levels $z - score < -0.5$ for the integrative analysis summarising the phenotypes - Cancer, hESC, iPS, F and DF. Intersections show the number of shared proteins.

Table C.2.: Part1: Absolute pool sizes of intermediates used for PCA of quantitative metabolomics data.

| Metabolite | Pathway | d0 | d6-DF | H1 | H1-DF | H9 | H9-DF | HT29 | MCF | MDA | RKO | SW480 |
|---|---|---|---|---|---|---|---|---|---|---|---|---|
| Ala | aa | 1054.89 | 2069.51 | 1042.55 | 3272.13 | 1397.07 | 2708.15 | 529.57 | 748.80 | 1024.46 | 783.57 | 645.87 |
| Cit | tca | 1733.89 | 3220.42 | 1408.63 | 4849.74 | 1300.39 | 5966.71 | 1822.63 | 2368.90 | 2273.92 | 1530.67 | 1748.15 |
| Fum | tca | 854.76 | 1298.85 | 801.44 | 2073.82 | 891.74 | 1213.92 | 829.25 | 1514.55 | 1131.53 | 841.30 | 2472.47 |
| Glu | glut | 47025.76 | 82428.89 | 30472.72 | 80249.18 | 28302.33 | 99000.78 | 117021.31 | 180510.34 | 14323.27 | 261133.60 | 167016.15 |
| Gly | aa | 18862.66 | 42757.30 | 19651.78 | 81303.06 | 15460.34 | 83576.90 | 15979.85 | 33110.18 | 23011.08 | 29106.01 | 24274.02 |
| Glyc | aa | 2308.64 | 1953.30 | 652.09 | 3819.84 | 1271.63 | 2949.07 | 1188.60 | 4502.67 | 2490.56 | 1753.26 | 2369.47 |
| Glyc3P | other | 461.63 | 1324.74 | 1691.26 | 5001.26 | 942.06 | 3859.01 | 1586.86 | 3142.96 | 1658.73 | 859.53 | 2335.25 |
| Iso | aa | 3846.07 | 18784.34 | 6928.78 | 39455.32 | 5929.40 | 35601.78 | 7374.61 | 9019.81 | 1796.28 | 8289.07 | 8376.14 |
| Lac | glyc | 17372.94 | 16006.84 | 109478.72 | 78104.74 | 42113.31 | 93023.82 | 26870.87 | 20370.18 | 54383.36 | 36433.76 | 24680.47 |
| Leu | aa | 36795.80 | 37061.49 | 13003.50 | 42499.55 | 11295.42 | 45811.53 | 25326.12 | 41109.00 | 40211.16 | 25813.67 | 35210.30 |
| Mal | tca | 3486.39 | 3264.12 | 1670.75 | 2970.62 | 1754.83 | 2491.61 | 2328.62 | 3711.55 | 3137.77 | 2440.71 | 7578.88 |
| Phe | aa | 11319.39 | 9017.04 | 5926.85 | 41966.11 | 8638.79 | 40222.74 | 12289.90 | 9332.57 | 1020.82 | 18388.64 | 6199.19 |
| Pro | aa | 16060.98 | 11722.09 | 12415.82 | 26863.70 | 9067.27 | 29246.59 | 4489.76 | 6383.43 | 7373.78 | 5482.33 | 4135.57 |
| Pyr | glyc | 14607.60 | 27849.18 | 41458.81 | 500518.69 | 22222.93 | 127940.71 | 33263.92 | 64695.96 | 17921.67 | 34976.70 | 72096.88 |
| Ser | aa | 11730.71 | 25941.02 | 14387.44 | 44397.53 | 17097.44 | 43697.26 | 83559.68 | 91580.81 | 28740.73 | 105984.36 | 95159.17 |
| Suc | tca | 609.78 | 973.15 | 689.46 | 1366.23 | 762.72 | 1451.97 | 754.88 | 1261.79 | 1082.97 | 935.33 | 1382.99 |
| Thr | aa | 23772.11 | 58244.66 | 17066.00 | 70629.71 | 31761.10 | 67278.55 | 29762.12 | 37920.36 | 4378.89 | 39409.31 | 37596.02 |
| Uracil | other | 1026.99 | 1355.10 | 1067.44 | 7050.17 | 3196.44 | 5855.64 | 788.31 | 1516.00 | 1586.50 | 717.51 | 1551.50 |
| Val | aa | 8157.07 | 22599.60 | 7980.68 | 39999.94 | 8779.79 | 36843.58 | 15027.01 | 17800.53 | 11651.14 | 16261.62 | 18519.99 |
| aKG | tca | 1282.19 | 2724.37 | 1381.70 | 5936.63 | 2014.78 | 6146.65 | 1906.72 | 1585.83 | 1706.43 | 1762.15 | 1867.56 |

Table C.3.: Part2: Absolute pool sizes of intermediates used for PCA of quantitative metabolomics data.

| Metabolite | Pathway | HFF1-F | iPS2-DF | iPS2 | iPS4-DF | iPS4 | BJ-F | iB4 | iB4-DF | iB5 | NFH2-F | OiPS3 | OiPS3-DF | OiPS6 | OiPS6-DF |
|---|---|---|---|---|---|---|---|---|---|---|---|---|---|---|---|
| Ala | aa | 1144.05 | 1937.20 | 874.75 | 1815.91 | 886.13 | 1420.27 | 1240.90 | 6553.20 | 1026.94 | 637.58 | 379.41 | 1786.21 | 235.56 | 685.10 |
| Cit | tca | 6874.42 | 5822.16 | 1250.65 | 6636.24 | 1246.60 | 8123.53 | 2068.73 | 15611.53 | 1476.72 | 10375.45 | 3103.89 | 19015.58 | 2019.81 | 7551.99 |
| Fum | tca | 1222.18 | 2017.32 | 314.16 | 1566.59 | 384.30 | 1607.54 | 791.01 | 3616.01 | 626.38 | 1558.77 | 1066.13 | 5920.97 | 882.11 | 1307.61 |
| Glu | glut | 123187.29 | 122220.58 | 9414.26 | 120744.66 | 12353.44 | 32251.21 | 22876.46 | 113842.00 | 18243.10 | 50329.85 | 35320.40 | 196663.79 | 17193.43 | 35036.86 |
| Gly | aa | 56481.95 | 50515.69 | 16947.91 | 43803.17 | 16176.53 | 62211.41 | 16170.05 | 89835.42 | 17406.90 | 72255.03 | 11207.83 | 101425.52 | 10564.37 | 43502.39 |
| Glyc | aa | 766.01 | 1834.17 | 172.93 | 1779.57 | 157.34 | 2986.28 | 1083.46 | 4997.80 | 1028.28 | 2998.77 | 589.55 | 3051.63 | 395.13 | 3930.37 |
| Glyc3P | other | 2543.50 | 3443.14 | 677.87 | 3017.83 | 792.90 | 4495.21 | 1266.05 | 7025.26 | 1235.54 | 1841.50 | 1230.07 | 5959.41 | 864.59 | 6041.35 |
| Iso | aa | 28412.56 | 33106.49 | 5915.58 | 31704.11 | 5945.21 | 46435.96 | 12450.85 | 47926.24 | 15203.75 | 58888.92 | 11569.94 | 59362.17 | 9610.06 | 52576.03 |
| Lac | glyc | 104210.89 | 154598.60 | 59641.81 | 150447.03 | 55277.51 | 78371.66 | 61683.55 | 86069.18 | 78893.23 | 70622.51 | 76929.94 | 111935.58 | 41049.20 | 53058.54 |
| Leu | aa | 51804.76 | 53978.34 | 10553.34 | 53541.71 | 9792.22 | 86920.65 | 36069.02 | 87668.48 | 34146.10 | 82944.90 | 17641.93 | 122930.33 | 19281.49 | 77246.78 |
| Mal | tca | 3730.95 | 4195.18 | 696.64 | 4355.39 | 757.10 | 3685.18 | 1769.40 | 7869.68 | 1149.57 | 3939.87 | 2917.85 | 16273.54 | 2338.15 | 3583.34 |
| Phe | aa | 13308.61 | 20383.96 | 4045.12 | 15962.16 | 3467.15 | 24724.79 | 6296.11 | 25041.04 | 7412.89 | 31224.95 | 5190.59 | 34588.14 | 4369.32 | 25141.89 |
| Pro | aa | 15892.45 | 12246.73 | 3847.49 | 14625.08 | 3855.30 | 17561.54 | 9433.43 | 10793.41 | 9193.13 | 20822.95 | 7315.61 | 88551.31 | 3712.73 | 1798.27 |
| Pyr | glyc | 310264.66 | 272649.25 | 40970.40 | 342398.78 | 43206.94 | 447852.33 | 70436.43 | 342923.81 | 65106.36 | 316172.55 | 45063.68 | 269425.50 | 44855.50 | 394666.94 |
| Ser | aa | 42416.59 | 44122.08 | 12640.18 | 45907.69 | 12917.10 | 64448.85 | 22254.60 | 93274.19 | 24270.45 | 61751.37 | 14388.31 | 120980.30 | 10800.53 | 58849.53 |
| Suc | tca | 3248.65 | 1789.58 | 271.84 | 1764.82 | 291.54 | 2529.30 | 662.78 | 1565.08 | 620.88 | 2416.18 | 740.06 | 3648.44 | 550.87 | 1510.78 |
| Thr | aa | 59483.74 | 62466.55 | 13707.78 | 64761.36 | 14223.10 | 209468.21 | 46022.69 | 103980.03 | 22127.87 | 60785.42 | 13547.47 | 120797.61 | 10350.81 | 302113.09 |
| Uracil | other | 6146.50 | 7326.96 | 922.78 | 6538.78 | 978.23 | 16317.71 | 2514.20 | 7634.29 | 2434.04 | 15868.97 | 2885.25 | 16136.40 | 2652.82 | 26844.43 |
| Val | aa | 36033.95 | 41638.22 | 6524.71 | 39691.74 | 6631.75 | 55580.46 | 14362.19 | 51663.21 | 15218.72 | 58335.98 | 10700.53 | 59409.02 | 9267.47 | 47989.04 |
| aKG | tca | 5191.78 | 5368.16 | 833.70 | 5822.92 | 1011.54 | 8157.53 | 1961.82 | 11264.24 | 1863.53 | 4988.01 | 2648.32 | 11154.28 | 1909.12 | 7714.86 |

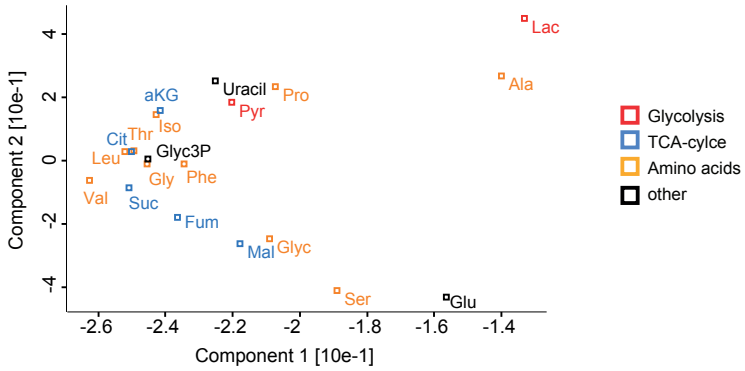


Figure C.2.: Loadings of rank-normalised PCA of quantitative pool sizes in cancer, hESCs, iPS cells, and their associated fibroblasts.

# D Supplementary: From pSIRM to MFA

Table D.1.: Conversion table for the metabolic flux map of LUHMES cells d0 and d6

| Substrate | Product | LUHMES d0 | | | | LUHMES d6 | | | |
|---|---|---|---|---|---|---|---|---|---|
| | | flux | mult | total flux | pt | d6 | mult | total flux | pt |
| Glc | GA3P | 240.00 | 1 | 240 | 1.4 | 76.5 | 1 | 76.5 | 1.5 |
| DHAP | GA3P | 238.00 | 1 | 238 | 1.4 | 76.5 | 1 | 76.5 | 1.5 |
| GA3P | Pyr | 464.00 | 1 | 464 | 2.8 | 153 | 1 | 153 | 3.0 |
| Pyr | Pyr mit | 124.00 | 1 | 124 | 0.7 | 44.7 | 1 | 44.7 | 0.9 |
| Pyr | Lac | 500.00 | 1 | 500 | 3.0 | 149 | 1 | 149 | 2.9 |
| Pyr | Ala | 80.60 | 1 | 80.6 | 0.5 | 11.1 | 1 | 11.1 | 0.2 |
| Pyr ex | Pyr im | 150.00 | 1 | 150 | 0.9 | 51.2 | 1 | 51.2 | 1.0 |
| Ala | Ala exp | 71.00 | 1 | 71 | 0.4 | 11.1 | 1 | 11.1 | 0.2 |
| Lac | Lac exp | 500.00 | 1 | 500 | 3.0 | 149 | 1 | 149 | 2.9 |
| Pyr | acetylCoA | 124.00 | 1 | 124 | 0.7 | 57.4 | 1 | 57.4 | 1.1 |
| Pyr | OAA | 23.30 | 1 | 23.3 | 0.1 | 40 | 1 | 40 | 0.8 |
| OAA aCoA | Cit | 63.60 | 1 | 63.6 | 0.4 | 62.4 | 1 | 62.4 | 1.2 |
| Cit | aKG | 63.60 | 1 | 63.6 | 0.4 | 62.4 | 1 | 62.4 | 1.2 |
| aKG | Sucu | 31.30 | 4 | 125.2 | 0.8 | 18.6 | 4 | 74.4 | 1.5 |
| Suc | Mal | 39.10 | 4 | 156.4 | 0.9 | 18.8 | 4 | 75.2 | 1.5 |
| Mal | OAA | 52.50 | 1 | 52.5 | 0.3 | 22.5 | 1 | 22.5 | 0.4 |
| OAA | Asp | 10.40 | 1 | 10.4 | 0.1 | 0.02 | 1 | 0.02 | 0.0 |
| Mal | Pyr | 104.00 | 1 | 104 | 0.6 | 52.6 | 1 | 52.6 | 1.0 |
| Gln im | Gln | 87.00 | 1 | 87 | 0.5 | 14.7 | 1 | 14.7 | 0.3 |
| Gln | Glu | 81.80 | 1 | 81.8 | 0.5 | 14.7 | 1 | 14.7 | 0.3 |
| Glu | aKG | 75.10 | 1 | 75.1 | 0.5 | 12.1 | 1 | 12.1 | 0.2 |
| G6P | R5P | 0.00 | 1 | 0 | 0.0 | 15.3 | 1 | 15.3 | 0.3 |
| Ser | Gly | 19.60 | 1 | 19.6 | 0.1 | 5.8 | 1 | 5.8 | 0.1 |
| Ser ex | Ser im | 17.00 | 1 | 17 | 0.1 | 1.1 | 1 | 1.1 | 0.0 |
| DHAP | Glyc3P | 190.00 | 1 | 190 | 1.1 | 0.003 | 1 | 0.003 | 0.0 |
| 3PGA | Ser | 11.10 | 1 | 11.1 | 0.1 | 4.72 | 1 | 4.72 | 0.1 |
| Glu ex | Glu | 10.00 | 1 | 10 | 0.1 | 0 | 1 | 0 | 0.0 |
| | PPP | 0.00 | 1 | 0 | 0.0 | 5.1 | 1 | 5.1 | 0.1 |

# E Supplementary: MTXQC

## Exemplary MTXQC output

The herein presented pdf-file represents theexemplary MTXQC output file of a pSIRM time course experiment in Luhmes cells, labeled with u-$^{13}C$)-Glucose for up to 24 hours. The details of biological question of the experiment is addressed in Section 3.1.4. The pdf-file includes the project-specific R-code. The pdf-file has been saved on the attached CD.

## Input and output files

Table E.1.: Input files for metQC pSIRM-TS v.7

| Part | Input | Information |
|---|---|---|
| general | ann-native-glc.csv | annotation of files |
| | conversion-metabolite.csv | Metabolite renaming list |
| | letter-pathway.csv | Annotation of metabolites and pathways |
| | letter-pathway-profile.csv | Annotation of metabolites and derivates per pathway |
| GC | Alcane-Intensities.csv | Areas of alcanes in all samples; including RT and RI information |
| | CinAcid.csv | Areas of internal extraction standard cinnamic acid |
| | MassSum-73.csv | Exported summed up areas for m/Z 73 for each file and scan; including RI information |
| | quantMassAreasMatrix-pTop5.csv | Areas based on Top5-Quantification of all annotated metabolites |
| Inc | 13C-Inc.csv | Calculated 13C-incorporation for each metabolite and file |
| | pSIRM-SpectraData.csv | Export of MIDs for each metabolite and file |
| Quant | ManualQuantTable-top5.csv | Table containing areas and concentration values for determination of calibration curves |
| | quantMassAreasMatrix-pTop5.csv | Areas based on Top5-Quantification of all annotated metabolites |

Table E.2.: Output files for metQC pSIRM-TS v.7 - HeatMap data

| | | |
|---|---|---|
| general | HM-GC | QC-factors regarding GC-MS measurement |
| | HM-Incorporation.csv | QC-factors regarding isotopic incorporation |
| | HM-Quant-pTop5.csv | QC-factors regarding top5 mass quantification |

Table E.3.: Output files for metQC pSIRM-TS v.7

| Part | Output | Information |
|---|---|---|
| GC | alcane-statistics.csv | Per file - mean and sd of all nine alkanes per file |
| | AreaSum-normFac.csv | Per file - N, sumArea and Area.fac for area<br>nomalization of all annotated metabolites |
| | CinAcid-normFactor.csv | Per file CinAcid - area, correction factor and evaluation if factor is within defined range $(0.65; 1.45)$ |
| | mz-73-statistics.csv | Per file N - mean.73, sd.73, max.73 and ratio of summed up areas of $m/z73$ |

Table E.4.: Output files for metQC pSIRM-TS v.7- Inc

| | | |
|---|---|---|
| Inc | 13C-statistics.csv | Per metabolite Mass.Pos and Time - t N, m.li and sd.li |
| | 13C-stats-zeros.csv | Per metabolite incorporation at $t = 0$ |
| | SE-calculation-Nascore.csv | Per metabolite - calculated number and fraction of spectra containing specific number of NA in comparison to backup MID - na.frac.r, N, fracr.prop |
| | SE-classification.csv | Per metabolite and file calculated sum of sample and backup MID, ist ratio (low3a.ratio), and the evaluation |
| | SE-validation.csv | Per metabolite statistics of goodQ and lowQ, calculated proportion |

Table E.5.: Output files for metQC pSIRM-TS v.7 - Quant pTop5

| | | |
|---|---|---|
| pTop5 | pTop5-CalculationFileData.tsv | Per metabolite and file - all normalization values, cell count to final concentration per 1e+6 cells (Top5 Quantification) |
| | pTop5-Calibration-Samples-lincheck.tsv | Per metabolite – counting entities within, below and above linear range and proportion of entities within the linear range (Top5 Quantification) |
| | top5-CalibrationInfo-unique.tsv | Per metabolite - Rsquared, intercept, slope and number of data points of calibration curve (Top5 Quantification) |
| | top5-QMQcurveInfo.tsv | Per metabolite - dilution, concentration and intensity vales for calculation of calibration curve (Top5 Quantification) |
| | pTop5-Quantities-steadystate-times-linear.csv | Per metabolite and Time - mean and sd value and average and sd overall time range (Top5 Quantification) |
| | pTop5-Quantities-steadystate-linear.csv | Per metabolite - pool sizes (N,mean, sd) - Top5 Quantification; only linear range |
| | Metabolic-profile-calc.csv | Data summary for the determination of the metabolic profile |
| | Metabolite-profile-summary.csv | Values of metabolic profile plot |

## GC-MS fragmentation analysis

Table E.6.: GC-fragments for determination of stable isotope incorporation

| Metabolite | Derivate | m+0 | Exact mass | C-body | Carbons |
|---|---|---|---|---|---|
| Ala | (2TMS) | 116 | 116.089 | C2 | not unique |
| Ala | (2TMS) | 190 | 190.1078 | C2 | |
| Ala | (3TMS) | 188 | 188.1285 | C2 | [2,3] |
| Ala | (3TMS) | 262 | 262.1473 | | |
| Asp | (2TMS) | 130 | 130.0319 | C2 | |
| Asp | (2TMS) | 160 | 160.0788 | C3 | |
| Asp | (3TMS) | 218 | 218.1027 | C2 | [1,2] |
| Asp | (3TMS) | 232 | 232.1184 | C3 | [2,3,4] |
| Asp | (3TMS) | 306 | 306.1371 | C3 | |
| Cit | (4TMS) | 273 | 273.0973 | C5 | [1,2,3,4,5] |
| Cit | (4TMS) | 347 | 347.1161 | C4 | |
| Cit | (4TMS) | 375 | 375.111 | C6 | all |
| Cit | (4TMS) | 465 | 465.1611 | C6 | all |
| DHAP | (1MEOX)(3TMS) | 400 | 400.1191 | C3 | all |
| Frc | (1MEOX)(5TMS) | 205 | 205.1075 | C2 | [5,6] |
| Frc | (1MEOX)(5TMS) | 217 | 217.1075 | C3 | [4,5,6] |
| Frc | (1MEOX)(5TMS) | 307 | 307.1576 | C3 | |
| FBP | (1MEOX)(7TMS) | 217 | 217.1075 | C3 | [4,5,6] |
| FBP | (1MEOX)(7TMS) | 387 | 387.1423 | | |
| F6P | (1MEOX)(6TMS) | 217 | 217.1075 | C3 | |
| F6P | (1MEOX)(6TMS) | 387 | 387.1423 | | |
| Fum | (2TMS) | 217 | 217.0711 | C3 | |
| Fuma | (2TMS) | 245 | 245.066 | C4 | all |
| 6PGA | (7TMS) | 217 | 217.1075 | C3 | |
| 6PGA | (7TMS) | 387 | 387.1423 | | |
| Glc | (1MEOX)(5TMS) | 160 | 160.27 | C2 | [1,2] |
| Glc | (1MEOX)(5TMS) | 205 | 205.1075 | C2 | [5,6] |
| Glc | (1MEOX)(5TMS) | 217 | 217.1075 | C3 | [4,5,6] |
| G1/6P | (1MEOX)(6TMS) | 217 | 217.1075 | C3 | [4,5,6] |
| G1/6P | (1MEOX)(6TMS) | 357 | 357.1133 | C2 | |
| G6P | (1MEOX)(6TMS) | 217 | 217.1075 | C3 | [4,5,6] |
| G6P | (1MEOX)(6TMS) | 357 | 357.1133 | C2 | |
| Glu | (2TMS) | 186 | 186.0581 | C4? | |
| Glu | (2TMS) | 230 | 230.1027 | C3? | |
| Glu | (2TMS) | 276 | 276.1082 | C5 | all |
| Glu | (3TMS) | 230 | 230.1027 | C3? | |
| Glu | (3TMS) | 246 | 246.134 | C4 | [1,2,3,5] * or 4? |

Continued on next page

**Table E.6 – continued from previous page**

| Metabolite | Derivate | m+0 | Exact mass | C-body | Carbons |
|---|---|---|---|---|---|
| Glu | (3TMS) | 348 | 348.1477 | C4 | |
| Gln | (3TMS) | 156 | 156.0839 | C4 | [2,3,4,5] |
| Gln | (3TMS) | 245 | 245.15 | C4 | |
| 2HG | (3TMS) | 185 | n.d. | C4 | |
| 2HG | (3TMS) | 231 | 231.0867 | C3 | |
| 2HG | (3TMS) | 247 | 247.118 | C4 | symmetry |
| 2HG | (3TMS) | 349 | 349.1317 | — | sec. structure |
| aKG | (1MEOX)(2TMS) | 156 | 156.0475 | C3 | |
| aKG | (1MEOX)(2TMS) | 198 | 198.0581 | C5 | symmetry |
| aKG | (1MEOX)(2TMS) | 288 | 288.1082 | C5 | all |
| GA3P | (1MEOX)(3TMS) | 217 | n.d. | C3 | all |
| 3PGA | (4TMS) | 357 | 357.1133 | C2 | [2,3] |
| 3PGA | (4TMS) | 387 | 387.1423 | | |
| Glyc | (3TMS) | 218 | 218.1153 | C3 | all |
| Glyc | (3TMS) | 293 | 293.1419 | | |
| Glyc3P | (4TMS) | 315 | 315.1028 | — | sec. structure |
| Glyc3P | (4TMS) | 357 | 357.1133 | C2 | [2,3] |
| Glyc3P | (4TMS) | 387 | 387.1423 | — | sec. structure |
| Gly | (2TMS) | 176 | 176.0921 | | |
| Gly | (2TMS) | 204 | 204.0871 | | |
| Gly | (3TMS) | 276 | 276.1266 | C2 | all |
| Gly | (3TMS) | 248 | 248.1317 | | |
| Lac | (2TMS) | 117 | 117.073 | C2 | [2,3] |
| Lac | (2TMS) | 191 | 191.0918 | C2 | |
| Lac | (2TMS) | 219 | 219.0867 | C3 | all |
| Mal | (3TMS) | 233 | 233.1024 | C3 | symmetry* |
| Mal | (3TMS) | 245 | 245.066 | C4 | all |
| Mal | (3TMS) | 335 | 335.1161 | C4 | all |
| PEP | (3TMS) | 369 | 369.0769 | C3 | all |
| Pyr | (1MEOX)(1TMS) | 158 | 158.0632 | C3 | |
| Pyr | (1MEOX)(1TMS) | 174 | 174.0581 | C3 | all |
| Pyr | (1MEOX)(1TMS) | 189 | 189.0816 | C3 | |
| R5P | (1MEOX)(5TMS) | 217 | 217.1075 | C3 | |
| R5P | (1MEOX)(5TMS) | 357 | 357.1133 | C2 | |
| Ser | (2TMS) | 116 | 116.0526 | C2 | not unique |
| Ser | (2TMS) | 132 | 132.0839 | C2 | |
| Ser | (3TMS) | 188 | 188.0921 | C2 | |
| Ser | (3TMS) | 204 | 204.1234 | C2 | [2,3] |
| Ser | (3TMS) | 218 | 218.1027 | C2 | [1,2] |
| Suc | (2TMS) | 172 | 172.055 | C3 | symmetry |
| Suc | (2TMS) | 247 | 247.0816 | C4 | all |

Table E.7.: GC-MS fragment analysis for central carbon metabolism related metabolites

| Metabolite | Derivate | m+0 | Exact mass | Formula | Comment |
|---|---|---|---|---|---|
| Alanine | (2TMS) | 116 | 116.089 | C5H14NSi | [M-COOTMS]+ |
| Alanine | (2TMS) | 190 | 190.1078 | C7H20NOSi2 | |
| Alanine | (3TMS) | 188 | 188.1285 | C8H22NSi2 | [M-COOTMS]+ |
| Alanine | (3TMS) | 262 | 262.1473 | C10H28NOSi3 | |
| Aspartic acid | (2TMS) | 130 | 130.0319 | C4H8NO2Si | [M-COOTMS]+ |
| Aspartic acid | (2TMS) | 160 | 160.0788 | C6H14NO2Si | |
| Aspartic acid | (3TMS) | 218 | 218.1027 | C8H20NO2Si2 | [Head]+ |
| Aspartic acid | (3TMS) | 232 | 232.1184 | C9H22NO2Si2 | [M-COOTMS]+ |
| Aspartic acid | (3TMS) | 306 | 306.1371 | C11H28NO3Si3 | |
| Citric acid | (4TMS) | 273 | 273.0973 | C11H21O4Si2 | |
| Citric acid | (4TMS) | 347 | 347.1161 | C13H27O5Si3 | |
| Citric acid | (4TMS) | 375 | 375.111 | C14H27O6Si3 | |
| Citric acid | (4TMS) | 465 | 465.1611 | C17H37O7Si4 | [M-CH3]+ |
| Dihydroxyacetone phosphate | (1MEOX)(3TMS) | 315 | 315.1028 | C9H28O4PSi3 | ! Pi + H ! |
| Dihydroxyacetone phosphate | (1MEOX)(3TMS) | 400 | 400.1191 | C12H31NO6PSi3 | [M-CH3]+ |
| Fructose_MP | (1MEOX)(5TMS) | 205 | 205.1075 | C8H21O2Si2 | |
| Fructose_MP | (1MEOX)(5TMS) | 217 | 217.1075 | C9H21O2Si2 | |
| Fructose_MP | (1MEOX)(5TMS) | 307 | 307.1576 | C12H31O3Si3 | |
| Fructose-1_6-diphosphate | (1MEOX)(7TMS) | 217 | 217.1075 | C9H21O2Si2 | |
| Fructose-1_6-diphosphate | (1MEOX)(7TMS) | 315 | 315.1028 | C9H28O4PSi3 | ! Pi + H ! |
| Fructose-1_6-diphosphate | (1MEOX)(7TMS) | 387 | 387.1423 | C12H36O4PSi4 | ! Pi + TMS ! |
| Fructose-6-phosphate | (1MEOX)(6TMS) | 217 | 217.1075 | C9H21O2Si2 | |
| Fructose-6-phosphate | (1MEOX)(6TMS) | 315 | 315.1028 | C9H28O4PSi3 | ! Pi + H ! |
| Fructose-6-phosphate | (1MEOX)(6TMS) | 387 | 387.1423 | C12H36O4PSi4 | ! Pi + TMS ! |
| Fumaric acid | (2TMS) | 217 | 217.0711 | C8H17O3Si2 | |

Continued on next page

**Table E.7 – continued from previous page**

| Metabolite | Derivate | m+0 | Exact mass | Formula | Comment |
|---|---|---|---|---|---|
| Fumaric acid | (2TMS) | 245 | 245.066 | C9H17O4Si2 | [M-CH3]+ |
| Gluconic acid-6-phosphate | (7TMS) | 217 | 217.1075 | C9H21O2Si2 | |
| Gluconic acid-6-phosphate | (7TMS) | 315 | 315.1028 | C9H28O4PSi3 | ! Pi + H ! |
| Gluconic acid-6-phosphate | (7TMS) | 387 | 387.1423 | C12H36O4PSi4 | ! Pi + TMS ! |
| Glucose_MP / BP | (1MEOX)(5TMS) | 160 | | C6H14NO2Si | |
| Glucose_MP / BP | (1MEOX)(5TMS) | 205 | 205.1075 | C8H21O2Si2 | |
| Glucose_MP / BP | (1MEOX)(5TMS) | 217 | 217.1075 | C9H21O2Si2 | |
| Glucose_MP / BP | (1MEOX)(5TMS) | 315 | 315.1028 | C9H28O4PSi3 | ! Pi + H ! |
| Glucose-1/6-phosphate | (1MEOX)(6TMS) | 217 | 217.1075 | C9H21O2Si2 | |
| Glucose-1/6-phosphate | (1MEOX)(6TMS) | 357 | 357.1133 | C11H30O5PSi3 | |
| Glucose-6-phosphate | (1MEOX)(6TMS) | 217 | 217.1075 | C9H21O2Si2 | |
| Glucose-6-phosphate | (1MEOX)(6TMS) | 357 | 357.1133 | C11H30O5PSi3 | |
| Glutamic acid | (3TMS) | 230 | 230.1027 | C9H20NO2Si2 | |
| Glutamic acid | (3TMS) | 246 | 246.134 | C10H24NO2Si2 | [M-COOTMS]+ |
| Glutamic acid | (3TMS) | 348 | 348.1477 | C13H30NO4Si3 | [M-CH3]+ |
| Glutamic acid | (2TMS) | 186 | 186.0581 | C7H12NO3Si | |
| Glutamic acid | (2TMS) | 230 | 230.1027 | C9H20NO2Si2 | |
| Glutamic acid | (2TMS) | 276 | 276.1082 | C10H22NO4Si2 | [M-CH3]+ |
| Glutamine | (3TMS) | 156 | 156.0839 | C7H14NOSi | |
| Glutamine | (3TMS) | 245 | 245.15 | C10H25N2OSi2 | [M-COOTMS]+ |
| Glutaric acid_ 2-hydroxy- | (3TMS) | 231 | 231.0867 | C9H19O3Si2 | |
| Glutaric acid_ 2-hydroxy- | (3TMS) | 247 | 247.118 | C10H23O3Si2 | [M-COOTMS]+ |
| Glutaric acid_ 2-hydroxy- | (3TMS) | 349 | 349.1317 | C13H29O5Si3 | [M-CH3]+ |
| Glutaric acid_ 2-oxo- | (1MEOX)(2TMS) | 156 | 156.0475 | C6H10NO2Si | |
| Glutaric acid_ 2-oxo- | (1MEOX)(2TMS) | 198 | 198.0581 | C8H12NO3Si | |
| Glutaric acid_ 2-oxo- | (1MEOX)(2TMS) | 288 | 288.1082 | C11H22NO4Si2 | |

Continued on next page

**Table E.7 – continued from previous page**

| Metabolite | Derivate | m+0 | Exact mass | Formula | Comment |
|---|---|---|---|---|---|
| Glutaric acid | (2TMS) | 233 | 233.1024 | C9H21O3Si2 | |
| Glutaric acid | (2TMS) | 261 | 261.0973 | C10H21O4Si2 | [M-CH3]+ |
| Glyceric acid-3-phosphate | (4TMS) | 315 | 315.1028 | C9H28O4PSi3 | ! Pi + H ! |
| Glyceric acid-3-phosphate | (4TMS) | 357 | 357.1133 | C11H30O5PSi3 | [M-COOTMS]+ |
| Glyceric acid-3-phosphate | (4TMS) | 387 | 387.1423 | C12H36O4PSi4 | ! Pi + TMS ! |
| Glycerol | (3TMS) | 218 | 218.1153 | C9H22O2Si2 | |
| Glycerol | (3TMS) | 293 | 293.1419 | C11H29O3Si3 | [M-CH3]+ |
| Glycerol-3-phosphate | (4TMS) | 315 | 315.1028 | C9H28O4PSi3 | ! Pi + H ! |
| Glycerol-3-phosphate | (4TMS) | 357 | 357.1133 | C11H30O5PSi3 | |
| Glycerol-3-phosphate | (4TMS) | 387 | 387.1423 | C12H36O4PSi4 | ! Pi + TMS ! |
| Glycine | (2TMS) | 176 | 176.0921 | C6H18NOSi2 | |
| Glycine | (2TMS) | 204 | 204.0871 | C7H18NO2Si2 | [M-CH3]+ |
| Glycine | (3TMS) | 276 | 276.1266 | C10H26NO2Si3 | [M-CH3]+ |
| Glycine | (3TMS) | 248 | 248.1317 | C9H26NOSi3 | |
| Lactic acid | (2TMS) | 117 | 117.073 | C5H13OSi | [M-COOTMS]+ |
| Lactic acid | (2TMS) | 191 | 191.0918 | C7H19O2Si2 | |
| Lactic acid | (2TMS) | 219 | 219.0867 | C8H19O3Si2 | [M-CH3]+ |
| Malic acid | (3TMS) | 233 | 233.1024 | C9H21O3Si2 | [M-COOTMS]+ |
| Malic acid | (3TMS) | 245 | 245.066 | C9H17O4Si2 | |
| Malic acid | (3TMS) | 335 | 335.1161 | C12H27O5Si3 | [M-CH3]+ |
| Phosphoenolpyruvic acid | (3TMS) | 211 | 211.0006 | C4H12O4PSi2 | |
| Phosphoenolpyruvic acid | (3TMS) | 369 | 369.0769 | C11H26O6PSi3 | [M-CH3]+ |
| Pyruvic acid | (1MEOX)(1TMS) | 158 | 158.0632 | C6H12NO2Si | |
| Pyruvic acid | (1MEOX)(1TMS) | 174 | 174.0581 | C6H12NO3Si | [M-CH3]+ |
| Pyruvic acid | (1MEOX)(1TMS) | 189 | 189.0816 | C7H15NO3Si | [M]+ |
| Ribose-5-phosphate | (1MEOX)(5TMS) | 217 | 217.1075 | C9H21O2Si2 | |

Continued on next page

**Table E.7 – continued from previous page**

| Metabolite | Derivate | m+0 | Exact mass | Formula | Comment |
|---|---|---|---|---|---|
| Ribose-5-phosphate | (1MEOX)(5TMS) | 315 | 315.1028 | C9H28O4PSi3 | ! Pi + H ! |
| Ribose-5-phosphate | (1MEOX)(5TMS) | 357 | 357.1133 | C11H30O5PSi3 | |
| Serine | (2TMS) | 116 | 116.0526 | C4H10NOSi | |
| Serine | (2TMS) | 132 | 132.0839 | C5H14NOSi | [M-COOTMS]+ |
| Serine | (3TMS) | 188 | 188.0921 | C7H18NOSi2 | |
| Serine | (3TMS) | 204 | 204.1234 | C8H22NOSi2 | [M-COOTMS]+ |
| Serine | (3TMS) | 218 | 218.1027 | C8H20NO2Si2 | [Head]+ |
| Succinic acid | (2TMS) | 172 | 172.055 | C7H12O3Si | |
| Succinic acid | (2TMS) | 247 | 247.0816 | C9H19O4Si2 | [M-CH3]+ |

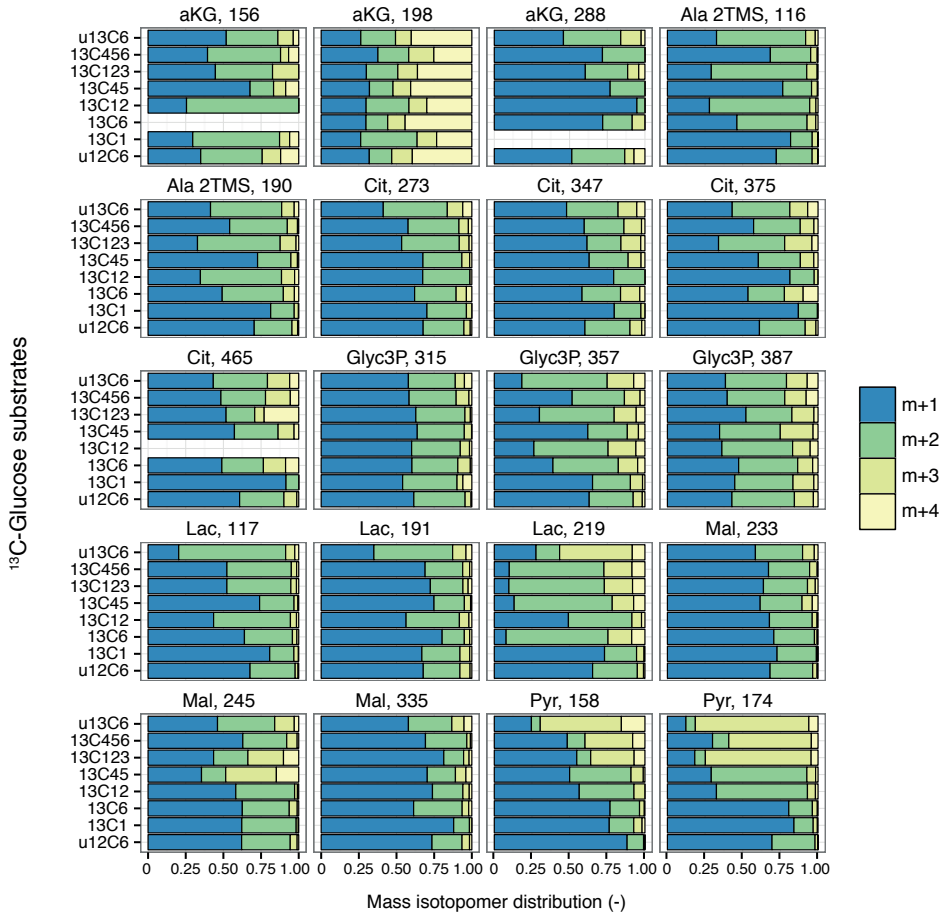


Figure E.1.: GC-MS fragment analysis applying different isotopes $^{13}$C-glucose in cell culture experiment.

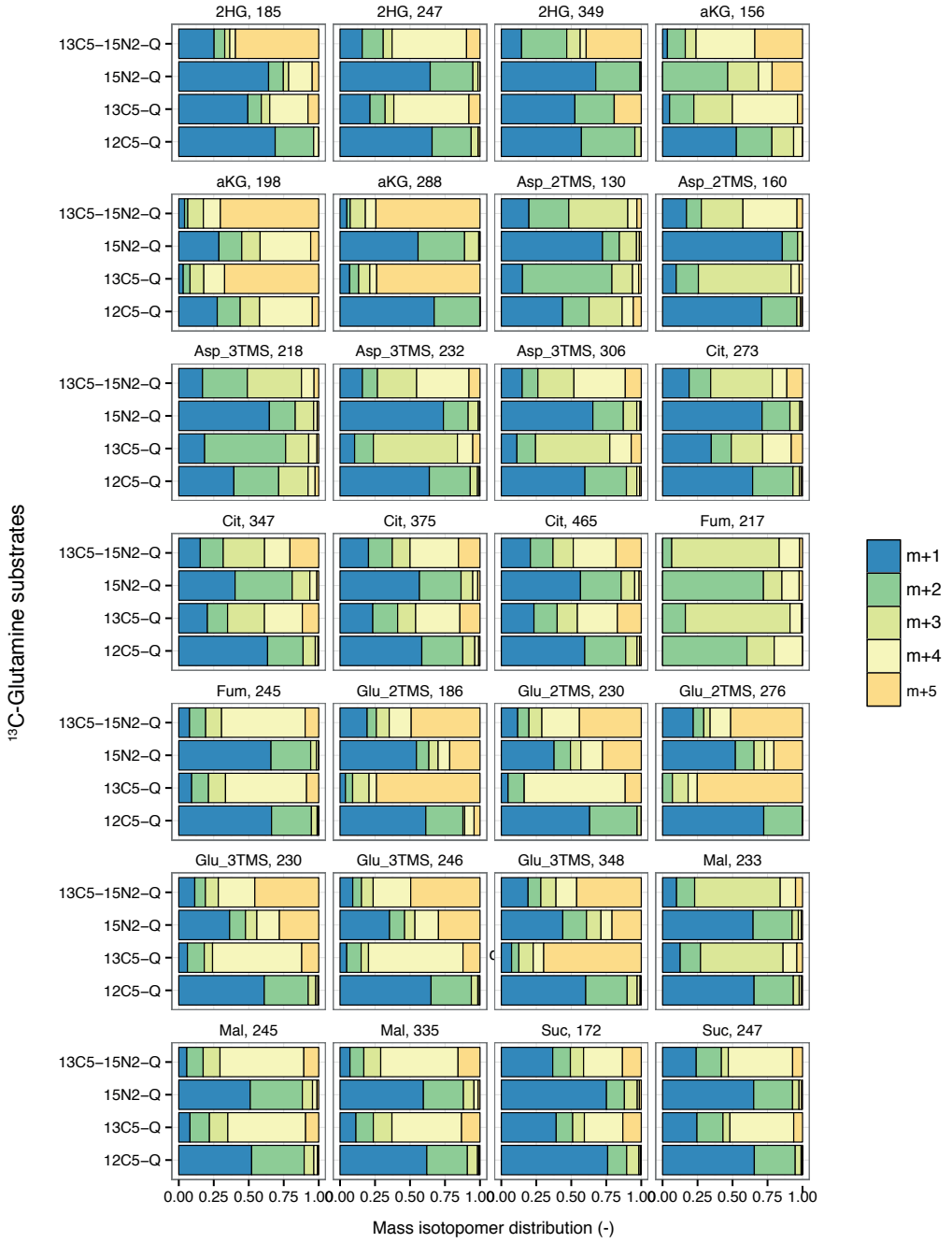


Figure E.2.: GC-MS fragment analysis applying different isotopes of $^{13}$C-glutamine in cell culture experiment.